Ferrocenyl Carbenes as Redox-Switchable Ligands in Gold Catalysis

Synthesis, Redox-Behaviour and Elucidation of Side Reactions

Dissertation

Zur Erlangung des Grades

„Doktor der Naturwissenschaften“

Im Promotionsfach Chemie

am Fachbereich Chemie, Pharmazie, Geographie

und Geowissenschaften

der Johannes Gutenberg-Universität Mainz

Philipp Veit

geboren in Kirchheimbolanden

Mainz, 2020

Die vorliegende Arbeit wurde im Zeitraum vom Juni 2015 bis Oktober 2020 unter Betreuung von [redacted] am Department Chemie der Johannes Gutenberg-Universität Mainz durchgeführt.

Mainz, 13.10.2020

Eigenständigkeitserklärung

Hiermit versichere Ich, Philipp Veit, Matrikelnummer [redacted] dass ich meine *Promotionsarbeit* selbstständig verfasst und keine anderen als die angegebenen schriftlichen und elektronischen Quellen, sowie andere Hilfsmittel benutzt habe. Alle Ausführungen, die anderen Schriften wörtlich oder sinngemäß entnommen wurden, habe ich kenntlich gemacht.

Datum _____ Unterschrift _____

Dekan: [redacted]

1. Berichterstatter: [redacted]

2. Berichterstatter: [redacted]

Tag der mündlichen Prüfung: 19.11.2020

Kurzzusammenfassung

N-heterozyklische Carbene waren die ersten stabilen kristallinen Carbene die 1991 von Arduengo et al. isoliert wurden. Analog zu einem *N*-heterozyklischen Carben wurde später ein Diferrocenyl-Carben postuliert und es gab Syntheseversuche von vielen Arbeitsgruppen mit unterschiedlichen Herangehensweisen, die bisher alle nicht zum Nachweis des Diferrocenyl-Carben ausgereicht haben.

Der erste Teil dieser Arbeit beschäftigt sich mit der Synthese von Dimetallocentosylhydrazonen als mögliche Vorstufe für das Diferrocenyl-Carben und beleuchtet die nicht klassische intramolekulare Metall-Wasserstoff-Brückenbindung die in diesen Verbindungen auftritt. Die Bindungsstärke der Wasserstoff-Brückenbindung zu Ferrocenyl- und Ruthenocenylgruppen wird untersucht und verglichen, wobei die Ruthenocenyl-Wasserstoff-Brückenbindung stärker ist. Durch zweifache Oxidation lässt sich die Wasserstoff-Brückenbindung in Diferrocenyltosylhydrazon öffnen und die Orientierung der vorher gebundenen Ferrocenyl-Gruppe ändert sich, wodurch es zu einem molekularen Schalter wird. Im gemischten Ferrocenylruthenocenyltosylhydrazon wird die intramolekulare Metall-Wasserstoff-Brückenbindung mit einem Verhältnis von 10:1 bevorzugt zur Ruthenocenyl-Gruppe ausgebildet. Durch Deprotonierung/Reprotonierung, thermische Behandlung oder Bestrahlung mit 400 nm können die beiden Isomere in einander umgewandelt werden und das Verhältnis von 10:1 verschiebt sich weiter zu Gunsten der Ruthenocenyl-Wasserstoff-Brückenbindung.

Fischer-Carben-Komplexe sind seit ihrer Entdeckung 1964 in vielen Bereichen der Organometall-Chemie vertreten. Die redox-aktiven Eigenschaften von Ferrocenyl-Fischer-Carben-Komplexen machen diese besonders interessant als Vorstufen für redox-schaltbare Katalysatoren.

In dieser Arbeit werden Ferrocenyl-Fischer-Carben-Komplexe sowohl mit Chrom, als auch mit Wolfram, mit einer oder auch mit zwei Ferrocenyl Gruppen auf ihre Stabilität und elektronischen Eigenschaften untersucht, um daraus redox-schaltbare Katalysatoren herzustellen. Der elektronische Kopplungsparameter H_{AB} von (*N*-Metylaminoferrocenyl)(ferrocenyl)carben(pentacarbonyl)wolfram(0) wird bestimmt und mit den homologen Carbox- und Thioamiden verglichen.

Es werden zwei neue Reaktionsmöglichkeiten von Ferrocenyl Fischer Carben Komplexen zu 2,*N*-Diferrocenylacetamid und 2,3,4-Triferrocenyl-cyclobut-2-enon beobachtet und die zugrunde liegenden Reaktionsmechanismen genauer untersucht. Der vorgeschlagene Mechanismus zu 2,3,4-Triferrocenyl-cyclobut-2-enon ähnelt dabei der Dötz-Benzannelierung. Die Bildung von 2,*N*-Diferrocenylacetamid verläuft dagegen wahrscheinlich über einen nucleophilen Angriff von Aminoferrocen an einem Carbonyl Kohlenstoff Atom mit anschließender Insertion in die Carben-Bindung.

Ferrocenyl-Ethoxy-Fischer-Carben wird mit einer Transmetallierung auf Gold(I) übertragen um einen redox-schaltbare Katalysator zu erhalten. Dieser Katalysator wird an einer Beispielreaktion auf seine Eigenschaften getestet um sowohl die Qualität der Reaktion als auch die Fähigkeit des Katalysators mehrmals an- und aus-geschaltet zu werden zu bewerten. Der Katalysator zeigt einen Umsatz von nahezu 100 % nach 8 h Reaktion und lässt sich mehrmals An- und Aus-schalten.

Abstract

N-Heterocyclic carbenes were the first stable crystalline carbenes isolated by Arduengo et al. in 1991. Later a diferrocenyl carbene has been postulated analogous to the *N*-heterocyclic carbenes. Many different research groups with various approaches failed to confirm the existence of this molecule.

In the first part of this work the synthesis of different dimetalllocene tosylhydrazones as potential precursors for dimetalllocene carbenes is discussed. In these compounds a strong *nonclassical* NH···M intramolecular hydrogen bond (IHB) to the metallocene site is present. The bond strength to the ferrocenyl and ruthenocenyl groups is investigated and compared to each other. The IHB to ruthenocenyl group is stronger than the IHB to the ferrocenyl group. Double oxidation of diferrocenyl tosylhydrazone leads to a cleavage of the IHB and a conformational change of the previous bound ferrocenyl group, making this compound a molecular switch. In the mixed ferrocenyl ruthenocenyl tosylhydrazone the IHB is preferably formed to the ruthenocenyl group with a ratio of 10:1. Deprotonation/reprotonation, thermal treatment or irradiation with 400 nm leads to an isomerization and a shift of the ratio towards the isomer with the ruthenocenyl IHB.

Since their discovery in 1964 Fischer carbene complexes have been applied in many parts of organometallic chemistry. The redox responsive characteristics of ferrocenyl Fischer carbene are precious precursors for redox switchable catalysts (RSC).

In this work different chromium and tungsten containing ferrocenyl Fischer carbene complexes with one or two ferrocenyl sites are studied according their stability and electrochemical properties in accordance to their aptitude as precursors for RSC. The electronic coupling parameter H_{AB} of (*N*-methylaminoferrocenyl)(ferrocenyl)carbene(pentacarbonyl)tungsten(0) is evaluated and compared to the corresponding diferrocenylcarbox- and thioamides.

Two new reaction paths from ferrocenyl Fischer carbene complexes to 2,*N*-diferrocenylacetamide and 2,3,4-triferrocenyl-cyclobut-2-enone are reported and the reaction mechanisms are studied in detail. The proposed mechanism to form 2,3,4-triferrocenyl-cyclobut-2-enone is similar to the well-known Dötz benzannulation reaction. The formation of 2,*N*-diferrocenylacetamide instead proceeds most likely via nucleophilic attack of aminoferrocene on a carbonyl carbon atom of the Fischer carbene complex with subsequent insertion into the carbene bond.

Ferrocenyl ethoxy Fischer Carbene is transferred to Gold(I) to get a prototype redox switchable catalyst. This RSC is used for a test reaction to probe the conversion properties and the ability to switch the catalyst on and off. The catalyst shows almost 100 % yield after 8 h and can be switched on and off several times.

Content

Abbreviations

°C	Degrees Celsius
Å	Ångström
Ad	adamantyl
ADC	acyclic diamino carbene
Alk	alkyl
B	magnet field strength
$BAr^F_4^-$	tetrakis(3,5-bis(trifluoromethyl)phenyl)borate anion
Bfc	1',1''.biferrocenyl
bfc	1',1''-biferrocenyl-1,1'''-diyl
Bn	benzyl group
br	broad (signal shape in IR- and NMR-spectroscopy)
CAACs	cyclic (alkyl)(amino)carbenes
Cc	cobaltocenyl
CcH	cobaltocene
Cc*	nonamethylcobaltocenyl
Cc^*CH_3	Decamethylcobaltocene
cod	1,5-cyclooctadiene
COSMO	conductor-like screening model
COSY	correlated spectroscopy
Cp	cyclopentadienyl
CV	Cyclic voltammetry
Cy	Cyclohexyl
d	duplet
DCM	dichloromethane
Dipp	2,6-diisopropylphenyl
dppc	1,1'-bis(diphenylphosphino)cobaltocene
dppf	1,1'-bis(diphenylphosphino)ferrocene
δ	chemical shift (NMR)
ΔE	potential difference
deprot.	deprotonated
DFT	density functional theory
E	electrochemical potential
$E_{rel.}$	relative potential energy
EA	elemental analysis
Et	ethyl
EPR	electron paramagnetic resonance
Eq.	equation
exc.	excess
exp.	experimental
EXSY	exchange spectroscopy
Fc	ferrocenyl
fc	ferrocenen-1,1'-diyl
FcH	Ferrocene

Fc*	nonamethylferrocenyl
Fc*CH_3	decamethylferrocene
FcDAC	diaminocarbene[3]ferrocenophane
FD/MS	field desorption mass spectrometry
FT	fourier transformation
HMBC	heteronuclear multiple quantum correlation
HOMO	highest occupied molecular orbital
HSQC	heteronuclear single quantum coherence
IBO	intrinsic bond orbital
IET	intramolecular electron transfer
IHB	intramolecular hydrogen bond
imag	imaginary
IMes	1,3-bis(2,4,6-trimethylphenyl) imidazol-2-ylidene
IPr**	1,3-bis{2,6-bis[bis(4-*tert*-butylphenyl)methyl]-4-methylphenyl}-2,3-dihydro-1*H*-imidazol-2-ylidene
IR	infrared
IR_s	solid state infrared spectroscopy
$IR_{solv.}$	infrared spectroscopy in solution (Solvent)
IS	isomer shift (Mößbauer spectroscopy)
IVCT	intervalence charge transfer
J	coupling constant (NMR)
K	Kelvin
KHMDS	potassium hexamethyldisilazide / potassium hexamethyldisilazane
λ	wavelength
LASER	Light Amplification by Stimulated Emission of Radiation
LUMO	lowest unoccupied molecular orbital
m	medium (signal intensity in IR-spectroscopy)
m	multiplet (NMR-spectrum)
'Magic Blue'	tris(4-bromphenyl)aminiumhexachloroantimonate
Me	methyl
Mes	mesityl
MIC	mesoionic carbene
mM	millimole per litre
mT	millitesla
m/z	mass to charge ratio
MO	molecular orbital
MS	mass spectrometry
$NaHCO_3$	sodium hydrogen carbonate
NaCl	sodium chloride
$NaSO_4$	natrium sulphate
NHC	N-heterocyclic carbene
NHE	normal hydrogen electrode
NMR	nuclear magnetic resonance
org.	organic
ox.	oxidation
PE	petroleum ether

pt	pseudo triplet (NMR)
$\tilde{\nu}$	wavenumber
ppm	parts per million
q	quartet (NMR)
QS	quadrupole splitting (Mößbauer spectroscopy)
quant.	quantitative
RCM	ring closing metathesis
Red.	reduction
R_f	retardation factor
RI	resolution-of-identity
ROMP	ring-opening metathesis polymerization
ROP	ring-opening polymerization
ROS	reactive oxygen species
RSC	redox switchable catalysis
r.t.	room temperature
s	strong (signal intensity in IR-spectroscopy)
s	singlet (NMR-spectrum)
SCE	standard calomel electrode
sh	shoulder (signal intensity in IR- or UV-spectroscopy)
simul.	simulated
subst.	substituted
SWV	square-wave-voltammetry
T	temperature
t	triplet (NMR-spectrum)
TD-DFT	time dependent density functional theory
TEP	tolman electronic parameter
Th	2-thienyl
th	2,5-thiendiyl
THF	Tetrahydrofurane
tol	*p*-tolyl
trz	1,2,3-triazol-5-ylidene
UV	ultraviolet
Vis	visible part of the electromagnetic spectrum
vs	very strong (signal intensity in spectroscopy)
vw	very weak (signal intensity in spectroscopy)
w	weak (signal intensity in spectroscopy)
XRD	X-ray diffraction
ZORA	zeroth order regular approximation

1 Introduction

1.1 Ferrocenylcarbenes and Diferrocenylcarbenes

1.1.1 α-Ferrocenylcarbenes

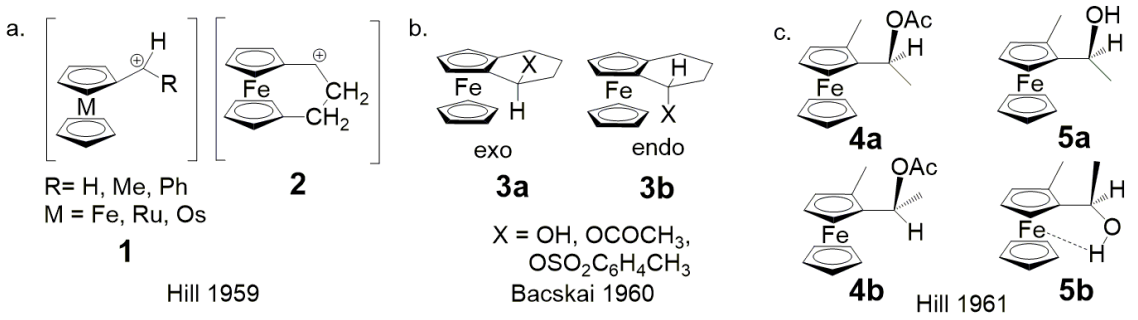

Scheme 1.1.1: a. Carbenium intermediates postulated for the solvolysis of metallocenylacetates[1], b. reaction rate of exo/endo-α-substituted-1,2-tetramethyleneferrocenes[2,3], c. diastereomeric isomers .[4]

Already in 1959 only a couple of years after the first discovery of ferrocene[5,6] the first α-metallocenylcarbeniumions of iron, ruthenium and osmium (Scheme 1.1.1 a.: **1**, **2**) were suggested as intermediates during the ethanolysis of metallocenylcarbinylacetates and the reactivity was compared to the trityl ion.[1] The reactivity of the osmocene homologue was 5.1 times faster than the methylferrocenecarbinylacetate, while the reaction rate of the methylruthenocenyl-carbinylacetate was only 1.34 times faster. The role of the metal centre in the stabilization of the carbenium ion was also investigated by comparison of the reaction rate of exo/endo-α-acetoxy-1,2-tetramethyleneferrocene **3a** and **3b,** respectively (Scheme 1.1.1 b.).[2,3] The exo-isomer **3a** shows a 2240 times higher relative reaction rate in the solvolysis reaction suggesting a participation of the iron electrons in the rate determining ionization process. Some molecular orbital descriptions of the interaction of the metal atom with the electron deficient carbon in metallocenylcarbeniumions suggested a shift of the coordination to the ring from η^5 to η^3 to enable a interaction with the carbenium carbon atom.[7] Ortho-substituents on the cyclopentadienyl ring of ferrocenylcarbeniumions are leading to diastereomeric isomers **4a/4b** and **5a/5b**, respectively (Scheme 1.1.1 c.).[4] The sole alcohol product after hydrolysis of the substituted ferrocenylcarbinylacetates had the same configuration as the starting acetate. The σ^+_{para} value for phenyl-, methoxy- and ferrocenyl-substituents on carbenium ions were reported and taken as measure of the ability for the stabilization of intermediates or transition states with delocalized electrons.[8] The resonance effect on solvolysis rates of the ferrocenyl group is about 25 kJ mol^{-1} higher than for the phenyl group. To further investigate the mesomeric form of the carbenium ion detailed NMR studies were conducted.[9] Deshielding of the β-protons, with respect to the α-protons, shifts the β-protons into the downfield and the α-protons into the upfield in the NMR spectrum. The electronic structure of the ferrocenyl carbenium ion could be explained by a movement of the iron atom towards the carbenium carbon atom. This results in a greater overlap of the iron orbitals with the orbitals of the α-protons and increases the electron density. Also, the anisotropy of the iron atom was taken into account to shield the α-protons. The effect of the other

substituent on the carbenium ion on the shift of the α-protons of the ferrocenyl substituent was reported. Aryl substituents decrease the additional shielding of the α-protons by the metal interaction compared to alkyl substituents.

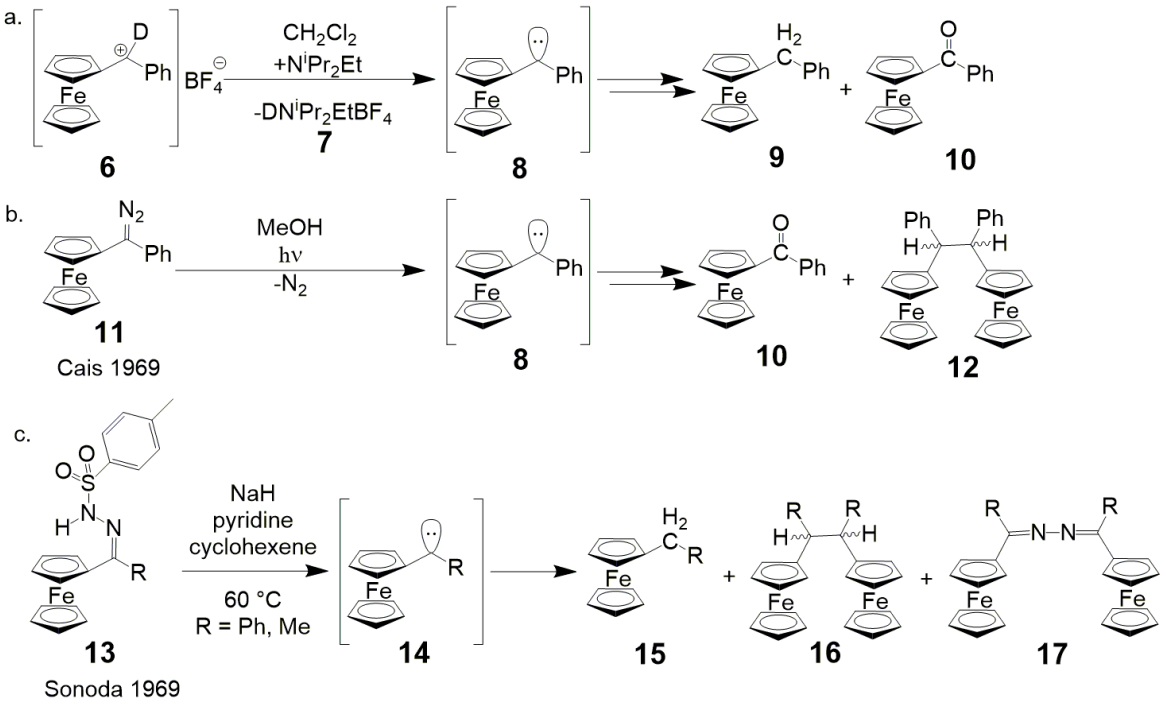

Scheme 1.1.2: Postulated α-ferrocenyl carbene intermediates via: a. deprotonation of ferrocenyl carbenium ions[10], b. photolysis of ferrocenyl diazomethanes[10], c. Bamford-Stevens reaction of ferrocenyl tosylhydrazones.[11]

In 1969, the first ferrocenylcarbene intermediates were proposed by Cais[10] and Sonoda[11] (Scheme 1.1.2). Deprotonation of the deuterated ferrocenyl phenyl carbenium ion salt **6** in dichloromethane with *N*,*N*-diisopropylethylamine leads to benzylferrocene **9** and benzoylferrocene **10** as products and the deuterated quaternary amine salt **7** as confirmed by NMR-spectroscopy (Scheme 1.1.2 a.).[10] Photolysis of ferrocenylphenyldiazomethane in methanol solution yields benzoylferrocene and 1,2-diferrocenyl-1,2-diphenylethane (Scheme 1.1.2 b.).[10] Both reactions propose ferrocenylphenylcarbene as intermediate but give no further conclusion about the singlet or triplet nature. UV irradiation of ferrocenylphenyldiazomethane in frozen methanolic matrix gives an EPR-signal which stays active when irradiation is stopped but the origin or the shape of the signal is not further specified. The group of Sonoda used a Bamford-Stevens reaction[12] of ferrocenyltoslyhydrazones to generate ferrocenyldiazomethanes in situ which could be detected by IR spectroscopy (Scheme 1.1.2 c.). As final products three species could be isolated. The azine product postulates a coupling of the carbene with the diazomethane. 1,1-Diphenylethylene was used as a triplet carbene trapping agent before and was also used to catch the ferrocenylphenylcarbene and yielded 1-ferrocenyl-1,2,2-triphenylcyclopropane. Also, the formation of benzylferrocene and 1,2-diferrocenyl-1,2-diphenyl-ethane suggest a triplet nature of the carbene which could abstract a hydrogen from the solvent to form an intermediate radical, which abstracts another hydrogen. The fact, that no addition of the carbene to the solvent cyclohexene is observed strengthens the hints for a triplet carbene. Singlet carbenes as

dichlorocarbene add to cyclohexene, styrene and vinylferrocene while triplet carbenes as diphenylcarbene only add to styrene and vinylferrocene.[11] Sonoda et al. also studied the reactions of ferrocenylmethylcarbene more in detail and found seven different products including the three shown in scheme 1.1.2 c. and additionally vinylferrocene, acetylferrocene, ferrocenylmethylcarbinol and 1,2-diferrocenyl-1-methylcyclopropane.[13] Formation of 1,2-diferrocenyl-1-methylcyclo-propane is explained by addition of the carbene at vinylferrocene. The reaction with the solvent carbon tetrachloride was investigated as well. 2-ferrocenyl-2-methyldichloroethylene could be isolated from this reaction which is proposed to form via reaction of the carbene with trichloromethyl radical with subsequent loss of a chlorine atom. 1,1-Diphenylethylene is a potent carbene catcher and is used to compare the reactivity of the α-ferrocenylcarbenes: ferrocenylcarbene, ferrocenylmethylcarbene and ferrocenylphenyl-carbene with the corresponding phenyl and *p*-anisylcarbenes.[14] The results suggest that the reactivity of *p*-anisylcarbenes is the highest, followed by phenylcarbenes and ferrocenylcarbenes showing the lowest reactivity with diphenylethylene.

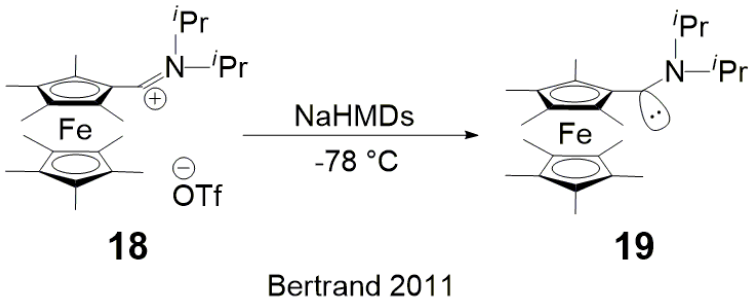

Scheme 1.1.3: The first persistent α-ferrocenyl carbene.[15]

In 2011 the first persistent α-ferrocenyl carbene **19** was reported by Bertrand et al. by the deprotonation of *N*,*N*-diisopropylnonamethylferrocenylaldiminium trifluoromethanesulfonate **18** with sodium hexamethydisilazane (Scheme 1.1.3).[15] The resulting carbene was stable enough to measure NMR at –50 °C and gave a resonance of 315 ppm for the carbene carbon in the ^{13}C-NMR spectrum.

1.1.2 *N*-heterocyclic Carbenes (NHCs)

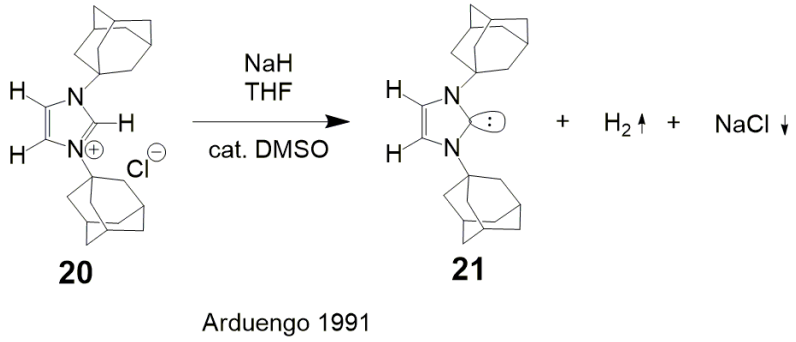

Scheme 1.1.4: The first stable crystalline carbene.[16]

In 1991 Arduengo et al. reported 1,3-di-1-adamantyl-imidazol-2-ylidene **21** as the first stable crystalline singlet carbene via the deprotonation of 1,3-di-1-adamantyl-imidazolium chloride **20**

(Scheme 1.1.4).[16,17] The amount of hydrogen generated by the reaction and also the amount of sodium chloride that was filtered off was determined and was in accordance to the theoretical calculated amounts. Stabilization was achieved by the two lone pairs of the nitrogen atoms in the imidazole heterocycle, but also the steric effect of the two adamantyl substituents was assumed to be crucial for the isolation. The N-C-N angle of 102.2° is quite prominent for this compound and was predicted by calculations in singlet carbenes before.[18] *N*-heterocyclic carbenes (NHCs) in general have been proposed in 1962 by Wanzlick with two *N*-phenyl substituents, but could not been isolated as the variety of accessible imidazolium salts was quite restricted at this time and Raman spectroscopy that would have been necessary to distinguish between the carbene and the dimer by showing the IR-inactive symmetrical vibrations was not common in the standard chemistry laboratory.[19–21]

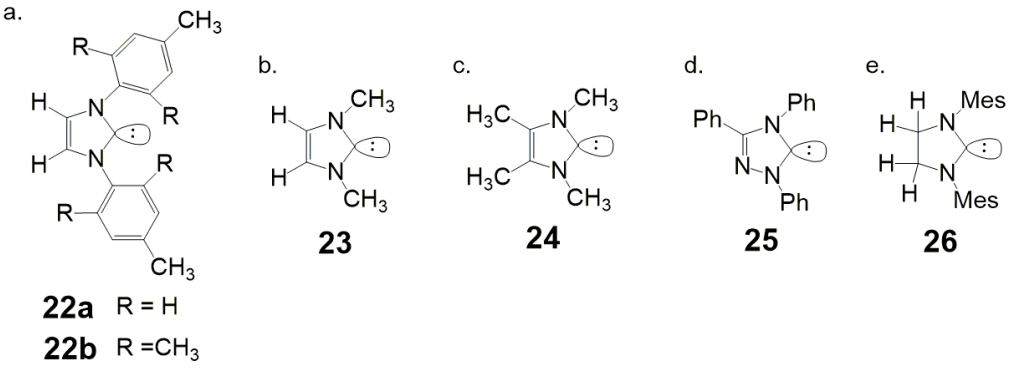

Scheme 1.1.5: Examples of stable NHCs: a. with aryl substituents[22], b. & c. with two and four methyl substituents[22,23], d. triazole[24], e. imidazoline[25].

Later also NHCs with other substituents were isolated (Scheme 1.1.5). 1,3-Di-*p*-tolylimidazol-2-yilidene **22a** and 1,3-di-mesitylimidazol-2-yilidene **22b** were the first aryl substituted NHCs (Scheme 1.1.5 a.).[22] The assumption that sterically demanding substituents were needed could be disproved by the isolation of 1,3-dimethylimidazol-2-yilidene **23** (Scheme 1.1.5 b.) and 1,3,4,5-tetramethylimidazol-2-yilidene **24** (Scheme 1.1.5 c.).[22,23] A third nitrogen atom in the five membered heterocycle also did not deteriorate the stability and yielded the stable carbene 1,3,4-triphenyl-4,5-dihydro-1H-1,2,4-triazol-5-ylidene **25** (Scheme 1.1.5 d.).[24] Also the double bond in the ring is not mandatory to stabilize the carbene as the isolation of 1,2-dimesitylimidazolin-2-yliden **26** proofed (Scheme 1.1.5 e.).[25]

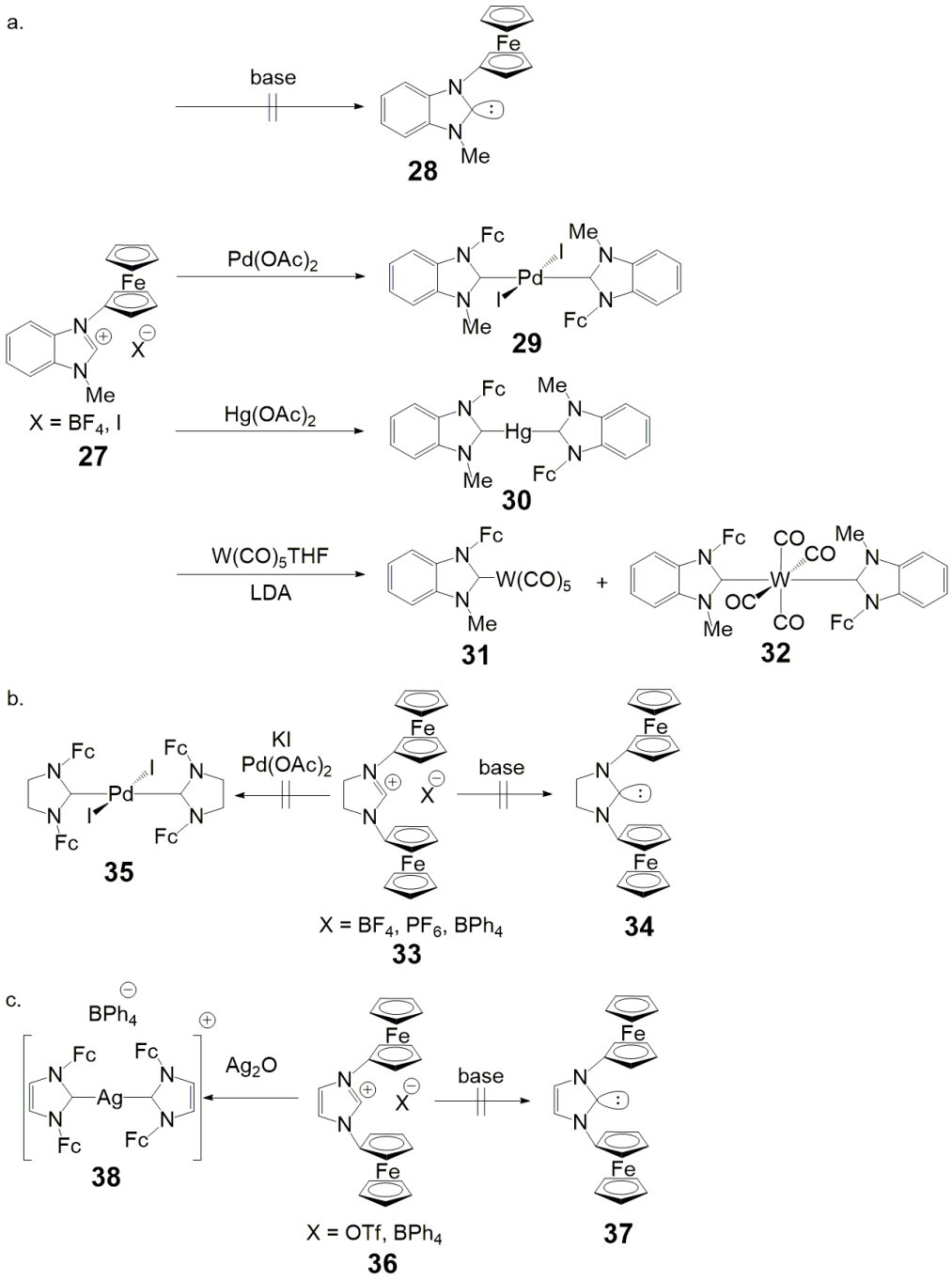

Scheme 1.1.6: Ferrocenyl containing NHCs: a. *N*-ferrocenyl-*N'*-methyl-benzimidazolium salt and corresponding metal carbene complexes,[26] b. N,N'-diferrocenylimidazolinium and c. imidazolium salts and corresponding metal carbene complexes.[27]

In 1999 Bildstein et al. synthesized the first benzimidazolium salts with a *N*-Fc-substituent **27** (Scheme 1.1.6 a.)[26] and later in the same year also some N,N'-diferrocenylimidazolinium salts **33** and N,N'-diferrocenylimidazolium salts **36** (Scheme 1.1.6 b-c.).[27] In none of the cases the corresponding carbenes (**28**, **34**, **37**) could be detected, but carbene complexes with silver (**38**), mercury (**30**), palladium (**29**) and tungsten carbonyl (**31**, **32**) could be isolated. For all carbenium salts the corresponding thioketone could be isolated in a reaction with methyl lithium and sulphur.[26,27]

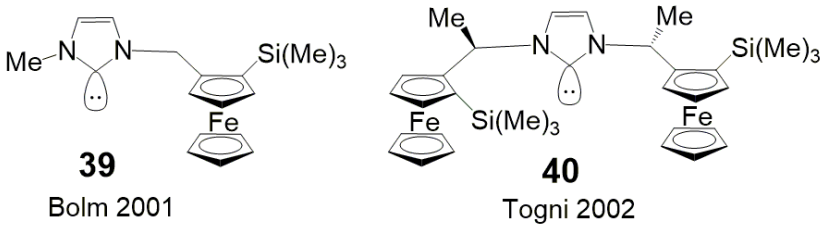

Scheme 1.1.7: Stable ferrocenyl containing *N*-heterocyclic carbenes.[28,29]

Bolm reported the first planar-chiral stable NHC enabled by the use of a ferrocenyl substituent **39**[28] and shortly after Togni et al. isolated a stable diferrocenyl substituted NHC also with β-ferrocenyl substituents and bulky trimethylsilyl groups on the cyclopentadienyl ring **40** (Scheme 1.1.7).[29]

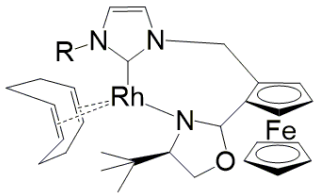

Scheme 1.1.8: Ferrocenyl containing NHC-complexes in catalysis.[30]

The chiral ferrocenyl substituted NHC-Rh-complex **41** by Bolm showed high catalytic activity in the hydrosilylation of acetophenone (Scheme 1.1.8).[30] A detailed review on all types of ferrocenyl and ruthenocenyl containing NHCs was published by Siemeling.[31] Bielawski et al. synthesized a wide range of redox-active N-heterocyclic carbenes containing one or two ferrocenyl moieties and investigated the TEP values of the corresponding metal complexes[32]

1.1.3 α,α-Diferrocenylcarbenes

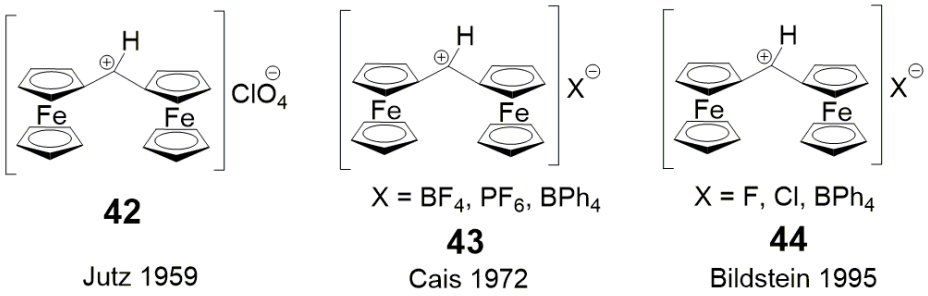

Scheme 1.1.9: Diferrocenylcarbeniumions with different counter ions.[33–36]

In 1959 the first diferrocenylcarbeniumion **42** was isolated by Jutz (Scheme 1.1.9).[33] Thirteen years later the structure and properties of this α,α-diferrocenylmethyliumion were investigated by Cais **43**[34] and also compared to other organometallic carbenium cations.[35] Bildstein et al. used this carbenium ions **44** to synthesize 1,1-diferrocenyl-n-alkanes in a reaction with carbanions.[36] All attempts to generate the diferrocenylmethylidene by deprotonation of the carbenium ion resulted in nucleophilic addition to $(Fc)_2CHR$.

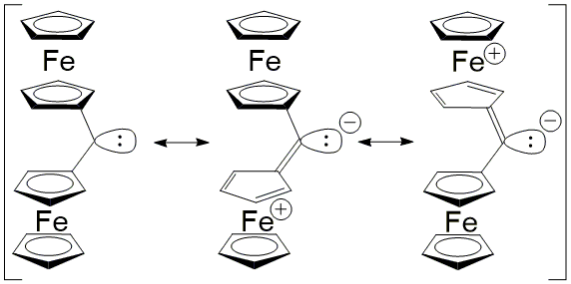

45

Scheme 1.1.10: Mesomeric structure of diferrocenylcarbene proposed by Bildstein.[37]

In a mini review Bildstein discussed four different routes that could lead to the isolation of diferrocenylcarbene **45** (Scheme 1.1.10), but none of them resulted in a successful isolation so far.[37] The four routes are as already discussed above in several examples: (i) homolytic cleavage of diazomethane by thermolysis or irradiation, (ii) Bamford-Stevens reaction of the tosyl hydrazone, (iii) thermolysis of telluroketone and (iv) deprotonation of carbenium salts. The cleavage of diferrocenyldiazomethane gave quantitative conversion to tetraferrocenylazine but no evidence for the carbene. Kay et al. isolated diferrocenylmethanobuckminsterfullerene ($C_{60}C(Fc)_2$) as the result of a Bamford-Stevens reaction of diferrocenyl tosyl hydrazone with sodium ethanolate in the presence of buckminsterfullerene.[38] Bildstein reported the selective formation of a tris addition product ($C_{60}[C(Fc)_2]_3$) under slightly different conditions.[37] Bis(ferrocenyl)telluroketone is one of the few room temperature stable telluroketones. Thermal decomposition should yield elemental tellurium and the carbene, but only tetraferrocenylethylene could be isolated[39]. Also trapping of the carbene with metal carbonyl complexes was not successful, which suggested a mechanism via a telluroketone [2+2] cyclodimer without any free intermediate diferrocenyl-methylidenes. Also, all attempts to synthesize the bulky bis(pentamethylferrocenyl)methylidene failed so far.

1.1.4 Ferrocenophanecarbenes

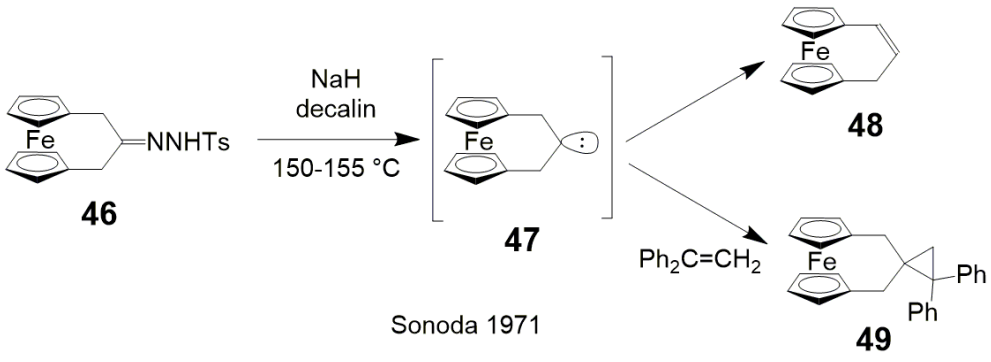

Scheme 1.1.11: Ferrocenophanecarbene as proposed intermediate.[40]

Already in 1971 the first [3]-ferrocenophanecarbene intermediate **47** was proposed by Sonoda (Scheme 1.1.11).[40] Following the well-known route via Bamford-Stevens reaction of [3]-ferrocenophan-2-one tosylhydrazone **46** as thermal, base assisted decomposition with in situ generation of the carbene. 1,2-dehydro-[3]-ferrocenophane **48** was isolated in 70 % yield as the

main product. With 1,1-diphenylethylene as carbene catcher the ferrocenyl spirane **49** could be isolated with 78 % yield. Performing the same decomposition reaction in 1-decene gave no addition of the carbene to the double bond and only 1,2-dehydro-[3]-ferrocenophane **48** as product. Both reactions give the hint for a triplet nature of the intermediate β-ferrocenylcarbene **47**. It must additionally be considered, that the hydrogen transfer reaction forming 1,2-dehydro-[3]-ferrocenophane most probably proceeds via singlet carbene stage and therefore a singlet-triplet equilibrium has to be considered.

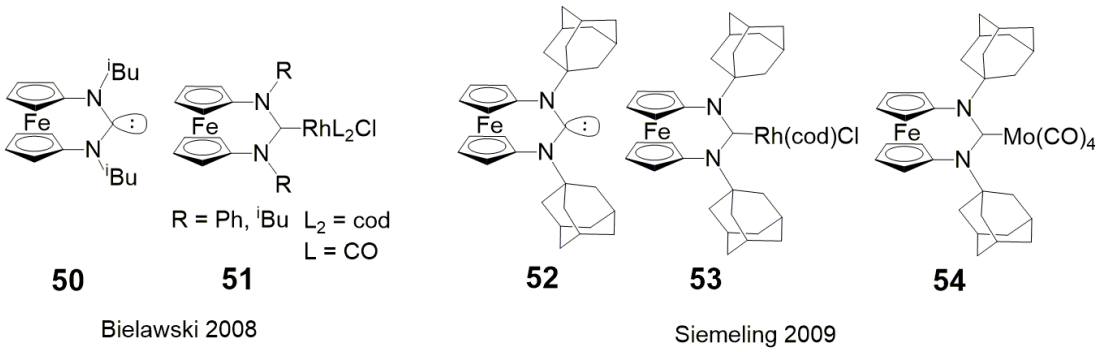

Scheme 1.1.12: Ferrocenophanecarbenes isolated by Bielawski[41] and Siemeling.[42,43]

In 2008 Bielawski discovered the first stable diaminocarbene[3]ferrocenophane (FcDAC) with *iso*-butyl substituents **50** and isolated the rhodium metal complexes with *iso*-butyl and phenyl substituents **51** (Scheme 1.1.12).[41] Shortly after Siemeling et al. synthesized another species of this new interesting compound class with 1-adamantyl substituents **52** and the corresponding rhodium and molybdenum complexes (**53**, **54**).[42,43] This type of redox switchable ligand with a wide N-C-N angle was already proposed in 1998 by Mirkin et al. as an enhancement of the widely used 1,1'-bis(diphenylphosphino)ferrocene ligand (dppf).[44] Also the alternatives with oxygen or sulphur as heteroatoms were discussed by Siemeling before.[45] Unsymmetrical NHC diaminocarbene[3]ferrocenophane with 1-neopentyl and 2-adamantyl substituents could be isolated, while the phenyl and 9-anthracenylmethyl derivates with 1-neopentyl could only be trapped as Rh complexes.[46] Benzyl substituted diaminocarbene[3]ferrocenophanes are also not stable for isolation and were trapped with elemental selenium as selenourea derivatives.[47] A quite interesting class of diaminocarbene[3]ferrocenophanes can be obtained by substitution on the cyclopentadienyl rings. 3,3'-Di-*tert*-butyl-*N,N'*-di-*iso*-pentyl-diaminocarbene[3]ferrocenophane is a stable planar-chiral carbene compared to the *tert*-butyl-free congener.[48]

1.2 Nonclassical Metal-Hydrogen Bonds

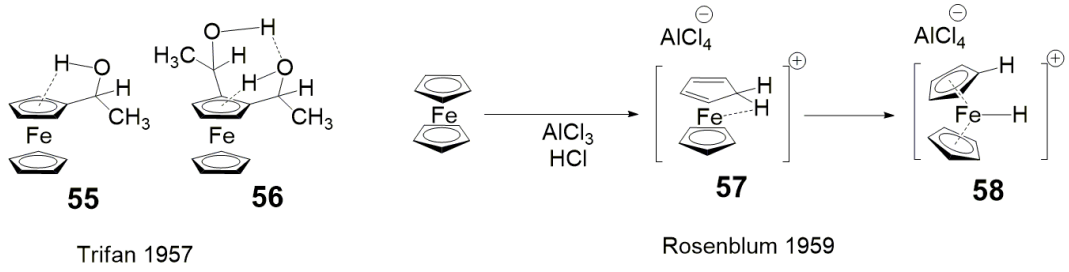

Scheme 1.2.1: First hydrogen-bonds observed in metallocene compounds[49] and protonation of ferrocene.[50–52]

Hydrogen bonds between hydrogen and oxygen, sulphur, nitrogen or fluorine are quite common, but also other hydrogen bonds are possible in metallocene compounds and other electron rich complexes. The first intramolecular hydrogen bond (IHB) to an aromatic ring was reported in 1957 by Trifan et al. in ferrocenylalcohols **55** and **56** (Scheme 1.2.1).[49] α-Hydroxyethylferrocene shows two different hydroxyl absorption bands in the infrared spectrum in CCl_4. The free hydroxyl vibration at 3617 cm^{-1} and another concentration-independent, but temperature-dependent band at 3574 cm^{-1} assigned to the ring-hydrogen bonded structure. In 1959 the first protonation of ferrocene has been reported (**57**, **58**).[50] The structure and mechanism were discussed for several years.[53] The high field NMR-absorption characteristic for a proton directly bonded to a metal atom and the magnetically equivalent cyclopentadienyl protons on both rings suggested structure **58**.[51] Detailed studies on the protonation mechanism were published by Mueller-Westerhoff et al. in 1994.[52] They could show, that the protonation of ferrocene begins with an exo attack followed by rapid equilibrium between ring and iron protonated species. Ruthenocene in contrast shows no ring protonation and only the ruthenium protonated species is present. Recent results from Seppelt et al. in 2017 confirmed structure **58** by low-temperature X-ray diffraction data of protonated ferrocene at 30 and 100 K.[54]

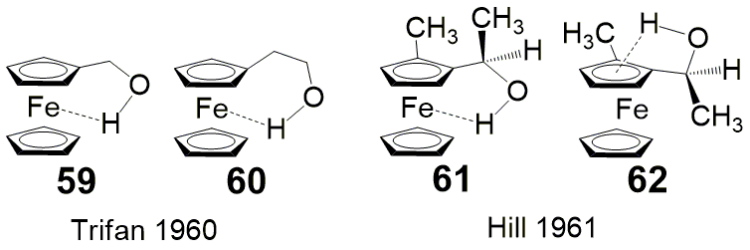

Scheme 1.2.2: Hydrogen-bonds to the iron centre in ferrocenyl compounds.[2,4]

Ferrocenyl alcohols **59**–**62** also show intramolecular hydrogen bonding to the iron centre (Scheme 1.2.2).[2,4] 2-Ferrocenylethanol **60** shows three different hydroxyl bands in the infrared spectrum at 3632, 3605 and 3533 cm^{-1} representing the free, π-bonded and Fe-bonded hydroxyl absorptions.[2] To quantify the strength of the hydrogen bond, $\Delta\nu$ the difference of the free hydroxyl absorption ν(free OH) and the hydroxyl absorption of the hydrogen bonded hydroxyl group ν(bonded OH) is used ($\Delta\nu$(OH) = ν(free OH) – ν(bonded OH)). The corresponding 2-ruthenocenylethanol shows a stronger IHB with $\Delta\nu$ of 171 cm^{-1} instead of 99 cm^{-1} for the ferrocenyl homologue. Methyl(2-methyl)-ferrocenyl)-carbinol shows two different isomers **61** and

62 (Scheme 1.2.2.). The *R*-isomer **61** shows stronger hydroxyl stretching absorption at 3580 cm^{-1} corresponding to the IHB to iron, while the *S*-isomer **62** has a stronger absorption at 3605 cm^{-1} assigned to the IHB to the π-system of the cyclopentadienyl ring.[4] By comparing the position of the OH band in the vibrational spectrum of different ferrocenyl alcohols with the free OH stretch the enthalpies for the IHB can be estimated.[55] The equation $-\Delta H = 75\ \Delta\nu\ /(\ \Delta\nu\ + 720)$; ΔH in kJ mol^{-1}; $\Delta\nu$(XH) = ν(free XH) – ν(bonded XH) in cm^{-1}; gives a good empirical correlation of the hydrogen bond enthalpy with the shift of the bonded XH-stretch compared to the free XH stretch.[56–60]

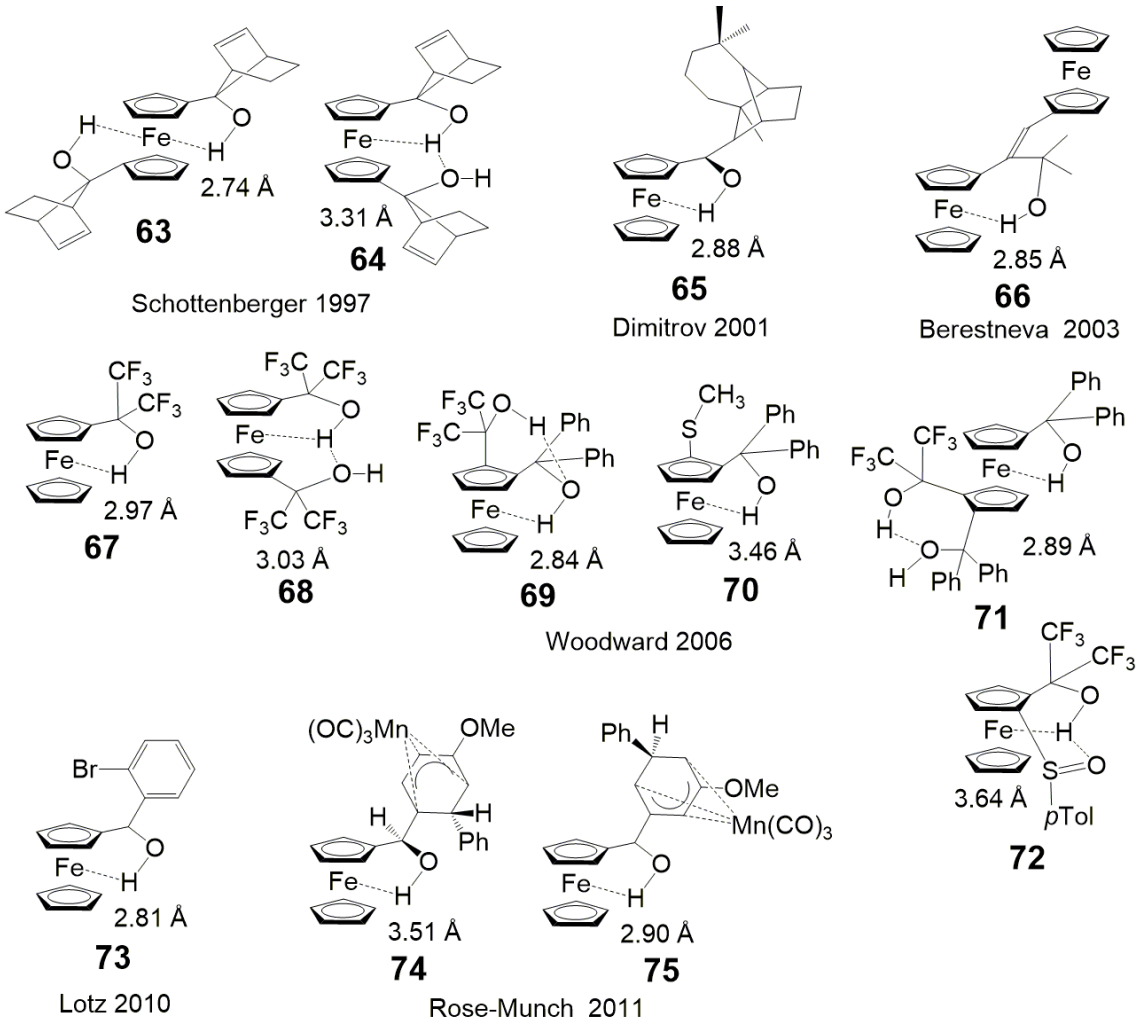

Scheme 1.2.3: More OH···Fe IHBs in ferrocenyl compounds.[61–66]

A search in the Cambridge Structural Database gives 13 structures with short OH···Fe distances **63–75** ranging from 2.74 Å in **63** to 3.64 Å **72** (H···Fe) and 3.35 Å in **63** to 4.01 Å in **72** (O···Fe), suggesting IHBs (Scheme 1.2.3).[61–66] The corresponding hydroxyl IR stretches are 3518 and 3464 cm^{-1} for **63** and 3524 and 3440 cm^{-1} for **64**.[61] The compounds **67**-**72** show several hydroxyl IR stretches for free hydroxyl groups, OH···O bonded and OH···Fe bonded hydroxyl groups: **67** (3102 cm^{-1}), **68** (3697 and 3484 cm^{-1}), **69** (3474 and 3234 cm^{-1}), **70** (3428 cm^{-1}), **71** (3598, 3480 and 3223 cm^{-1}), **72** (3252 cm^{-1}).[64] For the other structures no IR data is available. Although in the publications no IHB is discussed the IR stretches give a clear evidence for OH···O and OH···Fe

IHBs. Especially the compounds **67**-**72** described by Woodward[64] with two or three hydroxyl groups show the free OH-stretch, a OH···O IHB stretch and a OH···Fe IHB stretch.

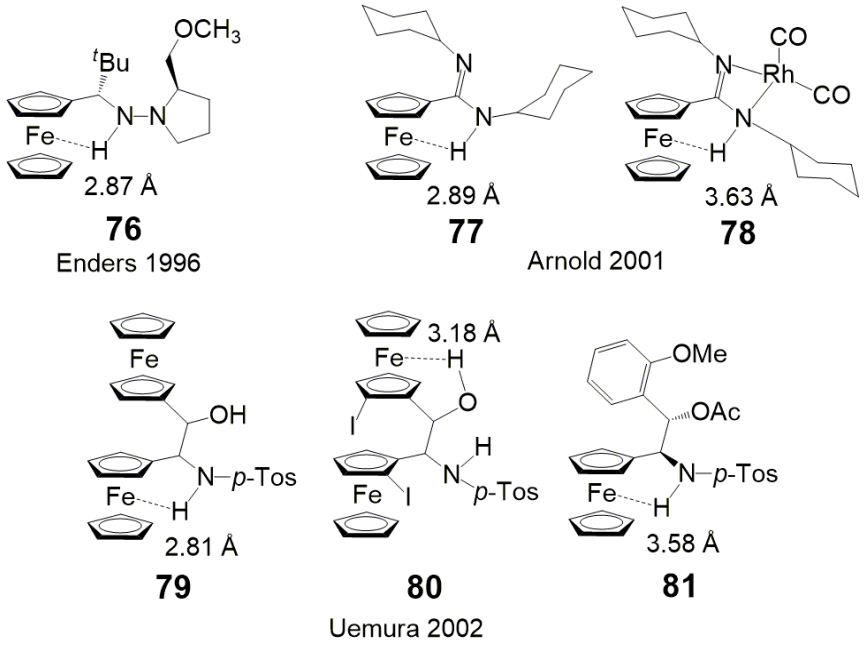

Scheme 1.2.4: NH···Fe IHBs in ferrocenyl compounds.[67–69]

Also, NH···Fe IHBs are present in the literature although the IHB was not discussed in the publications, the XRD suggest the IHB (Scheme 1.2.4). The reported N···Fe distances in the XRD data range between 3.40 Å for **77** and 3.83 Å for **78** and the corresponding NH···Fe distances range between 2.87 Å for **76** and 3.63 Å for **78**. The NH IR stretches are 3420 cm^{-1} for **77**, 3208 cm^{-1} for **78**[68] and 3250 cm^{-1} for **81**,[69] respectively. For all other compounds no IR data is available. The compound **80** shows no evidence for a NH···Fe IHB but instead hints for a OH···Fe IHB with a O···Fe distance of 3.60 Å and a OH···Fe distance of 3.18 Å. More inter- and intramolecular XH···M hydrogen bonds in organometallic compounds in general in a wide variety have been discussed since 1994 in the literature.[59,70–77]

1.3 Ferrocenyl Fischer Carbene Complexes

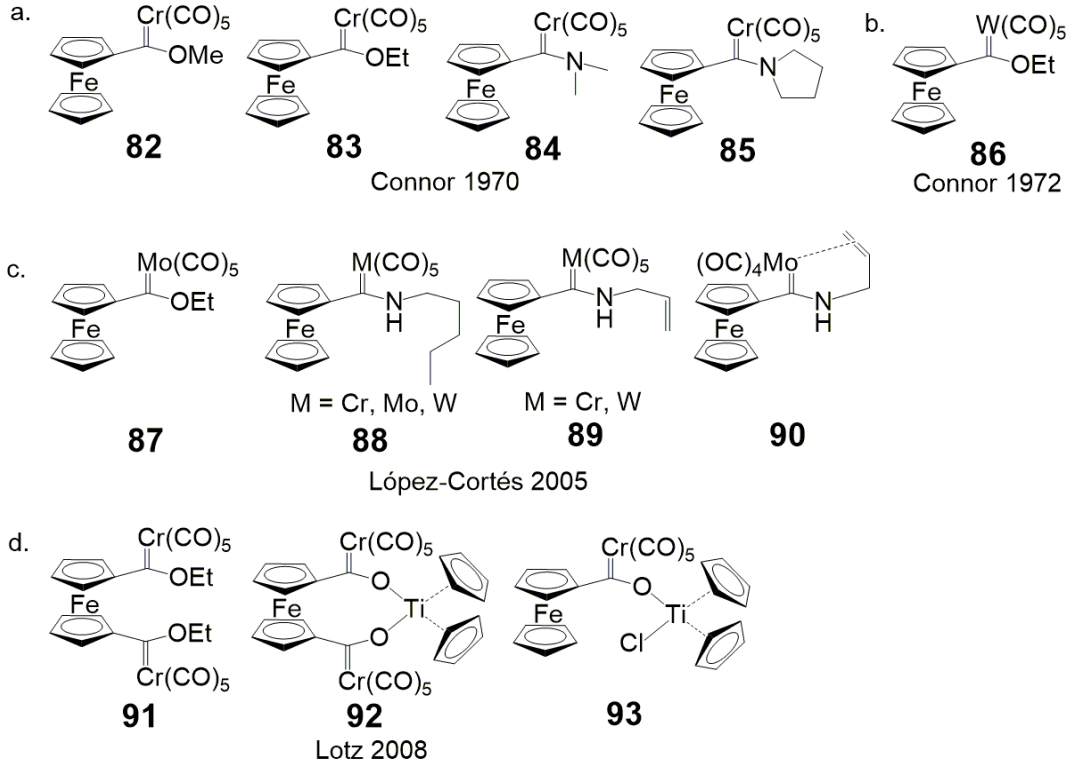

Scheme 1.3.1: Group VI ferrocenyl Fischer carbene complexes, a. with chromium[78,79], b. with tungsten[80,81], c. with molybdenum[82], d. biscarbenes and titanocene derivates.[83]

After the discovery of Fischer carbene complexes in 1964[84] the first ferrocenyl Fischer carbene complexes **82**–**85** have been reported by Connor et al. in 1970 (Scheme 1.3.1 a.)[78] and in the same year also by Fischer et al..[79] The heavier tungsten homologue **86** followed soon after (Scheme 1.3.1 b.).[80,81] Only the molybdenum homologue **87** was not synthesized until 2005 (Scheme 1.3.1 c.).[82] In general the yield for molybdenum carbene complexes is far lower than for their chromium and tungsten counter parts. López-Cortés et al. also synthesized the (ferrocenyl) (alkyl/allyl amino) carbene complexes **88**–**90** of all three group VI transition metals and observed coordination of the allyl group to molybdenum tetracarbonyl in **90**. Lotz et al. created the quite interesting bisethoxy ferrocenyl-1,1'-diyl bridged biscarbene complex **91** and the cyclic bisoxy titanocene bridged derivative **92** (Scheme 1.3.1 d.).[83] Also the mono carbene with oxy titanocene chloride substituent was isolated **93**. Similar tungsten compounds were synthesized by Bezuidenhout in 2011.[85]

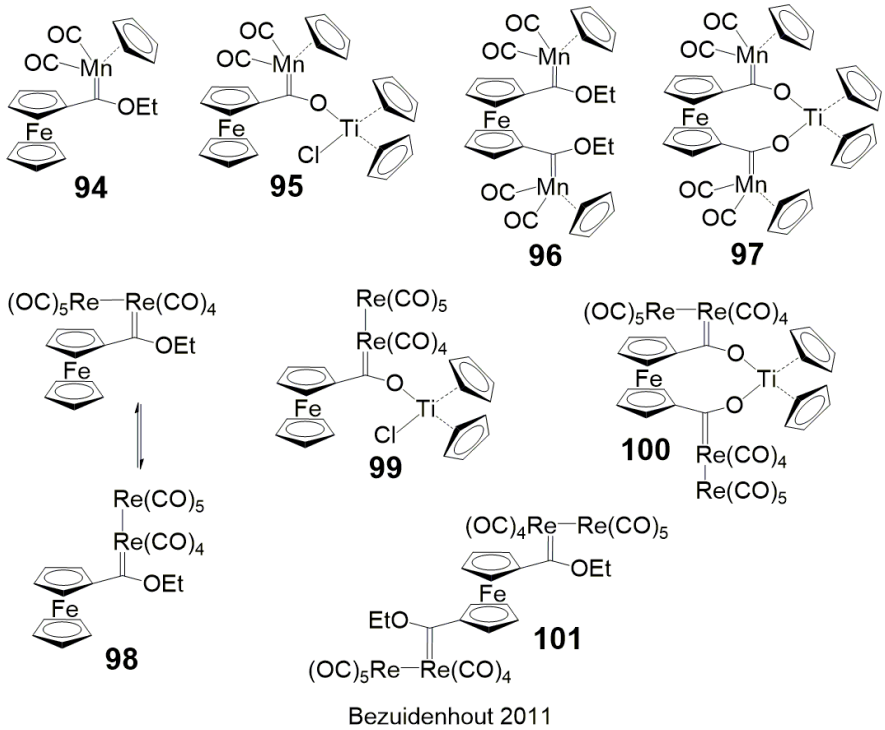

Scheme 1.3.2: Group VII ferrocenyl Fischer carbene complexes.[86]

The corresponding group VII transition metal carbene complexes **94**–**97** with $MnCp(CO)_3$-groups and **98**–**101** with $Re_2(CO)_9$-groups were reported by the same group shortly after (Scheme 1.3.2).[86] For the mono carbene ethoxy rhenium complex **98** the axial as well as the equatorial isomer are present. In the oxy titanocene chloride complex **99** the $Re_2(CO)_9$ group is axial. For the bisoxy titanocene bridged species **100** one $Re_2(CO)_9$ moiety is axial and the other is equatorial. The bisethoxy ferrocenyl-1,1'-diyl bridged biscarbene **101** shows both $Re_2(CO)_9$ groups in equatorial conformation. A review about multicarbene and multimetal Fischer carbene complexes was published by Bezuidenhout in 2012 which also shows a variety of ferrocenyl Fischer carbene complexes.[87]

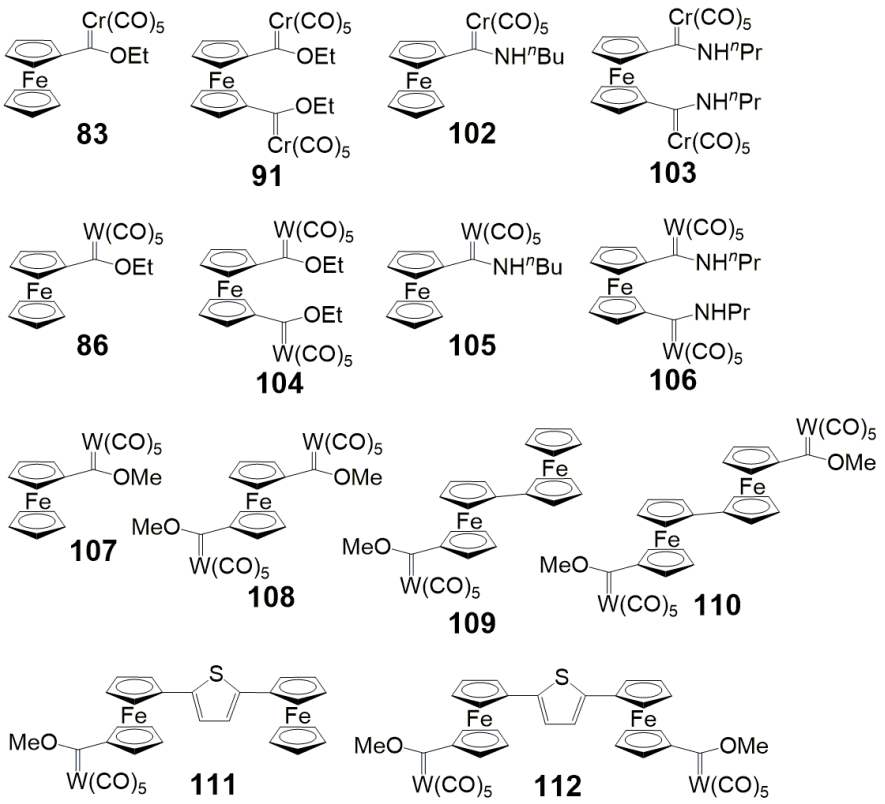

Scheme 1.3.3: Ferrocenyl Fischer carbene complexes investigated by cyclic voltammetry: 83, 91[88,89], 102, 103[90], 86, 104–106[91], 107–110[92], 111, 112[93].

The electrochemistry of ferrocenyl Fischer carbene complexes is quite interesting (Scheme 1.3.3). The ethoxy ferrocenyl carbene **83** and bisethoxy ferrocenyl-1,1'-diyl bridged biscarbene **91** of chromium pentacarbonyl show a reversible first oxidation at 289 and 499 mV, respectively (vs. FcH/FcH^+ in CH_2Cl_2 with $[N(^nBu)_4][PF_6]$ as supporting electrolyte).[88,89] This first oxidation was assigned to the chromium centre by comparison of cyclic voltammograms with other ferrocene free Fischer carbene complexes and by DFT-calculations. No spectroscopic prove for the localization of the oxidation was given. For the biscarbene complex **91** a second reversible oxidation is observed at 650 mV. This was assigned to the second chromium centre by the criteria mentioned above. Both carbene complexes **83** and **91** show a reversible oxidation after all at 700 and 730 mV, respectively. This oxidation was assigned to the ferrocenyl substituents. Further irreversible oxidation was observed at potentials over 950 mV for some of the corresponding heteroarene carbene complexes with furanyl and thienyl groups instead of the ferrocenyl group. This irreversible oxidation was assigned to $Cr^I \rightarrow Cr^{II}$. For the ferrocenyl Fischer carbene complexes **83** and **91** this oxidation lies outside of the solvent window. Reversible reduction of the carbene double bond in the ferrocenyl Fischer carbenes **83** and **91** was observed at –2.15 and –1.85 mV. The corresponding ethoxy tungsten carbene complex **86**, biscarbene **104** and alkylamino derivates **105** and **106** show a different behaviour.[91] First a reversible oxidation of the ferrocenyl group is observed at 285, 510, 206 and 540 mV. Assignment was done by IR spectroscopy of the mono oxidized species. The shift of the carbonyl stretching frequencies was only around 20 cm^{-1} and for oxidation on the tungsten centre a shift of more than 100 cm^{-1} would be expected. No EPR measurements to further confirm or disprove this assumption were performed. Depending on the supporting electrolyte an irreversible $W^0 \rightarrow W^{II}$ or $W^0 \rightarrow W^{III}$ oxidation is observed after the first

oxidation on the ferrocenyl moiety. The potentials for these oxidations are 809, 766, 611 and 591 mV for $W^0 \rightarrow W^{III}$ with $[N(^nBu)_4][PF_6]$ as supporting electrolyte and 1105, 922, 950 and 792 cm^{-1} $W^0 \rightarrow W^{II}$ with $[N(^nBu)_4][B(C_6F_5)_4]$ as supporting electrolyte, respectively. DFT calculations on the trication $[(CO)_5W^{II}=C(OEt)(Fc^+)]^{3+}$ **86^{3+}** show a W···H bond of 2.09 Å to the methylene group for stabilization. Similar structure with a Cr···H bond to the methylene group has already been calculated for $[(CO)_5Cr^{II}=C(OEt)(Th)]^{2+}$ and $[(CO)_5Cr^{II}=C(OEt)(th)(OEt)C=Cr^{II}(CO)_5]^{4+}$.[89] The structure of the tetracation **86^{4+}** $(CO)_5W^{III}=C(OEt)(Fc^+)$ could not be located on the potential energy surface. The electrochemical properties of the alkyl amino carbene species of chromium Fischer carbene $(CO)_5Cr=C(NH^nBu)Fc$ **102** and $(CO)_5Cr=C(NH^nPr)fc(NH^nPr)C=Cr(CO)_5$ **103** were elucidated.[90] They show reversible one electron oxidation on the chromium at 196 and 341 mV, respectively. The bis carbene **103** shows oxidation of the second chromium centre at 446 mV. The iron centres are oxidized at 539 and 700 mV, respectively. For **103** an irreversible $Cr^I \rightarrow Cr^{II}$ oxidation is observed at 977 mV. To study the interaction with more metal centres the biferrocenyl derivates $(CO)_5W=C(OMe)(fc)(Fc)$ **109** and $(CO)_5W=C(OMe)(fc)(fc)(OMe)C=W(CO)_5$ **110** were investigated and compared to **107** $(CO)_5W=C(OMe)(Fc)$ and **108** $(CO)_5W=C(OMe)(fc)(OMe)C=W(CO)_5$.[92] Two reversible oxidations on the iron centres are found at –14, 637 and 226, 715 mV, respectively. The mono cations show IVCT bands and are categorized as weakly coupled class II systems according to Robin Day.[94] The corresponding thienyl bridged biferrocenes $(CO)_5W=C(OMe)(fc)(th)(Fc)$ **111** and $(CO)_5W=C(OMe)(fc)(th)(fc)(OMe)C=W(CO)_5$ **112** show a quasi-reversible reduction of the carbene bond at –2095 and –2095 mV with $[N(^nBu)_4][B(C_6F_5)_4]$ as supporting electrolyte, two reversible oxidations of the ferrocene centres at 10 and 420 mV for the monocarbene **111** and at 230 and 475 mV for the biscarbene **112**.[93] The irreversible $W^0 \rightarrow W^{II}$ oxidation takes place at 1135 mV for both compounds **111** and **112**. The group VII transition metal Fischer carbene complexes $Cp(CO)_2Mn=C(OEt)Fc$ **94** and $Cp(CO)_2Mn=C(OEt)fc(OEt)C=Mn(CO)_2Cp$ **96** show reversible oxidation of the manganese centres before the ferrocenyl groups.[95] The manganese centre of the carbene complex is oxidized at –106 mV and the two manganese centres in the biscarbene complex at –74 and 55 mV. The ferrocenyl centres are oxidized at 442 and 714 mV, respectively. For $[Cp(CO)_2Mn=C(OEt)Fc][PF_6]$ **$[94][PF_6]$** the EPR spectrum shows a rhombic *g* tensor and ^{55}Mn hyperfine coupling.

1.3.1 Evaluation the electronic parameters of carbene ligands.

The electronic parameters of different ligands can be evaluated by measuring the CO stretching frequencies of their carbonyl complexes. In 1967 Strohmeier[96] and Bigorgne[97] used the CO stretching frequencies of $CpMn(CO)_2L$, $CpV(CO)_2L$, $Fe(CO)_4L$ and $Ni(CO)_3L$ to determine the π-acceptor strength and σ-donor capability of wide variety phosphine ligands giving the following series of increasing π-acceptor strength: $PR_3 < PPh_3 < PClPh_2 < PCl_2Ph < PCl_3 < PF_3$.[98] Ten years later, in 1977 Tolman introduced the Tolman electronic parameter (TEP) using the A_1 CO mode of $Ni(CO)_3L$ in CH_2Cl_2 as a ubiquitous standard for the π-acceptor strength of different ligands. This method has been also applied to $Ni(CO)_3NHC$ complexes[99], but due to the acute toxicity and stability problems of the nickel complexes better references were examined. The iridium $[(NHC)Ir(CO)_2Cl]$[100] and rhodium $[(NHC)Rh(CO)_2Cl]$[101–103] complexes are suitable alternatives for the nickel complexes. They can be easily synthesized by transmetalation of carbene complexes with $[Ir(cod)Cl]_2$ and $[Rh(cod)Cl]_2$[104] and subsequent carbonylation. Nolan et al. developed an equation (Eq.1) to convert the Ir-CO stretches into the TEP value.[100] The same was done by Glorius et al. for the corresponding Rh-CO stretches (Eq.2).[103]

$$TEP\ (cm^{-1}) = 0.8475 \cdot \nu_{CO}^{av/Ir} + 336\ cm^{-1} \quad \text{(Eq.1)}$$

$$TEP\ (cm^{-1}) = 0.8001 \cdot \nu_{CO}^{av/Rh} + 420\ cm^{-1} \quad \text{(Eq.2)}$$

This concept was also applied to ferrocenyl carbene ligands by Bezuidenhout et al. in 2015 (Scheme 1.3.4).[105] They measured the TEPs for $Cl(CO)_2Rh{=}C(OEt)Fc$ **114** and $Cl(CO)_2Rh{=}C(NH^nPr)Fc$ **117** with 2054 and 2049 cm^{-1}. These values lie between the classical phosphine ligands with TEPs between 2060 and 2069 cm^{-1} and NHC ligands with TEPs between 2049 and 2055 cm^{-1} (Scheme 1.3.5). Also the complexes $Cl(CO)LRh{=}C(OEt)Fc$ (L=PPh_3, PCy_3, $P(OPh)_3$, $AsPh_3$) **115** were synthesized. All eight Rh complexes **113**–**117** were used as catalyst precursors for the hydroformylation of 1-octene. The results were comparable to rhodium NHC complexes, regarding the conversion, TOFs, chemo- and regioselectivity toward the linear aldehyde.

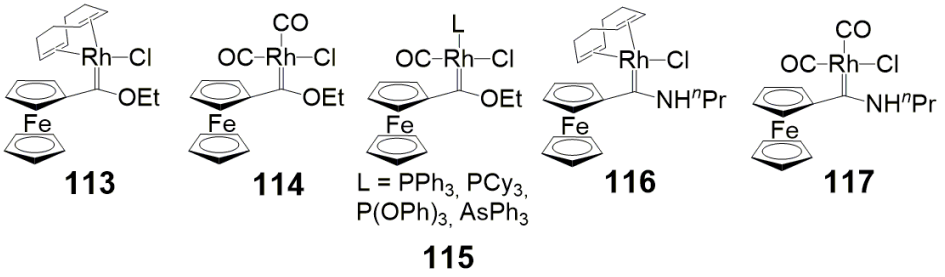

Scheme 1.3.4: Rh complexes of ferrocenyl carbene ligands.[105]

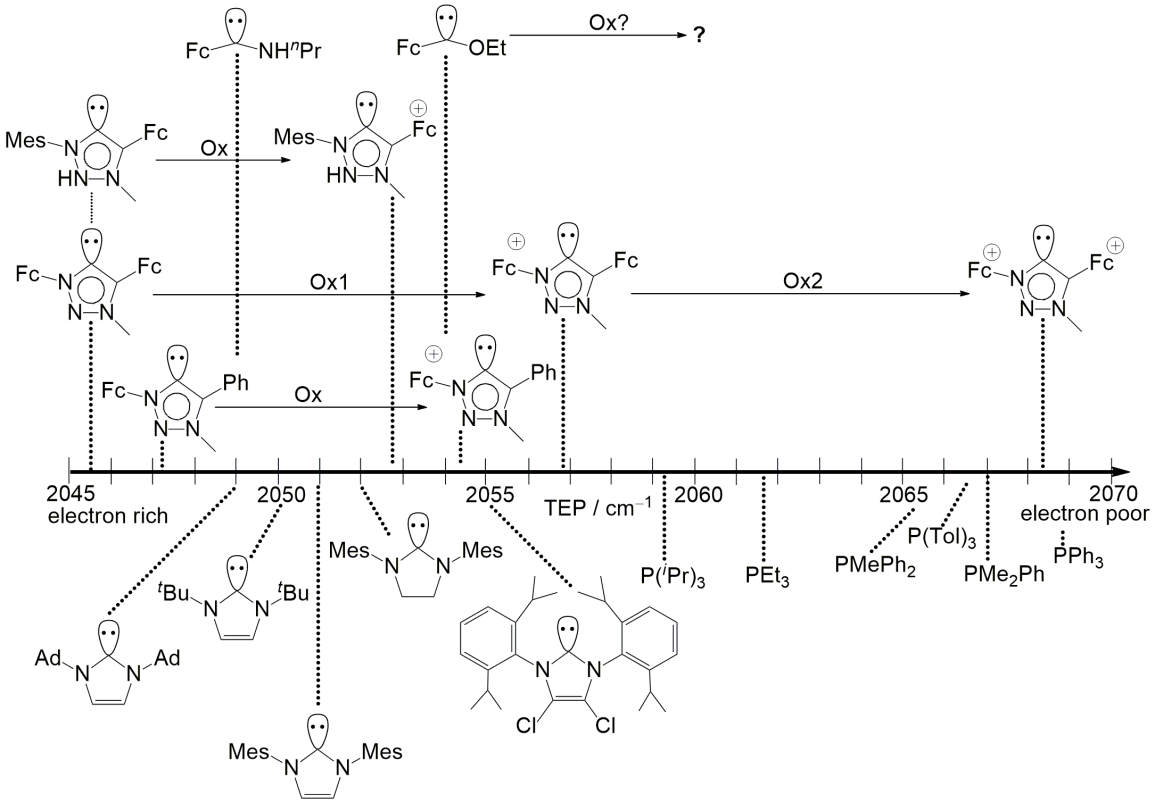

Scheme 1.3.5: TEP of ferrocenyl carbene ligands[105–107], NHCs[100,108] and phosphines[100,108].

Also the ^{13}C-NMR resonance of the carbene carbon of NHCs can be used to classify the electronic structure of carbene ligands.[109] Most imidazole-2-ylidenes show a ^{13}C resonance between 210 and 220 ppm. Whereas saturated imidazoline-2-ylidenes and acyclic diamino carbenes have a lower population of the carbene p_π-orbital and therefore show a higher anisotropy at the carbene carbon centre which results in downfield shifting of the resonances to 236–260 ppm.

Another technique to measure the π-accepting properties and σ-donor ability of carbene ligands is the synthesis of carbene-phosphinidene adducts and measurement of ^{31}P NMR resonances of the (carbene)=P-Ph adducts.[110] The phosphinidene adducts are formed by reaction of the free carbenes with pentaphenylcyclopentaphosphane or dichlorophenylphosphane with subsequent treatment with KC_8 or magnesium. The ^{31}P-NMR resonances range from –61.2 up to 126.3 ppm and are in correlation with the trend observed with the TEP or the ^{13}C resonances. High-field ^{31}P chemical shifts correspond to phosphorous atoms with a high electron density and therefore a carbene with a high σ-donor ability and low π-acceptor properties and vice versa for the low field ^{31}P chemical shifts. Also ^{77}Se-NMR can be used to investigate the properties of carbene ligands.[47,111–114] The high range between around –20 ppm for low carbene-π-acidity and roughly 900 ppm for high carbene-π-acidity gives a good scale to differentiate the compounds. It is important to highlight the non-linear behaviour of ^{77}Se-NMR for this method.

1.4 Gold Carbene Complexes

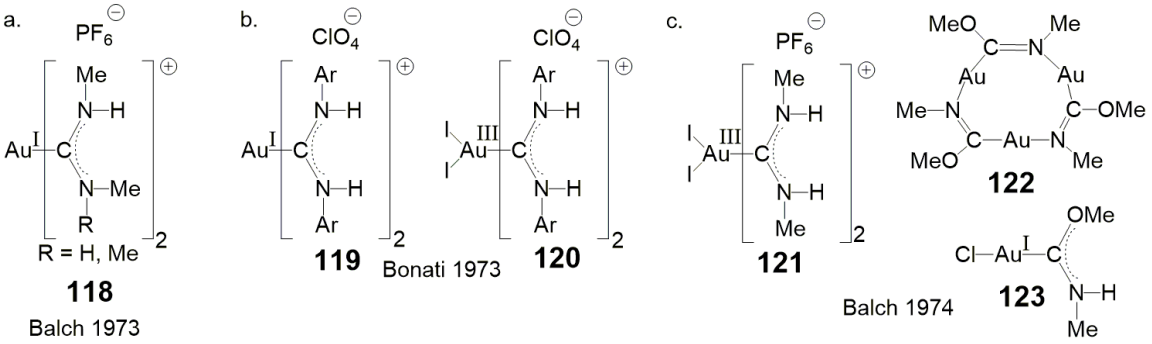

Scheme 1.4.1: Gold carbene complexes: a. Balch 1973[115], b. Bonati 1973[116], c. Balch 1974[117].

Already in 1973 gold carbene complexes **118** $[Au^{I}\{C(NHMe)NMeR\}_2][PF_6]$ (R = H, Me) were reported as intermediates in the α-addition of amines to isocyanides with tetrachloridoaurate(III) (Scheme 1.4.1 a.).[115] The gold carbene complexes react to formamidines under a variety of conditions and with quantitative yields. Bonati et al. observed square planar gold(III)-biscarbenes with two halides $[Au^{III}\{C(NHAr)_2\}_2I_2][ClO_4]$ **120** which are isoelectronic to platinum(II) complexes (Scheme 1.4.1 b.).[116] Balch et al. isolated similar gold(III)-biscarbenes $[Au^{III}\{C(NHMe)_2\}_2I_2][PF_6]$ **121**and also a trimeric cycle $[Au^{I}C(OMe)NMe]_3$ **122** which forms three equivalents of $[ClAu^{I}C(OMe)NHMe]$ **123** after treatment with hydrochloric acid (Scheme 1.4.1 c.).[117]

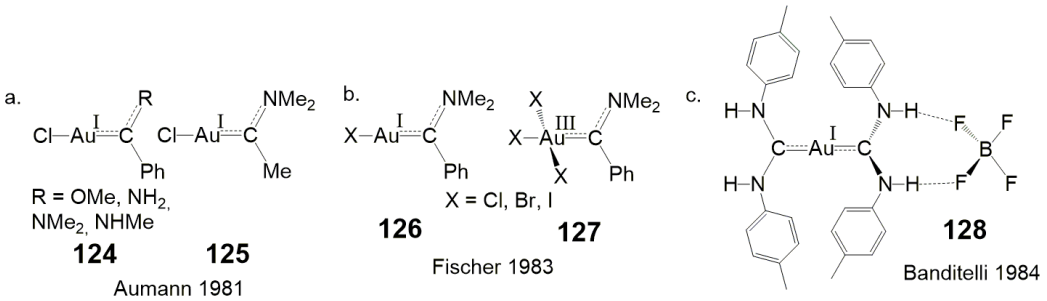

Scheme 1.4.2: Gold carbene complexes synthesized via transmetalation from Fischer carbene complexes: a. 124, 125[118], b. 126, 127[119,120], c. 128.[121]

Gold(I) carbene complexes **124** and **125** are accessible via carbene transfer reaction from tungsten Fischer carbene complexes with tetrachloridoaurate (Scheme 1.4.2 a.).[118] Phenyl and methyl carbenes with alkoxy and amino substituents are possible $[ClAu^{I}C(XR)R']$, XR = OMe, NH_2, NMe_2, NHMe, R' = Ph, Me. Replication of the carbene transfer with tungsten, chromium and molybdenum Fischer carbene complexes with tetrachloridoaurate gave the product $[ClAu^{I}C(NMe_2)Ph]$ **126** but also the gold(III) carbene complex $[Cl_3Au^{III}C(NMe_2)Ph]$ **127** could be isolated (Scheme 1.4.2 b.).[119,120] The corresponding bromide complexes $[BrAu^{I}C(NMe_2)Ph]$ and $[Br_3Au^{III}C(NMe_2)Ph]$ could be isolated by carbene transfer with tetrabromidoaurate from Fischer carbene complexes, but also by halide exchange from the chloride complexes with boron tribromide. The iodide complexes are not accessible by transmetalation with tetraiodidoaurate and could only be obtained by halogen exchange of the bromide complexes with boron triiodide. The biscarbene gold complex *trans*,*trans*-$[\{(p\text{-tolNH})_2C\}_2Au][BF_4]$ **128** (Scheme 1.4.2 c.) shows a quite interesting structure.[121] Both NH hydrogens point away from the gold atom. The *cis*,trans-

and the *cis,cis*-isomers are not observed. The two carbene ligands are colinear with 177.4° C-Au-C angle. The single crystal XRD structure also shows two NH···F hydrogen bonds to the BF_4 anion. The two carbene ligands show a dihedral angle of 68.1° to each other.

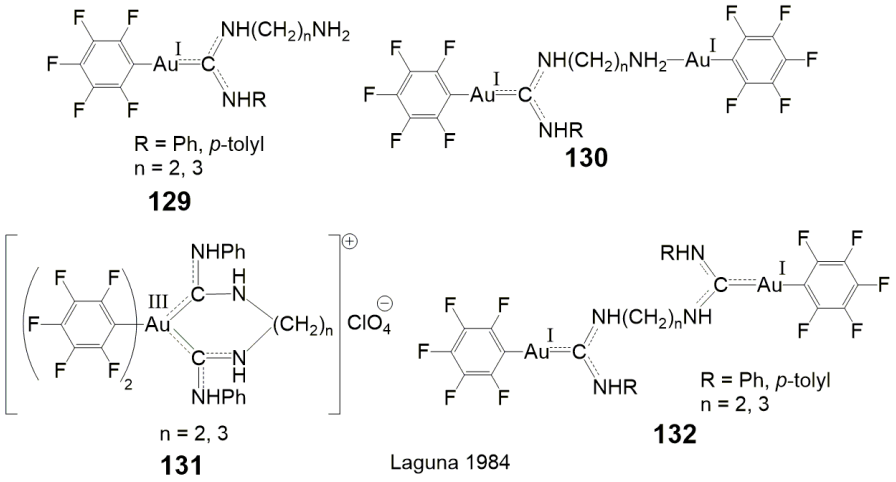

Scheme 1.4.3:Binuclear gold carbene complexes 129–132.[122]

Laguna et al. described some binuclear gold complexes **129**–**132** with diamine groups as bridging ligands that can be isolated as air and moisture stable solids (Scheme 1.4.3).[122] The reactions to synthesize the binuclear gold complexes are quite slow with reaction times between 3 and 30 days until full conversion.

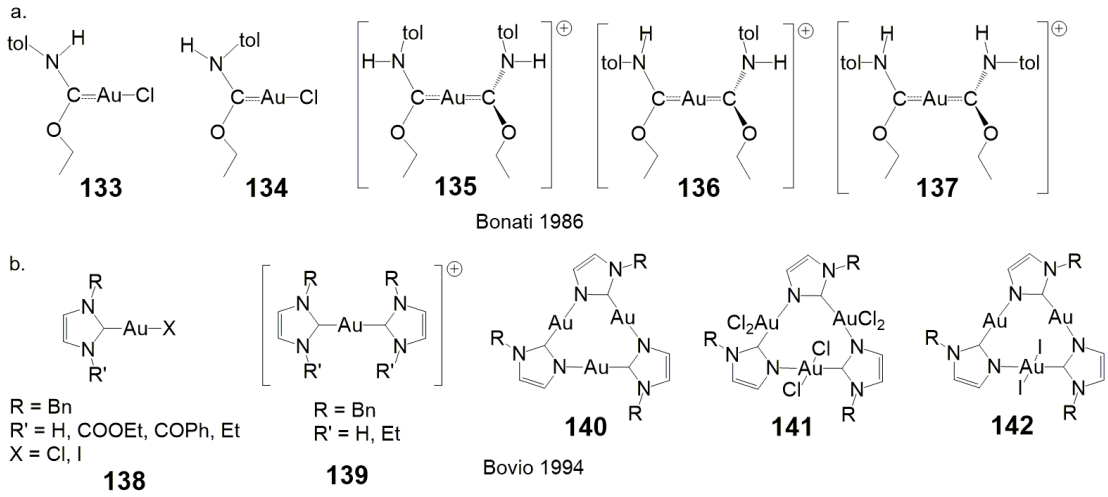

Scheme 1.4.4: Examples for mono- and trinuclear gold carbene complexes investigated by ^{197}Au Mössbauer spectroscopy, a. *cis/trans* isomers of aminocarbene gold complexes[123], b. NHC Au^{I} and Au^{III} gold complexes.[124]

A great method to investigate the properties of gold carbene complexes is ^{197}Au Mössbauer spectroscopy. Differentiation between Au^{I} and Au^{III} can be achieved quite easily. Linear correlation between quadrupole splitting QS and isomer shift IS of several mono- and trinuclear gold complexes **133**–**142** (Scheme 1.4.4) give an equation for Au^{I} (Eq.3) and another for Au^{III} (Eq.4).[123–125]

Au(I): QS = 1.34 IS + 4.36 (Eq.3)

Au(III): QS = 1.59 IS – 0.21 (Eq.4)

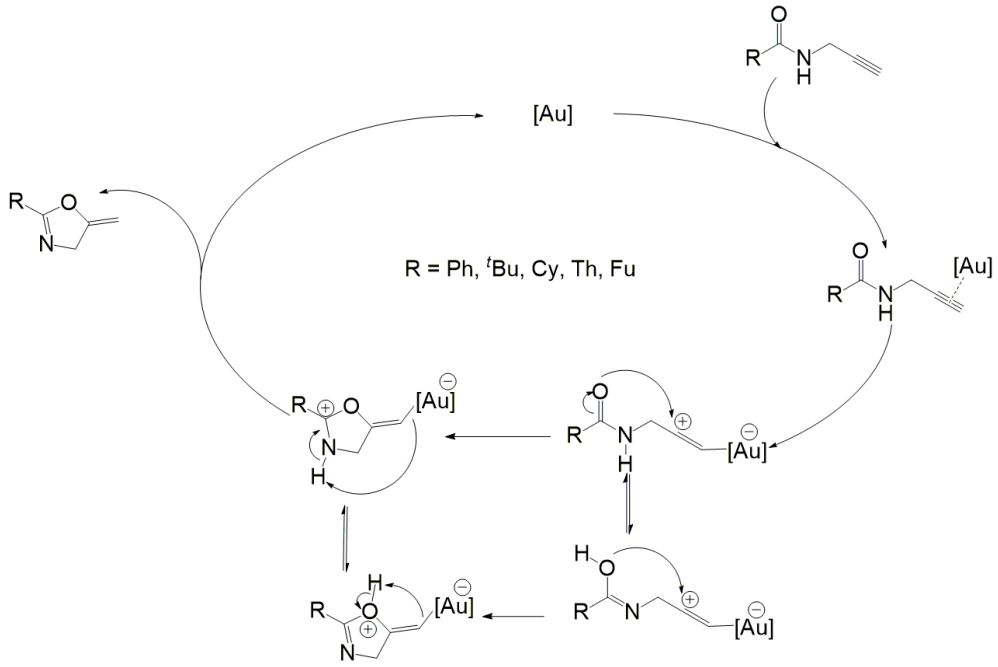

Scheme 1.4.5: Gold complexes in catalysis of the cycloisomerization of propargyl amides to oxazolines.[126]

Gold complexes can be used in catalysis of a variety of reactions that origin in the activation of carbon-carbon π-bonds e.g. the cycloisomerization of propargyl amides to oxazolines (Scheme 1.4.5). Because of the mild reaction conditions, it is often used in total synthesis on one of the last steps. For many years phosphane ligands have been used for this reactions,[126,127] but carbene ligands have gotten more and more interest in the last years.[128,129] The reaction mechanism of gold catalysis has been investigated in detail. The most important step is the η^2-coordination of the carbon-carbon π-bond on the gold centre, showing a significant lengthening of the π-bond and change in configuration of the carbon atoms.[130] The π-complexes of Au are quite similar to π-complexes of Pd, Pt and Ag but relativistic effects lead to better reactivity caused by a lower coordination number and different oxidation states.

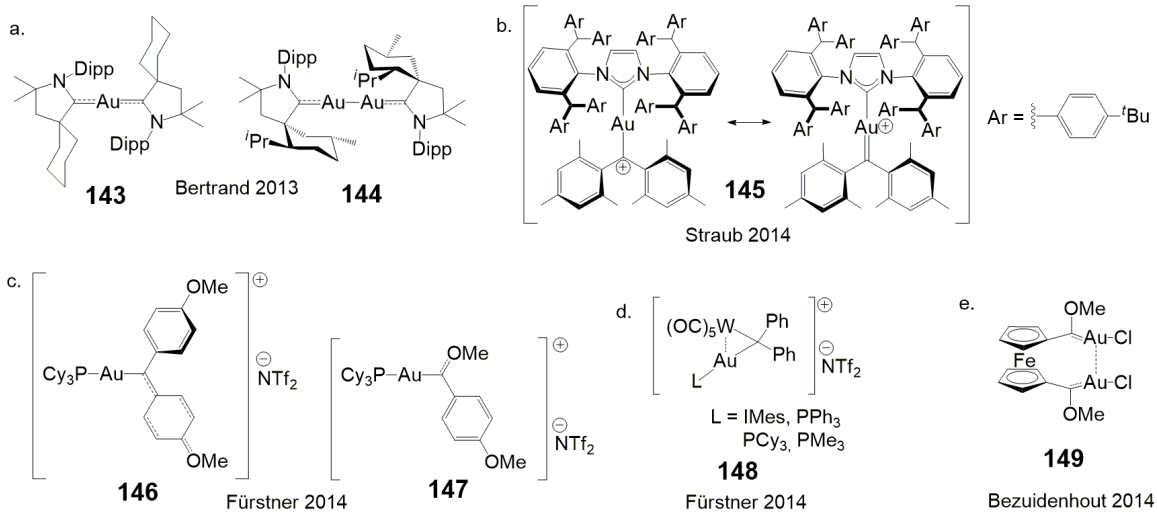

Scheme 1.4.6: a. Neutral mono- and dinuclear gold complexes[131], b. non-heteroatom-stabilized gold-carbene complex[132], c. gold carbenoid complex and gold Fischer carbene complex[133], d. hetero-bimetallic tungsten gold complex[134], e. gold Fischer carbene complex with aurophilic interaction.[135]

A lot of Au^{I} and Au^{III} carbene complexes have been reported but Au^{0} and Au^{II} carbene complexes were unknown so far. Bertrand et al. isolated neutral mono- and dinuclear gold(0) carbene complexes **143** and **144** (Scheme 1.4.6 a.).[131] They used cyclic (alkyl)(amino)carbene ligands with good π-electron accepting properties, which is necessary to form strong bonds to gold and to stabilize the paramagnetic gold(0) centre. EPR spectra and DFT calculations of the mononuclear complex **143** showed the location of the spin density mainly on the carbene carbons and the nitrogen atoms giving only a weak Au^{0} character. The dinuclear complex **144** shows a quite short Au-Au distance of 2.552 Å. The Au-C distance of 1.991 Å in the mononuclear complex **143** is shorter than in the dinuclear complex **144** with 2.082 and 2.088 Å, respectively, which origins in the different binding modes: electronic ^{2}S ($d^{10}s^{1}p^{0}$, J=1/2) ground state for **143** vs. ^{2}P ($d^{10}s^{0}p^{1}$, J=1/2) excited state for **144**.

Typically, gold carbene complexes are stabilized by a hetero atom like a halide in the coordination sphere. Straub et al. reported gold carbene complex **145** without a hetero atom stabilization using the bulky octa-*tert*-butyl IPr** imino ylide ligand (IPr** = 1,3-bis{2,6-bis[bis(4-*tert*-butylphenyl)methyl]-4-methylphenyl}-2,3-dihydro-1*H*-imidazol-2-ylidene) (Scheme 1.4.6 b.).[132] Three different bond orders are possible for gold carbene complexes: “carbene” character with Au=C bond order of two, “carbenium” character with Au-C bond order of one and also a “carbenoid” character with formal gold-carbon bond order of zero. Depending on the electronic structure one of them is preferred. In general, strong metal carbene bonds lead to metathesis reactions with alkenes, whereas weak metal-carbene bonds allow cyclopropanations of alkenes. In this case the bond order assigned by UV/Vis data is somewhere between one and zero. In literature the definition of gold carbene and carbenoid is discussed in detail.[136] Another representative of gold carbenoid complexes was synthesized by Fürstner et al. with a bis-*p*-anisyl carbene ligand **146**.[133] This complex catalyses the cyclopropanation of *p*-methoxystyrene to 1,1,2-tri-*p*-anisyl-cyclopropane. The gold carbene length in the solid state is 2.039 Å and therefore the same as in the corresponding gold Fischer carbene complex with the *p*-anisyl methoxy carbene

ligand **147**. Calculations with Kohn-Sham DFT and the intrinsic bond orbital (IBO) approach show the importance of π-stabilizing effects of the organic substituents at the carbene carbon atom, which are compensating the low π-backbonding from the gold atom.[137] The IBOs of the π-systems of the two aromatic rings and the carbene σ lone pair are mainly located at the carbene carbon atom. Transmetalation approaches with diphenylcarbene tungsten pentacarbonyl yielded hetero-bimetallic gold tungsten complexes **148**.[134] Transmetalation of ferrocene-1,1'-diyl biscarbene gave interesting complex **149** with aurophilic interaction between the two gold centres.[135] With an Au···Au distance of 3.035 Å in the single crystal XRD structure the interaction is stronger than in other gold carbene complexes without a ferrocenophane bridge that show Au···Au distances between 3.093 and 3.307 Å. Gold carbene complexes are also accessible by transmetalation from dirhodium carbene complexes, which can be synthesized from diazomethanes.[138] Beside catalysis, ferrocene containing gold carbene complexes of the type $[Au(NHC\text{-}(CH_2Fc)_x)_2]^+$ (x = 1-4) can also be used as anticancer agents by regulating the formation of reactive oxygen species (ROS) in cell studies.[139] Usually, silver salts are used to abstract the halide in gold(I) carbene complexes to generate the active species for catalysis, but also MeOTf or simple potassium salts can be used instead, although the catalytic activity of the silver activated species is much higher.[140] As already described in chapter 1.3.1 for NHCs in general, ^{13}C NMR spectroscopy can give a good measure for σ donation in gold(I) carbene complexes.[141] The counter ion influence in gold catalysis is some times more important, than the ligand effect. In a detailed study a variety of different counter ions are compared.[142] Sterically demanding but counter ions like $(BAr^F{}_4)^-$, $[B(C_6F_5)_4]^-$, $[Al(OC(CF_3)_3)_4]^-$ and $[B(C_6F_5)_3(OAc^F)]^-$ show higher catalytic activity than the counter ions Cl^-, NTf_2^-, OTf^-, SbF_6^-, BF_4^-, and OTs^- commonly used in industrial applications.

1.5 Redox Switchable Catalysis (RSC)

In general, there are two possible representatives in redox switchable catalysis (RSC). Catalysts that are inactive in the reduced state and can be switched into the active state by oxidation or vice versa. In most cases there is also no real “on” or “off”, but only a change in the catalytic activity.

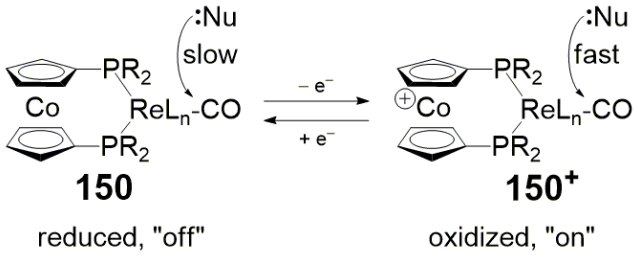

Scheme 1.5.1: Redox switchable catalysis in cobaltocenyl metal carbonyl complexes.[143]

One of the first examples for RSC with a metallocenyl ligand was reported by Wrighton et al. in 1994 (Scheme 1.5.1). They used a redox-active 1,1’-bis(diphenylphosphino)cobaltocene (dppc) ligand to reversibly change the reactivity of rhenium metal carbonyls towards nucleophiles.[143] In the oxidized state **150**$^+$ the electrophilicity of the carbonyl is higher, while in the reduced state **150** it is lower. By oxidation the reactivity towards tertiary amine *N*-oxides could be increased by a factor of 200, while the reactivity towards azide was increased by a factor of 5400 and $\Delta H^{\neq}$ was decreased by 13–17 kJ mol^{-1}. The same ligand can be used to reversibly change the rate of rhodium(I)-catalysed reduction and isomerization of ketones and alkenes.[144] Additionally to the control of the reaction rate redox switchable catalysts were also be used by Plenio et al. as phase tag for recycling of homogeneous catalyst **151** in Grubbs-Hoveyda ring closing metathesis (RCM) (Scheme 1.5.2).[145] By applying a voltage or adding an oxidant the catalyst can be oxidized twice and precipitates from the reaction solvent toluene. This way the metathesis can be stopped and the catalyst could be recovered. Reduction of the catalyst leads to redissolving and continuation of the metathesis reaction.

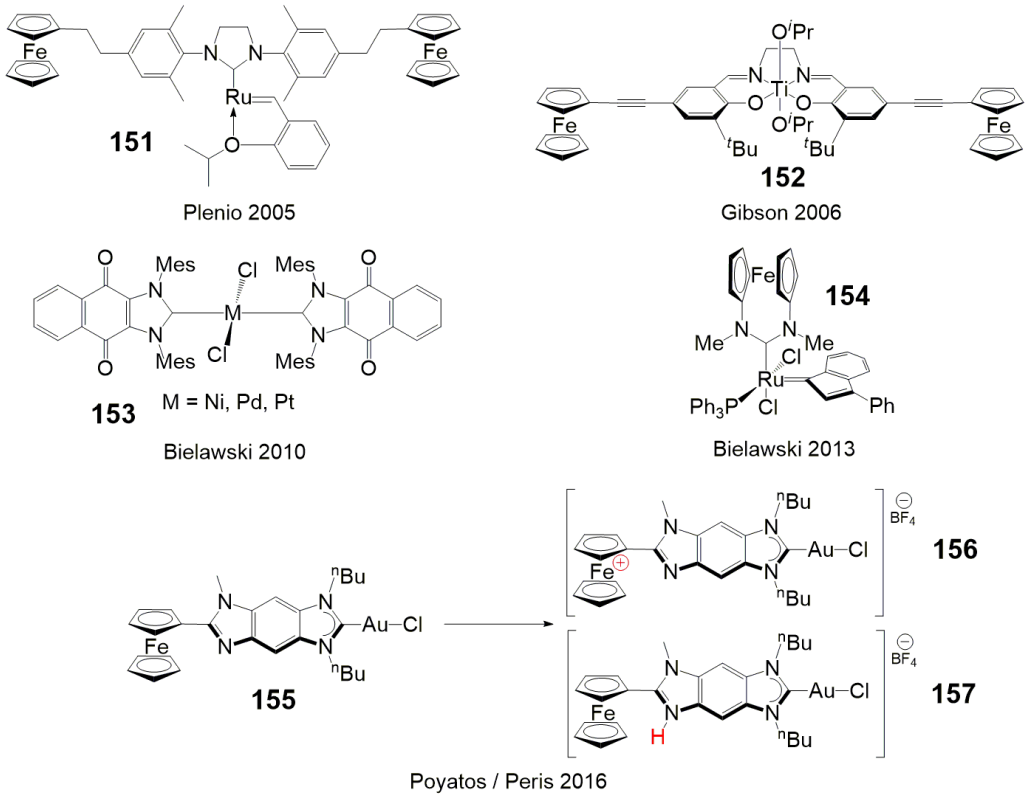

Scheme 1.5.2: Examples of redox switchable catalysts.[145–149]

Gibson et al. used the ferrocenium labelled salen titanium catalyst **151** for the ring-opening polymerization (ROP) of *rac*-lactide (Scheme 1.5.2).[146] In the non-oxidized state the catalyst was approximately 30 times more active than in the double-oxidized state, which was attributed to the electron withdrawing effect of the ferrocenium groups. The catalyst could be switched from the oxidized to the reduced state to recover the initial catalytic activity. This could be used to form micro-block copolymers. Bielawski et al. used NHC ligands with a redox active naphthoquinone moiety to synthesize nickel-, palladium- and platinum-complexes **153** that were used in redox-switchable Kumada coupling of different bromoarenes with phenylmagnesium chloride (Scheme 1.5.2).[147] Addition of cobaltocene as reducing agent decreased the catalytic activity, while subsequent oxidation with ferrocenium tetrafluoroborate restored the initial activity. In 2013 Bielawski et al. used the redox-switchable diaminocarbene[3]ferrocenophane Grubbs like catalyst **154** for the ring-opening metathesis polymerization (ROMP) of *cis-cis*-1,5-cyclooctadiene.[148] In the reduced state the conversion is approximately 25 % after 10 min with 0.04 mol% catalyst loading. After oxidation with DDQ almost a full stop of the reaction could be observed. UV/vis spectroscopy suggested, that the catalyst is still soluble after oxidation. EPR spectroscopy indicated an iron centred radical in the oxidized state. Poyatos and Peris et al. used an imidazolium salt with a fused benzoferrocenyl as precursor for the synthesis of the ferrocenyl-imidazolylidene-gold(I) complex **155**, which they used for RSC in the cyclization of alkynes with furans.[149] The neutral complex **155** shows no activity, while the oxidized species gives 53–75 % yield depending on the alkynes used for the reaction. Two active species **156** and **157** could be responsible for the catalysis. The expected Fe(III) complex **156**, but also the protonated Fe(II) complex **157** was observed after the oxidation. Separation of these two species to assign the catalytic activity was

not successful. More RSC of NHC complexes can be found in a detailed review of Peris published in 2017 about smart NHC ligands in catalysis.[150]

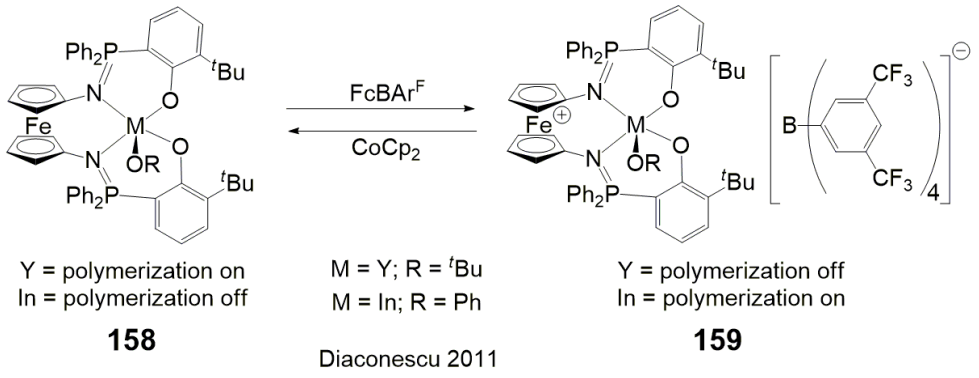

Scheme 1.5.3: Central metal dependent RSC.[151]

A quite interesting example for RSC was published by Diaconescu et al. in 2011 (Scheme 1.5.3).[108,151] The same catalyst with different central metal shows antithetic behaviour in RSC polymerization reactions. While the yttrium complex is active in the reduced state **158** and catalyses the ROP of L-lactide and can be switched off by oxidation with ferrocenium tetrakis(3,5-bis(trifluoromethyl)phenyl)borate (FcBAr^F), the corresponding indium complex is active in the oxidized state **159** and can be switched off by addition of cobaltocene.

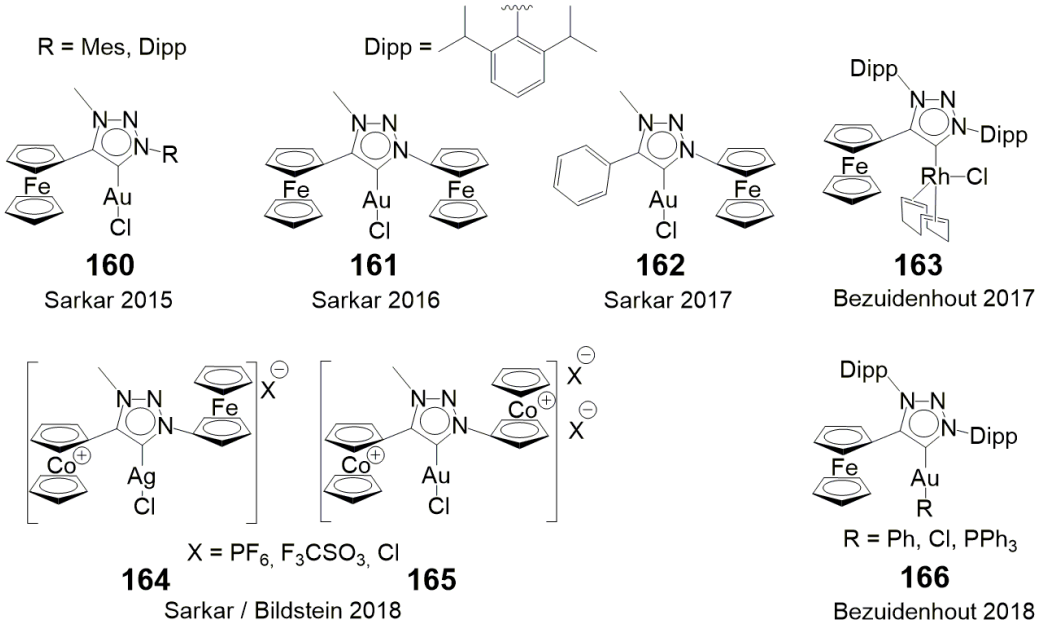

Scheme 1.5.4: Mesoionic carbene complexes in RSC, 4-ferroceny 160[152], 1,4-diferrocenyl 161[107], 1-ferrocenyl 162[106], mono/dicobaltoceniumyl 164 and 165[153],Dipp-Rh-complex 163[154], Dipp-Au-complex 166.[155]

The Group of Sarkar investigated several representatives of ferrocenyl containing mesoionic carbene (MIC) complexes of gold in RSC with a 1,2,3-triazol-5-ylidene (trz) scaffold (Scheme 1.5.4). The 4-ferrocenyl-1-mesityl triazolylidene gold(I) complex **160**[152] shows 88 % conversion after 24 h in the oxidized state **160$^+$**, but only 12 % conversion in the same time in the neutral state **160** for

the test reaction cyclization of *N*(2-propyn-1-yl)benzamide to 5-methylene-2-phenyl-4,5-dihydrooxazole with 1 mol% catalyst loading. The diferrocenyl triazolylidene gold(I) complex **161**[107] shows 10 % conversion for the same reaction. Oxidation to the mono cation **161**$^{+}$ leads to an increase of the TEP from 2045.4 cm^{-1} to 2056.9 cm^{-1} and a conversion of 30 % after 24 h. For the beforementioned 4-ferrocenyl,1-mesityl triazolylidene **161** the TEP changes from 2045.4 cm^{-1} to 2052.8 cm^{-1} upon oxidation.[107] The second oxidation of 4,N-diferrocenyl triazolylidene complex to **161**$^{2+}$ further increases the TEP to 2068.3 cm^{-1}, while the conversion of the test reaction shows 40 % after 24 h. For the 1-ferrocenyl,4-phenyl triazolylidene gold(I) complex **162** the reversibility of the RSC could be shown by switching the catalyst “on” and “off” for several times.[106] For this ligand the TEP changes from 2047.0 cm^{-1} to 2054.3 cm^{-1} upon oxidation. The conversion rate for the test reaction is 30 % after 24 h for the neutral species **162** and 100 % for the mono cation **162**$^{+}$. Expanding the concept of redox switchable MIC ligands to other metallocene moieties leads to cobaltocenium compounds **164** and **165**.[153] With TEPs of 2077.9 cm^{-1} for the 1-ferrocenyl,4-cobaltocenyl triazolylidene mono cation **164** and 2108.7 cm^{-1} for the 1,4-dicobaltocenyl triazolylidene dication **165** the ligands lie in the electron poor region compared to standard NHC ligands with TEPs between 2045–2053 cm^{-1}. The 1,4-dicobaltocenyl triazolylidene gold complex **165** shows 100 % conversion in the test reaction in less than 2 h. Addition of two equivalents of reducing agents fully stops the reaction, while re-oxidation does not activate the catalyst again, as the cobaltocenium complexes show lower redox stability than the ferrocenyl complexes. RSC in the hydroformylation of 1-octene has been investigated by Bezuidenhout et al. with a ferrocenyl-bis-Dipp trz Rh(I) complex **163**.[154] Similar ferrocenyl bis-Dipp trz gold complexes **166** have been used as anticancer agents.[155] A detailed review about different trz complexes and their application in catalysis, medicine and photophysics was published by Bugarin et al. in 2018. [156]

Also examples of RSC with more than two ferrocenyl sites are possible. Recent work of Hey-Hawkins et al. reported a *P*-chiral dendritic ferrocenyl phosphine ruthenium complex with 12 ferrocenyl units that shows RSC in the transfer hydrogenation of acetophenone to 1-phenylethanol.[157]

2 Aim of Work

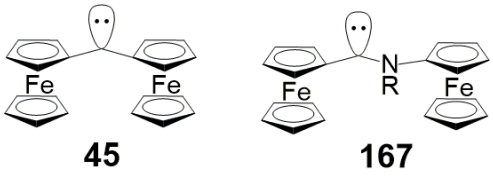

Scheme 2.1: Diferrocenyl carbene and ferrocenyl aminoferrocenyl carbene.

Redox switchable catalysis (RSC) is of great interest, as it allows to control a desired reaction and switch it on and off. This can be used for example in the synthesis of special block copolymers or also to recycle the catalyst after the reaction. The stability and good redox properties of the ferrocenyl moiety made it an important part of redox switchable carbene ligands. Ferrocenyl carbene complexes have a wide application in RSC, but most of them are based on NHCs of MICs and are synthesized in elaborate multi-step reactions that sometimes include explosive intermediates like ferrocenyl and aryl azides. Acyclic approaches showed no successful results in RSC so far. The primary aim of this work is the basic understanding of diferrocenyl carbene **45** and ferrocenyl aminoferrocenyl carbenes **167** (Scheme 2.1) as potential novel acyclic redox switchable carbene ligands for the application in catalysis. Different approaches for the synthesis of these elusive compounds are investigated. In the course of these studies, substituent patterns for stabilization of the carbenes are tested and unexpected side reactions are screened. One possible route to **45** is the base assisted Bamford-Stevens reaction of diferrocenyl tosyl hydrazone **168** (Scheme 2.2). As previously reported **168** shows a strong nonclassical NH···Fe intramolecular hydrogen bond (IHB).[158] But what happens if the Fe is replaced by Ru? Investigation of the IHB after substitution of one or both ferrocenyl groups by ruthenocenyl groups will be performed. The strength of the resulting NH···Ru IHB will be evaluated and compared to the NH···Fe IHB. Possible isomers in the mixed ferrocenyl ruthenocenyl tosyl hydrazone will be compared.

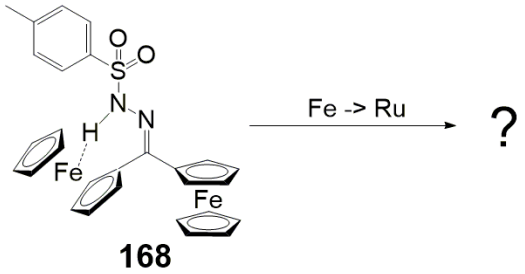

Scheme 2.2: Diferrocenyl tosyl hydrazone with IHB.[158]

Furthermore, one or two ferrocenyl groups will be introduced into Fischer carbene complexes and the products will be characterized (Scheme 2.3). Detection of free carbene intermediates or isolation and trapping of the free carbenes will be attempted. The side reaction to diferrocenyl imine will be investigated in detail to prevent it in future. The unexpected formation of 2,*N*-diferrocenyl acetamide from the ferrocenyl ethoxy Fischer carbene complex will be studied and mechanistic proposals will be given. Transmetalation of ferrocenyl ethoxy Fischer carbene complex to gold has been achieved by Bezuidenhout el at. but no catalytic experiment were

performed so far.[135] This gold(I) complex will be used as scaffolding to investigate the basics redox switchable catalysis of a test reaction and elucidate the nature of the active species. Further transmetalation approaches with the new carbene ligands will be attempted to get gold(I) catalysts with two active redox centres.

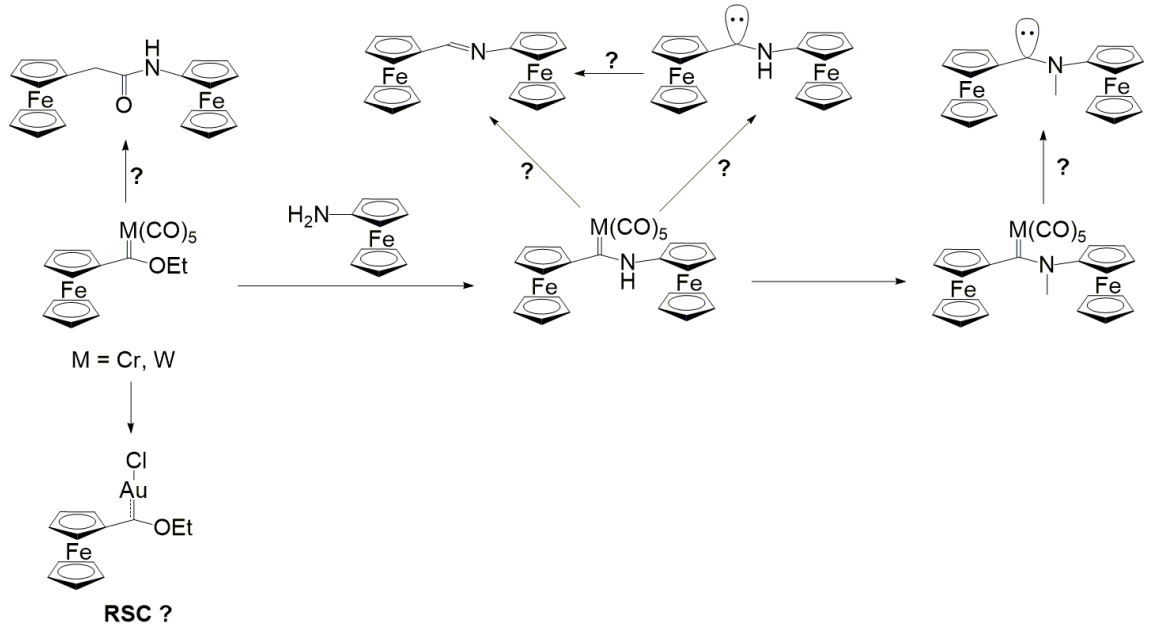

Scheme 2.3: Ferrocenyl carbene complexes investigated in this work.

3 Results and Discussion

The first five sections 3.1–3.5 of this dissertation have been published as scientific articles in peer reviewed chemistry journals. These articles will be reprinted in the following with the permission of the respective publisher. The section 3.6 is an unpublished manuscript that is in the submission process.

In section 3.1 *"Competitive NH···Ru/Fe Hydrogen Bonding in Ferrocenyl Ruthenocenyl Tosyl Hydrazone"* the *nonclassical* NH···M intramolecular hydrogen bond (IHB) to ferrocenyl and ruthenocenyl moieties in dimetallocenyl tosyl hydrazone is compared. IR spectroscopic measurements suggest that the NH···Ru IHB in diruthenocenyl tosyl hydrazone is 6 kJ mol^{-1} stronger than the NH···Fe IHB in diferrocenyl tosyl hydrazone. The mixed metallocenyl species ferrocenyl ruthenocenyl tosyl hydrazone shows two isomers which can be interconverted from *E* to *Z* by thermal and photochemical experiments as well as protonation.

In accordance to the N heterocyclic carbenes with two lone pairs of two nitrogen atoms stabilizing the carbene carbon atom the carbene complex (aminoferrocenyl) (ferrocenyl) carbene (pentacarbonyl) chromium(0) with at least one nitrogen atom in the proximity of the carbene carbon atom was synthesized. In section 3.2 *"Preparation, Properties, and Reactivity of (Aminoferrocenyl) (ferrocenyl) carbene (pentacarbonyl) chromium(0) as Bulky Isolobal Trimetallo-amide*" the carbene complex is characterized and compared to the isolobal diferrocenyl amide and diferrocenyl thioamide.

One big problem in the synthesis of aminoferrocenyl carbene complexes is the follow up reaction to an imine, that prevents the isolation of a carbene. In section 3.3 *"On the mechanism of imine elimination from Fischer tungsten carbene complexes"* the formation of the imine is investigated in detail by DFT calculations and kinetic and mechanistic experiments.

To prove the applicability of ferrocenyl Fischer carbene complexes as precursor for redox-switchable catalysis the transmetalation of the carbene fragment to gold and benchmark catalysis experiments were carried out. In the section 3.4 *"Gold(II) in redox-switchable gold(I) catalysis"* the synthesis of the gold complex as well as the redox-switchable catalysis experiments are described.

During the synthesis of the aminoferrocenyl ferrocenyl Fischer carbene complexes two unexpected side products could be identified. Diferrocenylacetamide is formed after nucleophilic attack of ferrocenylamide on a carbonyl carbon and triferrocenylcyclobutenone is formed in a multi-step reaction of three equivalents of ferrocenyl Fischer carbene complex. Mechanistic studies to these two products are described in the section 3.5 *"Unexpected C–C coupling reaction of Ferrocenyl Fischer Carbene Complexes leading to Acetamides and Cyclobutenones"*. The reaction to the cyclobutenone is compared to the literature known Dötz benzannulation reaction and differences are pointed out.

In section 3.6 *"Electrochemistry of the heterotrimetallic Fischer carbene complex (N-methylaminoferrocenyl) (ferrocenyl) carbene (pentacarbonyl) tungsten (0)"* the synthesis of the heterotrimetallic carbene complex is reported and characterized by NMR-, IR-, UV-vis spectroscopy, cyclic voltammetry and DFT calculations. The compound is compared to the lighter

isolobal analogous diferrocenyl amide and diferrocenyl thioamide. The communication of the two iron centres in dependence on the bridge (C=O, C=S, C=$M(CO)_5$) in the mixed valent ferrocene/ferrocenium mono cations is studied with spectroelectrochemical techniques and Robin Day classification is applied.

3.1 Competitive NH···Ru/Fe Hydrogen Bonding in Ferrocenyl Ruthenocenyl Tosyl Hydrazone

Philipp Veit, Ephraim Prantl, Christoph Förster,* and Katja Heinze*

Organometallics **2016**, *35*, 249-257.

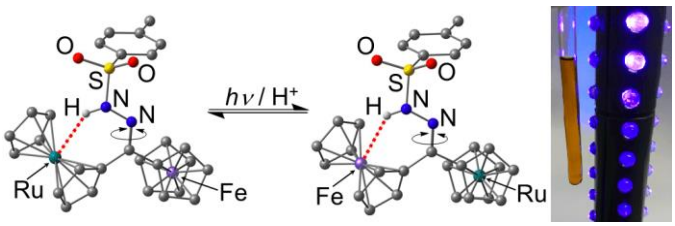

The literature-known diferrocenyl tosyl hydrazone (**1**) described in the last chapter shows a strong nonclassical NH···Fe intramolecular hydrogen bond (IHB). In this chapter, it is shown that an analogous NH···Ru IHB is present in the heavier homologue diruthenocenyl tosyl hydrazone (**2**). The IHB is confirmed by NMR and IR spectroscopy as well as by XRD methods. By IR spectroscopy it can be shown, that the NH···Fe IHB in **1** is weaker than the NH···Ru IHB in **2** by 6 kJ mol^{-1}. The synthesis of the mixed metallocenyl compound ferrocenyl ruthenocenyl tosyl hydrazone (**3**) shows the E/Z isomer directing abilities of NH···M IHBs. **3** is obtained as a mixture of the Z and E isomers (**3a,b**) with NH···Ru and NH···Fe IHBs, respectively. At 111 °C, **3a** with the NH···Ru IHB is preferred with an isomeric ratio of 10:1 (91% **3a**). The formation of the isomeric mixture allows a direct comparison of the competitive NH···Ru/Fe hydrogen bonding. The underlying reason for the **3a**:**3b** ratio is of thermodynamic nature, rooted in the differences in strengths of the NH···M IHBs of Fe and Ru. Thermal and photochemical approaches and protonation to the corresponding iminium/carbenium ions [**H-3a**]$^+$/[**H-3b**]$^+$ were employed to overcome the barrier for the E → Z isomerization **3b** → **3a**, with concomitant switching of the NH···M IHB.

Author contributions

The compounds were synthesized and characterized by Ephraim Prantl during his bachelor thesis under the supervision of Philipp Veit. The crystal structures were solved and refined by Christoph Förster. The irradiation experiments were conducted by Philipp Veit. All DFT-calculations were performed by Philipp Veit. The manuscript was written by Philipp Veit (40 %), Christoph Förster (20 %) and Katja Heinze (40 %).

Supporting Information

for this article is found in Chapter 6.1 at pp. 103. For full Supporting Information containing the coordinates of all relevant DFT calculated structures, refer to:
https://pubs.acs.org/doi/suppl/10.1021/acs.organomet.5b00963/suppl_file/om5b00963_si_004.pdf

„Reprinted with permission from Veit, P.; Prantl, E.; Förster, C.; Heinze, K. *Organometallics* **2016**, *35*, 249–257. Copyright © 2016 American Chemical Society. ACS AuthorChoice - This is an open access article published under an ACS AuthorChoice License, which permits copying and redistribution of the article or any adaptations for non-commercial purposes."

This is an open access article published under an ACS AuthorChoice License, which permits copying and redistribution of the article or any adaptations for non-commercial purposes.

ORGANOMETALLICS

Article

pubs.acs.org/Organometallics

Competitive NH···Ru/Fe Hydrogen Bonding in Ferrocenyl Ruthenocenyl Tosyl Hydrazone

Philipp Veit, Ephraim Prantl, Christoph Förster,* and Katja Heinze*

Institute of Inorganic Chemistry and Analytical Chemistry, Johannes Gutenberg-University of Mainz, Duesbergweg 10-14, 55128 Mainz, Germany

Supporting Information

ABSTRACT: A strong *nonclassical* NH···Fe intramolecular hydrogen bond (IHB) is present in the literature-known diferrocenyl tosyl hydrazone (**1**). Here, we confirm by NMR and IR spectroscopy as well as by XRD methods that an analogous NH···Ru IHB is present in the heavier homologue diruthenocenyl tosyl hydrazone (**2**). The NH···Ru IHB in **2** is stronger than the NH···Fe IHB in **1** by 6 kJ mol^{-1}, as determined by IR spectroscopy. Further, we probed the *E*/*Z* isomer directing abilities of NH···M IHBs in the synthesis of the mixed metallocenyl compound ferrocenyl ruthenocenyl tosyl hydrazone (**3**). **3** is obtained as a mixture of the *Z* and *E* isomers (**3a,b**) with NH···Ru and NH···Fe IHBs, respectively. At 111 °C, **3a** is preferred with an isomeric ratio of 10:1 (91% **3a**). The formation of the isomeric mixture allows a direct comparison of the competitive NH···Ru/Fe hydrogen bonding. The underlying reason for the **3a**:**3b** ratio is of thermodynamic nature, rooted in the differences in strengths of the NH···M IHBs of Fe and Ru. Thermal and photochemical approaches and protonation to the corresponding iminium/carbenium ions [**H-3a**]$^+$/[**H-3b**]$^+$ were employed to overcome the barrier for the *E* → *Z* isomerization **3b** → **3a**, with concomitant switching of the NH···M IHB.

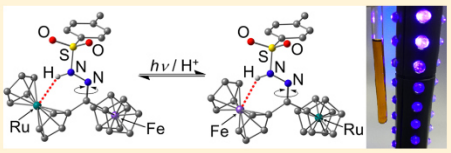

INTRODUCTION

Classical hydrogen bonds between electronegative elements are important in secondary structures of natural peptides[1] as well as in catalysis.[2,3] However, also *nonclassical* hydrogen bonds such as XH···M and XH···HM play a significant role in modern chemistry, especially in organometallics with rather electron rich metal centers.[4−9] Organometallic peptides with conventional hydrogen bond forming ingredients, such as amino acids,[10−21] sugars,[22] ureas,[23,24] and lactams,[25] based on classical hydrogen bonds[26,27] have been extensively studied and exploited. Molecular wires,[28−30] redox-responsive foldamers,[31−33] optically switchable valence tautomers,[34,35] porphyrin tweezers,[36] and anion sensors[37−42] have been devised from the combination of ferrocene and hydrogen bonds in organometallic systems. Utilization of stable, *nonclassical* hydrogen bonds[4−9] in the areas of organometallic crystal engineering[4−6,8] and especially in supramolecular organometallic chemistry, yet inspired by conventional, natural hydrogen bond based secondary structures, would expand our molecular universe in terms of structural diversity and reactivity.

Recently, a strong, *nonclassical* NH···Fe intramolecular hydrogen bond (IHB) has been discovered in the organometallic diferrocenyl tosyl hydrazone **1**.[43] This IHB is exceptionally thermally stable and persistent with respect to competition with external hydrogen atom acceptors such as THF and even DMSO.[43] The static NH···Fe IHB in **1** clearly distinguishes the two ferrocenyl sites in **1**, especially from an electrochemical point of view. Indeed, the non-hydrogen-bonded ferrocenyl substituent is oxidized to the ferrocenium ion (Fc$^+$) in the first place, while the IHB to the uncharged Fc remains intact in **1**$^+$. In the second oxidation process to **1**$^{2+}$, the IHB is disrupted due to accumulation of positive charge at the hydrogen-bonded Fc$^+$ moiety. The NH···Fe IHB confines charge and spin to the non-hydrogen-bonded Fc site in **1**$^+$, while in **1**$^{2+}$ the second positive charge splits the IHB, inducing a significant conformational rearrangement.[43]

We then became interested in the question whether the heavier homologue ruthenocene would behave similarly to ferrocene and whether the NH···Ru hydrogen bond would be stronger or weaker than the corresponding NH···Fe IHB. In terms of basicity, the reactivity of ferrocene and ruthenocene has to be divided into "ring basicity", the interaction of the electron-rich cyclopentadienyl (Cp) ligands with hydrogen donors, and "metal basicity", as a consequence of the interaction of the electron-rich metal centers with hydrogen donors. Ferrocene (K_b = 1.54) shows a higher ring basicity in protonation equilibria of the Cp ligands in comparison to ruthenocene (K_b = 0.48).[44,45] Ferrocene protonation at iron is achieved in boron trifluoride hydrate,[46] while $RuCp_2$ and $OsCp_2$ show a higher metal basicity and are protonated at the metal already by TFA in CH_2Cl_2.[47,48] These opposite trends in ring and metal basicity lead to different protonation mechanisms of the metal centers.[49] The protonation of ferrocene occurs via an exo attack of a proton at the Cp

Received: November 20, 2015
Published: January 13, 2016

ACS Publications © 2016 American Chemical Society

DOI: 10.1021/acs.organomet.5b00963
Organometallics 2016, 35, 249−257

Downloaded via UNIV MAINZ on August 5, 2019 at 12:33:13 (UTC).
See https://pubs.acs.org/sharingguidelines for options on how to legitimately share published articles.

ligand, while ruthenocene is directly protonated at the metal. Similar to protonation, intermolecular $OH_{phenol}\cdots Cp$ hydrogen bonds are formed exclusively for $FeCp_2$, while $OH_{phenol}\cdots M$ hydrogen bonds are detected additionally in the case of $RuCp_2$ and $OsCp_2$ by treating these metallocenes with phenols.[50] For IHBs of metallocenyl alcohols and phenols analogous observations have been made and the strength of the OH···M IHBs follows the trend Fe < Ru < Os.[50−53] Further, six-membered-ring conformations allow stronger intramolecular OH···Fe hydrogen bonds in ferrocenyl alcohols than five- or seven-membered rings.[51,53]

We envisaged that the dimetallocenyl tosyl hydrazone platform is ideally suited to address the fundamental question of which metal center (Fe/Ru) forms stronger NH···M hydrogen bonds in metallocenes for the following reasons: the hydrogen bond encompasses the stable six-membered-ring conformation and competition of the NH···Cp hydrogen bonding is essentially excluded due to the restricted conformational mobility caused by the C=N double bond. Next, we were interested in the *E*/*Z* isomer directing abilities as a consequence of the competition of the *nonclassical* NH···M hydrogen bonds in the synthesis of a mixed-metal (Ru/Fe) tosyl hydrazone as a prototype for imine type *E*/*Z* R(R′)C=NR″ compounds.[54]

Hence, we prepared the diruthenocenyl tosyl hydrazone **2** and the mixed ferrocenyl ruthenocenyl tosyl hydrazone **3** from the respective ketones[55−60] (Scheme 1) and investigated their

Scheme 1. Synthesis of 2 and 3a,b with Atom Numbering for NMR Assignment

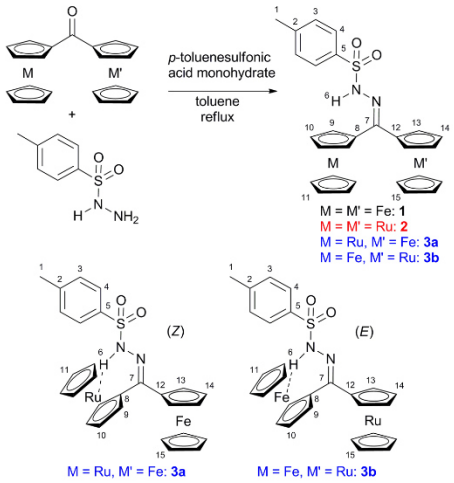

structures in solution and in the solid state by NMR and IR spectroscopy as well as by single-crystal XRD. For the heterobimetallic hydrazone **3**, *E*/*Z* isomers are envisaged, namely **3a** (*Z*) featuring a NH···Ru IHB and **3b** (*E*) with a NH···Fe IHB. The relative stability of these two isomers will be probed by NMR and IR spectroscopy in combination with density functional theory studies. A conceivable interconversion between the two hydrogen-bonded isomers **3a,b** will be attempted by thermal means, as described for ferrocenyl imines,[54] by photochemical means, and by acid assistance similarly to isomerization of purely organic hydrazones lacking XH···M IHBs.[61]

RESULTS AND DISCUSSION

The hydrazones **2** and **3** were conveniently[43,59,60] prepared from the respective literature-known dimetallocenyl ketones[55−58] by condensation with *p*-toluenesulfonyl hydrazide in refluxing toluene in good yields (Scheme 1). The compositions and purities of **2** and **3** were ascertained by mass spectrometry, showing the expected molecular ion peaks at *m*/*z* 656.8 and 611.7 with correct isotopic patterns, respectively (Figure S1 in the Supporting Information), and by satisfactory elemental analyses (Experimental Section). The UV/vis spectra of **2** and **3** in CD_2Cl_2 are unspectacular, displaying metallocene-associated absorption bands at 235, 254, 284, and 330 nm (**2**) and at 236, 295, 350, and 455 nm (**3a,b**), respectively (Figures S2 and S3 in the Supporting Information). According to time-dependent density functional theory (TD-DFT) calculations, most of these transitions involve the LUMO, which features large coefficients on the C=N double bond corresponding to the π^*(C=N) molecular orbital.

The diruthenium complex **2** shows two sets of Cp proton and carbon resonances (Scheme 1 and Figures S4 and S5 in the Supporting Information), a low-field NH^6 resonance at δ_{NH} 9.70 ppm (Figure 1), and an NOE cross peak of the NH proton

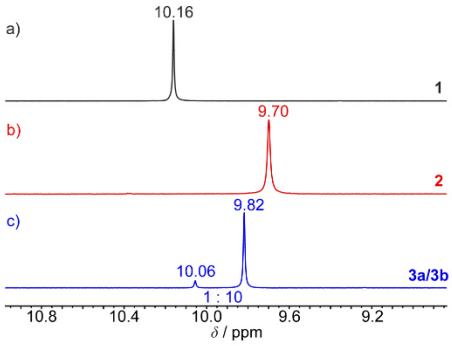

Figure 1. NH region of the ^{1}H NMR spectra of (a) **1**,[43] (b) **2**, and (c) a 10:1 mixture of **3a,b** in $CDCl_3$ (full spectra in Figure S8 in the Supporting Information).

to one C_5H_5 (H^{11}) ring in $CDCl_3$ solution (Figure S6 in the Supporting Information). This NOE distance constraint places the NH group in the vicinity of a ruthenium center. Hence, a NH···Ru IHB is also present in **2**, perfectly similar to the NH···Fe situation in **1**.[43] Completely analogous to **1**, the NH···Ru IHB in **2** is not disrupted by the strongly hydrogen accepting solvent DMSO, as shown by a ^{1}H NMR experiment in d_6-DMSO (δ_{NHRu} 9.67 ppm, Figure S7a in the Supporting Information).

The mixed dimetallocene **3** is obtained as a mixture of *E*/*Z* isomers **3a,b** (Scheme 1) in the nonstatistical ratio 10:1 at 111 °C (toluene reflux), as easily identified by the doubled set of proton resonances in a 10:1 (91% **3a**) integration ratio (NH proton resonances H^6, Figure 1; tosyl proton resonances $H^{1,3,4}$

DOI: 10.1021/acs.organomet.5b00963
Organometallics 2016, 35, 249−257

and Cp proton resonances $H^{9-11}$and H^{13-15}, Figure S9 in the Supporting Information). The two isomers proved to be inseparable by recrystallization, column chromatography, and HPLC, but they are easily identified by their significantly different proton NMR resonances. By comparison with the ^{1}H NMR resonances of **1** (ferrocenyl substituents with and without IHB[43]) and **2** (ruthenocenyl substituents with and without IHB, Figure S4 in the Supporting Information) it is even possible to assign the major isomer **3a** to that with a NH···Ru IHB (δ_{NHRu} 9.82 ppm, 91%) and the minor isomer **3b** to that with the NH···Fe IHB (δ_{NHFe} 10.06 ppm, 9%) (Figures S9 and S11 in the Supporting Information). DMSO leaves the IHBs in **3a,b** unaffected, as shown previously for **1**[43] and **2** (**3a** δ_{NHRu} 9.78 ppm and **3b** δ_{NHFe} 10.01 ppm in d_6-DMSO; Figure S7b in the Supporting Information). Variable-temperature ^{1}H NMR spectra in d_8-toluene reveal that the IHBs of **3a,b** are stable and thermal interconversion of **3a,b** (Scheme 2) is not achieved up to 100 °C (Figure S12 in the Supporting Information).

Scheme 2. Possible Pathways for the 3a,b Interconversion

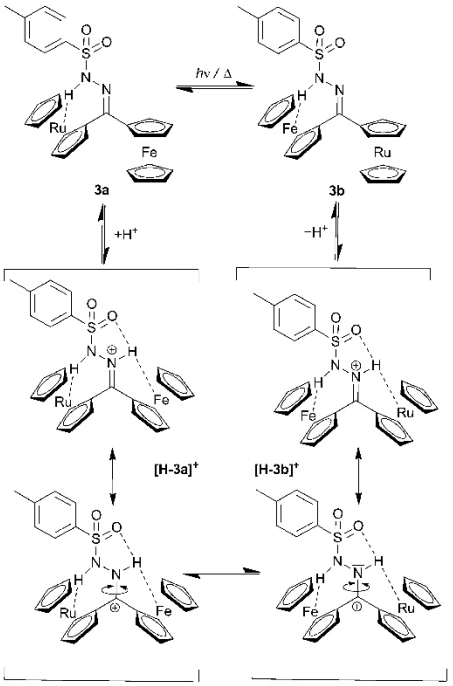

DFT calculations on **3a,b** (Figure 2 and the Supporting Information) suggest a thermodynamic preference for the NH···Ru hydrogen bonded isomer **3a** over **3b** by 8 kJ mol^{-1} at 298 K. This corresponds to a relative fraction of **3a** of 96%. Both non-hydrogen-bonded isomers are almost degenerate in terms of energy and are 14 kJ mol^{-1} higher in energy than the

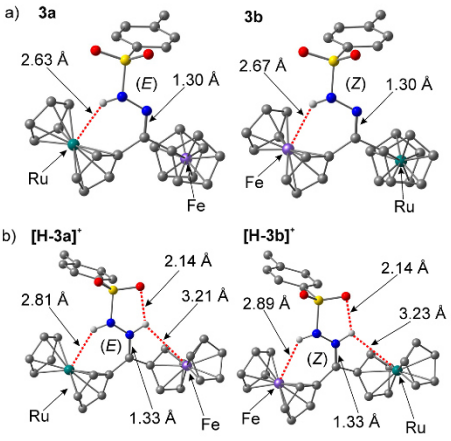

Figure 2. DFT calculated optimized geometries of (a) **3a,b** and (b) [**H-3a**]$^+$ and [**H-3b**]$^+$ showing NH···M/O IHBs.

hydrogen-bonded isomer **3a**. Hence, the preference of **3a** is essentially based on the more favorable NH···Ru IHB in comparison to **3b** with its NH···Fe IHB, while electronic differences between the *E* and *Z* isomers appear negligible. The NH···Ru IHB in **3a** is calculated to be slightly stronger than the NH···Fe IHB in **1**, with a difference between the conformers of **1** with and without IHB amounting to 10 kJ mol^{-1}. For the diruthenocenyl tosyl hydrazone **2** the corresponding energy difference is calculated as 12 kJ mol^{-1}.

As an indicator of the hydrogen bond strength, the NH stretching vibration without IHB as present in diphenyl tosyl hydrazone (**4**)[43,62] at 3219 cm^{-1} is compared to the NH vibration with NH···M IHB in the solid state. The NH stretching vibrations of **1**−**3** are observed at 3101, 3003, and 3001 cm^{-1}, respectively (Figure S16 in the Supporting Information). This significant shift to lower wavenumbers shows the presence of strong hydrogen bonds in **1**−**3**. For **2** and **3**, the NH stretching band overlaps with the CH_{cp} vibrations. To confirm the assignment, **2** was N-deuterated with D_2O to $\mathbf{2}^D$, giving an ND stretch at 2262 cm^{-1}. The isomer **3b** was not detected in the IR spectra of the **3a,b** mixture due to its low concentration. This further confirms the preference of the NH···Ru IHB in **3**.

Vibrational spectra in solution with a noncoordinating solvent are used to exclude packing effects or intermolecular hydrogen bonds. **1**, **2**, and **3a,b** show absorptions of NH stretching vibrations at 3118, 3028, and 3030 cm^{-1} in $CDCl_3$, respectively (Figure 3). Using the NH vibration of **4**[43,62] in CD_2Cl_2 with 3267 cm^{-1} as a reference value for the free NH stretch together with the empirical correlation of hydrogen bond enthalpies and XH wavenumber shifts $-\Delta H = 18\Delta\tilde{\nu}/(\Delta\tilde{\nu} + 720)$ (ΔH in kcal mol^{-1}; $\Delta\tilde{\nu}$ in cm^{-1}),[7,52,63] the hydrogen bond enthalpies are as follows: **1**,[43] $\Delta\tilde{\nu} \approx 149$ cm^{-1}, $-\Delta H \approx 13$ kJ mol^{-1}; **2**, $\Delta\tilde{\nu} \approx 239$ cm^{-1}, $-\Delta H \approx 19$ kJ mol^{-1}; **3a**, $\Delta\tilde{\nu} \approx 237$ cm^{-1}, $-\Delta H \approx 19$ kJ mol^{-1}. According to these values, the IHBs in **2** and **3a** are comparable in terms of strength while they are significantly stronger than the IHB in **1**, resulting in the conclusion that the NH···Ru IHB is stronger than the NH···

DOI: 10.1021/acs.organomet.5b00963
Organometallics 2016, 35, 249−257

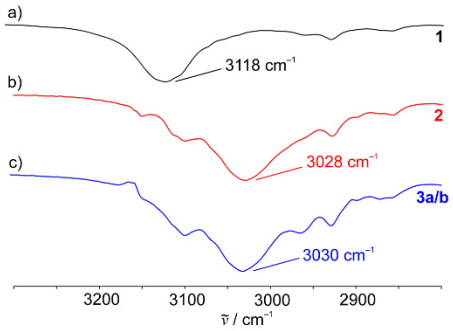

Figure 3. IR spectra of (a) **1** in CD_2Cl_2[43] and (b) **2** and (c) **3a,b** mixture (10:1) in $CDCl_3$ (NH region).

Fe IHB by 6 kJ mol^{-1}. This trend is also confirmed by the isomer ratio **3a**:**3b** in the ^{1}H NMR spectrum (Figure S9a in the Supporting Information) and the DFT calculations.

The final proof of IHBs involving ruthenium(II) in the solid state is given by single-crystal XRD analyses of **2** and **3a** (Figure 4 and Table 1). Only the *Z* isomer **3a** is detected in the single crystal. All dimetallocenyl tosyl hydrazones **1**,[13] **2**, and **3a** crystallize isotypically in the monoclinic space group $P2_1/c$. The Ru1···H2N (H2 was localized in the difference Fourier map) and Ru1···N2 distances are in accordance with the DFT calculations (Table 1). Although ruthenocenyl alcohols have been amply described in the literature,[51−53] only three examples of structurally confirmed XH···Ru IHBs in ruthenocenyl-containing compounds are deposited in the Cambridge Structural Database (CSD)[64] with O···Ru = 3.493 Å[65] and N···Ru = 3.687 Å,[66] 3.791 Å.[67] In **1** the corresponding distances to iron are 3.46 Å (Fe−N2) and 2.71 Å (Fe−H2N).[43] The heavier homologue **2** shows distances of 3.47 Å (Ru1−N2) and 2.67 Å (Ru1−H2N), and **3a** features distances of 3.46 Å (Ru1−N2) and 2.72 Å (Ru1−H2N). The torsion angles between the cyclopentadienyl and the hydrazone planes for **2** are 145° (N1−C11−C12−C13) and 170° (N1−C11−C6−C7), respectively, and for **3a** are 146° (N1−C11−C12−C13) and 170° (N1−C11−C6−C7) (Figure 4). The IHB forces the ruthenocenyl substituent out of conjugation, suggesting that the IHB overcompensates the energy loss resulting from the noncoplanar orientation. The non-hydrogen-bonded metallocenyl substituent shows almost coplanar sites in **1**−**3** with respect to the RR′C═N plane, allowing π conjugation.

As DFT calculations suggest a slightly higher fraction of **3a** of 96% at room temperature than at the applied synthesis temperature of 111 °C (94%), we attempted to increase the isomer ratio by reducing the synthesis temperature to room temperature. However, the reaction rate is too small at room temperature to obtain the hydrazones.

Hence, we considered a postsynthetic isomerization of **3b** to **3a**. An NMR sample of the 10:1 **3a**:**3b** mixture in toluene was heated to 100 °C, yet the isomer ratio remained constant. Obviously, the barrier for *E*/*Z* isomerization in **3** is too high for thermal activation. Next, a photochemical isomerization was attempted. Indeed, TD-DFT calculations of **3a** (Figure S3 in the Supporting Information) show that most electronic transitions between 236 and 455 nm involve the LUMO,

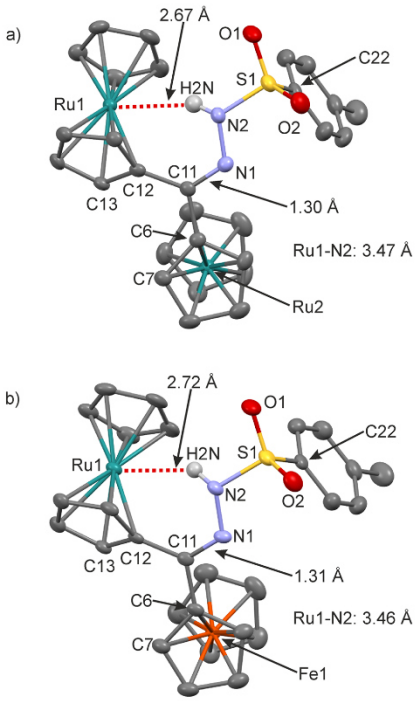

Figure 4. Molecular structures of (a) **2** and (b) **3a** from single crystal XRD (CH hydrogen atoms omitted, thermal ellipsoids at 50% probability).

which essentially corresponds to population of the π^* orbital of the C═N double bond. For **3a**, the low-energy band at 455 nm corresponds to a ruthenium → π^*(CN) transition. An analogous iron → π^*(CN) absorption is expected for **3b**. On the one hand, excitation into these bands should reduce the CN bond order, allowing facilitated rotation around this bond, and on the other hand weaken the corresponding NH···M hydrogen bond due to electron depletion at the electron-donating metal center. Facilitated rotation around the CN bond with concomitant cleavage of the IHB should interconvert **3b** to **3a** (Scheme 2). Indeed, irradiation of the **3a**,**b** mixture at 400 nm for 96 h at room temperature in $CDCl_3$ in an NMR tube increases the **3a**:**3b** ratio from 10:1 (94% **3a**) to 17:1 (95% **3a**) (Figure S13 in the Supporting Information). Performing the same experiment at −78 °C yielded a 15:1 **3a**:**3b** ratio (94% **3a**) after 140.5 h (Figure S13). Hence, irradiation overcomes the C═N rotational barrier and allows **3a**,**b** to equilibrate at room temperature and even at lower temperature. This confirms that the isomer ratio is thermodynamically controlled and the observed 10:1 ratio corresponds to the equilibrium ratio at 111 °C (synthesis temperature).

In addition to photochemically induced isomerization, this process might also be induced by protonation of the hydrazone at the C═N nitrogen atom to the iminium/carbenium ion [**H**-

DOI: 10.1021/acs.organomet.5b00963
Organometallics 2016, 35, 249−257

Table 1. Selected Bond Lengths (Å) and Angles (deg) of 1, 2, and 3a determined by XRD and of 1, 2, and 3a,b Determined by DFT Calculations

	1 (XRD)[43]	2 (XRD)	3a (XRD)	1 (DFT)[43]	2 (DFT)	3a (DFT)	3b (DFT)
M1	Fe	Ru	Ru	Fe	Ru	Ru	Fe
M2	Fe	Ru	Fe	Fe	Ru	Fe	Ru
M1···H2N	2.71(2)	2.67(2)	2.72(3)	2.674	2.640	2.627	2.673
M1···N2	3.463(2)	3.466(2)	3.461(3)	3.545	3.551	3.539	3.547
N1−C11−C12−C13	146.8(2)	145.2(3)	145.7(4)	149.2	147.0	146.7	148.8
N1−C11−C6−C7	168.6(2)	169.7(2)	169.6(5)	162.4	160.0	163.5	158.4
N1−C11	1.297(3)	1.296(3)	1.305(4)	1.297	1.297	1.297	1.297
N1−N2	1.396(2)	1.389(3)	1.386(4)	1.378	1.376	1.376	1.377
N2−S1	1.650(2)	1.652(2)	1.653(3)	1.706	1.706	1.705	1.706
C11−C12	1.473(3)	1.480(3)	1.477(5)	1.482	1.482	1.482	1.482
C11−C6	1.480(3)	1.476(3)	1.476(5)	1.478	1.477	1.477	1.477
N1−N2−S1−C22	54.2(2)	58.1(2)	56.9(3)	55.4	56.2	55.8	55.5
M1−X1[a]	1.660	1.818	1.801	1.696	1.877	1.877	1.696
M1−X2[b]	1.660	1.814	1.805	1.698	1.880	1.879	1.698
M2−X1[a]	1.655	1.811	1.663	1.691	1.876	1.601	1.875
M2−X2[b]	1.649	1.806	1.664	1.692	1.875	1.692	1.875
τ(M1)[c]	174.6	175.7	175.4	175.4	176.4	176.7	175.4
τ(M2)[c]	179.2	179.1	179.2	178.0	178.7	178.0	178.7

[a]X1 = centroid of coordinated C_5H_5 ring. [b]X2 = centroid of coordinated C_5H_4 ring. [c]τ = X1−M−X2.

3a]$^+$/[**H-3b**]$^+$ (Figure 2b and Scheme 2). Addition of TFA to the orange dichloromethane solution of **3a,b** at room temperature leads to formation of the respective brown iminium/carbenium ions [**H-3a**]$^+$/[**H-3b**]$^+$. Protonation results in bathochromic shifts of 295 → 310 nm, 350 → 420 nm, and 455 → 566 nm of the characteristic absorption bands (Figure S14 in the Supporting Information), as is common for ferrocenyl carbenium ions.[68] The ^{1}H NMR spectrum of [**H-3a**]$^+$/[**H-3b**]$^+$ shows two sets of signals for the two isomers [**H-3a**]$^+$ and [**H-3b**]$^+$ (Figure S15b in the Supporting Information). Isomerization/equilibration at room temperature for 22 h and subsequent deprotonation by K_2CO_3 restores the orange **3a,b** solution and yields a **3a**:**3b** ratio of approximately 16:1 (94% **3a**) according to the ratio of the respective cyclopentadienyl resonances in the ^{1}H NMR spectrum (Figure S15c). This experiment further substantiates that **3a** is thermodynamically preferred and its fraction increases at lower temperature. DFT calculations show an elongation of the NH···M IHB after protonation (**3a** → [**H-3a**]$^+$, 2.63 Å → 2.81 Å, Figure 2; **3b** → [**H-3b**]$^+$, 2.67 Å → 2.89 Å, Figure 2) as well as an elongation of the C═N bond by 3 pm reflecting the reduced double-bond character. The reduced CN bond order allows thermal rotation around the CN bond with concomitant dissociation of the NH···M IHB. The iminium/carbenium ions [**H-3a**]$^+$/[**H-3b**]$^+$ are calculated to be similar in energy within 2 kJ mol^{-1}. Additionally, the DFT calculations of the iminium/carbenium ions [**H-3a**]$^+$/[**H-3b**]$^+$ resulted in minimum structures with three IHBs which are preferred over conformations with fewer IHBs (Figure 2b). The additional proton forms bifurcated hydrogen bonds to a tosyl oxygen atom and the second metal center. The latter NH···M IHBs, forming five-membered rings, are considerably weaker (3.21 Å [**H-3a**]$^+$, 3.23 Å [**H-3b**]$^+$) than the IHBs involving the first metal center within a six-membered ring. Rotation around the CN bond transforms a NH···M IHB in a six-membered ring into a NH···M IHB in a five-membered ring. In summary, **3b** is accessible at higher temperature in small amounts and this less favored isomer can be isomerized to **3a** by reducing the CN bond order either by photochemical means by population of the π^*(CN) orbital or by protonation at the N atom which lowers the E/Z activation barriers (Scheme 2). A simple thermal isomerization is not achieved up to 100 °C.

As the NH···Fe IHB of the diferrocenyl tosyl hydrazone **1** can be opened by double oxidation to **1**$^{2+}$, the redox chemistry of the ruthenocenyl tosyl hydrazones **2** and **3** was investigated as well. The two ferrocenyl sites of **1** are reversibly oxidized at $E_{1/2}$ = 0.08 V vs FcH/FcH$^+$ (Fc without IHB) and $E_{1/2}$ = 0.57 V (Fc with IHB) (Figure 5a), resulting in disruption of the hydrogen bond upon accumulation of positive charge.[43] Ruthenocenes are quasi-reversibly oxidized in the presence of electrolytes containing weakly coordinating anions.[69,70] At lower temperature, the resulting 17-VE radical cations dimerize to form Ru−Ru bonds.[69,70] The RcH/RcH$^+$ potential is higher than the FcH/FcH$^+$ potential by 0.41 V.[69,70] Expectedly, the cyclic voltammogram of **2** (Figure 5b) shows an irreversible oxidation at E_p = 0.68 V, which is assigned to a double Ru$^{II/III}$ oxidation leading to follow-up reactions such as Ru−Ru bond formation[69,70] and preventing back-reduction to **2**. The mixed metallocenyl tosyl hydrazone **3** (Figure 5c) features a reversible oxidation wave at 0.31 V which is assigned to a reversible oxidation of the ferrocenyl moiety ($E_{1/2}$ = 0.25 V). As this Fc/Fc$^+$ oxidation occurs at the metallocene without IHB, no influence on the IHB is expected. All further Ru-based processes (E_p = 1.20 V) are irreversible and lead to follow-up reactions or decomposition. The irreversible nature of the ruthenocenyl oxidation precludes the use of **2** or **3** as redox switches, in contrast to the electrochemical switching possible in the diferrocenyl tosyl hydrazone **1**.

■ CONCLUSION

Diruthenocenyl tosyl hydrazone **2** features a NH···Ru IHB similar to its 3d homologue diferrocenyl tosyl hydrazone **1** displaying a NH···Fe IHB. The mixed dimetallocenyl hydrazone **3** is obtained as both conceivable Z/E isomers **3a,b** with a NH···Ru IHB and a NH···Fe IHB, respectively. The molecular geometries of **2** and **3a**, including the IHBs, have been fully confirmed by single-crystal XRD. The **3a** isomer with the NH···Ru IHB is thermodynamically favored by 8 kJ mol^{-1}

DOI: 10.1021/acs.organomet.5b00963
Organometallics 2016, 35, 249−257

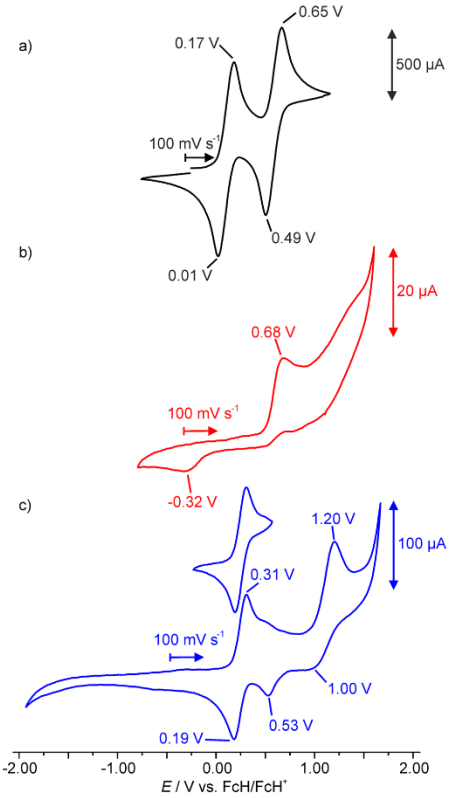

Figure 5. Cyclic voltammograms of (a) **1**[43] (b) **2**, and (c) **3a,b** mixture (10:1) in $[^nBu_4N][B(C_6F_5)_4]/CH_2Cl_2$.

according to DFT calculations. The NH···Ru IHB in **3a** is significantly stronger than the NH···Fe IHB in **1**, as deduced from the different energies of the NH stretching vibrations ($\Delta(-\Delta H)$ = 6 kJ mol^{-1}) and as confirmed by DFT calculations (4 kJ mol^{-1}) on **1** and **3a** with and without IHBs. Interconversion between the *Z*/*E* isomers **3a,b** is achieved by photochemical excitation as well as by protonation and subsequent deprotonation. Together with various protonation studies of metallocenes[44−49,71−74] and XH···M hydrogen-bonding studies,[43,50−53] our results suggest that ferrocene is more easily protonated at the Cp ring than ruthenocene, while ruthenocene forms the more stable NH···M hydrogen bond. Hence, metal-based and ligand-based reactivity patterns are clearly different in these two fundamental metallocenes. The strong IHBs to Fe and Ru will be exploited in the future to design redox- or light-switchable systems and molecular machines based on stable *nonclassical* NH···M hydrogen bonds.

EXPERIMENTAL SECTION

General Procedures. All reactions were performed under an argon atmosphere unless otherwise noted. A glovebox of the type UniLab/MBraun (Ar 4.8, O_2 <1 ppm, H_2O <1 ppm) was used for storage and weighing of sensitive compounds. All analytical samples that required the absence of oxygen were prepared in the same glovebox. Dichloromethane was dried with CaH_2 and distilled prior to use. THF and toluene were distilled from potassium. All reagents were used as received from commercial suppliers (ABCR, Acros Organics, Alfa Aesar, Fischer Scientific, Fluka, and Sigma-Aldrich). Deuterated solvents were purchased from Euriso-top. Ruthenocene,[75] ruthenocene monocarboxylic acid,[76] diruthenocenyl ketone,[55] and ferrocenyl ruthenocenyl ketone[55] were synthesized using literature procedures. The corresponding tosyl hydrazones were obtained similarly to the procedure for diferrocenyl tosyl hydrazone.[43,59,60]

NMR spectra were recorded on a Bruker Avance DRX 400 spectrometer at 400.31 MHz (^{1}H) and 100.07 MHz (^{13}C{^{1}H}). All resonances are reported in ppm vs the solvent signal as internal standard: CD_2Cl_2 (^{1}H, δ 5.32 ppm; ^{13}C, δ 54.0 ppm), d_8-toluene (^{1}H, δ 2.09, 7.09 ppm), $CDCl_3$ (^{1}H, δ 7.26 ppm; ^{13}C, δ 77.2 ppm), d_6-DMSO (^{1}H, δ 2.50 ppm), and d_8-THF (^{1}H, δ 1.72, 3.58 ppm).[77] IR spectra were recorded with a BioRad Excalibur FTS 3100 spectrometer as KBr disks or by using KBr cells in CD_2Cl_2 or $CDCl_3$. Electrochemical experiments were carried out on a BioLogic SP-50 voltammetric analyzer by using a platinum working electrode, a platinum wire as the counter electrode, and a 0.01 M $Ag/AgNO_3$ electrode as the reference electrode. The measurements were carried out at a scan rate of 100 mV s^{-1} for cyclic voltammetry experiments and at 50 mV s^{-1} for square wave voltammetry experiments in 0.1 M $[n\text{Bu}_4\text{N}]][B(C_6F_5)_4]$ as supporting electrolyte in CH_2Cl_2. Potentials are referenced against the decamethylferrocene/decamethylferrocenium couple ($E_{1/2}$ = 550 ± 5 mV vs ferrocene/ferrocenium under our experimental conditions) and are given relative to the ferrocene/ferrocenium couple. UV/vis/NIR spectra were recorded on a Varian Cary 5000 spectrometer by using 1.0 cm cells (Hellma, Suprasil). FD mass spectra were recorded on a Thermo Fisher DFS mass spectrometer with a LIFDI upgrade. Elemental analyses were performed by the microanalytical laboratory of the chemical institutes of the University of Mainz.

Density Functional Theory Calculations. Density functional theory calculations were carried out with the Gaussian09/DFT series[78] of programs. The B3LYP[79] formulation of density functional theory was used employing the LANL2DZ[80−83] basis set. No symmetry constraints were imposed on the molecules. The presence of energy minima of the ground states was checked by analytical frequency calculations. Solvent modeling was done employing the integral equation formalism polarizable continuum model (IEFPCM, dichloromethane). The approximate free energies at 298 K were obtained through thermochemical analysis of the frequency calculation, using the thermal correction to Gibbs free energy as reported by Gaussian09. Grimme's D3 dispersion correction[84] favors all systems with an IHB by 10 kJ mol^{-1} relative to the respective non-hydrogen-bonded structure. The relative stability of **3a,b** is hence not affected.

Crystal Structure Determination. Intensity data were collected with a Bruker AXS Smart1000 CCD diffractometer with an APEX II detector and an Oxford cooling system and corrected for absorption and other effects using Mo Kα radiation (λ = 0.71073 Å). The diffraction frames were integrated using the SAINT package, and most were corrected for absorption with MULABS.[85,86] The structures were solved by direct methods and refined by the full-matrix method based on F^2 using the SHELXTL software package.[87,88] All non-hydrogen atoms were refined anisotropically, while the positions of all hydrogen atoms were generated with appropriate geometric constraints and allowed to ride on their respective parent carbon/nitrogen atoms with fixed isotropic thermal parameters. H2N of **2** and **3a** was found in the difference Fourier map with further riding refinement with a fixed N2−H2N distance of 0.88 Å. See the Supporting Information for crystal data of **1**,[43] **2**, and **3a**. CCDC-1426094 and CCDC-1426095 contain supplementary crystallographic data for this paper. These data

DOI: 10.1021/acs.organomet.5b00963
Organometallics 2016, 35, 249−257

can be obtained free of charge from The Cambridge Crystallographic Data Centre via www.ccdc.cam.ac.uk/data_request/cif.

Diruthenocenyl Tosyl Hydrazone (2). Diruthenocenyl ketone (600 mg, 1.23 mmol, 1 equiv), *p*-toluenesulfonyl hydrazide (456 mg, 2.45 mmol, 2 equiv), and *p*-toluenesulfonic acid (6 mg, 0.03 mmol, 0.02 equiv) were dissolved in toluene (40 mL) and heated to reflux for 19 h. Purification via column chromatography (silica, 20 cm × 7 cm, dichloromethane, R_f = 0.2) yielded 370 mg of **2** (0.56 mmol, 45.5%) as a yellow powder after removing the solvent under reduced pressure.

Suitable crystals for structure determination were obtained by dissolving 50 mg of **2** in chloroform (5 mL). Subsequent diffusion of diethyl ether into this solution resulted in pale yellow rodlike crystals.

^{1}H NMR ($CDCl_3$): δ 9.70 (s, 1 H, H^6), 7.92 (d, ^3J = 8 Hz, 2 H, H^4), 7.38 (d, ^3J = 8 Hz, 2 H, H^3), 5.04 (pt, ^3J = 2 Hz, 2 H, H^9), 5.00 (pt, ^3J = 2 Hz, 2 H, H^{13}), 4.74 (pt, ^3J = 2 Hz, 2 H, H^{10}), 4.65 (pt, ^3J = 2 Hz, 2 H, H^{14}), 4.57 (s, 5 H, H^{11}), 4.33 (s, 5 H, H^{15}), 2.46 (s, 3 H, H^1) ppm. ^{13}C NMR ($CDCl_3$): δ 148.4 (C^7), 144.0 (C^2), 135.9 (C^5), 129.4 (C^3), 128.2 (C^4), 85.6 (C^{12}), 76.4 (C^8), 72.6 (C^9, C^{10}), 72.2 (C^{11}), 72.0 (C^{14}), 71.8 (C^{15}), 71.1 (C^{13}), 21.8 (C^1) ppm. MS (FD): *m*/*z* 658.0 (M^+). IR (KBr): $\tilde{\nu}$ 457 (s), 552 (s), 682 (s), 812 (s), 1166 (s), 1342 (s), 1402 (m), 2785 (w), 2922 (w), 2958 (sh), 2976 (sh), 3003 (s, br), 3086 (w), 3094 (w), 3102 (w), 3116 (w) cm^{-1}. IR ($CDCl_3$): $\tilde{\nu}$ 554 (s), 821 (s), 1167 (vs), 1344 (s), 1400 (m), 2262 (s), 2872 (w), 2928 (w), 2965 (w), 3028 (s, br), 3099 (w), 3175 (w) cm^{-1}. UV/vis (CH_2Cl_2): λ_{max} (ε) 235 (14200), 254 (11050), 284 (5080), 330 (2590 M^{-1} cm^{-1}) nm. CV (CH_2Cl_2, vs FcH/FcH$^+$): $E_{p,ox}$ = 0.68 V, $E_{p,red}$ = −0.32 V. Anal. Calcd for $C_{28}H_{26}N_2O_2Ru_2S$ (656.7): C, 51.21; H, 3.99; N, 4.27; S, 4.88. Found: C, 50.78; H, 3.76; N, 4.18; S, 5.35.

^{D}2. **2** (100 mg, 0.15 mmol, 1 equiv) was dissolved in THF (5 mL), and dichloromethane (4 mL), D_2O (1 mL), and one drop of of concentrated aqueous hydrochloric acid were added. The solution was stirred for 2 h at room temperature. The solvents were removed under reduced pressure. The degree of deuterium incorporation at the NH group was 58% as estimated by ^{1}H NMR spectroscopy.

Ferrocenyl Ruthenocenyl Tosyl Hydrazone (3a,b). A mixture of ferrocenyl ruthenocenyl ketone (600 mg, 1.35 mmol, 1 equiv), *p*-toluenesulfonyl hydrazide (500 mg, 2.69 mmol, 2 equiv), and *p*-toluenesulfonic acid (5.4 mg, 0.03 mmol, 0.02 equiv) was heated in toluene (30 mL) to reflux for 19 h. Purification via column chromatography (silica, 20 cm × 7 cm, dichloromethane, R_f = 0.2) yielded 330 mg of a 10:1 mixture of **3a,b** (0.54 mmol, 39.9%) as an orange powder after removing the solvent under reduced pressure. The isomeric ratio was determined by ^{1}H NMR spectroscopy.

Suitable crystals for structure determination were obtained by dissolving 50 mg of **3a,b** in chloroform (5 mL). Subsequent diffusion of diethyl ether into this solution resulted in red rodlike crystals. In the measured crystal only **3a** is present without any disorder.

^{1}H NMR for **3a** ($CDCl_3$): δ 9.82 (s, 1 H, H^6), 7.99 (d, ^3J = 8 Hz, 2 H, H^4), 7.42 (d, ^3J = 8 Hz, 2 H, H^3), 5.08 (pt, ^3J = 2 Hz, 2 H, H^9), 4.80 (pt, ^3J = 2 Hz, 2 H, H^{10}), 4.65 (pt, ^3J = 2 Hz, 2 H, H^{13}), 4.63 (s, 5 H, H^{11}), 4.31 (pt, ^3J = 2.0 Hz, 2H, H^{14}), 3.93 (s, 5 H, H^{15}), 2.45 (s, 3 H, H^1) ppm. ^{1}H NMR for **3b** ($CDCl_3$): δ 10.06 (s, 1 H, H^6), 7.96 (2 H, H^4), 7.38 (2 H, H^3), 4.94 (pt, ^3J = 2 Hz, 2 H, H^{13}), 4.71 (pt, ^3J = 2 Hz, 2 H, H^9), 4.63 (2 H, H^{14}), 4.46 (pt, ^3J = 2 Hz, 2 H, H^{10}), 4.41 (s, 5 H, H^{15}), 4.14 (s, 5 H, H^{11}), 2.45 (s, 3 H, H^1) ppm. ^{13}C NMR for **3a** ($CDCl_3$): δ 148.9 (C^7), 144.0 (C^2), 135.9 (C^5), 129.4 (C^3), 128.3 (C^4), 82.2 (C^{12}), 76.6 (C^8), 72.6 (C^{10}), 72.5 (C^9), 72.4 (C^{11}), 70.0 (C^{14}), 69.7 (C^{15}), 68.6 (C^{13}), 21.8 (C^1) ppm. MS (FD): *m*/*z* 612.0 (M^+). IR (KBr): $\tilde{\nu}$ = 554 (s), 814 (s), 1049 (s), 1165 (s), 1342 (s), 2777 (w), 2922 (w), 2964 (sh), 3001 (s, br), 3117 (w), 3094 (w), 3084 (w) cm^{-1}. IR ($CDCl_3$): $\tilde{\nu}$ 554 (s), 816 (s), 1165 (s), 1344 (s), 1400 (m), 2261 (s), 2857 (w), 2925 (w), 3030 (s, br), 3099 (w), 3149 (w) cm^{-1}. UV/vis (CH_2Cl_2): λ_{max} (ε) 236 (14540), 295 (7290), 350 (1510), 455 (430 M^{-1} cm^{-1}) nm. CV (CH_2Cl_2, vs FcH/FcH$^+$): $E_{1/2}$ = 0.25 V, $E_{p,ox}$ = 1.20 V, $E_{p,red}$ = 0.53, 1.00 V. Anal. Calcd for $C_{28}H_{26}FeN_2O_2RuS$ (611.5): C, 55.00; H, 4.29; N, 4.58; S, 5.24. Found: C, 53.66; H, 4.15; N, 4.37; S, 5.35.

■ ASSOCIATED CONTENT

Supporting Information

The Supporting Information is available free of charge on the ACS Publications website at DOI: 10.1021/acs.organomet.5b00963.

Crystallographic data for **2** (CIF)
Crystallographic data for **3a** (CIF)
Cartesian coordinates of DFT optimized structures (XYZ)
X-ray crystallographic data of **1**, **2**, and **3a**, ^{1}H NMR spectra of **1**, **2** and **3a,b** in $CDCl_3$ and in d_6-DMSO, ^{13}C NMR spectra of **2** and **3a,b**, variable-temperature ^{1}H NMR spectra of **3a,b** in d_8-toluene up to 100 °C, UV/vis spectra of **2** and **3a,b** in CH_2Cl_2 together with TD-DFT calculations of the major transitions, a plot showing the percentage of **3a** after irradiation of a **3a,b** mixture with a 400 nm LED torch, UV/vis spectra of a **3a,b** mixture with addition of TFA and K_2CO_3, ^{1}H NMR spectra of a **3a,b** mixture in CH_2Cl_2 after addition of TFA and K_2CO_3, and IR spectra of **1**, **2** and **3a,b** in the solid state (PDF)

■ AUTHOR INFORMATION

Corresponding Authors

*C.F.: e-mail, cfoerster@uni-mainz.de.
*K.H.: fax, +49 6131 39-27277; e-mail, katja.heinze@uni-mainz.de.

Notes

The authors declare no competing financial interest.

■ ACKNOWLEDGMENTS

We are grateful to Prof. Benno Bildstein (University of Innsbruck, Innsbruck, Austria) for inspiring discussions and preparative advice concerning ruthenocenyl ketones. We thank Regine Jung-Pothmann for the collection of the diffraction data and the Johannes Gutenberg University of Mainz (Germany) for financial support to C.F. (Internal University Research Funding).

■ REFERENCES

(1) Kabsch, W.; Sander, C. *Biopolymers* **1983**, *22*, 2577−2637.
(2) Doyle, A. G.; Jacobsen, E. N. *Chem. Rev.* **2007**, *107*, 5713−5743.
(3) Taylor, M. S.; Jacobsen, E. N. *Angew. Chem., Int. Ed.* **2006**, *45*, 1520−1543; *Angew. Chem.* **2006**, *118*, 1550−1573.
(4) Braga, D.; Grepioni, F.; Tedesco, E.; Biradha, K.; Desiraju, G. R. *Organometallics* **1997**, *16*, 1846−1856.
(5) Braga, D.; Grepioni, F.; Desiraju, G. R. *Chem. Rev.* **1998**, *98*, 1375−1406.
(6) Braga, D.; Grepioni, F. *Acc. Chem. Res.* **2000**, *33*, 601−608.
(7) Epstein, L. M.; Shubina, E. S. *Coord. Chem. Rev.* **2002**, *231*, 165−181.
(8) Braga, D. *Chem. Commun.* **2003**, 2751−2754.
(9) Brammer, L. *Dalton Trans.* **2003**, 3145−3157.
(10) Moriuchi, T.; Hirao, T. *Chem. Soc. Rev.* **2004**, *33*, 294−301.
(11) Heinze, K.; Beckmann, M. *Eur. J. Inorg. Chem.* **2005**, *2005*, 3450−3457.
(12) Kirin, S. I.; Kraatz, H.-B.; Metzler-Nolte, N. *Chem. Soc. Rev.* **2006**, *35*, 348−354.
(13) Lapić, J.; Siebler, D.; Heinze, K.; Rapić, V. *Eur. J. Inorg. Chem.* **2007**, *2007*, 2014−2024.
(14) Heinze, K.; Wild, U.; Beckmann, M. *Eur. J. Inorg. Chem.* **2007**, *2007*, 617−623.
(15) Djaković, S.; Siebler, D.; Semenčić, M. Č.; Heinze, K.; Rapić, V. *Organometallics* **2008**, *27*, 1447−1453.

DOI: 10.1021/acs.organomet.5b00963
Organometallics 2016, 35, 249−257

(16) Lataifeh, A.; Beheshti, S.; Kraatz, H.-B. *Eur. J. Inorg. Chem.* **2009**, *2009*, 3205−3218.
(17) Semenčić, M. Č.; Siebler, D.; Heinze, K.; Rapić, V. *Organometallics* **2009**, *28*, 2028−2037.
(18) Hirao, T. *J. Organomet. Chem.* **2009**, *694*, 806−811.
(19) Semenčić, M. Č.; Heinze, K.; Förster, C.; Rapić, V. *Eur. J. Inorg. Chem.* **2010**, *2010*, 1089−1097.
(20) Moriuchi, T.; Hirao, T. *Acc. Chem. Res.* **2010**, *43*, 1040−1051.
(21) Martić, S.; Labib, M.; Shipman, P. O.; Kraatz, H.-B. *Dalton Trans.* **2011**, *40*, 7264−7290.
(22) Förster, C.; Kovačević, M.; Barišić, L.; Rapić, V.; Heinze, K. *Organometallics* **2012**, *31*, 3683−3694.
(23) Lapić, J.; Pavlović, G.; Siebler, D.; Heinze, K.; Rapić, V. *Organometallics* **2008**, *27*, 726−735.
(24) Lapić, J.; Djaković, S.; Cetina, M.; Heinze, K.; Rapić, V. *Eur. J. Inorg. Chem.* **2010**, *2010*, 106−114.
(25) Kovač, V.; Radolović, K.; Habuš, I.; Siebler, D.; Heinze, K.; Rapić, V. *Eur. J. Inorg. Chem.* **2009**, *2009*, 389−399.
(26) Desiraju, G. R.; Steiner, T. *The Weak Hydrogen Bond in Chemistry and Biology*; Oxford University Press: Oxford, U.K., 1999.
(27) Steiner, T. *Angew. Chem., Int. Ed.* **2002**, *41*, 48−76; *Angew. Chem.* **2002**, *114*, 50−80.
(28) Okamura, T.-a.; Sakauye, K.; Ueyama, N.; Nakamura, A. *Inorg. Chem.* **1998**, *37*, 6731−6736.
(29) Heinze, K.; Schlenker, M. *Eur. J. Inorg. Chem.* **2004**, *2004*, 2974−2988.
(30) Heinze, K.; Siebler, D. *Z. Anorg. Allg. Chem.* **2007**, *633*, 2223−2233.
(31) Siebler, D.; Förster, C.; Heinze, K. *Dalton Trans.* **2011**, *40*, 3558−3575.
(32) Siebler, D.; Linseis, M.; Gasi, T.; Carrella, L. M.; Winter, R. F.; Förster, C.; Heinze, K. *Chem. - Eur. J.* **2011**, *17*, 4540−4551.
(33) Kienz, T.; Förster, C.; Heinze, K. *Organometallics* **2014**, *33*, 4803−4812.
(34) Fukuzumi, S.; Yoshida, Y.; Okamoto, K.; Imahori, H.; Araki, Y.; Ito, O. *J. Am. Chem. Soc.* **2002**, *124*, 6794−6795.
(35) Neidlinger, A.; Ksenofontov, V.; Heinze, K. *Organometallics* **2013**, *32*, 5955−5965.
(36) Melomedov, J.; Ochsmann, J. R.; Meister, M.; Laquai, F.; Heinze, K. *Eur. J. Inorg. Chem.* **2014**, *2014*, 2902−2915.
(37) Beer, P. D.; Cadman, J. *Coord. Chem. Rev.* **2000**, *205*, 131−155.
(38) Beer, P. D.; Gale, P. A. *Angew. Chem., Int. Ed.* **2001**, *40*, 486−516; *Angew. Chem.* **2001**, *113*, 502−532.
(39) Beer, P. D.; Bayly, S. R. *Top. Curr. Chem.* **2005**, *255*, 125−162.
(40) Heinze, K.; Schlenker, M. *Eur. J. Inorg. Chem.* **2005**, *2005*, 66−71.
(41) Molina, P.; Tárraga, A.; Caballero, A. *Eur. J. Inorg. Chem.* **2008**, *2008*, 3401−3417.
(42) Siebler, D.; Förster, C.; Heinze, K. *Eur. J. Inorg. Chem.* **2010**, *2010*, 523−527.
(43) Förster, C.; Veit, P.; Ksenofontov, V.; Heinze, K. *Chem. Commun.* **2015**, *51*, 1514−1516.
(44) Floris, B.; Illuminati, G.; Ortaggi, G. *Tetrahedron Lett.* **1972**, *13*, 269−272.
(45) Floris, B.; Illuminati, G.; Jones, P. E.; Ortaggi, G. *Coord. Chem. Rev.* **1972**, *8*, 39−43.
(46) Curphey, T. J.; Santer, J. O.; Rosenblum, M.; Richards, J. H. *J. Am. Chem. Soc.* **1960**, *82*, 5249−5250.
(47) Shubina, E. S.; Krylov, A. N.; Kreindlin, A. Z.; Rybinskaya, M. I.; Epstein, L. M. *J. Organomet. Chem.* **1994**, *465*, 259−262.
(48) Cerichelli, G.; Illuminati, G.; Ortaggi, G.; Maria Giuliani, A. *J. Organomet. Chem.* **1977**, *127*, 357−370.
(49) Mueller-Westerhoff, U. T.; Haas, T. J.; Swiegers, G. F.; Leipert, T. K. *J. Organomet. Chem.* **1994**, *472*, 229−246.
(50) Shubina, E. S.; Krylov, A. N.; Kreindlin, A. Z.; Rybinskaya, M. I.; Epstein, L. M. *J. Mol. Struct.* **1993**, *301*, 1−5.
(51) Baker, A. W.; Bublitz, D. E. *Spectrochim. Acta* **1966**, *22*, 1787−1799.
(52) Shubina, Y.; Epstein, L. M. *J. Mol. Struct.* **1992**, *265*, 367−384.
(53) Trifan, D. S.; Bacskai, R. *J. Am. Chem. Soc.* **1960**, *82*, 5010−5011.
(54) Saloman, S.; Hildebrandt, A.; Korb, M.; Schwind, M.; Lang, H. *Z. Anorg. Allg. Chem.* **2015**, *641*, 2282−2290.
(55) Denifl, P. Ph.D. Thesis, University of Innsbruck, Innsbruck, Austria, 1994.
(56) Rausch, M. D.; Fischer, E. O.; Grubert, H. *J. Am. Chem. Soc.* **1960**, *82*, 76−82.
(57) Small, G. J.; Trotter, J. *Can. J. Chem.* **1964**, *42*, 1746−1748.
(58) Watanabe, M.; Motoyama, I.; Sano, H. *Inorg. Chim. Acta* **1994**, *225*, 103−109.
(59) Kay, K.-Y.; Kim, L. H.; Oh, I. C. *Tetrahedron Lett.* **2000**, *41*, 1397−1400.
(60) Bildstein, B. *J. Organomet. Chem.* **2001**, *617*−*618*, 28−38.
(61) Su, X.; Aprahamian, I. *Chem. Soc. Rev.* **2014**, *43*, 1963−1981.
(62) Roy, S.; Nangia, A. *Cryst. Growth Des.* **2007**, *7*, 2047−2058.
(63) Belkova, N. V.; Shubina, E. S.; Gutsul, E. I.; Epstein, L. M.; Eremenko, I. L.; Nefedov, S. E. *J. Organomet. Chem.* **2000**, *610*, 58−70.
(64) CSD search (ConQuest) (www.ccdc.cam.ac.uk) on October 13th, 2015. Search parameters: Ru···H−X, X = element of groups 15−17: *d*(Ru-H) = 2.0−3.2 Å (3−50 bonds), *d*(Ru−X) = 2.0−4.2 A (2−50 bonds). Results: OH···Ru = 2.969 Å,[65] NH···Ru = 3.161 Å,[66] NH···Ru = 3.137 Å.[67]
(65) Maschke, M.; Alborzinia, H.; Lieb, M.; Wölfl, S.; Metzler-Nolte, N. *ChemMedChem* **2014**, *9*, 1188−1194.
(66) Ramakrishnan, S.; Srinivasan, A. *Org. Lett.* **2007**, *9*, 4769−4772.
(67) Enders, M.; Kohl, G.; Pritzkow, H. *Organometallics* **2002**, *21*, 1111−1117.
(68) Bildstein, B.; Denifl, P.; Wurst, K. *J. Organomet. Chem.* **1995**, *496*, 175−186.
(69) Swarts, J. C.; Nafady, A.; Roudebush, J. H.; Trupia, S.; Geiger, W. E. *Inorg. Chem.* **2009**, *48*, 2156−2165.
(70) Trupia, S.; Nafady, A.; Geiger, W. E. *Inorg. Chem.* **2003**, *42*, 5480−5482.
(71) Borisov, Y. A.; Ustynyuk, N. A. *Russ. Chem. Bull.* **2002**, *51*, 1900−1908.
(72) Sharma, N.; Ajay, J. K.; Venkatasubbaiah, K.; Lourderaj, U. *Phys. Chem. Chem. Phys.* **2015**, *17*, 22204−22209.
(73) Evchenko, S. V.; Kamounah, F. S.; Schaumburg, K. *J. Labelled Compd. Radiopharm.* **2005**, *48*, 209−218.
(74) Meot-Ner, M. *J. Am. Chem. Soc.* **1989**, *111*, 2830−2834.
(75) Kündig, E. P.; Monnier, F. R. *Adv. Synth. Catal.* **2004**, *346*, 901−904.
(76) Hellmuth, T.; Rieckhoff, S.; Weiss, M.; Dorst, K.; Frey, W.; Peters, R. *ACS Catal.* **2014**, *4*, 1850−1858.
(77) Fulmer, G. R.; Miller, A. J. M.; Sherden, N. H.; Gottlieb, H. E.; Nudelman, A.; Stoltz, B. M.; Bercaw, J. E.; Goldberg, K. I. *Organometallics* **2010**, *29*, 2176−2179.
(78) Frisch, M. J.; Trucks, G. W.; Schlegel, H. B.; Scuseria, G. E.; Robb, M. A.; Cheeseman, J. R.; Scalmani, G.; Barone, V.; Mennucci, B.; Petersson, G. A.; Nakatsuji, H.; Caricato, M.; Li, X.; Hratchian, H. P.; Izmaylov, A. F.; Bloino, J.; Zheng, G.; Sonnenberg, J. L.; Hada, M.; Ehara, M.; Toyota, K.; Fukuda, R.; Hasegawa, J.; Ishida, M.; Nakajima, T.; Honda, Y.; Kitao, O.; Nakai, H.; Vreven, T.; Montgomery, J. A., Jr.; Peralta, J. E.; Ogliaro, F.; Bearpark, M.; Heyd, J. J.; Brothers, E.; Kudin, K. N.; Staroverov, V. N.; Kobayashi, R.; Normand, J.; Raghavachari, K.; Rendell, A.; Burant, J. C.; Iyengar, S. S.; Tomasi, J.; Cossi, M.; Rega, N.; Millam, J. M.; Klene, M.; Knox, J. E.; Cross, J. B.; Bakken, V.; Adamo, C.; Jaramillo, J.; Gomperts, R.; Stratmann, R. E.; Yazyev, O.; Austin, A. J.; Cammi, R.; Pomelli, C.; Ochterski, J. W.; Martin, R. L.; Morokuma, K.; Zakrzewski, V. G.; Voth, G. A.; Salvador, P.; Dannenberg, J. J.; Dapprich, S.; Daniels, A. D.; Farkas, Ö.; Foresman, J. B.; Ortiz, J. V.; Cioslowski, J.; Fox, D. J. *Gaussian09, Revision A.02*; Gaussian, Inc., Wallingford CT, 2009.
(79) Becke, A. D. *J. Chem. Phys.* **1993**, *98*, 5648−5652.
(80) Dykstra, C. E. *Chem. Phys. Lett.* **1977**, *45*, 466−469.
(81) Hay, P. J.; Wadt, W. R. *J. Chem. Phys.* **1985**, *82*, 299−310.
(82) Hay, P. J.; Wadt, W. R. *J. Chem. Phys.* **1985**, *82*, 270−283.
(83) Wadt, W. R.; Hay, P. J. *J. Chem. Phys.* **1985**, *82*, 284−298.

DOI: 10.1021/acs.organomet.5b00963
Organometallics 2016, 35, 249−257

(84) Grimme, S.; Antony, J.; Ehrlich, S.; Krieg, H. *J. Chem. Phys.* **2010**, *132*, 154104.
(85) *SMART Data Collection and SAINT-Plus Data Processing Software for the SMART System (various versions)*; Bruker Analytical X-Ray Instruments, Inc., Madison, WI, 2000.
(86) Blessing, B. *Acta Crystallogr., Sect. A: Found. Crystallogr.* **1995**, *51*, 33–38.
(87) Sheldrick, G. M. *SHELXTL, Version 5.1*; Bruker AXS, Madison, WI, 1998.
(88) Sheldrick, G. M. *SHELXL-97*; University of Göttingen, Göttingen, Germany, 1997.

DOI: 10.1021/acs.organomet.5b00963
Organometallics 2016, 35, 249–257

3.2 Preparation, Properties, and Reactivity of (Aminoferrocenyl) (ferrocenyl) carbene (pentacarbonyl) chromium(0) as Bulky Isolobal Trimetallo-amide

Philipp Veit, Christoph Förster,* Sebastian Seibert, and Katja Heinze*

Z. Anorg. Allg. Chem. **2015**, *641*, 2083–2092.

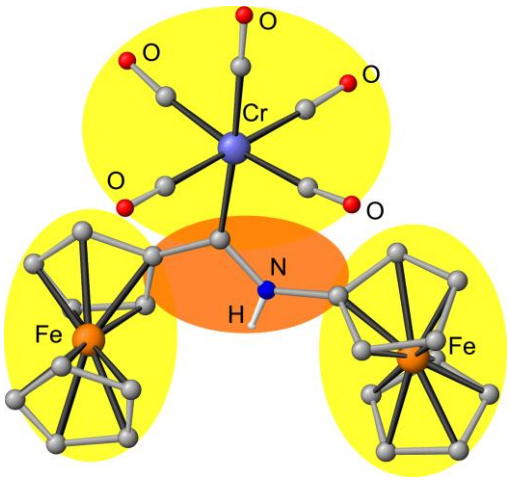

Nucleophilic substitution of the ethoxy substituent in the Fischer carbene complex (ethoxy) (ferrocenyl) carbene (pentacarbonyl) chromium(0) by ferrocenyl amide gives the hetero trimetallic complex (aminoferrocenyl) (ferrocenyl) carbene (pentacarbonyl) chromium(0) (**1**). As the $Cr(CO)_5$ fragment is isolobal to oxygen or sulfur the carbene complex can be viewed as an isolobal metallo analogue to di ferrocenylamide (Fc)(FcNH)C=O and diferrocenyl-thioamide (Fc)(FcNH)C=S. The impact of the formal replacement of O/S by $Cr(CO)_5$ is studied with respect to steric and electronic consequences as well as reactivity by spectroscopic, diffraction, electrochemical and theoretical methods.

Author contributions

1 was first synthesized by Sebastian Seibert during a research internship in the Heinze group under the supervision of Christoph Förster. Single crystals suitable for XRD analysis were isolated by Sebastian Seibert. The crystal structure was solved and refined by Christoph Förster. The optimization of the synthesis strategy for **1** was done by Philipp Veit during his diploma thesis and the beginning of his PhD thesis, as well as the full characterization and all other experiments. All DFT calculations were performed by Philipp Veit. The manuscript was written by Philipp Veit (20 %) Christoph Förster (40 %) and Katja Heinze (40 %).

Supporting Information

for this article is found in Chapter 6.2 at pp. 117. For full Supporting Information containing a List of DFT calculated electronic transitions and the coordinates of all relevant DFT calculated structures, refer to:

https://onlinelibrary.wiley.com/action/downloadSupplement?doi=10.1002%2Fzaac.201500562&file=zaac_201500562_sm_miscellaneous_information.pdf

“Reprinted with the permission of Veit, P.; Förster, C.; Seibert, S.; Heinze, K.; *Z. Anorg. Allg. Chem.* **2015**, *641*, 2083–2092. Copyright © 2015 WILEY-VCH Verlag GmbH & Co. KGaA, Weinheim”

Journal of Inorganic and General Chemistry
ZAAC
Zeitschrift für anorganische und allgemeine Chemie
www.zaac.wiley-vch.de
ARTICLE

DOI: 10.1002/zaac.201500562

Preparation, Properties, and Reactivity of (Aminoferrocenyl)(ferrocenyl) carbene(pentacarbonyl)chromium(0) as Bulky Isolobal Trimetallo-amide

Philipp Veit,[a] Christoph Förster,*[a] Sebastian Seibert,[a] and Katja Heinze*[a]

Dedicated to Professor F. Ekkehardt Hahn on the Occasion of His 60th Birthday

Keywords: Carbene; Chromium; Ferrocene; Fischer carbene complex; Imine

Abstract. Nucleophilic substitution of the ethoxy substituent in the Fischer carbene complex (ethoxy)(ferrocenyl)carbene(pentacarbonyl) chromium(0) (**1**) by ferrocenyl amide [Fc-NH]$^-$ [**2**-H]$^-$ gives the hetero trimetallic complex (aminoferrocenyl)(ferrocenyl)carbene (pentacarbonyl)chromium(0) (**3**). As the $Cr(CO)_5$ fragment is isolobal to oxygen or sulfur **3** can be viewed as an isolobal metallo analogue to diferrocenylamide (Fc)(FcNH)C=O (**4**) and diferrocenylthioamide (Fc)(FcNH)C=S (**5**). The impact of the formal replacement of O/S by $Cr(CO)_5$ in **3** is studied with respect to steric and electronic consequences as well as reactivity by spectroscopic, diffraction, electrochemical and theoretical methods.

Introduction

Since the reports of the first example of a carbene complex (Me)(OMe)C=W(CO)$_5$ by *E. O. Fischer* 50 years ago[1] and of a stable *N*-heterocyclic carbene by *A. J. Arduengo* almost 30 years later,[2] carbenes and their transition metal complexes have attracted considerable and still growing attention,[3,4] especially in the fields of organometallic catalysis and organic synthesis.[5] An interesting sub-class are carbenes with ferrocenyl (Fc) or nonamethylferrocenyl (Fc*) substituents, respectively. The Fc substituent can be directly bound to the carbene carbon atom (α-ferrocenyl carbenes, Scheme 1a: **I**–**III**), attached directly or indirectly to the nitrogen atom in N-heterocyclic carbenes (NHCs, Scheme 1a: **IV**, **V**) or located in the backbone of NHCs (Scheme 1a: **VI**).[6–10] The ferrocenyl unit introduces reversible redox-switching in the carbenes[11] and their complexes, e.g. in ferrocenyl-appended Grubbs-Hoyveda catalysts[12] or Grubbs II catalysts.[13] A ferrocenophane backbone in NHCs **VI** (Scheme 1a) increases their reactivity towards the addition of small molecules, such as ammonia or carbon monoxide.[14] Planar chirality can be achieved in ferrocenyl carbenes as well.[6b,15] The strong electron donating power of Fc groups stabilizes electron deficient centres as found for example in α-ferrocenyl carbenium ions.[16] Consequently, a strong motivation in the efforts towards the preparation of α-ferrocenyl carbenes is to stabilize the carbene center by an electron-donating Fc substituent. In spite of extensive studies, only a single persistent α-ferrocenyl carbene, namely (Fc*)(N*i*Pr$_2$)C **III**, bearing a Fc* substituent in the α position of the carbene carbon atom has been reported so far by *G. Bertrand*.[7] This report and earlier studies underline that Fc or Fc* units are rather classified as spectator substituents similar to aryl substituents.[5,8] Access to "protected" α-ferrocenyl carbenes is provided via Fischer carbene complexes. This route gives the opportunity of a post-modification of the carbene ligand in the complex, e.g. via nucleophilic substitution. The first (ferrocenyl)(alkoxy)carbene(pentacarbonyl)metal(0) representatives (Cr, Mo, W) were already prepared by *E. O. Fischer*.[17] Their electrochemical properties[18] and reactivity[19] have been subsequently investigated as well. Post-functionalization to (amino)(ferrocenyl)(pentacarbonyl) metal(0) complexes is readily achieved by treating (Fc)(*R*O)C=*M*(CO)$_5$ (*R* = alkyl, *M* = Cr, Mo, W) with saturated or unsaturated amines,[17,20] according to the classical procedure by *E. O. Fischer*.[21]

The isolobal relationship of *M*(CO)$_5$ (*M* = Cr, Mo, W) complex fragments and the chalcogens O and S[5e] has been utilized in the synthesis of ferrocenyl thioesters and thio- and selenoamides (Fc)(*R*)C=*X* [*X* = S; *R* = OEt, NH*R*′; *R*′ = H, Me, Et, Pr; *X* = Se: *R* = NH*R*′; *R*′ = $(CH_2)_n$OH, *n* = 1–3, CH_2(C(H)OH)Me, CH_2(C(H)OH)Me], as formal oxidation products of corresponding Fischer carbene complexes (Fc)(*R*)C=*M*(CO)$_5$ [*X* = S: *R* = OEt, NH*R*′; *R*′ = H, Me, Et, Pr, *M* = Cr, Mo, W; *X* = Se: R = NH*R*′; *R*′ = $(CH_2)_n$OH, *n* = 1–3, CH_2(C(H)OH)Me, CH_2(C(H)OH)Me, *M* = Cr].[20a,20b] From this perspective, we envisaged the title compound (Fc)(NHFc)C=Cr(CO)$_5$ (**3**) as a metallo amide analogous to

* Dr. C. Förster
E-Mail: cfoerster@uni-mainz.de
* Prof. Dr. K. Heinze
Fax: +49-6131-39-27277
E-Mail: katja.heinze@uni-mainz.de
[a] Institute of Inorganic Chemistry and Analytical Chemistry
Johannes Gutenberg-University of Mainz
Duesbergweg 10–14
55128 Mainz, Germany
Supporting information for this article is available on the WWW under **http://dx.doi.org/10.1002/zaac.201500562** or from the author.

Dedicated Cluster

 © 2015 WILEY-VCH Verlag GmbH & Co. KGaA, Weinheim

Journal of Inorganic and General Chemistry
ZAAC
Zeitschrift für anorganische und allgemeine Chemie
www.zaac.wiley-vch.de
ARTICLE

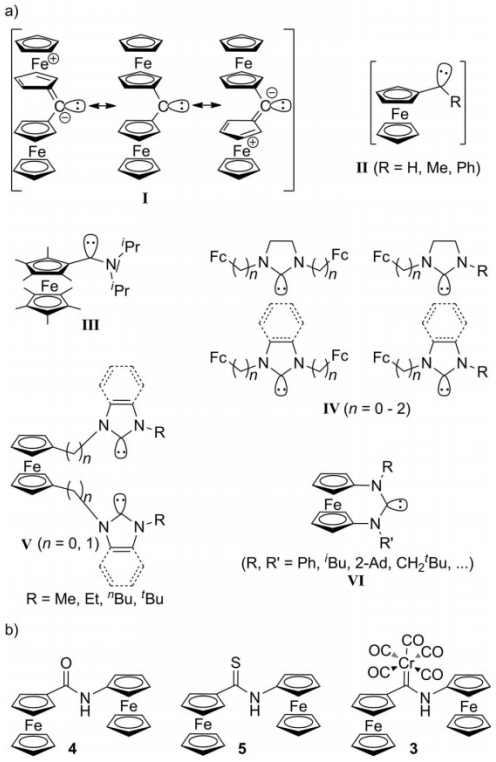

Scheme 1. (a) Selected types of ferrocenyl containing carbenes: elusive diferrocenyl carbene **I**,[6] α-ferrocenyl carbenes **II**,[7] nonamethylferrocenyl(diisopropylamino)carbene **III**,[8] ferrocenyl-substituted NHCs **IV**, **V**,[6,9] [3]ferrocenophane-NHCs **VI**;[10] and (b) diferrocenyl amide **4** (X = O),[22a] diferrocenyl thioamide **5** (X = S),[22b] and (aminoferrocenyl)(ferrocenyl)carbene(pentacarbonyl) chromium(0) complex (**3**) [X = $Cr(CO)_5$] (this study).

the respective diferrocenyl chalcogene amides (Fc)(NHFc)C=X (Scheme 1b, **4**: X = O; **5**: X = S) in addition to the description of **3** as a novel oligometallic heteroatom stabilized Fischer carbene complex.[17e,23]

Oligoferrocenyl complexes with amide bridges show distinct secondary zigzag structures with intramolecular NH···O hydrogen bonds in solution similar to α-helices of organic peptides in competition with intermolecular NH···O hydrogen bonds in the solid state.[24,25] While ferrocenyl carboxamides (X = O) prefer intramolecular hydrogen bonding patterns with eight-membered rings, the homologous thioamides (X = S) form six-membered rings with intramolecular NH···S hydrogen bonds.[22,24,25] This demonstrates that rather small changes (O → S) already result in larger structural rearrangements. For carboxamides (Fc)(NHR)C=O the *trans* amide configuration is generally strongly favoured with respect to the *cis* amide, while some thioamides, such as (Fc)(NHMe)C=S, feature both configurations.[22] With respect to electronic communication of the ferrocenyl substituents in oligoferrocenyl (thio)amides via the (thio)amide bridge the differences are only marginal. Electronic coupling of the redox sites (H_{AB} = 140–260 cm^{-1}) within the Robin-Day class II[26] mixed-valent species [(Fc)(NHFc)C=X]$^+$ (X = O, S) is essentially independent of X. In all cases reported so far, the first oxidation to mixed-valent cations [(Fc)(NHFc)C=X]$^+$ is largely localized on the *N*-substituted ferrocenyl unit as expected from the electron donating character of the substituent.[22]

The following study aims to elucidate the impact of the formal substitution of oxygen or sulfur with the electropositive sterically demanding isolobal $Cr(CO)_5$ fragment in Fc(NHFc)C=X [**3**: X = $Cr(CO)_5$; **4**: X = O; **5**: X = S]. In particular, in this study we address the effect of the bulky $Cr(CO)_5$ fragment onto the conformation of **3**, the ability of **3** to form hydrogen bonds and the steric and electronic effects of the electropositive $Cr(CO)_5$ fragment onto the reactivity and redox behavior of **3**.

Results and Discussion

Unexpectedly, straightforward treatment of the Fischer carbene complex (ethoxy)(ferrocenyl)carbene (pentacarbonyl)chromium(0) (**1**)[17] with ferrocenylamine Fc-NH_2 (**2**)[27] in refluxing ethyl ether according to the Fischer route[21] did not furnish the desired (aminoferrocenyl)(ferrocenyl)carbene(pentacarbonyl) chromium(0) complex **3**. This is possibly due to the insufficient nucleophilicity of Fc-NH_2. To amplify the nucleophilicity of the amine, **2** is deprotonated in situ to **[2-H]**$^-$ with *n*-butyllithium in diethyl ether and **1** is added to the resulting suspension of lithium(ferrocenyl)amide at –8 °C (Scheme 2). After warming to room temperature and column chromatographic workup, amino carbene **3** is isolated in low yield (6 %) in addition to *trans*-1,2-diferrocenylimine **6**[28] and an as yet unidentified compound as side products (Scheme 2). Deprotonation of **2** with one equivalent potassium hexamethyldisilazide (KHMDS) in tetrahydrofuran at room temperature and reaction with **1** for 20 h slightly increases the isolated yield

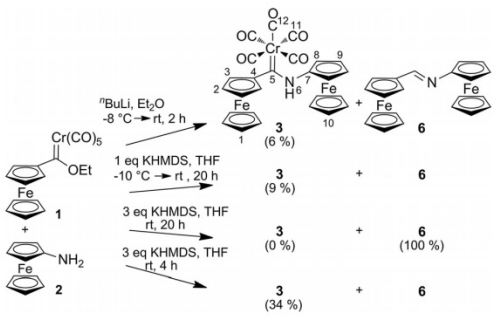

Scheme 2. Reactions of (ethoxy)(ferrocenyl)carbene (pentacarbonyl)-chromium(0) **1** with ferrocenylamine **2** in the presence of bases to give **3** and **6**. Atom numbering of **3** for NMR assignments.

 © 2015 WILEY-VCH Verlag GmbH & Co. KGaA, Weinheim

Journal of Inorganic and General Chemistry
ZAAC
Zeitschrift für anorganische und allgemeine Chemie
www.zaac.wiley-vch.de
ARTICLE

of **3** to 9%. Increasing the amount of base to three equivalents with the same reaction time yields no product. Reducing the reaction time to 4 h and using three equivalents of KHMDS gives **3** up to 34% (Scheme 2). The mechanism of the imine formation from **3** will be discussed below.

Composition and purity of **3** is substantiated by mass spectrometry and elemental analysis (Experimental Section, Supporting Information). Carbene complex **3** is furthermore characterized by multinuclear and two-dimensional NMR techniques. All ^{1}H and ^{13}C NMR resonances are assigned based on coupling patterns and NOE contacts. Only the resonances of the two unsubstituted C_5H_5 ligands (H^1, H^{10} and C^1, C^{10}) could not be discriminated by these methods due to the absence of through-bond coupling pathways and short-enough through-space H···H distances to other groups (Experimental Section, Supporting Information). The proton resonances H^2/H^3 and H^8/H^9 can be distinguished by the $^{1}H,^{1}H$-NOE spectrum (Figure 1). Both H^3 and H^8 show cross peaks to the amine proton H^6 with the cross peak to H^3 being significantly more intense. XRD and DFT analyses (see below) reveal a smaller distance between H^3 and H^6 compared to the H^6···H^8 distance. Hence, H^3 (δ = 4.63 ppm) is assigned to the *C*-substituted Cp ring and H^8 (δ = 4.77 ppm) to the *N*-substituted Cp ring. Proton coupling between H^3 and H^2 as well as between H^8 and H^9 allows assigning the H^2 and H^9 resonances as well. Interestingly, the amine proton H^6 shows further cross peaks to both unsubstituted Cp rings at δ = 4.38 and 4.31 ppm (Figure 1). These two contacts suggest that the NH group is located in between both ferrocenyl moieties with rather short NH···C_5H_5 distances. Consequently, this arrangement places the NH group in close proximity to both central iron atoms. A similar NH···C_5H_5 contact has been reported recently for diferrocenyl tosylhydrazone, which displays a very strong NH···Fe hydrogen bond.[29] The proton resonance of H^6 (δ = 10.90 ppm in CD_2Cl_2) is indeed shifted to lower field, compared to other aminocarbene(pentacarbonyl) chromium(0) complexes [(Fc)(NH*R*)C=Cr(CO)$_5$ (*R* = Me, Et, Pr, Bu, Pent): δ = 9.45–9.52 ppm in $CDCl_3$[17d,20a,20c]]. The shift is even more pronounced compared to those of amide **4** (δ = 8.95 ppm in [D_6]DMSO) and thioamide **5** (δ = 8.29 ppm in CD_2Cl_2).[22]

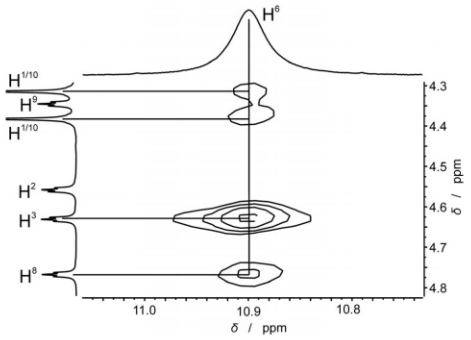

Figure 1. Section of the $^{1}H,^{1}H$-NOE spectrum of **3** in CD_2Cl_2 (t_{mix} = 0.8 s).

A clear trend is also observed for the ^{13}C NMR resonances of the carbene carbon nucleus C^5 [**3**: δ = 282.4 ppm; (Fc)(NH*R*)C=Cr(CO)$_5$ (*R* = Me, Et, Pr, Bu, Pent): δ = 270.6–273.3 ppm;[17d,20a,20c] **4**: δ = 167.2 ppm; **5**: δ = 198.2 ppm]. These shifts are likely a consequence of ring current effects of the substituted cyclopentadienyl ligands and of the NH···Fe hydrogen bonds.[29,30] In comparison to **4** and **5** the larger paramagnetic deshielding term,[31] based on lower energy electronic "π–π^*" and "n– π^*" transitions of the C=*X* chromophore [*X* = O, S, Cr(CO)$_5$] strongly affects the chemical shift of the carbene C nucleus.

The Cr(CO)$_5$ fragment displays the expected absorption pattern in its IR spectra (Experimental Section; A_1, B_1, E and A_1 symmetry). Generally, CO stretching vibrations of A_1 symmetry in *M*(CO)$_5$L complexes are sensitive towards the π-donor/π-acceptor capabilities of the ligand L.[21d] Yet, the character of (amino)carbene ligands is not strongly affected by the nature of its *N*-substituents, as observed earlier.[21] Hence, the frequencies of the CO A_1 vibrations in (*R*)(N*R*′*R*′′)C=Cr(CO)$_5$ are rather constant and **3** represents no exception.[17b,17d,20,21] The IR spectrum of **3** as a solid (KBr disk) shows an absorption for the N–H stretching vibration at 3271 cm^{-1} similar to (Fc)(NH-allyl)C=Cr(CO)$_5$ (3225 cm^{-1}).[17d] In CD_2Cl_2 solution the absorption for the NH stretch is found at 3233 cm^{-1} (Experimental Section, Supporting Information). For the chalcogen analogues **4** and **5** the corresponding NH stretches are found at 3320 and 3270 cm^{-1} in the solid (intermolecular NH···O/S hydrogen bonds) and at 3439 and 3397 cm^{-1} in dichloromethane solution (free NH group), respectively.[22] The low-energy NH stretching vibrations of **3** supports the presence of a hydrogen bond in the solid state as well as in solution as already deduced from proton NMR spectroscopic data.

Suitable crystals for X-ray diffraction analysis of **3** were obtained from a solution of **3** in petroleum ether-40/60:dichloromethane (5:1) at 7 °C. **3** crystallizes as the *trans* isomer in the monoclinic space group $P2_1/n$ with one molecule in the asymmetric unit (Figure 2, Table 1). No intermolecular contacts between the individual molecules of **3** are observed in the solid state ruling out significant intermolecular NH···OC contacts. The central chromium atom shows a slightly distorted octahedral coordination with a typical umbrella-like distortion[32] of the Cr(CO)$_5$ fragment (Figure 2). The carbene unit adopts a staggered conformation with respect to the Cr(CO)$_4$ plane. Expectedly, the Cr–C bond of the axial CO ligand is shorter and the corresponding C–O distance is larger than the respective distances of the equatorial CO ligands. The metrical data of **3** lie in range of that of the seven known solid-state structures of related (ferrocenyl)(R)carbene(pentacarbonyl) chromium(0) complexes (Table 1).[17d,17e,20a,33,34] Remarkably, the Cr–$C_{carbene}$ distance [2.097(2) Å] is shorter whereas the $C_{carbene}$–N distance is longer [1.322(3) Å] in **3** than the corresponding distances in (Fc)(NH$_2$)C=Cr(CO)$_5$ (Cr–$C_{carbene}$: 2.118 Å; $C_{carbene}$–N: 1.307 Å) and in (Fc)(NH($C_3H_6N(CH_3)_2$)C=Cr(CO)$_5$ (Cr–$C_{carbene}$: 2.128 Å; $C_{carbene}$–N: 1.308 Å).[20a] Obviously, the *N*-ferrocenyl substituent does not increase the π-donor capability of the amine towards the carbene center in

Dedicated Cluster

 © 2015 WILEY-VCH Verlag GmbH & Co. KGaA, Weinheim

Journal of Inorganic and General Chemistry
ZAAC
Zeitschrift für anorganische und allgemeine Chemie
www.zaac.wiley-vch.de
ARTICLE

Table 1. Selected bond lengths /Å and angles /° of **3** determined by XRD and of **3**, **[3-H]**$^-$, ***cis*-3^{Me}** and ***trans*-3^{Me}** determined by DFT calculations.

	3 (XRD)	**3** (DFT)	**[3-H]**$^-$ (DFT)	***cis*-3^{Me}** (DFT)	***trans*-3^{Me}** (DFT)
Cr1–C1	2.097(2)	2.113	2.224	2.205	2.185
Cr1–C22	1.865(3)	1.858	1.833	1.851	1.851
Cr1–C23	1.903(3)	1.890	1.872	1.881	1.887
Cr1–C24	1.900(3)	1.879	1.867	1.884	1.879
Cr1–C25	1.910(3)	1.885	1.886	1.880	1.890
Cr1–C26	1.907(3)	1.880	1.867	1.881	1.879
C1–C2	1.477(3)	1.487	1.505	1.479	1.495
C1–N1	1.322(3)	1.347	1.306	1.370	1.352
N1–C12	1.424(3)	1.433	1.397	1.444	1.451
Fe1–*X*1[a]	1.653	1.730	1.729	1.735	1.738
Fe1–*X*2[b]	1.644	1.731	1.729	1.731	1.741
Fe2–*X*1[a]	1.658	1.728	1.732	1.734	1.736
Fe2–*X*2[b]	1.654	1.726	1.735	1.733	1.740
Fe1···N1	3.484(2)	3.506	3.682	4.083	3.917
Fe2···N1	3.061(2)	3.132	3.184	3.225	3.281
Fe1···H1	3.130	2.954	–	–	–
Fe2···H1	3.094	3.149	–	–	–
C1–Cr1–C22	176.48(11)	177.78	179.02	175.43	176.91
C1–Cr1–C_{eq}[c]	87.69(9)–95.57(9)	86.62–95.63	83.00–94.91	83.80–97.54	85.567–98.02
Cr1–C22–O1	178.4(2)	179.89	179.65	175.44	179.77
Cr–C_{eq}–O	172.7(2)–177.3(2)	172.12–179.14	171.08–178.68	171.33–179.08	169.68–178.58
N1–C1–C2	109.5(2)	110.56	112.63	114.55	116.65
C1–N1–C12	129.1(2)	129.56	128.98	124.55	123.05
N1–C1–C2–C3	156.55	142.13	156.97	–162.03	147.98
C1–N1–C12–C13	–68.62	–71.05	–78.42	–141.23	107.96
τ(Fe1)[d]	178.83	177.28	179.45	175.55	174.13
τ(Fe2)[d]	179.80	179.04	179.39	177.23	175.59

a) *X*1 = centroid of coordinated C_5H_5 ring. b) *X*2 = centroid of coordinated C_5H_4 ring. c) C_{eq} carbon atom of equatorial carbonyl ligands. d) τ = *X*1–Fe–*X*2.

3. This is traced back to the out-of-plane orientation of the *N*-ferrocenyl moiety with respect to the carbene plane (torsion angle –68.6°) while the observed ferrocenyl orientation itself is caused by the steric interaction of the *N*-ferrocenyl substituent with the $Cr(CO)_5$ fragment (Figure 2). In contrast, in amide and thioamide oligoferrocenyl complexes the bound Cp rings of both ferrocenyl units are essentially co-planar with the (thio)amide bridges.[22,25] The resulting diminished π-donor ability of the amine towards the carbene carbon atom in **3** hence increases the chromium–carbene π back-bonding which is manifested in the slightly shorter Cr–$C_{carbene}$ bond in **3**.[35]

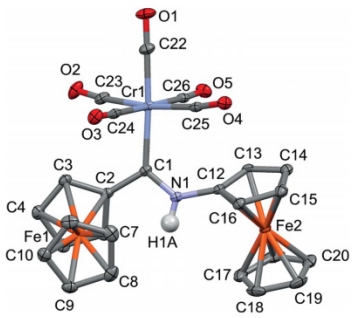

Figure 2. Molecular structure of **3** in the solid state (CH hydrogen atoms are omitted for clarity, thermal ellipsoids at 30% probability).

As already deduced from the NMR and IR data in CD_2Cl_2 solution the molecular structure in the solid state features non-classical NH···Fe hydrogen bonds,[29,30] forming a five-membered ring with Fe1 [N1···Fe1: 3.484(2) Å, N1H···Fe1: 3.13 Å] and a four-membered ring with Fe2 [N1···Fe2: 3.061(2) Å, NH···Fe2: 3.09 Å]. The sterically demanding $Cr(CO)_5$ fragment places both bulky ferrocenyl substituents in flanking positions with respect to the NH group effectively shielding the NH group from conceivable intermolecular NH···OC contacts (Figure 2).[36] DFT optimization of the geometry of **3** (B3LYP, LANL2DZ, IEF-PCM CH_2Cl_2) places the Fc moieties in essentially identical orientations as found in the solid-state structure of **3** with N···Fe1 and N···Fe2 distances of 3.506 and 3.132 Å, respectively. This confirms that the Fc orientations are intrinsic molecular properties and do not result from packing effects.

The electronic spectrum of **3** in CH_2Cl_2 shows a prominent absorption band at λ_{max} = 392 nm flanked by two shoulders (λ = 350, 450 nm) (Figure 3). Characteristic ferrocene absorption bands of the O/S analogues **4** and **5** are found at 445 and 470 nm, respectively.[22] Earlier studies on the electronic structure of Fischer carbene complexes assign three absorptions to a spin-forbidden metal-to-ligand charge transfer (MLCT) band at approximately 500 nm and spin-allowed ligand-field (LF) bands around 350–450 nm and around 300–350 nm, respectively.[37] Time-dependent DFT calculations (TD-DFT, B3LYP, LANL2DZ, IEF-PCM CH_2Cl_2) of **3** at the geometry optimized at the same level of theory indicate mixed MLCT/LF transi-

 © 2015 WILEY-VCH Verlag GmbH & Co. KGaA, Weinheim

Journal of Inorganic and General Chemistry
ZAAC
Zeitschrift für anorganische und allgemeine Chemie
www.zaac.wiley-vch.de
ARTICLE

tions for the three discernible absorptions. The lowest-energy absorption band (450 nm; DFT: 366 nm) is composed of *N*-Fc→carbene charge transfer (HOMO→LUMO) and a *C*-Fe(dd) ligand field transition. The central absorption at 392 nm (DFT: 348 nm) is a combination of *C*-Fe(dd) transitions (HOMO-3→LUMO+5), Cr→carbene (HOMO5→LUMO) and *C*-Fc→carbene (HOMO3→LUMO) charge transfer. The high energy shoulder at 350 nm (DFT: 316 nm) consists of a Cr→CO CT (HOMO-5→LUMO+2) and another Cr→CO CT admixed with ligand field (*C*-Fc, *N*-Fc) transitions (HOMO-2→LUMO+3) (Figure 4b). The mixed character of these bands suggests close-lying excited states of different parentage (Fe, Cr; carbene, CO). The close-lying electronically excited states might also affect the redox properties of **3**.

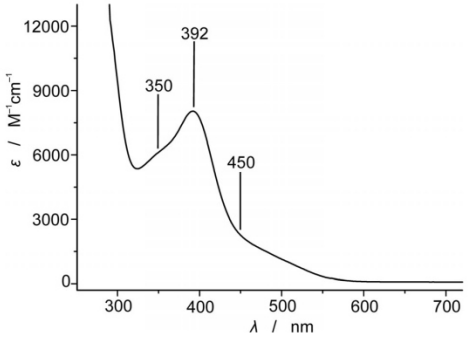

Figure 3. UV/Vis spectrum of **3** in CH_2Cl_2.

Diferrocenylamide **4** and thioamide **5** are reversibly oxidized to $[\mathbf{4}]^{\bullet+}$ and $[\mathbf{5}]^{\bullet+}$ at the *N*-substituted ferrocenyl site at –0.110 V and –0.065 V vs. FcH, respectively. The second oxidation at the *C*-substituted ferrocenyl moiety occurs at 0.300 V ($[\mathbf{4}]^{\bullet+}$) and 0.240 V ($[\mathbf{5}]^{\bullet+}$) vs. FcH, respectively.[22,38] The $Cr(CO)_5$ fragment in amino carbene complexes is typically oxidized at potentials around 0.196–0.499 V vs. FcH.[20c,38–41] Furthermore, the electron-deficient carbene center in **3** successfully competes with the (out-of-plane oriented) *N*-Fc site for electron density rendering the *N*-Fc moiety in **3** less susceptible towards oxidation as compared to other Fc-NHR derivatives. Hence, it is unclear a priori which redox site *N*-Fc, *C*-Fc, or $Cr(CO)_5$ is oxidized in **3** in the first place.

The cyclic voltammogram of **3** in $[n\mathrm{Bu_4N}][\mathrm{B(C_6F_5)_4}]$/$CH_3CN$ (Figure 5) shows an irreversible reduction at E_p = –2.300 V vs. FcH which is assigned to the reduction of the electron deficient carbene ligand.[18b,20c,41] This is in accordance with the LUMO of **3** being located at the carbene according to DFT calculations (Figure 4b and Supporting Information). A quasi-reversible oxidation is observed at E_p = 0.020 V closely followed by three quasi-reversible oxidations at E_p = 0.250, 0.370 and 0.560 V, respectively. A reduction wave of a follow-up product of the third oxidation is found at E_p = –1.460 V (^{*1}) vs. FcH. The oxidation at E_p = –0.440 V (^{*2}) is assigned to a follow-up product of the reduction of **3** at E_p = –2.300 V (Figure 5, Supporting Information). The three

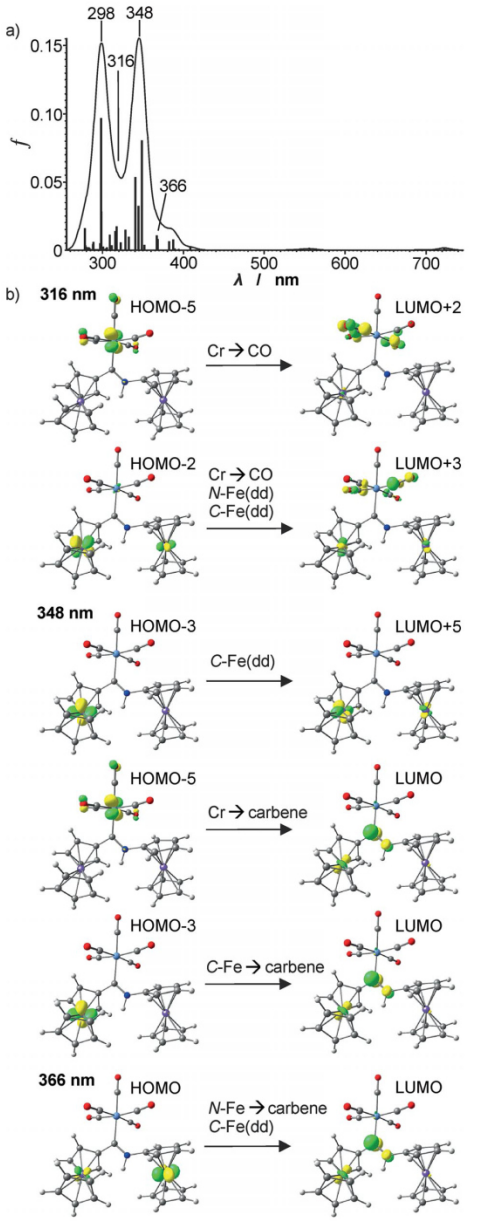

Figure 4. (a) TD-DFT (B3LYP, LANL2DZ, IEF-PCM CH_2Cl_2) calculated UV/Vis spectrum of **3** and (b) major orbital contributions (isosurface value 0.1 a.u.) to the indicated transitions.

redox steps at E_p = 0.020, 0.250 and 0.370 V are attributed to the oxidation of the $Cr(CO)_5$, *C*-Fc, and *N*-Fc moieties. The

 © 2015 WILEY-VCH Verlag GmbH & Co. KGaA, Weinheim

Journal of Inorganic and General Chemistry
ZAAC
Zeitschrift für anorganische und allgemeine Chemie
www.zaac.wiley-vch.de
ARTICLE

redox process at 0.560 V possibly corresponds to the $Cr^{I/II}$ couple of the chromium fragment[18b,20c,41] or of a chromium-based follow-up product, which is quasi-reversibly oxidized. An unambiguous assignment of the oxidation processes is impossible solely based on the comparison with the redox potentials of amino carbene chromium complexes[20c,41] and (thio)amides **4**, **5**.[22]

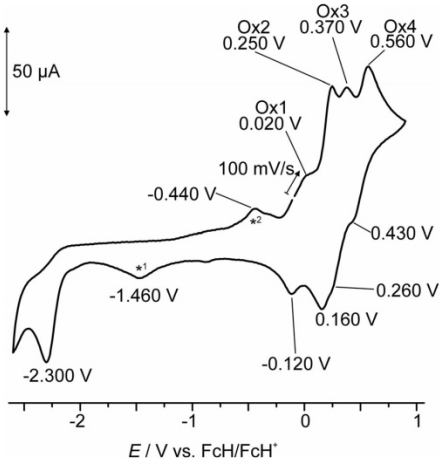

Figure 5. Cyclic voltammogram of **3** in $[n\mathrm{Bu_4N}][\mathrm{B(C_6F_5)_4}]/\mathrm{CH_3CN}$.

DFT (B3LYP, LANL2DZ, IEF-PCM CH_2Cl_2) optimizations of the two ferrocenium valence isomers of **[3]**$^{\bullet+}$ (Fc$^{\bullet+}$)(NH*R*)C=Cr(CO)$_5$ and (Fc)(NHFc$^{\bullet+}$)C=Cr(CO)$_5$ yield very similar energies while the (Fc)(NHR)C=Cr$^{\bullet+}$(CO)$_5$ valence isomer converged to the (Fc$^{\bullet+}$)(NHR)C=Cr(CO)$_5$ isomer (Supporting Information). Furthermore, *Bezuidenhout* et al. showed that the most stable DFT calculated electronic situation of **[1]**$^{\bullet+}$ depends on the choice of basis set and functional.[20c] Hence, neither the redox potentials of **3** nor DFT calculations of **[3]**$^{\bullet+}$ allow for a definitive assignment.

Although the close-lying redox potentials will lead to partial disproportionation of **[3]**$^{\bullet+}$ and higher oxidized species as well as to the possibility for valence isomerism[42] of **[3]**$^{\bullet+}$ assessing the redox site in **[3]**$^{\bullet+}$ by EPR spectroscopy was attempted. Treating **3** with 0.95 equivalents "magic blue" ([N(*p*-$C_6H_4Br)_3$][$SbCl_6$], $E_{½}$ = 0.67 V vs. FcH[38]) in THF indeed yields an EPR-active solution featuring an isotropic EPR resonance centred at g = 1.988 at room temperature (Figure 6). As ferrocenium radicals are EPR-silent at room temperature this resonance is ascribed to a chromium(I) centered radical. Values below the free-electron value are typically found for comparable Cr^I complexes featuring a low-spin d^5 electron configuration (S = ½).[43] Treating the alkoxy carbene complex **1** analogously yields an EPR resonance as well, yet at significantly lower field (g = 2.013, Figure 6). This suggests a lower contribution of the chromium centre in Cr^I radicals derived from **[1]**$^{\bullet+}$ as in the radical derived from **[3]**$^{\bullet+}$. As disproportionation and follow-up reactions of **[3]**$^{\bullet+}$ might play a significant role the experimentally derived Cr^I oxidation state cannot necessarily be ascribed to **[3]**$^{\bullet+}$ but to a follow-up or disproportionation product as well.

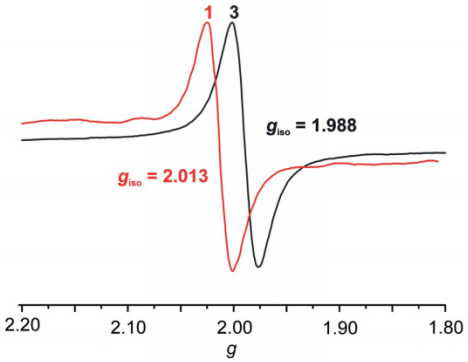

Figure 6. X-band (9.4 GHz) EPR spectra of **3** + 0.95 equiv. magic blue and **1** + 0.95 equiv. magic blue in THF at room temperature.

To elucidate the nature of the chromium centred radical, solution IR spectroscopic experiments with **3** in tetrahydrofuran in the presence of magic blue were carried out (Supporting Information). Indeed, the CO stretching bands of **3** decrease in intensity with increasing amounts of magic blue. No further bands assignable to Cr(CO)$_n$ fragments were detected. This observation is in full agreement with the IR spectroelectrochemical study on Ar(NMe$_2$)C=Cr(CO)$_5$ complexes showing the evolution of a gas at the electrode.[39d] Similarly, chemical oxidation of **1** and characterization of oxidation product(s) were reported as unsuccessful.[20c] Clearly, CO ligands dissociate in the primary oxidation products **[1]**$^{\bullet+}$ and **[3]**$^{\bullet+}$. In essence, the exact nature of the observed Cr^I radicals derived from **1** and **3** remains unclear.

In contrast to oxidation, deprotonation of **3** to **[3-H]**$^-$ is straightforward using strong bases such as KO*t*Bu. The successful deprotonation of **3** to **[3-H]**$^-$ is clearly corroborated by the strong shift of the A_1 CO stretch to lower energy by 31 cm^{-1} from 2051 cm^{-1} to 2020 cm^{-1} in THF as a result of increased π back-bonding of Cr to CO (Figure 7). DFT calcu-

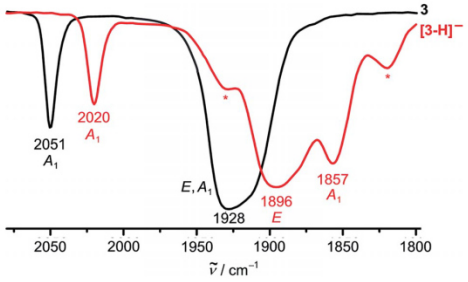

Figure 7. IR spectra of **3** and **3** + KO*t*Bu in THF at room temperature [assignments according to idealized C_{4v} point group of Cr(CO)$_5$; * denote CO bands of some decomposition product].

Dedicated Cluster

 © 2015 WILEY-VCH Verlag GmbH & Co. KGaA, Weinheim

Journal of Inorganic and General Chemistry
ZAAC
Zeitschrift für anorganische und allgemeine Chemie
www.zaac.wiley-vch.de
ARTICLE

lations of **3** and **[3-H]**$^-$ (Supporting Information) predict a shift of 36 cm^{-1} for the deprotonation of **3** to **[3-H]**$^-$ in very good agreement with the experiment. Similarly, the deprotonation also affects the second A_1 CO stretch (1857 cm^{-1}) to a higher degree than the vibrations of *E* symmetry due to the different *trans* influence of the deprotonated carbene (Figure 7). Expectedly, the Cr–$C_{carbene}$ bond in **[3-H]**$^-$ is elongated from 2.113 to 2.224 Å according to DFT calculations resulting in an (iminoacyl)(pentacarbonyl) chromate(0) valence description for **[3-H]**$^-$ (Figure 8a, Table 1). The anion **[3-H]**$^-$ is quite persistent at room temperature, yet after 20 h in the presence of three equivalents of base *trans*-1,2-diferrocenylimine **6** is quantitatively formed. Refluxing **[3-H]**$^-$ in toluene results in rapid quantitative formation of **6** according to ^{1}H NMR spectroscopy and mass spectrometry. On the other hand, **3** is thermally stable in the absence of a base. Hence, imine formation from **3** starts with a facile deprotonation at nitrogen by a suitable base followed by a rate-determining reprotonation at carbon with concomitant elimination of a $Cr(CO)_5$ fragment. The $Cr(CO)_5$ dissociation is certainly favoured due to the bulkiness of the two ferrocenyl substituents and the pentacarbonyl metal fragment itself.

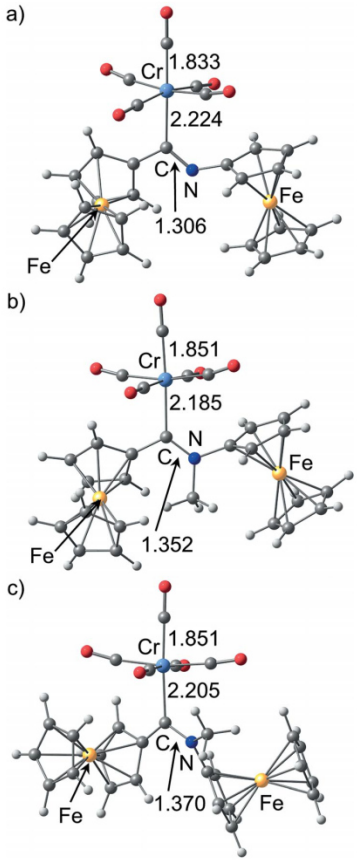

Figure 8. DFT optimized geometries and relevant distances /Å of (a) **[3-H]**$^-$, (b) ***trans*-3^{Me}**, and (c) ***cis*-3^{Me}**.

Trapping the sterically shielded **[3-H]**$^-$ anion by *N*-methylation with excess MeI in THF is successful according to ^{1}H NMR spectroscopy (approximately 50% spectroscopic yield of **3^{Me}**) and mass spectrometry (Supporting Information). The incomplete transformation can be ascribed to the sterically congested amide in **[3-H]**$^-$ hindering the nucleophilic attack at MeI. Interestingly, all Cp proton resonances of **3^{Me}** are considerably shifted to higher field with respect to those of **3** ($\Delta\delta$ = –0.07, –0.42, –0.25, –0.27, –0.31, –0.12 for H^{1,2,3,8,9,10}; Supporting Information) which is uncommon for such a minor chemical change in (*R*)(N*R*′*R*′′)C=*M*(CO)$_5$ complexes (*M* = Cr, W; *R*′ = H, Me, allyl).[44] However, the conformational effect of the H→Me substitution in the **3/3^{Me}** pair is appreciable due to the three sterically demanding substituents at the carbene center. The *trans* conformation of ***trans*-3^{Me}** similar to that of **3** (Figure 2, Figure 8b,c; C_{ipso}–$C_{carbene}$–N–C_{ipso} = 172.4°) is sterically congested and hence a major reorientation occurs to ***cis*-3^{Me}** (stabilized according to DFT calculations; C_{ipso}–$C_{carbene}$–N–C_{ipso} = 27.7°) to better accommodate the *N*-methyl group (Figure 8b, c). This reorientation significantly affects the chemical shifts of the Cp protons. Possibly, the expansion of the NH-Fc unit at the already congested carbene centre by *N*-methylation appears to approach the steric limit in these carbene complexes.

Conclusions

The heterotrimetallic isolobal amide (aminoferrocenyl)-(ferrocenyl)carbene(pentacarbonyl) chromium(0) complex **3** was prepared from the alkoxy Fischer carbene complex **1** by nucleophilic substitution of the alkoxide with ferrocenyl amide [Fc-NH]$^-$ **[2-H]**$^-$. Apart from an unidentified ferrocene-containing side product a significant side reaction is the elimination of *trans*-1,2-diferrocenylimine (**6**), which is suppressed at low temperature and by using only a slight excess of base. The formation of **6** is probably favoured by the considerable steric crowding by the three substituents $Cr(CO)_5$, *C*-Fc, *N*-Fc at the carbene center facilitating the $Cr(CO)_5$ dissociation. Indeed, the $Cr(CO)_5$ fragment forces the two Fc substituents in positions flanking the NH group in **3**, which results in two NH···Fe1/Fe2 hydrogen bonds as shown by XRD, NMR, IR, and DFT studies. Oxidation of **3** to the cation radical **[3]$^{•+}$** is likely followed by decarbonylation giving a chromium-centered radical according to EPR studies. *N*-Deprotonation of neutral **3** to anionic **[3-H]**$^-$ at higher temperature quantitatively releases the imine **6**, while at room temperature the anion **[3-H]**$^-$ can be trapped by methylation to yield the *N*-methylated carbene complex **3^{Me}**. NMR spectroscopy and DFT calculations of **3^{Me}** suggest a different conformation of **3^{Me}** (***cis*-3^{Me}**) as compared to **3** to accommodate the methyl group. Future work aims at the extension of the work towards other trimetallic amides (Fc)(FcNH)C=*ML*$_n$ with different steric and electronic impact of the *ML*$_n$ fragments.

 © 2015 WILEY-VCH Verlag GmbH & Co. KGaA, Weinheim

Journal of Inorganic and General Chemistry
ZAAC
Zeitschrift für anorganische und allgemeine Chemie
www.zaac.wiley-vch.de
ARTICLE

Experimental Section

General Procedures: All reactions were performed under standard Schlenk and glovebox conditions. A glovebox of the type UniLab/MBraun (Ar 4.8, O_2 < 1 ppm, H_2O < 1 ppm) was used for storage and weighing of sensitive compounds. All analytical samples that required the absence of oxygen were prepared in the same glovebox. Solvents were dried and distilled under argon prior to use. **1**[17d] and **2**[27] were prepared according to literature procedures.

NMR spectra were recorded with a Bruker Avance DRX 400 spectrometer at 400.31 MHz (^{1}H) and 100.657 MHz (^{13}C). Chemical shifts δ (ppm) are reported with respect to residual solvent signals as internal standards (^{1}H, ^{13}C): CD_2Cl_2 $\delta(^1H)$ = 5.32 ppm, $\delta(^{13}C)$ = 54.0 ppm. (s) = singlet; (pt) = pseudo triplet = unresolved doublet of doublets. UV/Vis spectra were recorded with a Varian Cary 5000 spectrometer in 1 cm cuvettes. Vibrational spectra were recorded with a Varian 3100 FT-IR Excalibur Series spectrometer. Measurements were carried out with the sample as KBr pellet or in solution in a KBr cell. FD mass spectra were recorded with a FD Finnigan MAT90 spectrometer. Electrochemical investigations were carried out with a SP-50 Analyzator of BioLogic in the glovebox to prevent follow-up reactions with oxygen or moisture. Two platinum wires were used as working and counter electrode and a Ag/$AgNO_3$ electrode was employed as reference (0.01 M $AgNO_3$, CH_3CN). $[(n\text{Bu})_4\text{N}][B(C_6F_5)_4]$[45] (0.1 M in CH_3CN) was used as electrolyte with 1 mM of the sample. The potentials are given vs. ferrocene/ferrocenium (FcH/FcH^+) (E = 0.40 V vs. SCE, 0.64 V vs. NHE).[38] EPR spectra were recorded with a Miniscope MS 300 X-band CW spectrometer (Magnettech GmbH, Germany). Values of g are referenced to Mn^{2+} in ZnS as external standard (g = 2.118, 2.066, 2.027, 1.986, 1.946). Simulations were performed with the EasySpin program package.[46] Elemental analyses were performed by the microanalytical laboratory of the chemical institutes of the University of Mainz.

DFT calculations were carried out with the Gaussian09/DFT[47] series of programs. The B3LYP[48] formulation of DFT was used employing the LANL2DZ[49] basis set. No symmetry constraints were imposed on the molecules. The presence of energy minima was checked by analytical frequency calculations. The integral-equation-formalism polarisable continuum model (IEFPCM, CH_2Cl_2) was employed for solvent modeling.

X-ray diffraction data were collected with a Bruker AXS Smart 1000 CCD diffractometer with an APEX II detector and an Oxford cooling system and corrected for absorption and other effects using Mo-K_α radiation (λ = 0.71073 Å) at 173(2) K. The diffraction frames were integrated using the SAINT package, and most were corrected for absorption with MULABS.[50,51] The structure was solved by direct methods and refined by the full-matrix method based on F^2 using the SHELXTL software package.[52,53] All non-hydrogen atoms were refined anisotropically, while the positions of hydrogen atoms were generated with appropriate geometric constraints and allowed to ride on their respective parent atoms with fixed isotropic thermal parameters.

Crystallographic data (excluding structure factors) for the structure in this paper have been deposited with the Cambridge Crystallographic Data Centre, CCDC, 12 Union Road, Cambridge CB21EZ, UK. Copies of the data can be obtained free of charge on quoting the depository number CCDC-1409670 (Fax: +44-1223-336-033; E-Mail: deposit@ccdc.cam.ac.uk, http://www.ccdc.cam.ac.uk).

Crystallographic Data of 3: $C_{26}H_{19}CrFe_2NO_5$ (589.12); monoclinic; $P2_1/n$; a = 11.5067(15) Å, b = 12.4663(15) Å, c = 17.305(2) Å, β = 106.089(3)°, V = 2385.1(5) Å^3; Z = 4; density, calcd. = 1.641 g·cm^{-3}, μ = 1.686 mm^{-1}; F(000) = 1192; crystal size 0.90×0.67×0.07 mm; θ = 2.45 to 28.04 deg.; $-14 \le h \le 15$, $-16 \le k \le 16$, $-22 \le l \le 21$; rfln collected = 24542; rfln unique = 5766 [R(int) = 0.0542]; completeness to θ = 28.04 = 99.7%; semi-empirical absorption correction from equivalents; max. and min. transmission 0.8911 and 0.3122; data 5766; restraints 0, parameters 316; goodness-of-fit on F^2 = 1.018; final R indices [$I > 2\sigma(I)$] R_1 = 0.0353, wR_2 = 0.0848; R indices (all data) R_1 = 0.0502, wR_2 = 0.0896; largest diff. peak and hole 0.584 and −0.457 e·Å^{-3}.

(Aminoferrocenyl)(ferrocenyl)carbene(pentacarbonyl) chromium(0) (3): Aminoferrocene **2** (100 mg, 0.5 mmol) and **1** (217 mg, 0.5 mmol) were dissolved in dry THF (10 mL). Potassium hexamethyl disilazide (KHMDS, 300 mg, 1.5 mmol) in dry THF (15 mL) was added within 4 h at room temperature whilst stirring. Saturated aqueous $NaHCO_3$ solution (20 mL) and petroleum ether 40/60 (10 mL) were added. The aqueous phase was extracted with petroleum ether 40/60 (10 mL) and CH_2Cl_2 (10 mL). The combined organic phases were evaporated under reduced pressure to obtain the crude product (249 mg). Purification by column chromatography (SiO_2, 26 cm×3.5 cm, petroleum ether 40/60:CH_2Cl_2 2:1, R_f = 0.5) yielded **3** as a dark red solid (99 mg, 0.168 mmol, 34%). $C_{26}H_{19}CrFe_2NO_5$: C 52.94 (calcd. 53.01); H 3.01 (calcd. 3.25); N 2.52% (calcd. 2.38%). **^{1}H NMR** (400.32 MHz, CD_2Cl_2): δ = 10.90 (s, 1 H, H^6), 4.77 (pt, 2 H, H^8), 4.63 (pt, 2 H, H^3), 4.56 (pt, 2 H, H^2), 4.38 (s, 5 H, H$^{1/10}$), 4.35 (pt, 2 H, H^9), 4.31 (s, 5 H, H$^{1/10}$) ppm. **^{13}C{^{1}H} NMR** (100.55 MHz, CD_2Cl_2): δ = 282.4 (C^5), 224.8 (C^{12}), 218.2 (C^{11}), 99.1 (C^4), 98.6 (C^7), 71.3 (C^2), 70.4 (C$^{1/10}$), 70.2 (C$^{1/10}$), 69.5 (C^3), 69.3 (C^8), 67.9 (C^9) ppm. **MS(FD)**: m/z (int.) = 589.0 (100%, **[3]$^{+\bullet}$**), 561.1 (1%, **[3]$^{+\bullet}$**–CO). **IR** (KBr): $\tilde{\nu}$ = 3271 (w, NH), 3092 (w, CH), 2052 (vs, CO A_1), 1981 (m, CO B_1), 1971 (m), 1913–1898 (br., CO E, A_1) cm^{-1}. **IR** (THF): $\tilde{\nu}$ = 2051 (vs, CO A_1), 1928 (br., CO E, A_1) cm^{-1}. **IR** (CD_2Cl_2): $\tilde{\nu}$ = 3233 (m, NH) cm^{-1}. **UV/Vis** (CH_2Cl_2): λ (ε/M^{-1}·cm^{-1}) = 350 (6100), 392 (8035), 450 (2260) nm.

Supporting Information (see footnote on the first page of this article): Mass spectra, NMR and IR spectra of **3**; relevant molecular orbitals of **3**. ^{1}H NMR and mass spectra of a **3**/**3^{Me}** mixture, Table of TD-DFT calculated electronic transitions of **3**; cartesian coordinates of all DFT optimized structures.

Acknowledgements

We thank *Regine Jung-Pothmann* for the collection of the diffraction data and the Johannes Gutenberg University, Mainz (Germany) for financial support to *C. F.* (Internal University Research Funding).

References

[1] E. O. Fischer, A. Maasböl, *Angew. Chem.* **1964**, *76*, 645; *Angew. Chem. Int. Ed. Engl.* **1964**, *3*, 580.
[2] A. J. Arduengo III, R. L. Harlow, M. Kline, *J. Am. Chem. Soc.* **1991**, *113*, 361–363.
[3] For recent reviews see: a) D. Bourissou, O. Guerret, F. P. Gabbaï, G. Bertrand, *Chem. Rev.* **2000**, *100*, 39–91; b) P. de Frémont, N. Marion, S. P. Nolan, *Coord. Chem. Rev.* **2009**, *253*, 862–892; c) K. Hitai, T. Itoh, H. Tomioka, *Chem. Rev.* **2009**, *109*, 3275–3332; d) J. Vignolle, X. Cattoën, D. Bourissou, *Chem. Rev.* **2009**, *109*, 3333–3384; e) T. Dröge, F. Glorius, *Angew. Chem.* **2010**, *122*, 7094–7107; *Angew. Chem. Int. Ed.* **2010**, *49*, 6940–6952; f) M. Soleilhavoup, G. Bertrand, *Acc. Chem. Res.* **2015**, *48*, 256–266.
[4] Themed issue towards *N*-heterocyclic carbenes: *Dalton Trans.* **2009**, *35*.

 © 2015 WILEY-VCH Verlag GmbH & Co. KGaA, Weinheim

Journal of Inorganic and General Chemistry
ZAAC
Zeitschrift für anorganische und allgemeine Chemie
www.zaac.wiley-vch.de
ARTICLE

[5] For reviews see: a) D. J. Nelson, *Eur. J. Inorg. Chem.* **2015**, 2012–2027; b) H. G. Raubenheimer, *Dalton Trans.* **2014**, *43*, 16959–16973, and reviews cited therein; c) J. W. Herndon, *Coord. Chem. Rev.* **2013**, *257*, 2800–3003; d) K. H. Dötz, J. Stendel Jr., *Chem. Rev.* **2009**, *109*, 3227–3274; e) A. Meijere, H. Schirmer, M. Duetsch, *Angew. Chem.* **2000**, *112*, 4124–4162; *Angew. Chem. Int. Ed.* **2000**, *39*, 3964–4002.

[6] For comprehensive reviews see: a) B. Bildstein, *J. Organomet. Chem.* **2001**, *617–618*, 28–38; b) U. Siemeling, *Eur. J. Inorg. Chem.* **2012**, 3523–3536.

[7] a) P. Ashkenazi, S. Lupan, A. Schwarz, M. Cais, *Tetrahedron Lett.* **1969**, *10*, 817–820; b) A. Sonoda, I. Moritani, T. Saraie, T. Wada, *Tetrahedron Lett.* **1969**, *10*, 2943–2946; c) A. Sonoda, I. Moritani, S. Yasuda, T. Wada, *Tetrahedron* **1970**, *26*, 3075–3081; d) A. Sonoda, I. Moritani, *Bull. Chem. Soc. Jpn.* **1970**, *43*, 3522–3527.

[8] A. DeHope, D. Mendoza-Espinosa, B. Donnadieu, G. Bertrand, *New J. Chem.* **2011**, *35*, 2037–2042.

[9] a) K. S. Coleman, S. Turberville, S. I. Pascu, M. L. H. Green, *J. Organomet. Chem.* **2005**, *690*, 653–658; b) C. D. Varnado Jr., V. M. Lynch, C. W. Bielawski, *Dalton Trans.* **2009**, 7253–7261.

[10] a) D. M. Khramov, E. L. Rosen, V. M. Lynch, C. W. Bielawski, *Angew. Chem.* **2008**, *120*, 2299–2302; *Angew. Chem. Int. Ed.* **2008**, *47*, 2267–2270; b) U. Siemeling, C. Färber, C. Bruhn, *Chem. Commun.* **2009**, 98–100; c) U. Siemeling, C. Färber, M. Leibold, C. Bruhn, P. Mücke, R. F. Winter, B. Sarkar, M. von Hopffgarten, G. Frenking, *Eur. J. Inorg. Chem.* **2009**, *2009*, 4607–4612; d) S. Rittinghaus, C. Färber, C. Bruhn, U. Siemeling, *Dalton Trans.* **2014**, *43*, 3508–3520.

[11] E. L. Rosen, C. D. Varnado Jr., A. G. Tennyson, D. M. Khramov, J. W. Kamplain, D. H. Sung, P. T. Cresswell, V. M. Lynch, C. W. Bielawski, *Organometallics* **2009**, *28*, 6695–6706.

[12] a) M. Süßner, H. Plenio, *Angew. Chem.* **2005**, *117*, 7045–7048; *Angew. Chem. Int. Ed.* **2005**, *44*, 6885–6888; b) L. H. Peeck, S. Leuthäusser, H. Plenio, *Organometallics* **2010**, *29*, 4339–4345.

[13] C. D. Varnado Jr., E. L. Rosen, M. S. Collins, V. M. Lynch, C. W. Bielawski, *Dalton Trans.* **2013**, *42*, 13251–13264.

[14] U. Siemeling, C. Färber, C. Bruhn, M. Leibold, D. Selent, W. Baumann, M. von Hopffgarten, C. Goedecke, G. Frenking, *Chem. Sci.* **2010**, *1*, 697–704.

[15] a) C. Bolm, M. Kesselgruber, G. Raabe, *Organometallics* **2002**, *21*, 707–710; b) A. Bertogg, F. Camponovo, A. Togni, *Eur. J. Inorg. Chem.* **2005**, 347–356; c) D. Broggini, A. Togni, *Helv. Chim. Acta* **2002**, *85*, 2518–2522.

[16] a) U. T. Mueller-Westerhoff, A. Nazzal, W. Prössdorf, J. L. Mayerle, R. L. Collins, *Angew. Chem.* **1982**, *94*, 314–314; *Angew. Chem. Int. Ed. Engl.* **1982**, *21*, 293–294; b) J. Lukasser, H. Angleitner, H. Schottenberger, H. Kopacka, M. Schweiger, B. Bildstein, K.-H. Ongania, K. Wurst, *Organometallics* **1995**, *14*, 5566–5578; c) R. Gleiter, C. Bleiholder, F. Rominger, *Organometallics* **2007**, *26*, 4850–4859.

[17] a) J. A. Connor, E. M. Jones, J. P. Lloyd, *J. Organomet. Chem.* **1970**, *24*, C20–C22; b) J. A. Connor, J. P. Loyd, *J. Chem. Soc., Dalton Trans.* **1972**, 1470–1476; c) G. A. Moser, E. O. Fischer, M. D. Rausch, *J. Organomet. Chem.* **1971**, *27*, 379–382; d) J. G. López-Cortés, L. F. Contreras de la Cruz, M. C. Ortega-Alfaro, R. A. Toscano, C. Alvarez-Toledano, H. Rudler, *J. Organomet. Chem.* **2005**, *690*, 2229–2237; e) D. I. Bezuidenhout, W. Barnard, B. van der Westhuizen, E. van der Watt, D. C. Liles, *Dalton Trans.* **2011**, *40*, 6711–6721.

[18] a) M. K. Lloyd, J. A. McCleverty, D. G. Orchard, J. A. Connor, M. B. Hall, I. H. Hillier, E. M. Jones, G. K. McEwen, *J. Chem. Soc., Dalton Trans.* **1973**, 1743–1747; b) B. van der Westhuizen, P. J. Swarts, I. Strydom, D. C. Liles, I. Fernández, J. C. Swarts, D. I. Bezuidenhout, *Dalton Trans.* **2013**, *42*, 5367–5378; c) B. van der Westhuizen, J. M. Speck, M. Korb, J. Friedrich, D. I. Bezuidenhout, H. Lang, *Inorg. Chem.* **2013**, *52*, 14253–14263; d) D. I. Bezuidenhout, I. Fernández, B. van der Westhuizen, P. J. Swarts, J. C. Swarts, *Organometallics* **2013**, *32*, 7333–7344.

[19] a) M. Zora, E. Ü. Güngör, *Tetrahedron Lett.* **2001**, *42*, 4733–4735; b) M. Zora, B. Yucel, N. B. Peynircioglu, *J. Organomet. Chem.* **2002**, *656*, 11–17.

[20] a) C. Sandoval-Chávez, J. G. López-Cortés, A. I. Gutiérrez-Hernández, M. C. Ortega-Alfaro, A. Toscano, C. Alvarez-Toledano, *J. Organomet. Chem.* **2009**, *694*, 3692–3700; b) A. I. Gutiérrez-Hernández, J. G. López-Cortés, M. C. Ortega-Alfaro, M. T. Ramírerz-Apan, J. de Cázares-Marinero, R. A. Toscano, *J. Med. Chem.* **2012**, *55*, 4652–4663; c) D. I. Bezuidenhout, B. van der Westhuizen, I. Strydom, P. J. Swarts, J. C. Swarts, I. Fernández, *Inorg. Chim. Acta* **2014**, *423*, 184–192.

[21] a) E. O. Fischer, U. Klabunde, *J. Am. Chem. Soc.* **1967**, *89*, 7141–7142; b) E. O. Fischer, J. A. Connor, *J. Chem. Soc. A* **1969**, 578–584; c) E. O. Fischer, B. Heckl, H. Werner, *J. Organomet. Chem.* **1971**, *28*, 359–365; d) E. O. Fischer, M. Leupoldt, *Chem. Ber.* **1972**, *105*, 599–608.

[22] a) K. Heinze, D. Siebler, *Z. Anorg. Allg. Chem.* **2007**, *633*, 2223–2233; b) T. Kienz, C. Förster, K. Heinze, *Organometallics* **2014**, *33*, 4803–4812.

[23] M. A. Sierra, *Coord. Chem. Rev.* **2000**, *100*, 3591–3637.

[24] a) H.-J. Lee, Y.-S. Choi, K.-B. Lee, J. Park, C.-J. Yoon, *J. Phys. Chem. A* **2002**, *106*, 7010–7017; b) C. Alemán, *J. Phys. Chem. A* **2001**, *105*, 6717–6723; c) D. R. Artis, M. A. Lipton, *J. Am. Chem. Soc.* **1998**, *120*, 12200–12206.

[25] a) D. Siebler, M. Linseis, T. Gasi, L. M. Carrella, R. F. Winter, C. Förster, K. Heinze, *Chem. Eur. J.* **2011**, *17*, 4540–4551; b) D. Siebler, C. Förster, K. Heinze, *Dalton Trans.* **2011**, *40*, 3558–3575; c) K. Heinze, K. Hüttinger, D. Siebler, in: *Modeling of Molecular Properties* (Ed.: P. Comba), Wiley-VCH, Weinheim, **2011**, pp. 325–346.

[26] a) M. B. Robin, P. Day, *Adv. Inorg. Chem. Radiochem.* **1967**, *9*, 247–422; b) B. S. Brunschwig, N. Sutin, *Coord. Chem. Rev.* **1999**, *187*, 233–254.

[27] a) B. Bildstein, M. Malaun, H. Kopacka, K. Wurst, M. Mitterböck, K.-H. Ongania, G. Opromolla, P. Zanello, *Organometallics* **1999**, *18*, 4325–4336; b) K. Heinze, M. Schlenker, *Eur. J. Inorg. Chem.* **2004**, *2004*, 2974–2988.

[28] M. A. Sierra, M. J. Mancheño, R. Vicente, M. Gómez-Gallego, *J. Org. Chem.* **2001**, *66*, 8920–8925.

[29] C. Förster, P. Veit, V. Ksenofontov, K. Heinze, *Chem. Commun.* **2015**, *51*, 1514–1516.

[30] For pertinent reviews see: a) L. Brammer, *Dalton Trans.* **2003**, 3145–3157; b) D. Braga, F. Grepioni, E. Tedesco, K. Biradha, G. R. Desiraju, *Organometallics* **1997**, *16*,1846–1856.

[31] *Multinuclear NMR* (Ed.: Joan Mason), Plenum Press, New York, London, **1987**.

[32] CCDC search (date: June 25, 2015) for $Cr(CO)_5L$ complexes with one Cr–C–O angle: 160–173°: 180 entries, e.g. CCDC no./ref. code: 701008, 265878, 611353/ BIGHAA, GAMQAM, CEBZAK10.

[33] CCDC search (date: June 25, 2015) for (ferrocenyl)(*R*)carbene(pentacarbonyl)chromium(0) complexes: CCDC no.: 217906, 263965, 701006, 701007, 701008, 729446, 729448.

[34] D. I. Bezuidenhout, E. van der Watt, D. C. LIles, M. Landmann, S. Lotz, *Organometallics* **2008**, *27*, 2447–2456.

[35] M. Cases, G. Frenking, M. Duran, M. Solà, *Organometallics* **2002**, *21*, 4182–4191.

[36] a) K. Heinze, V. Jacob, *J. Chem. Soc., Dalton Trans.* **2002**, 2379–2385; b) K. Heinze, *J. Chem. Soc., Dalton Trans.* **2002**, 540–547.

[37] a) L. S. Hegedus, *Tetrahedron* **1997**, *53*, 4105–4128; b) M. L. Lage, I. Fernández, M. J. Mancheño, M. A. Sierra, *Inorg. Chem.* **2008**, *47*, 5253–5258.

[38] N. G. Connelly, W. E. Geiger, *Chem. Rev.* **1996**, *96*, 877–910.

[39] a) I. Hoskovcová, J. Roháčová, L. Meca, T. Tobrman, D. Dvořák, J. Ludvík, *Electrochim. Acta* **2005**, *50*, 4911–4915; b) I. Hoskovcová, J. Roháčová, D. Dvořác, T. Tobrman, S. Záliš, R. Zvěřinová, J. Ludvík, *Electrochim. Acta* **2010**, *55*, 8341–8351; c) I. Hoskovcová, R. Zvěřinová, J. Roháčová, D. Dvořác, T. Tobrman, S. Záliš, J. Ludvík, *Electrochim. Acta* **2011**, *56*, 6853–6859; d) R.

Dedicated Cluster

 © 2015 WILEY-VCH Verlag GmbH & Co. KGaA, Weinheim

Journal of Inorganic and General Chemistry
ZAAC
Zeitschrift für anorganische und allgemeine Chemie
www.zaac.wiley-vch.de
ARTICLE

Metelková, T. Tobrman, H. Kvapilova, I. Hoskovcová, J. Ludvík, *Electrochim. Acta* **2012**, *82*, 470–477.
[40] H. Kvapilová, I. Hoslovcová, J. Ludvík, S. Záliš, *Organometallics* **2014**, *33*, 4964–4972.
[41] B. van der Westhuizen, P. J. Swarts, L. M. van Jaarsveld, D. C. Liles, U. Siegert, J. C. Swarts, I. Fernández, D. I. Bezuidenhout, *Inorg. Chem.* **2013**, *52*, 6674–6684.
[42] T. Tezgerevska, K. G. Alley, C. Boskovic, *Coord. Chem. Rev.* **2014**, *268*, 23–40.
[43] a) C. J. Picket, D. Fletcher, *J. Chem. Soc., Dalton Trans.* **1975**, 879–886; b) R. N. Bagchi, A. M. Bond, R. Colton, D. L. Luscombe, J. E. Moir, *J. Am. Chem. Soc.* **1986**, *108*, 3352–3358.
[44] a) E. Moser, E. O. Fischer, *J. Organomet. Chem.* **1968**, *13*, 387–398; b) A. Parlier, H. Rudler, J. C. Daran, C. Alvarez, *J. Organomet. Chem.* **1987**, *333*, 245–252.
[45] R. J. LeSuer, C. Buttolph, W. E. Geiger, *Anal. Chem.* **2004**, *76*, 6395–6401.
[46] S. Stoll, A. Schweiger, *J. Magn. Reson.* **2006**, *178*, 42–55.
[47] M. J. Frisch, G. W. Trucks, H. B. Schlegel, G. E. Scuseria, M. A. Robb, J. R. Cheeseman, G. Scalmani, V. Barone, B. Mennucci, G. A. Petersson, H. Nakatsuji, M. Caricato, X. Li, H. P. Hratchian, A. F. Izmaylov, J. Bloino, G. Zheng, J. L. Sonnenberg, M. Hada, M. Ehara, K. Toyota, R. Fukuda, J. Hasegawa, M. Ishida, T. Nakajima, Y. Honda, O. Kitao, H. Nakai, T. Vreven, J. A. Montgomery Jr., J. E. Peralta, F. Ogliaro, M. Bearpark, J. J. Heyd, E. Brothers, K. N. Kudin, V. N. Staroverov, R. Kobayashi, J. Normand, K. Raghavachari, A. Rendell, J. C. Burant, S. S. Iyengar, J. Tomasi, M. Cossi, N. Rega, J. M. Millam, M. Klene, J. E. Knox, J. B. Cross, V. Bakken, C. Adamo, J. Jaramillo, R. Gomperts, R. E. Stratmann, O. Yazyev, A. J. Austin, R. Cammi, C. Pomelli, J. W. Ochterski, R. L. Martin, K. Morokuma, V. G. Zakrzewski, G. A. Voth, P. Salvador, J. J. Dannenberg, S. Dapprich, A. D. Daniels, O. Farkas, J. B. Foresman, J. V. Ortiz, J. Cioslowski, D. J. Fox *Gaussian 09, revision A.02*, Gaussian, Inc., Wallingford CT, USA, **2000**.
[48] A. D. Becke, *J. Chem. Phys.* **1993**, *98*, 5648.
[49] a) C. E. Dykstra, *Chem. Phys. Lett.* **1977**, *45–52*, 466–469; b) P. J. Hay, W. R. Wadt, *J. Chem. Phys.* **1985**, *82*, 270; c) P. J. Hay, W. R. Wadt, *J. Chem. Phys.* **1985**, *82*, 299; d) W. R. Wadt, P. J. Hay, *J. Chem. Phys.* **1985**, *82*, 284.
[50] *SMART* Data Collection and *SAINT-Plus* Data Processing Software for the SMART System, various versions, Bruker Analytical X-ray Instruments, Inc., Madison, WI, USA, **2000**.
[51] R. H. Blessing, *Acta Crystallogr., Sect. A* **1995**, *51*, 33–38.
[52] a) G. M. Sheldrick, *SHELXTL*, version 5.1, Bruker AXS, Madison, WI, USA, **1998**; b) C. B. Hübschle, G. M. Sheldrick, B. Dittrich, *J. Appl. Crystallogr.* **2011**, *44*, 1281–1284.
[53] a) G. M. Sheldrick, *SHELXL-97*, University of Göttingen, Göttingen, Germany, **1997**; b) G. M. Sheldrick, *Acta Crystallogr., Sect. A* **2008**, *64*, 112–122.

Received: July 1, 2015
Published Online: August 11, 2015

Dedicated Cluster

 © 2015 WILEY-VCH Verlag GmbH & Co. KGaA, Weinheim

3.3 On the mechanism of imine elimination from Fischer tungsten carbene complexes

Philipp Veit, Christoph Förster*, Katja Heinze*

Beilstein J. Org. Chem. **2016**, *12*, 1322-1333.

Thematic Series: "Organometallic Chemistry" dedicated to the memory of Prof. Peter Hofmann.

(Aminoferrocenyl)(ferrocenyl)carbene(pentacarbonyl)tungsten(0) (**W(CO)$_5$(*E*-2)**) is synthesized by nucleophilic substitution of the ethoxy group of (CO)$_5$W=C(OEt)Fc by ferrocenyl amide Fc-NH$^-$ (Fc = ferrocenyl). **W(CO)$_5$(*E*-2)** thermally and photochemically eliminates bulky *E*-1,2-diferrocenylimine (***E*-3**) via a formal 1,2-H shift from the nitrogen atom to the carbene carbon atom. Kinetic and mechanistic studies to the formation of imine ***E*-3** are performed by NMR, IR and UV–vis spectroscopy and liquid injection field desorption ionization (LIFDI) mass spectrometry as well as by trapping experiments for low-coordinate tungsten complexes with triphenylphosphane. **W(CO)$_5$(*E*-2)** decays thermally in a first-order rate-law with a Gibbs free energy of activation of $\Delta G^{\ddagger}_{298K}$ = 112 kJ mol^{-1}. Three proposed mechanistic pathways are taken into account and supported by detailed (time-dependent) density functional theory [(TD)-DFT] calculations. The preferred pathway is initiated by an irreversible CO dissociation, followed by an oxidative addition/pseudorotation/reductive elimination pathway with short-lived, elusive sevencoordinate hydrido tungsten(II) intermediates ***cis*(N,H)-W(CO)4(H)(*Z*-15)** and ***cis*(C,H)-W(CO)4(H)(*Z*-15)**.

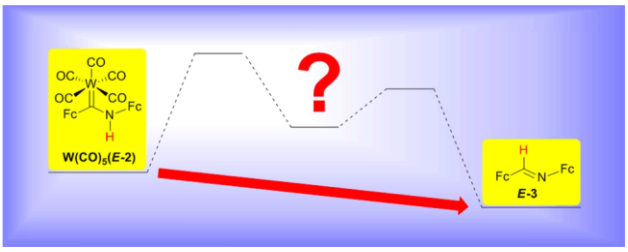

Author contributions

All experiments were performed by Philipp Veit. All DFT calculations were performed by Christoph Förster. The manuscript was written by Philipp Veit (20 %), Christoph Förster (40 %) and Katja Heinze (40 %).

Supporting Information

for this article is found in Chapter 6.3 at pp. 125. For full Supporting Information containing the coordinates of all relevant DFT calculated structures, refer to:

https://www.beilstein-journals.org/bjoc/content/supplementary/1860-5397-12-125-S1.pdf

This is an Open Access article under the terms of the Creative Commons Attribution License (http://creativecommons.org/licenses/by/2.0), which permits unrestricted use, distribution, and reproduction in any medium, provided the original work is properly cited.
The license is subject to the Beilstein Journal of Organic Chemistry terms and conditions: (http://www.beilstein-journals.org/bjoc) The definitive version of this article is the electronic one which can be found at: doi:10.3762/bjoc.12.125

BEILSTEIN JOURNAL OF ORGANIC CHEMISTRY

On the mechanism of imine elimination from Fischer tungsten carbene complexes

Philipp Veit, Christoph Förster* and Katja Heinze*

Full Research Paper

Open Access

Address:
Institute of Inorganic and Analytical Chemistry, Johannes Gutenberg-University, Duesbergweg 10-14, 55128 Mainz, Germany

Email:
Christoph Förster* - cfoerster@uni-mainz.de;
Katja Heinze* - katja.heinze@uni.mainz.de

* Corresponding author

Keywords:
carbene complexes; ferrocene; imine; mechanism; tungsten

Beilstein J. Org. Chem. **2016,** *12,* 1322–1333.
doi:10.3762/bjoc.12.125

Received: 15 April 2016
Accepted: 07 June 2016
Published: 27 June 2016

This article is part of the Thematic Series "Organometallic chemistry".
In memoriam Prof. Dr. Peter Hofmann.

Guest Editor: B. F. Straub

© 2016 Veit et al.; licensee Beilstein-Institut.
License and terms: see end of document.

Abstract

(Aminoferrocenyl)(ferrocenyl)carbene(pentacarbonyl)tungsten(0) $(CO)_5W{=}C(NHFc)Fc$ (**$W(CO)_5$(*E*-2)**) is synthesized by nucleophilic substitution of the ethoxy group of $(CO)_5W{=}C(OEt)Fc$ (**$M(CO)_5(1^{Et})$**) by ferrocenyl amide $Fc\text{-}NH^-$ (Fc = ferrocenyl). **$W(CO)_5$(*E*-2)** thermally and photochemically eliminates bulky *E*-1,2-diferrocenylimine (***E*-3**) via a formal 1,2-H shift from the N to the carbene C atom. Kinetic and mechanistic studies to the formation of imine ***E*-3** are performed by NMR, IR and UV–vis spectroscopy and liquid injection field desorption ionization (LIFDI) mass spectrometry as well as by trapping experiments for low-coordinate tungsten complexes with triphenylphosphane. **$W(CO)_5$(*E*-2)** decays thermally in a first-order rate-law with a Gibbs free energy of activation of $\Delta G^{\ddagger}_{298K}$ = 112 kJ mol^{-1}. Three proposed mechanistic pathways are taken into account and supported by detailed (time-dependent) densitiy functional theory [(TD)-DFT] calculations. The preferred pathway is initiated by an irreversible CO dissociation, followed by an oxidative addition/pseudorotation/reductive elimination pathway with short-lived, elusive seven-coordinate hydrido tungsten(II) intermediates ***cis*(N,H)-$W(CO)_4$(H)(*Z*-15)** and ***cis*(C,H)-$W(CO)_4$(H)(*Z*-15)**.

Introduction

Since the first example of a Fischer carbene complex $(CO)_5W{=}C(OMe)Me$ [1] in 1964, these compounds have evolved into a huge substance class with versatile applications as chemical multitalents in organic synthesis [2-5] as well as in light-driven organic reactions [6-8]. Carbene complexes of pentacarbonyl metal fragments (M = Cr, Mo, W) have further proven to be effective carbene transfer agents to late transition metals in transmetalation reactions [9-15]. The manifold synthetic access routes to carbene complexes even allows the assembly of multicarbene and multimetal carbene complexes [16,17]. First representatives of multimetal carbene complexes **$M(CO)_5(1^R)$** bear α-ferrocenyl alkoxy carbenes :C(OR)Fc (**1^R**,

Beilstein J. Org. Chem. 2016, 12, 1322–1333.

M = Cr, Mo, W; R = Me, Et; Fc = ferrocenyl) [18-22]. Nucleophilic substitution of the alkoxy substituent OR by amines gives access to α-ferrocenylamino Fischer carbene complexes [18,20,21,23-27], according to the classical Fischer route [28-31]. In contrast to conventional aromatic substituents, the Fc unit in **M(CO)$_5$(1^R)** is characterized by its redox activity and its large cylindrical steric bulk [32,33]. The electrochemical behaviour of ferrocenyl carbene complexes has been extensively investigated [25-27,34-39]. A second ferrocenyl unit can be incorporated by employing aminoferrocene (Fc-NH$_2$) [40,41] in a nucleophilic substitution reaction [27]. The trimetallic complex **Cr(CO)$_5$(*E*-2)** with the (aminoferrocenyl)ferrocenylcarbene ligand *E*-**2** is readily synthesized from **Cr(CO)$_5$(1^{Et})** by nucleophilic substitution of the ethoxy group with in situ generated ferrocenyl amide Fc-NH$^-$. Unlike the facile synthesis of the diphenyl derivative **Cr(CO)$_5$(*E*-4)** from **Cr(CO)$_5$(1^{Et})** and aniline [30,42], the preparation of the diferrocenyl derivative **Cr(CO)$_5$(*E*-2)** from bulky Fc-NH$_2$ [40,41] requires the presence of a base to increase the nucleophilicity of Fc-NH$_2$ by deprotonation. In the presence of base, **Cr(CO)$_5$(*E*-2)** decomposes readily in solution at room temperature releasing *E*-1,2-diferrocenylimine [43] *E*-**3** (Scheme 1a) [27]. Base assisted imine formation of NH carbene complexes typically occurs under rather harsh conditions. Thermal treatment of the significantly less encumbered complex **Cr(CO)$_5$(*E*/*Z*-4)** for 18 h in a 1:10 (v:v) pyridine (py)/hexane mixture yields imine *E*-**5** and *fac*-[Cr(CO)$_3$(py)$_3$] as side-product (Scheme 1b) [44]. Formation of the imine *E*-**7** and Cr(CO)$_6$ from the carbene complex **Cr(CO)$_5$(*Z*-6)** requires heating to 170 °C for 3 days under CO pressure (Scheme 1c) [42]. At room temperature and in the presence of base (KO*t*-Bu), **M(CO)$_5$(*Z*-8)** (M = Cr, W) simply isomerize to a mixture of *E*/*Z* isomers **M(CO)$_5$(*E*-8)**/

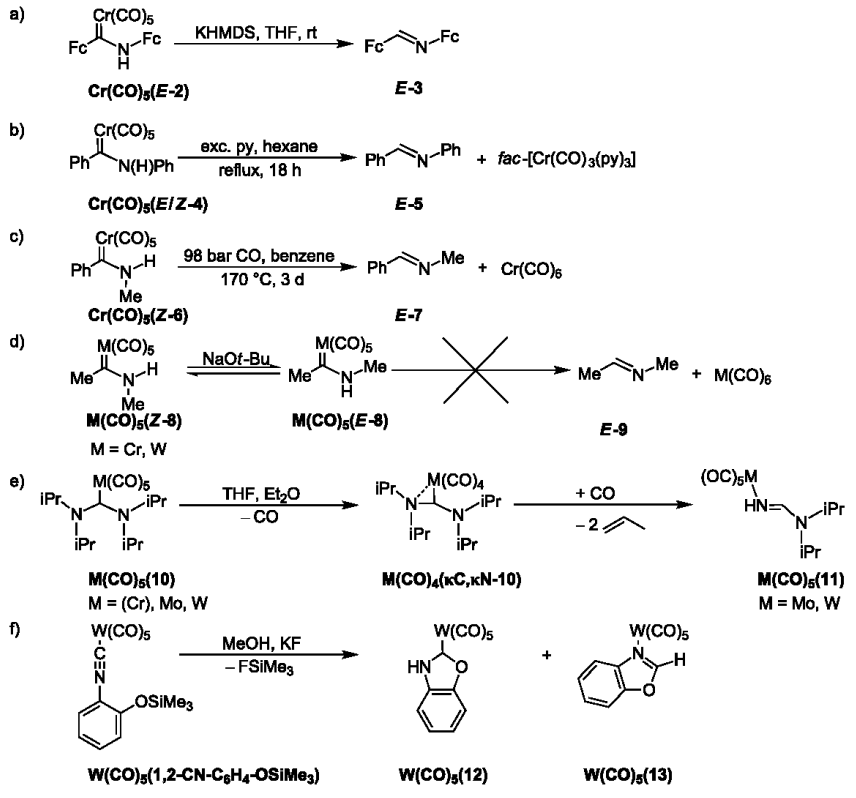

Scheme 1: Imine formation and isomerization reactions from NH carbene complexes **Cr(CO)$_5$(*E*-2)** (a) [27], **Cr(CO)$_5$(*E*/*Z*-4)** (b) [44], **Cr(CO)$_5$(*Z*-6)** (c) [42], **M(CO)$_5$(*Z*-8)** (d) [45,46], **M(CO)$_5$(10)** (e) [50-52] and during Si–O cleavage in the isonitrile complex **W(CO)$_5$(1,2-CN-C$_6$H$_4$-OSiMe$_3$)** (f) [53].

Beilstein J. Org. Chem. 2016, 12, 1322–1333.

M(CO)$_5$(*Z*-8) without ligand loss or formation of imine ***E*-9** (Scheme 1d) [45,46]. It appears that the bulky diferrocenylcarbene ***E*-2** facilitates formation of imine ***E*-3**. Mechanistically, a base-assisted 1,2-H shift can be conceived either at the coordinated carbene or at the free carbene [47,48] after ligand exchange at chromium (by py or CO) for **Cr(CO)$_5$(*E*/*Z*-4)** and **Cr(CO)$_5$(*Z*-6)**. Both pathways are compatible with the formation of the metal-containing products *fac*-[Cr(CO)$_3$(py)$_3$] and Cr(CO)$_6$ by dissociation of the imines ***E*-5** or ***E*-7** or by dissociation of the carbenes ***E*-4** or ***E*-6**, respectively (Scheme 1b,c) [42,44].

The related pentacarbonyl complexes of bis[di(isopropyl)amino]carbene **10** [49] **M(CO)$_5$(10)** (M = Cr, Mo, W) readily decarbonylate at room temperature to give the tetracarbonyl complexes **M(CO)$_4$(κC,κN-10)** with a side-on coordinated carbene ligand (Scheme 1e) [50-52]. Under CO atmosphere, the molybdenum and tungsten complexes **M(CO)$_{4/5}$(10)**, (M = Mo, W) eliminate two equivalents of propene giving the imine complexes **M(CO)$_5$(11)**. Formation of the imine complex tungsten(benzoxazole)(pentacarbonyl) **W(CO)$_5$(13)** has been reported by Tamm and Hahn during the synthesis of the carbene complex tungsten(benzoxazolin-2-ylidene)(pentacarbonyl) **W(CO)$_5$(12)** (Scheme 1f) [53].

In principle, the formation of imines from NH carbene complexes can occur by three conceivable fundamental pathways. The first pathway starts with the dissociation of the carbene followed by a 1,2-H shift at the free carbene (elimination–migration). The second one operates via a hydrogen atom shift at the coordinated carbene followed by dissociation of the resulting imine (migration–elimination). A third conceivable pathway could start with CO loss, followed by H atom migration. To the best of our knowledge, the mechanism of the imine formation from NH carbene complexes is not yet established.

In the absence of a base, the bulky diferrocenylcarbene complex **Cr(CO)$_5$(*E*-2)** is stable even in refluxing toluene and hence, a simple migration–elimination or elimination–migration reaction is not anticipated in this case. We report here the heavier tungsten analogue **W(CO)$_5$(*E*-2)** which is thermally reactive and smoothly forms the imine ***E*-3** without the need of prior deprotonation. This apparently simpler reaction allows the investigation of the mechanism of imine formation from NH carbene complexes.

Herein, the synthesis and characterization of **W(CO)$_5$(*E*-2)** followed by detailed mechanistic studies regarding the formation of imine ***E*-3** are presented including mass spectrometric, NMR, IR and UV–vis spectroscopic kinetic studies in combination with (TD)-DFT methods.

Results and Discussion

Synthesis of W(CO)$_5$(*E*-2)

The diferrocenyl NH carbene complex **W(CO)$_5$(*E*-2)** is obtained by treating **W(CO)$_5$(1^{Et})** [20,21] with aminoferrocene (Fc-NH$_2$) [40,41] in the presence of potassium hexamethyldisilazide (KHMDS) in tetrahydrofuran at room temperature (Scheme 2). In an analogous reactivity to **Cr(CO)$_5$(*E*-2)** (Scheme 1a) [27], the formation of the imine ***E*-3** is observed as a side-reaction under the alkaline conditions. Due to this reactivity, **W(CO)$_5$(*E*-2)** is obtained in only 28% yield as a deep-red crystalline compound after purification via column chromatography.

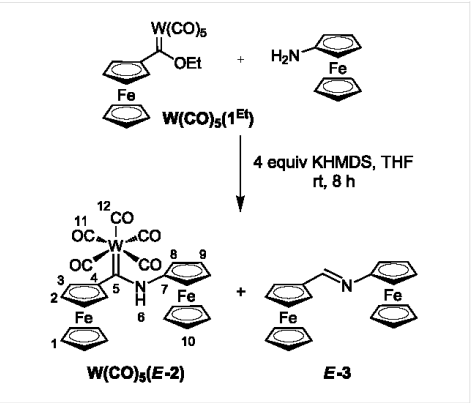

Scheme 2: Synthesis of **W(CO)$_5$(*E*-2)** from **W(CO)$_5$(1^{Et})** [20,21] and aminoferrocene [40,41] with concomitant formation of *E*-1,2-diferrocenylimine ***E*-3** [43] as side-product and atom numbering of **W(CO)$_5$(*E*-2)** for NMR assignments.

Characterization of W(CO)$_5$(*E*-2)

The composition and purity of **W(CO)$_5$(*E*-2)** is ascertained by mass spectrometry, showing the expected molecular ion peak at m/z = 721 with appropriate isotopic pattern, and elemental analysis (Experimental section and Supporting Information File 1). At increasing temperature in the FD mass spectrometer, peaks at m/z = 397 appear which can be assigned to a molecular ion of the composition $C_{21}H_{19}NFe_2$. A tiny peak cluster at m/z = 693, assignable to the loss of CO from **W(CO)$_5$(*E*-2)**, and peaks at higher m/z ratios, assignable to tungsten clusters, are also observed when traces of oxygen/water were present. Using ^{1}H and ^{13}C NMR spectroscopy as well as 2D NMR (^{1}H,^{1}H COSY, ^{1}H,^{1}H NOESY, ^{13}C,^{1}H HSQC, ^{13}C,^{1}H HMBC techniques), all ^{1}H and ^{13}C NMR resonances of **W(CO)$_5$(*E*-2)** are assigned based on coupling patterns and NOE contacts (Experimental section and Supporting Information File 1). Only the resonances of the unsubstituted C_5H_5 ligands (H^1, H^{10} and C^1, C^{10}) could not be discriminated. The proton resonances are

Beilstein J. Org. Chem. 2016, 12, 1322–1333.

found in a similar region as for other (pentacarbonyl)tungsten complexes **W(CO)$_5$(*E*-14^R)** with the α-ferrocenyl NH carbene ligand :C(NHR)Fc ***E*-14^R** (R = Me, Et, *n*-Pr [23], *n*-Bu [25], *n*-Pent [21]). Due to additional ring-current effects and non-classical NH···Fe hydrogen bonding [54-59] of the NH-Fc moiety, the resonance for the amine proton NH[6] (δ = 10.50 ppm in CD_2Cl_2) is shifted to lower field as compared to that of alkylamine substituted NH carbene complexes **M(CO)$_5$(*E*-14^R)** (δ = 9.00–9.11 ppm in $CDCl_3$) [21,23]. The NH···Fe interaction is also supported by the low-energy NH stretching vibration of **W(CO)$_5$(*E*-2)** at 3240 cm^{-1} in CD_2Cl_2, which matches to that of **Cr(CO)$_5$(*E*-2)** (3233 cm^{-1}) [27] (Experimental section and Supporting Information File 1). A weak absorption band at 3439 cm^{-1} is tentatively assigned to some **W(CO)$_5$(*Z*-2)** isomer lacking the NH···Fe interaction. In the solid state (KBr) the NH stretching vibration appears at 3335 cm^{-1} (Experimental section and Supporting Information File 1). The C–N–H bending vibration is observed as a single sharp relatively strong band at 1508 cm^{-1}. These IR data reveal that the main isomer in solution as well in the solid state is the *E* isomer in accordance with the IR data of **W(CO)$_5$(*E*/*Z*-8)** [46]. The carbonyl region of IR spectra of **W(CO)$_5$(*E*-2)** are in accordance with those of **Cr(CO)$_5$(*E*-2)** [27] and related amino(ferrocenyl)carbene(pentacarbonyl)tungsten complexes **W(CO)$_5$(*E*-14^R)** (R = Me, Et, *n*-Pr [23], *n*-Bu [25], *n*-Pent [21]). The UV–vis spectrum of **W(CO)$_5$(*E*-2)** (Supporting Information File 1) is similar to that of **Cr(CO)$_5$(*E*-2)** [27] and to those of carbene(pentacarbonyl)metal complexes (Cr, W) [60,61].

Thermolysis of **W(CO)$_5$(*E*-2)** in refluxing toluene gives imine ***E*-3** [43] after ca. 24 h in almost quantitative yield, as monitored by ^{1}H NMR spectroscopy. Accordingly, **W(CO)$_5$(*E*-2)** is a suitable candidate to investigate the imine formation from NH carbene complexes in a simple one-component system under relatively mild conditions and, importantly, in the absence of a base.

DFT studies on the formation of imine *E*-3 from W(CO)$_5$(*E*-2)

Three conceivable reaction pathways for the formation of imine ***E*-3** have been considered. For each pathway, density functional theory (DFT) calculations on the B3LYP/LANL2DZ (IEF-PCM toluene) level of theory have been performed to localize minimum structures and energies of the intermediates which are connected by transition states. The Gibbs free energies are reported at 298 K.

The first pathway comprises the migration–elimination mechanism involving a 1,2-H shift at the coordinated carbene ligand ***E*-2** or ***Z*-2** in **W(CO)$_5$(*E*-2)** or **W(CO)$_5$(*Z*-2)** followed by dissociation of the respective imine ***E*-3** (pathway 1a, Scheme 3) or ***Z*-3** (pathway 1b, Scheme 3), respectively. In the

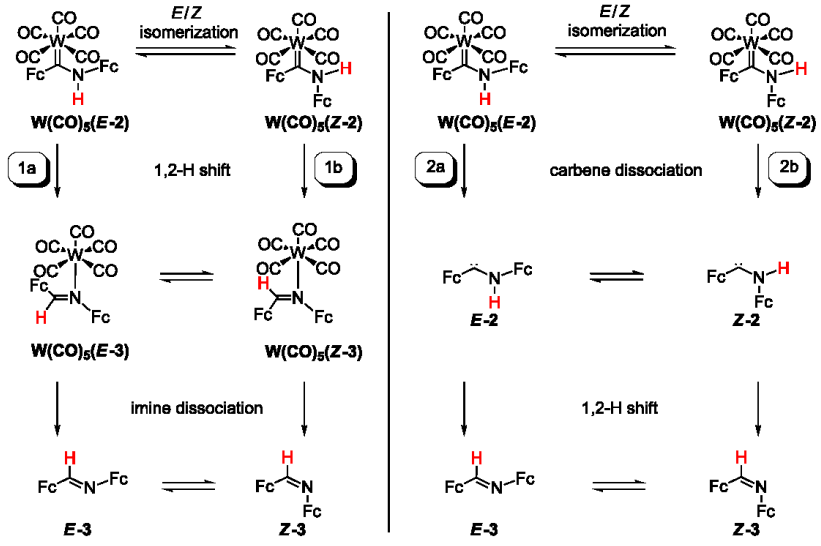

Scheme 3: Reaction pathways 1a/1b (migration–elimination) and 2a/2b (elimination–migration) for the formation of imine ***E*-3** from **W(CO)$_5$(*E*-2)**.

Beilstein J. Org. Chem. 2016, 12, 1322–1333.

latter case, *Z*-**3** isomerizes to the thermodynamically preferred isomer *E*-**3**. The second pathway (carbene elimination–migration) starts with the elimination of the carbenes *E*-**2** or *Z*-**2** followed by an 1,2-H shift to give the imines *E*-**3** (pathway 2a, Scheme 3) or *Z*-**3** (pathway 2b, Scheme 3). In the latter case, a *Z*-**3** → *E*-**3** isomerization follows.

The initial step of the third pathway is a CO dissociation yielding the tetracarbonyl complexes **W(CO)$_4$(*E*-2)** or **W(CO)$_4$(*Z*-2)**. This elimination is followed by a hydrogen atom shift at the coordinated carbene ligands *E*-**2** or *Z*-**2** (pathway 3a and 3b, Scheme 4) giving **W(CO)$_4$(*E*-3)** or **W(CO)$_4$(*Z*-3)**, respectively. Furthermore, the free coordination site in **W(CO)$_4$(*E*-2)** or **W(CO)$_4$(*Z*-2)** offers an oxidative addition/pseudorotation/reductive elimination pathway via the hydrido tungsten(II) complexes **W(CO)$_4$(H)(*Z*-15)** with the formally anionic ligand [Fc-C=N-Fc]$^-$ (**15**$^-$) as further alternative (pathway 3c, Scheme 4).

The calculated Gibbs free energies for **W(CO)$_5$(*E*-2)** and **W(CO)$_5$(*Z*-2)** are basically identical (Supporting Information File 1, Figure S16, Scheme 3). The calculated barrier for the *E*/*Z* isomerization **W(CO)$_5$(*E*-2)** → **W(CO)$_5$(*Z*-2)** amounts to $\Delta G^{\ddagger}$ = 108 kJ mol^{-1}. This barrier is significantly higher than that reported for (methoxy)(methyl)carbene(pentacarbonyl)chromium(0) Cr(CO)$_5$(C(OMe)Me) (52 kJ mol^{-1} (experimental) and ca. 61 kJ mol^{-1} (theoretical)) due to the larger steric bulk of the (aminoferrocenyl)ferrocenylcarbene **2**, the higher π-donating character of the amino substituent vs the alkoxy substituent thus increasing the C(carbene)–X double bond character (X = N, O) [62-64] and the loss of some attractive NH···Fe interaction (H···Fe(Fc-C) = 2.98 Å) in **W(CO)$_5$(*E*-2)** [27,54-59]. The Gibbs free energy of activation for the 1,2-H shift in **W(CO)$_5$(*Z*-2)** to give the imine complex **W(CO)$_5$(*Z*-3)** amounts to $\Delta G^{\ddagger}$ = 333 kJ mol^{-1} which is prohibitively large. For **W(CO)$_5$(*E*-2)** → **W(CO)$_5$(*E*-3)**, this barrier is somewhat smaller ($\Delta G^{\ddagger}$ = 284 kJ mol^{-1}), yet this 1,2-

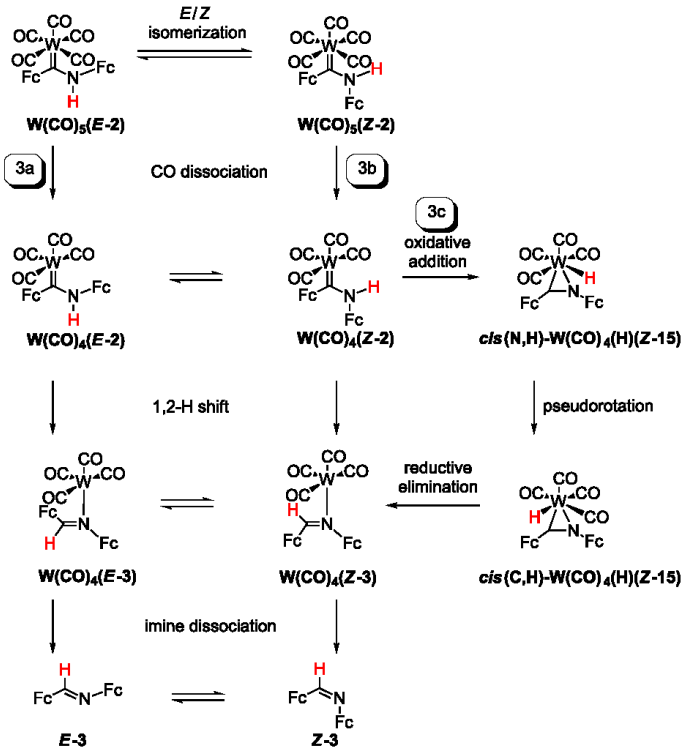

Scheme 4: Reaction pathways 3a/3b/3c (CO dissociation) for the formation of imine *E*-**3** from **W(CO)$_5$(*E*-2)**.

H shift initially only leads to a van-der-Waals adduct of the imine ***E*-3 [W(CO)$_5$···*E*-3]**. Hence, this hydrogen atom shift is coupled with a W–C(carbene) bond dissociation.

The turn over frequency (TOF) of catalytic cycles can be estimated from the energies of the TOF-determining transition state (TDTS) and the TOF-determining intermediate (TDI) [65]. The given energy difference between TDTS and TDI is the maximum energy span between a given intermediate and all following transition states of the cycle and can be understood as the overall Gibbs free energy of activation of the whole catalytic cycle [65]. This procedure can be translated to competing reaction paths. For pathways 1a and 1b (Scheme 3), the rate-determining intermediate (RDI) is **W(CO)$_5$(*Z*-2)** and the rate-determining transition states (RDTS's) are TS(**W(CO)$_5$(*E*-2)** → **W(CO)$_5$···*E*-3**) (pathway 1a) and TS(**W(CO)$_5$(*Z*-2)** → **W(CO)$_5$(*Z*-3)** (pathway 1b) giving the overall Gibbs free energies of activation $\Delta G^{\ddagger}_{total}$ = 287 kJ mol^{-1} and $\Delta G^{\ddagger}_{total}$ = 333 kJ mol^{-1}, respectively. The lower energy pathway 1a is associated with the dissociation of the carbene ligand (Supporting Information File 1, Figure S16). Hence, the initial dissociation of the carbenes ***E*-2** and ***Z*-2** is considered in pathways 2a and 2b (Scheme 3).

Dissociation of the carbenes ***E*-2**/***Z*-2** from **W(CO)$_5$(*E*-2)**/**W(CO)$_5$(*Z*-2)** is calculated endergonic (ΔG = 141 kJ mol^{-1} and ΔG = 167 kJ mol^{-1}, respectively, Scheme 3). Transition states for the carbene dissociation could not be identified. Hence, this initial dissociative step is probably not the one with the lowest energy. Nonetheless, the 1,2-H shift in the free carbenes has been calculated as well (Scheme 3).

The carbene ***E*-2** is 23 kJ mol^{-1} more stable than the ***Z*-2** isomer (Supporting Information File 1, Figure S17). The interconversion between these isomers ***E*-2** → ***Z*-2** ($\Delta G^{\ddagger}$ = 130 kJ mol^{-1}) proceeds via a bending vibration of the Cp–C(carbene)–N moiety. This reaction coordinate is fully analogous to the proposed mechanism of the *E*/*Z* isomerization of imines [66,67]. During the 1,2-H-shift of ***E*-2** to ***E*-3**, the migrating hydrogen atom interacts with the empty p_π-type orbital of the carbene carbon atom ($\Delta G^{\ddagger}$ = 250 kJ mol^{-1}), which is in accordance with the established mechanism of 1,2-migration reactions of carbenes [47,48,68-71]. Interestingly, the 1,2-H-shift of ***Z*-2** (***Z*-2** → ***Z*-3**: $\Delta G^{\ddagger}$ = 179 kJ mol^{-1}) with a lower barrier occurs within the C–C(carbene)–N plane via a direct interaction of the n_σ orbital at the carbene carbon atom with the hydrogen 1s orbital. Because of the non-crossing rule, this path is symmetry forbidden for aromatic carbenes [47,72]. The calculated barrier of the *E*/*Z* isomerization ***Z*-3** → ***E*-3** ($\Delta G^{\ddagger}$ = 52 kJ mol^{-1}) is in good agreement with experimental data for other imines with similar steric bulk, e.g., (Fc)$_2$C=NAr, leading to the global minimum ***E*-3** of pathways 2a and 2b (Scheme 3) [66,67]. ***E*-2** is the RDI for pathways 2a and 2b. The transition states TS(***E*-2** → ***E*-3**) ($\Delta G^{\ddagger}_{total}$ = 250 kJ mol^{-1}, pathway 2a) and TS(***Z*-2** → ***Z*-3**) ($\Delta G^{\ddagger}_{total}$ = 202 kJ mol^{-1}, pathway 2b) are the RDTS's. The 1,2-H-shift of the free carbenes **2** preferably proceeds via pathway 2b (Supporting Information File 1, Figure S17).

Compared to the carbene dissociation, significantly smaller endergonicities are calculated for the dissociation of a carbonyl ligand (pathways 3a and 3b, Scheme 4) giving the tetracarbonyl complexes **W(CO)$_4$(*E*-2)** and **W(CO)$_4$(*Z*-2)** with ΔG = 86 kJ mol^{-1} and 115 kJ mol^{-1}, respectively (Scheme 4). The **W(CO)$_4$(*E*-2)** isomer is stabilized with respect to **W(CO)$_4$(*Z*-2)** by 26 kJ mol^{-1}. The *E*/*Z* isomerization of **W(CO)$_4$(2)** proceeds via an intermediate **W(CO)$_4$(κ*C*,κ*N*-2)** with a side-on coordination of the carbene ligand **2** exploiting the free coordination site at tungsten similar to **M(CO)$_4$(κC,κN-10)** [50-52] (Scheme 1, Supporting Information File 1, Figure S18). The barrier for this *E*/*Z* carbene isomerization amounts to only $\Delta G^{\ddagger}$ = 99 kJ mol^{-1}. This represents the lowest barrier for the ***E*-2**/***Z*-2** isomerization calculated in the systems **W(CO)$_5$(*E*-2**/***Z*-2)**, **W(CO)$_4$(*E*-2**/***Z*-2)** and ***E*-2**/***Z*-2** (vide supra). However, the following 1,2-H shifts have high barriers of 294 and 248 kJ mol^{-1} for **W(CO)$_4$(*E*-2)** → **W(CO)$_4$(*E*-3)** and **W(CO)$_4$(*Z*-2)** → **W(CO)$_4$(*Z*-3)**, respectively. For the former reaction and similar to the 1,2-H shift in **W(CO)$_5$(*E*-2)** (vide supra), the van-der-Waals adduct **[W(CO)$_4$···*E*-3]** is the initial product implying the dissociation of the W–C(carbene) bond. The RDI for pathways 3a and 3b is **W(CO)$_4$(*E*-2)**. The RDTS's are TS(**W(CO)$_4$(*E*-2)** → **[W(CO)$_4$···*E*-3]**) ($\Delta G^{\ddagger}_{total}$ = 294 kJ mol^{-1}, pathway 3a) and TS(**W(CO)$_4$(*Z*-2)** → **W(CO)$_4$(*Z*-3)**) ($\Delta G^{\ddagger}_{total}$ = 274 kJ mol^{-1}, pathway 3b). Both pathways 3a and 3b are quite energy demanding and require even more energy than the ***E*-2** → ***E*-3** and ***Z*-2** → ***Z*-3** hydrogen atom migrations in the free carbenes (vide supra). The free coordination site at tungsten in **W(CO)$_4$(*Z*-2)** provides a third sequence for the formation of imine ***E*-3** (Scheme 4, Figure 1). Oxidative addition of the NH bond to the unsaturated tungsten center ($\Delta G^{\ddagger}$ = 157 kJ mol^{-1}) gives the seven-coordinate hydrido tungsten(II) complex ***cis*(N,H)-W(CO)$_4$(H)(*Z*-15)** with formally anionic [Fc-C=N-Fc]$^-$ (**15**$^-$) and hydrido ligands (Scheme 4, Figure 1 and Figure 2).

A similar oxidative addition has been proposed in the literature for the iron (aminophenyl)phenylcarbene complex [Cp(CO)(S(SiEt$_3$))Fe(**4**)] leading to an intermediate hydrido species followed by the elimination of *E*-1,2-diphenylimine ***E*-5** [73]. Pseudorotation of ***cis*(N,H)-W(CO)$_4$(H)(*Z*-15)** to the isoenergetic rotamer ***cis*(C,H)-W(CO)$_4$(H)(*Z*-15)** ($\Delta G^{\ddagger}$ = 86 kJ mol^{-1}) enables a low-energy reductive elimination

Beilstein J. Org. Chem. 2016, 12, 1322–1333.

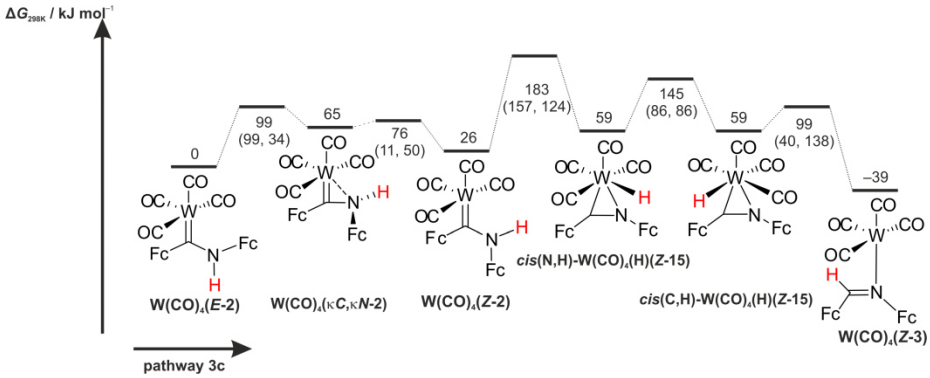

Figure 1: DFT calculated oxidative addition/pseudorotation/reductive elimination pathway 3c from **W(CO)$_4$(*E*-2)** to **W(CO)$_4$(*Z*-3)**.

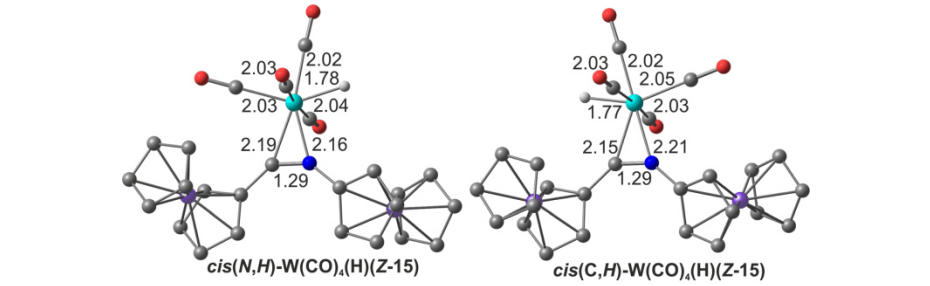

Figure 2: DFT calculated geometries of the two hydrido intermediates ***cis*(*N,H*)-W(CO)$_4$(H)(*Z*-15)** and ***cis*(*C,H*)-W(CO)$_4$(H)(*Z*-15)** and selected bond distances in Å.

($\Delta G^{\ddagger}$ = 40 kJ mol^{-1}) to give the imine complex **W(CO)$_4$(*Z*-3)** (Figure 1).

The overall Gibbs free energy of activation amounts to only $\Delta G^{\ddagger}_{total}$ = 183 kJ mol^{-1} with the RDI **W(CO)$_4$(*E*-2)** and the RDTS TS(**W(CO)$_4$(*Z*-2)** → ***cis*(*N,H*)-W(CO)$_4$(H)(*Z*-15)**) (pathway 3c) for this preferred reaction sequence (Figure 1 and Supporting Information File 1, Figure S19).

All overall Gibbs free energies of activation for the discussed pathways 1a/1b and 3a/3b in the coordination sphere of the metal center are higher than for the carbene → imine isomerization in the metal-free systems ***E*-2** → ***E*-3** and ***Z*-2** → ***Z*-3** (pathways 2a/2b). This suggests that W(CO)$_5$ or W(CO)$_4$ coordination to ***E*-2** or ***Z*-2** kinetically stabilizes the carbene ligand. All pathways 1a/1b, 2a/2b and 3a/3b have large overall Gibbs free energies of activation with $\Delta G^{\ddagger}_{total}$ > 200 kJ mol^{-1}. The alternative pathway 3c via CO dissociation, oxidative addition, pseudorotation and reductive elimination features the lowest overall Gibbs free energy of activation of $\Delta G^{\ddagger}_{total}$ = 183 kJ mol^{-1}. Although activation barriers for CO and carbene ligand dissociation steps could not be determined by DFT calculations, the formation of tetracarbonyl complexes is very probable, while the carbene dissociation is less likely. The experimentally determined barrier for CO dissociation from tungsten hexacarbonyl amounts to 193 kJ mol^{-1} [74]. According to the calculations, the **W(CO)$_4$(*Z*-2)** isomer is accessible from the thermodynamically preferred **W(CO)$_4$(*E*-2)** isomer. The following oxidative addition pathway 3c from **W(CO)$_4$(*Z*-2)** via the hydrido complexes ***cis*(*N,H*)-W(CO)$_4$(H)(*Z*-15)** and ***cis*(*C,H*)-W(CO)$_4$(H)(*Z*-15)** provides the lowest energy pathway for the formation of the imines ***Z*-3** and ***E*-3**. Important calculated bond distances in these key intermediates amount to W–C(carbene) = 2.19, 2.15 Å, W–N = 2.16, 2.21 Å, W–H = 1.78, 1.77 Å and C–N = 1.29, 1.29 Å for ***cis*(*N,H*)-W(CO)$_4$(H)(*Z*-15)** and ***cis*(*C,H*)-W(CO)$_4$(H)(*Z*-15)**, respec-

Beilstein J. Org. Chem. 2016, 12, 1322–1333.

tively (Figure 2). These hydrido intermediates act as hydrogen atom shuttle from the nitrogen to the carbon atom in NH carbene tetracarbonyl tungsten complexes. Oxidative additions of XY bonds to low-coordinate $W(CO)_n$ fragments is a common reactivity pattern for tungsten carbonyl complexes [75-80] and appears to be operative in the present case as well.

Experimental studies on the formation of imine *E*-3 from W(CO)$_5$(*E*-2)

Heating of a toluene solution of **W(CO)$_5$(*E*-2)** results in the formation of the imine ***E*-3** according to ^{1}H NMR spectroscopy (monitored by the NH proton resonance of **W(CO)$_5$(*E*-2)** at δ = 10.16 ppm and the CH proton resonance of ***E*-3** at δ = 8.33 ppm; Supporting Information File 1, Figures S20–S24). The appearance of a resonance at δ = 9.68 ppm is assigned to a trace amount of **W(CO)$_5$(*Z*-2)**. A dark precipitate (possibly tungsten nanoparticles [81,82]) forms during the thermolysis. The half-lives at 60, 70, 80, 90 and 100 °C amount to 145.9, 39.4, 28.9, 16.2 and 12.2 h. The time traces fit to a first order kinetics as anticipated in the absence of a base. An Eyring–Polanyi plot gives an activation enthalpy of $\Delta H^{\ddagger}$ = 54.5 ± 10.4 kJ mol^{-1} and an activation entropy of $\Delta S^{\ddagger}$ = –193 ± 30 J mol^{-1} K^{-1} (Supporting Information File 1, Figure S25). These values give a Gibbs free energy of activation of $\Delta G^{\ddagger}_{298K}$ = 112 kJ mol^{-1}.

The ^{1}H NMR spectra during thermolysis provide no hint for a long-lived intermediate and the reaction cleanly proceeds from the starting material **W(CO)$_5$(*E*-2)** to the product ***E*-3**. No hydride resonances have been detected up to δ = −30 ppm in the ^{1}H NMR spectra. This suggests that subsequent reactions after ligand dissociation proceed faster and the irreversible ligand dissociation is the rate-determining step.

Attempts to intercept low-coordinate tungsten intermediates were conducted by thermolysis of **W(CO)$_5$(*E*-2)** in the presence of triphenylphosphane. In case of aminocarbenes, experiments on the synthesis and decomposition of carbene(tetracarbonyl)(phosphane) complexes of chromium and tungsten revealed the exclusive formation of ***cis*-M(CO)$_4$(PR$_3$)(carbene)** (R = *n*-Bu, Ph) [83-85]. **M(CO)$_5$(PR$_3$)** and ***trans*-M(CO)$_4$(PR$_3$)$_2$** (M = Cr, W) have been detected as side-products [83,84].

W(CO)$_5$(PPh$_3$) gives a ^{31}P resonance at δ = 20.9 ppm ($^1J_{WP}$ = 243 Hz) in $CDCl_3$ and ***trans*-W(CO)$_4$(PR$_3$)$_2$** at δ = 27.4 ppm ($^1J_{WP}$ = 282 Hz) [86], while reported $W(CO)_4(PPh_3)$(carbene) complexes resonate in CD_2Cl_2 at δ = 24–25 ppm ($^1J_{WP}$ = 232–236 Hz) (*cis*) and at δ = 23 ppm ($^1J_{WP}$ = 209 Hz) (*trans*) and exhibit significantly smaller $^1J_{WP}$ coupling constants [85]. A ^{31}P NMR resonance of a toluene-d_8 solution of **W(CO)$_5$(*E*-2)** with one equivalent PPh_3 heated to 100 °C for 1 h was observed at δ = 27.3 ppm with ^{183}W satellites ($^1J_{WP}$ = 238 Hz) fitting to the carbene tetracarbonyl phosphane complex ***cis*-W(CO)$_4$(PPh$_3$)(*E*-2)** (23%) in addition to residual PPh_3 (δ = −4.2 ppm, 73%) (Scheme 5, Supporting Information File 1, Figure S13). A less intense resonance (4%) at δ = 28.9 ppm ($^1J_{WP}$ = 283 Hz) is assigned to ***trans*-W(CO)$_4$(PPh$_3$)$_2$** [86]. At later stages of the reaction, isomerization to another *cis* isomer of ***cis*-W(CO)$_4$(PPh$_3$)(*E*-2)** with δ = 24.0 ppm ($^1J_{WP}$ = 234 Hz), according to the $^1J_{WP}$ coupling constant [85], probably occurs. After 4 h another ^{31}P resonance appears at δ = 22.2 ppm ($^1J_{WP}$ = 244 Hz). Comparison of $^1J_{WP}$ coupling constants confirms the presence of **W(CO)$_5$(PPh$_3$)** [86], with up to 67% spectroscopic yield after 25 h. Hence, the ^{31}P NMR data suggest the following sequence as a main pathway: The sequence starts with initial loss of a CO ligand from **W(CO)$_5$(*E*-2)**, followed by formation of ***cis*-W(CO)$_4$(PPh$_3$)(*E*-2)** complexes. Substitution of imine ***E*-3** by a second PPh_3 ligand gives ***trans*-W(CO)$_4$(PPh$_3$)$_2$**. Finally, **W(CO)$_5$(PPh$_3$)** is formed, presumably along with elemental tungsten (Scheme 5).

FD mass spectrometry confirms the most probable decomposition of **W(CO)$_4$(PPh$_3$)(*E*-2)** to ***trans*-W(CO)$_4$(PPh$_3$)$_2$** (*m*/*z* = 820), **W(CO)$_5$(PPh$_3$)** (*m*/*z* = 586) and imine ***E*-3** (*m*/*z* = 397) (Supporting Information File 1, Figure S14). The carbonyl and CN stretching frequencies (2072, 2018, 1982, 1938, 1889,

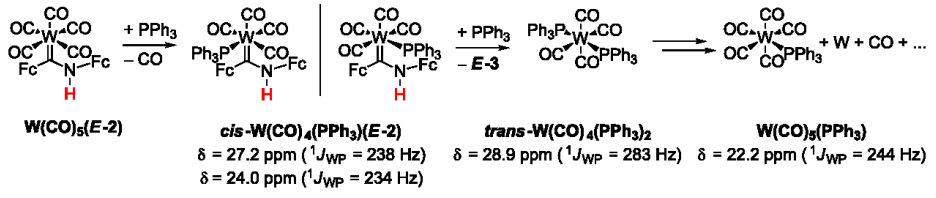

Scheme 5: Proposed reaction sequence from **W(CO)$_5$(*E*-2)** to **W(CO)$_5$(PPh$_3$)** in the presence of triphenylphosphane.

Beilstein J. Org. Chem. 2016, 12, 1322–1333.

1614 cm^{-1}) and relative intensities of partially overlapping bands obtained by IR spectroscopy (Supporting Information File 1, Figure S15) fit to a mixture of **W(CO)$_5$(PPh$_3$)** ($\tilde{\nu}$ = 2072, 1982, 1938 cm^{-1}) [87,88], **W(CO)$_4$(PPh$_3$)$_2$** in *cis* ($\tilde{\nu}$ = 2018 cm^{-1}) and *trans* ($\tilde{\nu}$ = 1938, 1889 cm^{-1}) configuration [89,90] as well as imine ***E*-3** ($\tilde{\nu}$ = 1614 cm^{-1}). Hence, the initial thermally induced dissociation of a CO ligand is more favourable than carbene dissociation in agreement with the DFT calculations (vide supra).

Similarly, photochemical activation (400 nm LEDs) in toluene produces imine ***E*-3** in 31% yield after 120 h from **W(CO)$_5$(*E*-2)** already at room temperature, while only 1% ***E*-3** is formed in the dark at room temperature. This observation additionally supports the hypothesis that the key initial step is the dissociation of CO from **W(CO)$_5$(*E*-2)** to give **W(CO)$_4$(*E*-2)** (Scheme 4).

Attempts to observe the tetracarbonyl intermediates in the absence of PPh_3 by LIFDI mass spectrometry were unsuccessful. The mass spectra recorded at several time intervals during the heating procedure (reflux in toluene under strictly inert conditions) display the peak of the starting material at m/z = 721 and the peak of the imine product ***E*-3** at m/z = 397. The former peak decreases while the latter one increases during the heating process (Supporting Information File 1, Figure S26). No other intermediates appear in the FD mass spectra. Tentatively, the concomitantly formed tungsten species aggregate under these conditions and form the observed dark precipitate. This further supports the hypothesis that no intermediates accumulate during the reaction and that the rate-determining step is the CO ligand dissociation.

IR spectroscopic monitoring of a **W(CO)$_5$(*E*-2)** solution in 1,2-dichloroethane under reflux (ca. 84 °C) shows that **W(CO)$_5$(*E*-2)** simply decays to a carbonyl-free species (likely the dark precipitate) and no soluble CO-containing intermediates such as **W(CO)$_4$(*E*-2)**, **W(CO)$_4$(*Z*-2)** or hydrido carbonyl complexes are detected (Supporting Information File 1, Figure S27).

In full accordance with the above observations, UV–vis spectra recorded during the thermal treatment of **W(CO)$_5$(*E*-2)** in toluene (100 °C) show the clean decay of the characteristic bands of **W(CO)$_5$(*E*-2)** at 360 and 391 nm. The ferrocene based absorption band around 500 nm remains essentially constant indicating the stability of the Fc units. Isosbestic points are observed at 337 and 500 nm corroborating the clean conversion of **W(CO)$_5$(*E*-2)** to ***E*-3** without long-lived soluble intermediates (Supporting Information File 1, Figure S28). The final UV–vis spectrum after 6 h closely resembles that of the calculated TD-DFT spectrum of imine ***E*-3** (Supporting Information File 1, Figure S29). All spectroscopic and analytical data suggest that the imine formation is faster than the CO dissociation.

Conclusion

The thermally induced formation of *E*-1,2-diferrocenylimine ***E*-3** from the NH carbene pentacarbonyl tungsten complex **W(CO)$_5$(*E*-2)** was investigated by density functional theory methods and mechanistic experimental studies (NMR, IR, UV–vis spectroscopy, FD mass spectrometry, kinetic studies, trapping of intermediates). All available data support the initial dissociation of a CO ligand to give the tetracarbonyl complex **W(CO)$_4$(*E*-2)**. Isomerization to the **W(CO)$_4$(*Z*-2)** isomer allows for an oxidative addition of the NH bond to give the seven-coordinate hydrido tungsten(II) complex ***cis*(N,H)-W(CO)$_4$(H)(*Z*-15)**. After pseudorotation to the ***cis*(C,H)-W(CO)$_4$(H)(*Z*-15)** rotamer, a reductive elimination yields the imine complex **W(CO)$_4$(*Z*-3)**. All other conceivable pathways, namely 1,2-H shifts within the free carbene or within the carbonyl complexes **W(CO)$_5$(*E*-2)** or **W(CO)$_4$(*E*-2)**, are significantly more energy demanding. The possibility of a seven-coordinate tungsten(II) intermediate opens the oxidative addition/pseudorotation/reductive elimination pathway shuttling the hydrogen atom from the nitrogen atom via the W atom to the carbene carbon atom. This pathway is unfeasible for homologous chromium complexes and explains the resistance of **Cr(CO)$_5$(*E*-2)** towards thermal ***E*-3** formation. A base-assisted pathway for imine formation is operative both for **Cr(CO)$_5$(*E*-2)** and **W(CO)$_5$(*E*-2)**, but the thermal imine formation is only feasible for **W(CO)$_5$(*E*-2)**.

Experimental

General procedures: All reactions were performed under argon atmosphere unless otherwise noted. A glovebox of the type UniLab/MBraun (Ar 4.8, O_2 < 1 ppm, H_2O < 1 ppm) was used for storage and weighing of sensitive compounds. All analytical samples that required the absence of oxygen were prepared in the same glovebox. Dichloromethane and 1,2-dichloroethane were dried with CaH_2 and distilled prior to use. THF and toluene were distilled from potassium. All reagents were used as received from commercial suppliers (ABCR, Acros Organics, Alfa Aesar, Fischer Scientific, Fluka and Sigma-Aldrich). Deuterated solvents were purchased from euriso-top. (Ethoxy)(ferrocenyl)carbene(pentacarbonyl)tungsten(0) **W(CO)$_5$(1^{Et})** [21] and Fc–NH_2 [40,41] were prepared according to literature procedures.

NMR spectra were recorded on a Bruker Avance DRX 400 spectrometer at 400.31 MHz (^{1}H), 100.07 MHz (^{13}C{^{1}H}) and 162.05 MHz (^{31}P{^{1}H}). All resonances are reported in ppm vs the solvent signal as internal standard [CD_2Cl_2 (^{1}H: δ =

5.32 ppm; ^{13}C: δ = 53.8 ppm), toluene-d_8 (^{1}H: δ = 2.08 ppm)] [91] and versus external H_3PO_4 (85%) (^{31}P: δ = 0 ppm). IR spectra were recorded with a BioRad Excalibur FTS 3100 spectrometer as KBr disks or by using KBr cells in CH_2Cl_2 or in CD_2Cl_2. Electrochemical experiments were carried out on a BioLogic SP-50 voltammetric analyzer by using a platinum working electrode, a platinum wire as counter electrode and a 0.01 M Ag/$AgNO_3$ electrode as reference electrode. The measurements were carried out at a scan rate of 100 mV s^{-1} for cyclic voltammetry experiments and at 50 mV s^{-1} for square wave voltammetry experiments in 0.1 M [*n*-Bu_4N][$B(C_6F_5)_4$] as supporting electrolyte in THF. Potentials are referenced against the decamethylferrocene/decamethylferrocenium couple ($E_{½}$ = −525 ± 5 mV vs ferrocene/ferrocenium under our experimental conditions) and are given relative to the ferrocene/ferrocenium couple. UV–vis/NIR spectra were recorded on a Varian Cary 5000 spectrometer by using 1.0 cm cells (Hellma, suprasil). FD mass spectra were recorded on a Thermo Fisher DFS mass spectrometer with a LIFDI upgrade. Elemental analyses were performed by the microanalytical laboratory of the chemical institutes of the University of Mainz.

Density functional theory calculations were carried out with the Gaussian09/DFT series [92] of programs. The B3LYP [93] formulation of density functional theory was used employing the LANL2DZ [94-97] basis set. No symmetry constraints were imposed on the molecules. The presence of energy minima of the ground states was checked by analytical frequency calculations. The calculated transition states exhibit a single imaginary frequency and they were additionally verified by intrinsic reaction coordinate (IRC) calculations. Solvent modelling was done employing the integral equation formalism polarizable continuum model (IEFPCM, toluene). The approximate free energies at 298 K were obtained through thermochemical analysis of the frequency calculation, using the thermal correction to the Gibbs free energy as reported by Gaussian09.

(Aminoferrocenyl)(ferrocenyl)carbene(pentacarbonyl)tungsten(0) ($W(CO)_5$(*E*-2)): 402 mg (2.0 mmol) of Fc-NH_2 and 1132 mg (2.0 mmol) of **$W(CO)_5(1^{Et})$** where dissolved in dry THF (40 mL). 1595 mg (8.0 mmol) of potassium hexamethyldisilazide (KHMDS) in dry THF (40 mL) were added within 5.5 h while stirring at room temperature. The reaction was monitored by TLC to check the reaction progress and to stop the reaction before extensive imine formation occurs. After 8 h, the solvent was removed under reduced pressure and an aqueous saturated $NaHCO_3$ solution (100 mL) was added. The aqueous phase was extracted with dichloromethane (3 × 100 mL) and the combined organic phases were washed with aqueous saturated $NaHCO_3$ solution (2 × 100 mL) and brine (2 × 100 mL). The organic phase was dried over $MgSO_4$. After evaporation of the solvent under reduced pressure, a crude red product was obtained (1.04 mg). Purification by column chromatography (SiO_2; 40 cm × 5.5 cm; petroleum ether (40/60):CH_2Cl_2 1:1; R_f(Fc–NH_2) = 0.0, R_f(***E*-3**) = 0.5, R_f(**$W(CO)_5$(*E*-2)**) = 0.8) yielded 403 mg (0.56 mmol, 28%) of deep red crystalline needles. ^{1}H NMR (CD_2Cl_2): δ 10.50 (s, 1H, H6), 4.73 (pt, 2H, H8), 4.71 (pt, 2H, H3), 4.62 (pt, 2H, H2), 4.37 (s, 5H, H1/10), 4.33 (pt, 2H, H9), 4.32 (s, 5H, H1/10) ppm; ^{13}C NMR (CD_2Cl_2) δ 259.6 (C5), 204.4 (C12), 199.3 (C11, $^1J_{WC}$ = 127 Hz), 99.7 (C7), 97.7 (C4), 72.1 (C2), 70.7 (C3), 70.6 (C1/10), 70.2 (C1/10), 69.1 (C8), 67.8 (C9) ppm; MS (FD) *m/z* (int.): 721.0 (100, $[M]^+$); IR (KBr) $\tilde{\nu}$: 3335 (m, NH), 3107 (s, CH), 2058 (vs, CO), 1977 (vs, CO), 1899 (br, CO), 1508 (s), 1350 (m), 1238 (m), 1057 (m), 822 (m), 600 (s), 579 (m), 480 (m) cm^{-1}; IR (CH_2Cl_2) $\tilde{\nu}$: 2060 (vs, CO A_1), 1975 (s, CO B_1), 1921 (br, CO *E*, A_1), 1503 (m) cm^{-1}; IR (CD_2Cl_2) $\tilde{\nu}$: 3439 (w, NH($W(CO)_5$(*Z*-2))), 3240 (m, NH($W(CO)_5$(*E*-2))) cm^{-1}; UV–vis (CH_2Cl_2) λ_{max} (ε): 290 sh (15370), 355 (11020), 387 (11680), 468 sh (2570 M^{-1} cm^{-1}) nm; CV (THF, vs FcH/FcH^+): $E_{1/2}$ = −2.38 V (qrev.), $E_{p,ox}$ = 0.26, 0.48 V, $E_{p,red}$ = 0.17, −0.15, −0.76 V; Anal. calcd for $C_{26}H_{19}Fe_2NO_5W$ (720.95): C, 43.31; H, 2.66; N, 1.94; found: C, 43.30; H, 2.69; N, 1.91.

Supporting Information

Supporting Information File 1

Experimental spectra and DFT derived data.
[http://www.beilstein-journals.org/bjoc/content/supplementary/1860-5397-12-125-S1.pdf]

Acknowledgements

We are grateful to the Johannes Gutenberg University of Mainz (Germany) for financial support to C.F. (Internal University Research Funding). We thank Petra Auerbach and Dr. Mihail Mondeskhi for collecting the LIFDI mass spectra.

References

1. Fischer, E. O.; Maasböl, A. *Angew. Chem., Int. Ed. Engl.* **1964,** *3,* 580–581. doi:10.1002/anie.196405801
2. Dötz, K. H.; Stendel, J., Jr. *Chem. Rev.* **2009,** *109,* 3227–3274. doi:10.1021/cr900034e
3. de Meijere, A.; Schirmer, H.; Duetsch, M. *Angew. Chem., Int. Ed.* **2000,** *39,* 3964–4002. doi:10.1002/1521-3773(20001117)39:22<3964::AID-ANIE3964>3.0.CO;2-C
4. Barluenga, J.; Flórez, J.; Fañanás, F. J. *J. Organomet. Chem.* **2001,** *624,* 5–17. doi:10.1016/S0022-328X(00)00837-8
5. Barluenga, J.; Fernández-Rodríguez, M. A.; Aguilar, E. *J. Organomet. Chem.* **2005,** *690,* 539–587. doi:10.1016/j.jorganchem.2004.10.032

Beilstein J. Org. Chem. **2016,** *12,* 1322–1333.

6. Hegedus, L. S. *Top. Organomet. Chem.* **2004,** 157–201. doi:10.1007/b98765
7. Hegedus, L. S. *Tetrahedron* **1997,** *53,* 4105–4128. doi:10.1016/S0040-4020(96)01186-6
8. Fernández, I.; Cossío, F. P.; Sierra, M. A. *Acc. Chem. Res.* **2011,** *44,* 479–490. doi:10.1021/ar100159h
9. Gómez-Gallego, M.; Mancheño, M. J.; Sierra, M. A. *Acc. Chem. Res.* **2005,** *38,* 44–53. doi:10.1021/ar040005r
10. Raubenheimer, H. G. *Dalton Trans.* **2014,** *43,* 16959–16973. doi:10.1039/c4dt01943a
11. Aumann, R.; Fischer, E. O. *Chem. Ber.* **1981,** *114,* 1853–1857. doi:10.1002/cber.19811140523
12. Bezuidenhout, D. I.; van der Westhuizen, B.; Rosenthal, A. J.; Wörle, M.; Liles, D. C.; Fernández, I. *Dalton Trans.* **2014,** *43,* 398–401. doi:10.1039/c3dt52961d
13. Ramollo, G. K.; López-Gómez, M. J.; Liles, D. C.; Matsinha, L. C.; Smith, G. S.; Bezuidenhout, D. I. *Organometallics* **2015,** *34,* 5745–5753. doi:10.1021/acs.organomet.5b00843
14. Seidel, G.; Gabor, B.; Goddard, R.; Heggen, B.; Thiel, W.; Fürstner, A. *Angew. Chem., Int. Ed.* **2014,** *53,* 879–882. doi:10.1002/anie.201308842
15. Seidel, G.; Fürstner, A. *Angew. Chem., Int. Ed.* **2014,** *53,* 4807–4811. doi:10.1002/anie.201402080
16. Sierra, M. A. *Chem. Rev.* **2000,** *100,* 3591–3638. doi:10.1021/cr9804137
17. Bezuidenhout, D. I.; Lotz, S.; Liles, D. C.; van der Westhuizen, B. *Coord. Chem. Rev.* **2012,** *256,* 479–524. doi:10.1016/j.ccr.2011.12.003
18. Connor, J. A.; Jones, E. M.; Lloyd, J. P. *J. Organomet. Chem.* **1970,** *24,* C20–C22. doi:10.1016/S0022-328X(00)80254-5
19. Mose, G. A.; Fischer, E. O.; Rausch, M. D. *J. Organomet. Chem.* **1971,** *27,* 379–382. doi:10.1016/S0022-328X(00)82169-5
20. Connor, J. A.; Lloyd, J. P. *J. Chem. Soc., Dalton Trans.* **1972,** 1470–1476. doi:10.1039/dt9720001470
21. López-Cortés, J. G.; Contreras de la Cruz, L. F.; Ortega-Alfaro, M. C.; Toscano, R. A.; Alvarez-Toledano, C.; Rudler, H. *J. Organomet. Chem.* **2005,** *690,* 2229–2237. doi:10.1016/j.jorganchem.2005.02.022
22. Schobert, R.; Kempe, R.; Schmalz, T.; Gmeiner, A. *J. Organomet. Chem.* **2006,** *691,* 859–868. doi:10.1016/j.jorganchem.2005.10.047
23. Sandoval-Chávez, C.; López-Cortés, J. G.; Gutiérrez-Hernández, A. I.; Ortega-Alfaro, M. C.; Toscano, A.; Alvarez-Toledano, C. *J. Organomet. Chem.* **2009,** *694,* 3692–3700. doi:10.1016/j.jorganchem.2009.07.044
24. Gutiérrez-Hernández, A. I.; López-Cortés, J. G.; Ortega-Alfaro, M. C.; Ramírez-Apan, M. T.; Cázares-Marinero, J. d. J.; Toscano, R. A. *J. Med. Chem.* **2012,** *55,* 4652–4663. doi:10.1021/jm300150t
25. Bezuidenhout, D. I.; Fernández, I.; van der Westhuizen, B.; Swarts, P. J.; Swarts, J. C. *Organometallics* **2013,** *32,* 7334–7344. doi:10.1021/om400865m
26. Bezuidenhout, D. I.; van der Westhuizen, B.; Strydom, I.; Swarts, P. J.; Swarts, J. C.; Fernández, I. *Inorg. Chim. Acta* **2014,** *423,* 184–192. doi:10.1016/j.ica.2014.07.068
27. Veit, P.; Förster, C.; Seibert, S.; Heinze, K. *Z. Anorg. Allg. Chem.* **2015,** *641,* 2083–2092. doi:10.1002/zaac.201500562
28. Klabunde, U.; Fischer, E. O. *J. Am. Chem. Soc.* **1967,** *89,* 7141–7142. doi:10.1021/ja01002a070
29. Connor, J. A.; Fischer, E. O. *J. Chem. Soc. A* **1969,** 578–584. doi:10.1039/J19690000578
30. Fischer, E. O.; Heckl, B.; Werner, H. *J. Organomet. Chem.* **1971,** *28,* 359–365. doi:10.1016/S0022-328X(00)88016-X
31. Grotjahn, D. B.; Dötz, K. H. *Synlett* **1991,** *1991,* 381–390. doi:10.1055/s-1991-20736
32. Togni, A.; Hayashi, T., Eds. *Ferrocenes;* Wiley-VCH: Weinheim, Germany, 1994.
33. Štěpnička, P., Ed. *Ferrocenes. Ligands, materials and biomolecules;* Wiley & Sons: Chichester, England, 2008.
34. van der Westhuizen, B.; Speck, J. M.; Korb, M.; Friedrich, J.; Bezuidenhout, D. I.; Lang, H. *Inorg. Chem.* **2013,** *52,* 14253–14263. doi:10.1021/ic402202w
35. Lloyd, M. K.; McCleverty, J. A.; Orchard, D. G.; Connor, J. A.; Hall, M. B.; Hillier, I. H.; Jones, E. M.; McEwen, G. K. *J. Chem. Soc., Dalton Trans.* **1973,** 1743–1747. doi:10.1039/dt9730001743
36. van der Westhuizen, B.; Swarts, P. J.; Strydom, I.; Liles, D. C.; Fernández, I.; Swarts, J. C.; Bezuidenhout, D. I. *Dalton Trans.* **2013,** *42,* 5367–5378. doi:10.1039/c3dt32913e
37. van der Westhuizen, B.; Swarts, P. J.; van Jaarsveld, L. M.; Liles, D. C.; Siegert, U.; Swarts, J. C.; Fernández, I.; Bezuidenhout, D. I. *Inorg. Chem.* **2013,** *52,* 6674–6684. doi:10.1021/ic4007422
38. van der Westhuizen, B.; Matthäus Speck, J.; Korb, M.; Bezuidenhout, D. I.; Lang, H. *J. Organomet. Chem.* **2014,** *772–773,* 18–26. doi:10.1016/j.jorganchem.2014.08.025
39. Bezuidenhout, D. I.; van der Westhuizen, B.; Swarts, P. J.; Chatturgoon, T.; Munro, O. Q.; Fernández, I.; Swarts, J. C. *Chem. – Eur. J.* **2014,** *20,* 4974–4985. doi:10.1002/chem.201304711
40. Bildstein, B.; Malaun, M.; Kopacka, H.; Wurst, K.; Mitterböck, M.; Ongania, K.-H.; Opromolla, G.; Zanello, P. *Organometallics* **1999,** *18,* 4325–4336. doi:10.1021/om990377h
41. Heinze, K.; Schlenker, M. *Eur. J. Inorg. Chem.* **2004,** 2974–2988. doi:10.1002/ejic.200300897
42. Fischer, E. O.; Leupold, M. *Chem. Ber.* **1972,** *105,* 599–608. doi:10.1002/cber.19721050225
43. Sierra, M. A.; Mancheño, M. J.; Vicente, R.; Gómez-Gallego, M. *J. Org. Chem.* **2001,** *66,* 8920–8925. doi:10.1021/jo015961q
44. Connor, J. A.; Rose, P. D. *J. Organomet. Chem.* **1972,** *46,* 329–334. doi:10.1016/S0022-328X(00)88335-7
45. Moser, E.; Fischer, E. O. *J. Organomet. Chem.* **1968,** *15,* 147–155. doi:10.1016/S0022-328X(00)86334-2
46. Moser, E.; Fischer, E. O. *J. Organomet. Chem.* **1969,** *16,* 274–282. doi:10.1016/S0022-328X(00)81115-8
47. Bourissou, D.; Guerret, O.; Gabbaï, F. P.; Bertrand, G. *Chem. Rev.* **2000,** *100,* 39–92. doi:10.1021/cr940472u
48. Vignolle, J.; Cattoën, X.; Bourissou, D. *Chem. Rev.* **2009,** *109,* 3333–3384. doi:10.1021/cr800549j
49. Alder, R. W.; Allen, P. R.; Murray, M.; Orpen, A. G. *Angew. Chem., Int. Ed. Engl.* **1996,** *35,* 1121–1123. doi:10.1002/anie.199611211
50. Tafipolsky, M.; Scherer, W.; Öfele, K.; Artus, G.; Pedersen, B.; Herrmann, W. A.; McGrady, G. S. *J. Am. Chem. Soc.* **2002,** *124,* 5865–5880. doi:10.1021/ja011761k
51. Herrmann, W. A.; Öfele, K.; von Preysing, D.; Herdtweck, E. *Organometallics* **2003,** *684,* 235–248. doi:10.1016/S0022-328X(03)00754-X
52. Frey, G. D.; Herdtweck, E.; Herrmann, W. A. *J. Organomet. Chem.* **2006,** *691,* 2465–2478. doi:10.1016/j.jorganchem.2006.01.033
53. Hahn, F. E.; Tamm, M. *J. Organomet. Chem.* **1993,** *456,* C11–C14. doi:10.1016/0022-328X(93)80442-E
54. Förster, C.; Veit, P.; Ksenofontov, V.; Heinze, K. *Chem. Commun.* **2015,** *51,* 1514–1516. doi:10.1039/C4CC08868A

55. Veit, P.; Prantl, E.; Förster, C.; Heinze, K. *Organometallics* **2016,** *35*, 249–257. doi:10.1021/acs.organomet.5b00963
56. Braga, D.; Grepioni, F.; Tedesco, E.; Biradha, K.; Desiraju, G. R. *Organometallics* **1997,** *16*, 1846–1856. doi:10.1021/om9608364
57. Braga, D.; Grepioni, F. *Acc. Chem. Res.* **2000,** *33*, 601–608. doi:10.1021/ar990143u
58. Epstein, L. M.; Shubina, E. S. *Coord. Chem. Rev.* **2002,** *231*, 165–181. doi:10.1016/S0010-8545(02)00118-2
59. Brammer, L. *Dalton Trans.* **2003,** 3145–3157. doi:10.1039/b303006g
60. Lage, M. L.; Fernández, I.; Mancheño, M. J.; Sierra, M. A. *Inorg. Chem.* **2008,** *47*, 5253–5258. doi:10.1021/ic800187r
61. Kvapilová, H.; Hoskovcová, I.; Kayanuma, M.; Daniel, C.; Záliš, S. *J. Phys. Chem. A* **2013,** *117*, 11456–11463. doi:10.1021/jp4074027
62. Kreiter, C. G.; Fischer, E. O. *Angew. Chem., Int. Ed. Engl.* **1969,** *8*, 761–762. doi:10.1002/anie.196907611
63. Cases, M.; Frenking, G.; Duran, M.; Solà, M. *Organometallics* **2002,** *21*, 4182–4191. doi:10.1021/om0203330
64. Fernández, I.; Cossío, F. P.; Arrieta, A.; Lecea, B.; Mancheño, M. J.; Sierra, M. A. *Organometallics* **2004,** *23*, 1065–1071. doi:10.1021/om0343263
65. Ananikov, V. P., Ed. *Understanding organometallic reaction mechanisms and catalysis. Computational and experimental tools;* Wiley-VCH: Weinheim, 2015.
66. Wurmb-Gerlich, D.; Vögtle, F.; Mannschreck, A.; Staab, H. A. *Justus Liebigs Ann. Chem.* **1967,** *708*, 36–50. doi:10.1002/jlac.19677080103
67. Saloman, S.; Hildebrandt, A.; Korb, M.; Schwind, M.; Lang, H. *Z. Anorg. Allg. Chem.* **2015,** *641*, 2282–2290. doi:10.1002/zaac.201500557
68. Heinemann, C.; Thiel, W. *Chem. Phys. Lett.* **1994,** *217*, 11–16. doi:10.1016/0009-2614(93)E1360-S
69. Sulzbach, H. M.; Platz, M. S.; Schaefer, H. F., III; Hadad, C. M. *J. Am. Chem. Soc.* **1997,** *119*, 5682–5689. doi:10.1021/ja970181d
70. McGibbon, G. A.; Heinemann, C.; Lavorato, D. J.; Schwarz, H. *Angew. Chem., Int. Ed. Engl.* **1997,** *36*, 1478–1481. doi:10.1002/anie.199714781
71. Shustov, G. V.; Liu, M. T. H.; Rauk, A. *J. Phys. Chem. A* **1997,** *101*, 2509–2513. doi:10.1021/jp963730v
72. Solé, S.; Gornitzka, H.; Guerret, O.; Bertrand, G. *J. Am. Chem. Soc.* **1998,** *120*, 9100–9101. doi:10.1021/ja980797i
73. Fukumoto, K.; Sakai, A.; Hayasaka, K.; Nakazawa, H. *Organometallics* **2013,** *32*, 2889–2892. doi:10.1021/om400304v
74. Lewis, K. E.; Golden, D. M.; Smith, G. P. *J. Am. Chem. Soc.* **1984,** *106*, 3905–3912. doi:10.1021/ja00326a004
75. Umland, P.; Vahrenkamp, H. *Chem. Ber.* **1982,** *115*, 3555–3564. doi:10.1002/cber.19821151108
76. Van der Sluys, L. S.; Kubat-Martin, K. A.; Kubas, G. J.; Caulton, K. G. *Inorg. Chem.* **1991,** *30*, 306–310. doi:10.1021/ic00002a028
77. Kubas, G. J.; Kiss, G.; Hoff, C. D. *Organometallics* **1991,** *10*, 2870–2876. doi:10.1021/om00054a062
78. Lang, R. F.; Ju, T. D.; Kiss, G.; Hoff, C. D.; Bryan, J. C.; Kubas, G. J. *J. Am. Chem. Soc.* **1994,** *116*, 7917–7918. doi:10.1021/ja00096a067
79. Butts, M. D.; Bryan, J. C.; Luo, X.-L.; Kubas, G. J. *Inorg. Chem.* **1997,** *36*, 3341–3353. doi:10.1021/ic960870a
80. Adrjan, B.; Szymańska-Buzar, T. *J. Organomet. Chem.* **2008,** *693*, 2163–2170. doi:10.1016/j.jorganchem.2008.03.017
81. Magnusson, M. H.; Deppert, K.; Malm, J.-O. *J. Mater. Res.* **2000,** *15*, 1564–1569. doi:10.1557/JMR.2000.0224
82. Sahoo, P. K.; Kalyan Kamal, S. S.; Premkumar, M.; Jagadeesh Kumar, T.; Sreedhar, B.; Singh, A. K.; Srivastava, S. K.; Chandra Sekhar, K. *Int. J. Refract. Met. Hard Mater.* **2009,** *27*, 784–791. doi:10.1016/j.ijrmhm.2009.01.005
83. Fischer, E. O.; Fischer, H. *Chem. Ber.* **1974,** *107*, 657–672. doi:10.1002/cber.19741070238
84. Fischer, H.; Fischer, E. O.; Kreissl, F. R. *J. Organomet. Chem.* **1974,** *64*, C41–C44. doi:10.1016/S0022-328X(00)92169-7
85. Landman, M.; Pretorius, R.; Fraser, R.; Buitendach, B. E.; Conradie, M. M.; van Rooyen, P. H.; Conradie, J. *Electrochim. Acta* **2014,** *130*, 104–118. doi:10.1016/j.electacta.2014.02.127
86. Schenk, W. A.; Buchner, W. *Inorg. Chim. Acta* **1983,** *70*, 189–196. doi:10.1016/S0020-1693(00)82801-7
87. Cotton, F. A.; Kraihanzel, C. S. *J. Am. Chem. Soc.* **1962,** *84*, 4432–4438. doi:10.1021/ja00882a012
88. Malosh, T. J.; Wilson, S. R.; Shapley, J. R. *Inorg. Chim. Acta* **2009,** *362*, 2849–2855. doi:10.1016/j.ica.2009.01.011
89. Graziani, M.; Zingales, F.; Belluco, U. *Inorg. Chem.* **1967,** *6*, 1582–1586. doi:10.1021/ic50054a034
90. Ardon, M.; Hogarth, G.; Oscroft, D. T. W. *J. Organomet. Chem.* **2004,** *689*, 2429–2435. doi:10.1016/j.jorganchem.2004.04.030
91. Fulmer, G. R.; Miller, A. J. M.; Sherden, N. H.; Gottlieb, H. E.; Nudelman, A.; Stoltz, B. M.; Bercaw, J. E.; Goldberg, K. I. *Organometallics* **2010,** *29*, 2176–2179. doi:10.1021/om100106e
92. *Gaussian 09*, Revision A.02; Gaussian, Inc.: Wallingford CT, 2009.
93. Becke, A. D. *J. Chem. Phys.* **1993,** *98*, 5648–5652. doi:10.1063/1.464913
94. Dykstra, C. E. *Chem. Phys. Lett.* **1977,** *45*, 466–469. doi:10.1016/0009-2614(77)80065-1
95. Hay, P. J.; Wadt, W. R. *J. Chem. Phys.* **1985,** *82*, 270–283. doi:10.1063/1.448799
96. Wadt, W. R.; Hay, P. J. *J. Chem. Phys.* **1985,** *82*, 284–298. doi:10.1063/1.448800
97. Hay, P. J.; Wadt, W. R. *J. Chem. Phys.* **1985,** *82*, 299–310. doi:10.1063/1.448975

License and Terms

This is an Open Access article under the terms of the Creative Commons Attribution License (http://creativecommons.org/licenses/by/2.0), which permits unrestricted use, distribution, and reproduction in any medium, provided the original work is properly cited.

The license is subject to the *Beilstein Journal of Organic Chemistry* terms and conditions: (http://www.beilstein-journals.org/bjoc)

The definitive version of this article is the electronic one which can be found at: doi:10.3762/bjoc.12.125

3.4 Gold(II) in redox-switchable gold(I) catalysis

Philipp Veit, Carla Volkert, Christoph Förster, Vadim Ksenofontov, Steffen Schlicher, Matthias Bauer, Katja Heinze*

Chem. Commun. **2019**, *55*, 4615-4618.

The paper was highlighted as a cover in the journal Chemical Communications. This article is part of the themed collection: Switchable Catalysis.

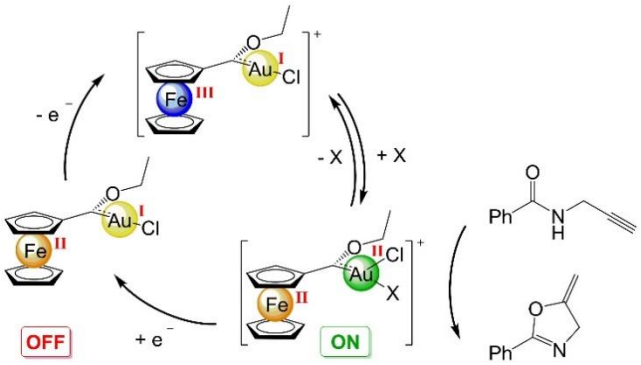

The redox switchable catalyst AuCl[C(Fc)OEt] is synthesized by transmetalation from $W(CO)_5$[C(Fc)OEt]. After oxidation the gold(II) species catalyses the cyclisation of *N*-(2-propyn-1-yl)benzamide to 2-phenyl-5-vinylidene-2-oxazoline without halide abstraction while the saturated gold(I) complex is inactive. Redox-switching between gold(II) and gold(I) turns the catalytic turnover on and off. Reversibility is proofed by switching the catalyst "on" and "off" for several catalytic cycles. Detailed EPR studies and DFT calculations underline the formation of a gold(II) species upon oxidation.

Author contributions

The synthesis, characterization and catalysis experiments were done by Carla Volkert during her bachelor thesis under the supervision of Philipp Veit. The EPR-measurements, the EPR calibration, ^{1}H DOSY experiments and all DFT calculations were performed by Philipp Veit. The Mößbauer measurements were done by Vadim Ksenofontov. The Au L_3-edge XANES spectra were recorded and analysed by Steffen Schlicher of the group of Matthias Bauer at beamline P64 of PETRA III (Hamburg, Germany). The manuscript was written by Philipp Veit (40 %) Christoph Förster (20 %) and Katja Heinze (40 %).

Supporting Information

for this article is found in Chapter 6.4 at pp. 146.

For full Supporting Information containing the coordinates of all relevant DFT calculated structures, refer to: http://www.rsc.org/suppdata/c9/cc/c9cc00283a/c9cc00283a1.pdf

"Reprinted with permission from Veit, P.; Volkert, C.; Förster, C.; Ksenofontov, V.; Schlicher, S.; Bauer, M.; Heinze, K. *Chem. Commun.* **2019**, *55*, 4615-4618.This journal is © The Royal Society of Chemistry 2015."

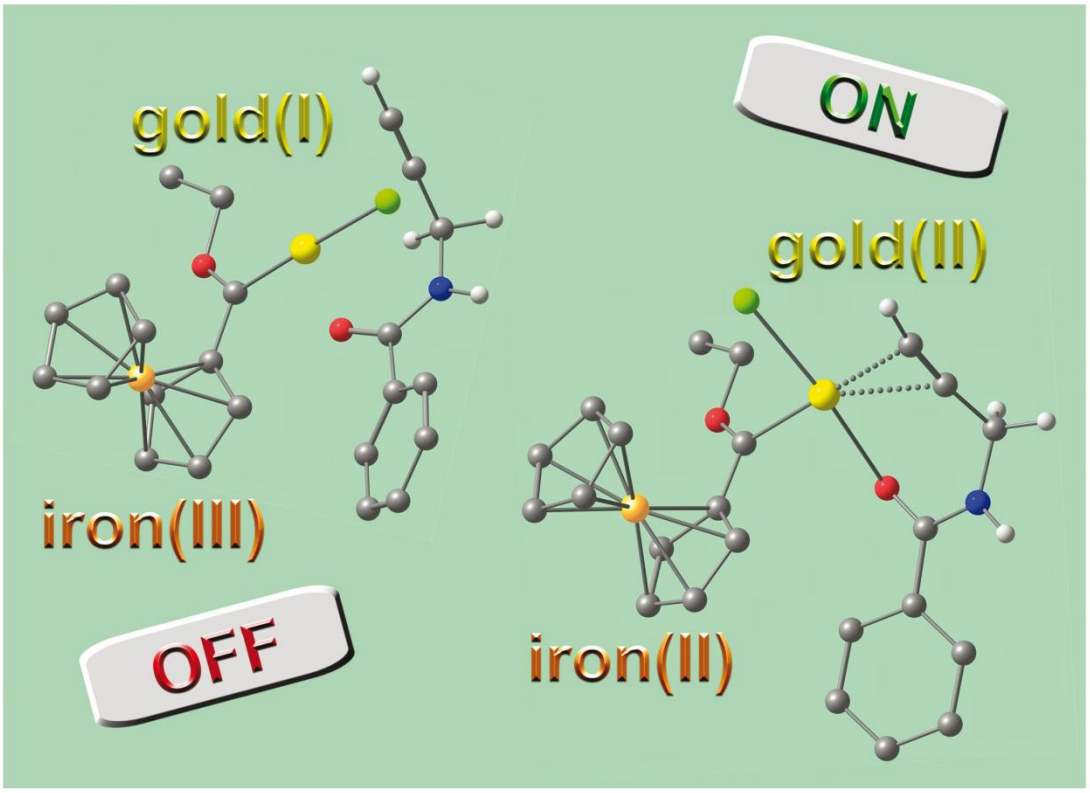

Showcasing research from Professor Katja Heinze's laboratory, Institute of Inorganic Chemistry, Johannes Gutenberg University of Mainz, Germany.

Gold(II) in redox-switchable gold(I) catalysis

Gold(II) species catalyse the cyclisation of *N*(2-propyn-1-yl)-benzamide to 2-phenyl-5-vinylidene-2-oxazoline without halide abstraction while the neutral, two-coordinate gold(I) complex is inactive indicating a gold(II/I) redox-switch.

As featured in:

See Katja Heinze *et al.*, *Chem. Commun.*, 2019, **55**, 4615.

ROYAL SOCIETY OF CHEMISTRY | Celebrating IYPT 2019

rsc.li/chemcomm

Registered charity number: 207890

ChemComm

COMMUNICATION

View Article Online
View Journal | View Issue

Check for updates

Cite this: Chem. Commun., 2019, 55, 4615

Received 11th January 2019,
Accepted 1st March 2019

DOI: 10.1039/c9cc00283a

rsc.li/chemcomm

Published on 01 March 2019. Downloaded on 5/6/2019 4:22:48 PM.

Gold(II) in redox-switchable gold(I) catalysis†

Philipp Veit,[a] Carla Volkert,[a] Christoph Förster,[a] Vadim Ksenofontov,[a] Steffen Schlicher,[b] Matthias Bauer[b] and Katja Heinze *[a]

Gold(II) species catalyse the cyclisation of *N*(2-propyn-1-yl)benzamide to 2-phenyl-5-vinylidene-2-oxazoline without halide abstraction while the saturated gold(I) complex is inactive. Redox-switching between gold(II) and gold(I) turns catalytic turnover on and off.

Molecular gold complexes have attracted great attention as (pre-)catalysts in homogeneous catalysis, especially in the activation of alkynes.[1–3] (Pre-)catalysts and intermediates feature gold in its favoured oxidation states I+ and III+.[4–7] In photocatalysis however, transient mononuclear gold(II) key intermediates have been postulated but remained elusive so far.[8–14] Apart from very few examples, the chemistry of mononuclear gold(II) complexes is underdeveloped due to the favoured disproportionation or dimerisation of gold(II).[15–19]

In gold(I) catalysed reactions, gold(I) halide complexes are usually employed as precatalysts. Typically, silver(I) salts, copper(II) triflate[20] or alkali metal salts[21] activate the precatalyst by halide abstraction. Chlorido gold(I) complexes with N-heterocyclic,[22] or acyclic diamino[23,24] carbene ligands are successfully employed in a plethora of catalytic applications in conjunction with halide scavengers.[1–7] The group of Peris recently reported a chlorido gold(I) complex bearing a redox-active ferrocenyl-imidazolylidene ligand. The presence of an oxidant increases the catalytic performance of the complex. Yet, this effect was ascribed to the formation of cationic protonated complexes under the reaction conditions.[25] On the other hand, the group of Sarkar demonstrated in seminal studies that ferrocenyl-substituted mesoionic carbene (Fc-MIC) ligands enable ON/OFF switching of the catalytic performance of gold(I) catalysts AuCl(Fc-MIC) by oxidation/reduction cycles (redox-switchable catalysis, RSC) without additional halide scavengers.[26–28] Indeed, RSC is a strongly expanding field in homogeneous catalysis.[26–40] The redox-switching event occurs either at a remote redox-active unit, *e.g.* a Fc unit located on the ligand[26–28,30,33,34,36–38] or directly at the catalytic metal centre, *e.g.* Ce^{III}/Ce^{IV}.[32] In gold(I) catalysis, activation by oxidation of the remote Fc unit increases the Lewis acidity of the Au^{I} ion.[26–28] Thus, carbene ligands with low donor ability should be beneficial for high catalytic activity in gold catalysis. The Tolman electronic parameter (TEP)[41] of the Fc-MICs increases from a very high donicity (TEP ≈ 2046 cm^{-1}) to a lower one (TEP ≈ 2054 cm^{-1}) upon oxidation of the Fc unit.[27,28] The neutral carbene ligand :C(Fc)OEt already possesses a similar donor strength (TEP = 2054 cm^{-1}) as the oxidised Fc-MICs.[27,28,42] Consequently, the oxidised carbene ligand $[:C(Fc)OEt]^+$ should have an even lower donor ability and could enable high catalytic activity with AuCl[C(Fc)OEt] **1** as precatalyst (Scheme 1).

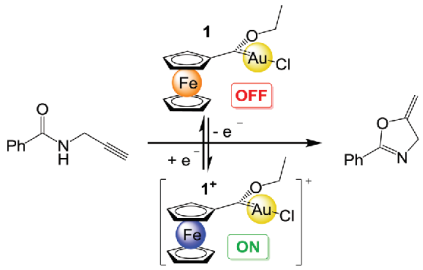

Scheme 1 Switchable gold-catalysed cyclisation of *N*(2-propyn-1-yl)-benzamide to 2-phenyl-5-vinylidene-2-oxazoline.

Compared to Fc-MICs with redox-active Fc substituents in a β position relative to the carbene donor, the Fc moiety in **1** located in the α position might have an even larger impact on the ligand's donor properties. Furthermore, the redox potentials for the Fc/Fc^+ oxidation of :C(Fc)OEt and Fc-MICs are very different,[28,42] opening the possibility of different valence isomers for cationic gold complexes $[AuCl(Fc\text{-}MIC)]^+$ and $\mathbf{1}^+$ and consequently a different reactivity. For comparison of $[AuCl(Fc\text{-}MIC)]^{0/+}$ and $\mathbf{1}^{0/+}$, we studied

[a] Institute of Inorganic Chemistry and Analytical Chemistry, Johannes Gutenberg University of Mainz, Duesbergweg 10-14, 55128 Mainz, Germany. E-mail: katja.heinze@uni-mainz.de
[b] Department Chemie and Center for Sustainable Systems Design (CSSD), University of Paderborn, Warburger Straße 100, D-33098 Paderborn, Germany

† Electronic supplementary information (ESI) available: Experimental procedures, spectral details, (TD-)DFT calculations. See DOI: 10.1039/c9cc00283a

Published on 01 March 2019. Downloaded on 5/6/2019 4:22:48 PM.

the gold catalysed cyclisation of *N*(2-propyn-1-yl)benzamide to 2-phenyl-5-vinylidene-2-oxazoline (Scheme 1).[20,26–28]

Pre-catalyst AuCl[C(Fc)OEt] **1** is accessible by transmetalation[43] from W(CO)$_5$[C(Fc)OEt][44] to AuCl(SMe$_2$) and fully characterised by ^{1}H and ^{13}C NMR, IR and UV/Vis spectroscopy, LIFDI mass spectrometry and cyclic voltammetry (ESI,† Fig. S1–S9). The cyclic voltammograms of **1** with [*n*Bu$_4$N][BAr$^F_4$] (Ar^F = C$_6$F$_5$) as supporting electrolyte show a reversible one-electron oxidation wave at $E_{\frac{1}{2}}$ = 0.58 V and 0.60 V in CH_2Cl_2 and THF, respectively (*vs.* FcH/FcH$^+$; ESI,† Fig. S7 and S9). These processes occur at significantly higher potential than the oxidation of Fc-MIC gold(I) complexes.[26–28] Changing the electrolyte from [*n*Bu$_4$N][BAr$^F_4$] to [*n*Bu$_4$N][PF$_6$] lowers the oxidation potential by approximately 100 mV similar to Fc-MIC gold(I) complexes.[27] Irreversible or quasi-reversible carbene reduction waves are additionally observed at negative potentials (ESI,† Fig. S6–S9). Interestingly, small oxidation waves appear at potentials 140 to 310 mV lower than the reversible oxidation wave. Potential and intensity depend on the solvent and the electrolyte but not on the batch of **1** employed. Hence, this is an intrinsic property of **1** in a given environment. We tentatively ascribe this wave to the oxidation of dimers **(1)$_2$** present to a minor extent in solution. In fact, dimers and oligomers of AuCl(carbene) complexes with small carbene ligands (but not for the Fc-MIC ligands[26–28]) held together by aurophilic interactions[45,46] form in the solid state.[43] The presence of Au···Au contacts in solution has been suggested using diffusion-ordered spectroscopy (DOSY).[47–49] ^{1}H DOSY experiments of **1** in dichloromethane with W(CO)$_5$[C(Fc)OEt] as internal monomeric reference confirm the mainly monomeric nature of **1** as suggested by the electrochemical experiments (ESI,† Fig. S10). However, dimerisation *via* Au···Au contacts in the minor species **(1)$_2$** should hardly affect oxidation of the remote Fc substituents but rather the gold centres. Hence, we investigated the chemical oxidation of **1** by a suitable oxidant (Magic Blue, [*N*(*p*-C$_6$H$_4$Br)$_3$][SbCl$_6$] and ammonium cerium(IV) nitrate, CAN) using X-band EPR spectroscopy in more detail. Irrespective of the oxidant and solvent (THF, CH_2Cl_2/DMF) employed, a broad resonance around g = 2 is detected for the **1**/oxidant mixture both at 77 and 295 K (Fig. 1a and ESI,† Fig. S11–S16). Hence, the EPR resonance derives from **1$^+$**. The observation of a signal already at room temperature and the lacking axial symmetry in frozen solution rules out the assignment of this resonance to a Fc$^+$ ion.[39,50,51] On the other hand, gold(II) species have been reported to possess g tensors with small g anisotropy and hyperfine coupling to the gold nucleus (^{197}Au: I = 3/2).[15–18] Due to the non-resolved coupling(s), only the g_{iso} value of 2.017 is given which fits to reported values for gold(II) complexes.[15–18] Furthermore, the resonance increases in intensity over time at room temperature converging to a limiting value after 5 h. Quantification of the EPR resonance after 5 h by double integration and calibration (ESI,† Fig. S17 and S18) confirms that the EPR resonance accounts for 75 ± 5% of the paramagnetic species (Fig. 1b). Hence, we suggest that Magic Blue first oxidises the Fc unit in **1** yielding the cationic Fe^{III}Au^I electromer of **1$^+$**. Ferrocenium is typically EPR-silent at room temperature and hence not observed at 295 K. The absence of an axial Fc$^+$ resonance also at 77 K may be ascribed to fast spin relaxation.[50] Then, the

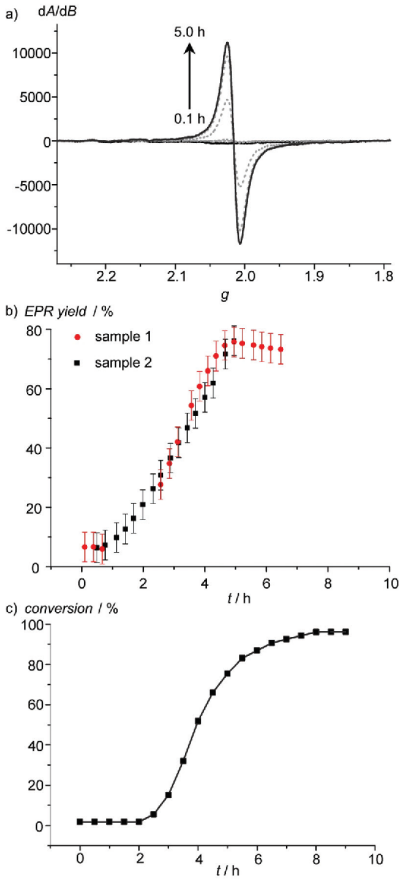

Fig. 1 (a) EPR spectra of **1**/Magic Blue in THF over time at 295 K, (b) doubly integrated intensity of the EPR resonance *versus* time plot and (c) conversion *versus* time plot for the cyclisation catalysed by **1**/Magic Blue in dichloromethane (Scheme 1).

Fe^{III}Au^I isomer slowly converts to a Fe^{II}Au^{II} isomer almost quantitatively suggesting that significant reorganisation takes place after the initial Fc/Fc$^+$ oxidation. Some gold(II) might also form directly starting from minor amounts of a dimeric species **(1)$_2$**.

Gratifyingly, geometry optimisations using Density Functional Theory (DFT) calculations on **[1]**[SbCl$_6$] converged to two electromers, namely a gold(I)/iron(III) and a gold(II)/iron(II) isomer in a contact ion-pair with the counter ion coordinating the gold with an Au–Cl(SbCl$_5$) distance of 2.47 Å (Fig. 2a). The spin density in the gold(II) isomer is mainly shared between the gold ion and the chlorido ligand (Fig. 2a). The original linear coordination of the Au^I center with a 177° C–Au–Cl angle is expanded yielding a 3 + 1 coordination of the gold(II) ion with a 92° C–Au–Cl angle in the Au^{II} species. This bending might raise

 This journal is © The Royal Society of Chemistry 2019

View Article Online
ChemComm Communication

Published on 01 March 2019. Downloaded on 5/6/2019 4:22:48 PM.

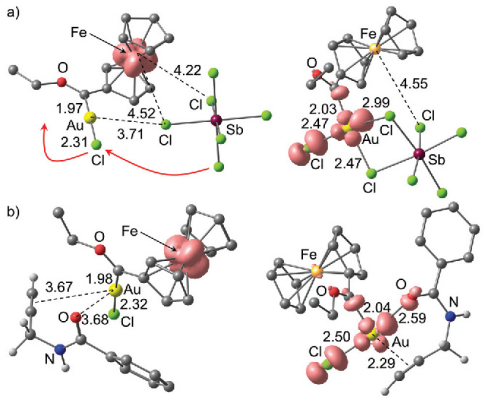

Fig. 2 DFT calculated optimised geometries and spin densities of $Fe^{III}Au^{I}$ and $Fe^{II}Au^{II}$ isomers of (a) **[1]**[$SbCl_6$] and (b) [**1** + substrate]$^+$. Distances given in Å, hydrogen atoms omitted (except for the propargyl amide unit), contour value at 0.01 a.u.

the activation barrier for the intramolecular electron transfer from Au^{I} to Fe^{III} giving the $Au^{II}Fe^{II}$ isomer (Fig. 2a).

Coordination of [$SbCl_6$]$^-$ to Au (Fig. 2a, right) shifts the spin density to give gold(II). A similar impact of ion coordination is observed in gold(II) porphyrin/gold(III) porphyrin radical anion valence isomers.[17] Conceptually similar, heterobimetallic molybdenum(IV)/ferrocenium complexes $Mo^{IV}Fe^{III}$ undergo intramolecular electron transfer to yield $Mo^{V}Fe^{II}$ electromers.[39,40] Fully analogously, rhodium(I) complexes bearing a ferrocenyl phosphine-NHC ligand are first oxidised at the Fc unit, while the second oxidation is rhodium centered initiating a further intramolecular electron transfer from rhodium to Fc^+.[35] In these examples, the Fc/Fc^+ redox couple acts as intermediate parking position for a positive charge.

DFT calculations suggest that coordination of oxygen nucleophiles such as amides (*e.g.* *N*(2-propyn-1-yl)benzamide) to the gold centre of **1**$^+$ instead of counter ions also stabilises the $Au^{II}Fe^{II}$ valence isomer over the $Au^{I}Fe^{III}$ isomer (Fig. 2b). In the gold(II) isomer the C–Au–Cl angle is compressed to 93° and the triple bond of the substrate coordinates to gold(II) (Fig. 2b).

Hence, we employed the gold(I) complex **1** and **1**/Magic Blue in the cyclisation reaction of *N*(2-propyn-1-yl)benzamide to the oxazoline in dichloromethane (Scheme 1). Neither **1** nor oxidant alone yield the heterocyclic product, while the mixture **1**/Magic Blue (1 mol%) quantitatively converts the substrate to the product within a few hours (Fig. 1c, TOF = (8.3 ± 1.1) × 10^{-3} s^{-1}; ESI,† Fig. S19 and S20). This is significantly faster than observed with the oxidised Fc-MIC gold complexes.[26–28] Interestingly, an induction period of *ca.* 2.5 h is observed (Fig. 1c). This time scale matches the development of the gold(II) EPR resonance (Fig. 1). Complementary, the paramagnetically broadened and shifted ^{1}H NMR resonances of the initial mixture of **1** and Magic Blue re-appear at typical diamagnetic values during a similar time span suggesting the re-reduction of an initially formed Fc^+ species (ESI,† Fig. S21). With these spectroscopic correlations, we propose that a gold(II) centre slowly forms from the initially present ferrocenium ion. The gold(II) centre presumably features a C–Au–Cl angle close to 90° (Fig. 2b), which enables substrate coordination in contrast to the initially present linearly coordinated gold(I) centre. The exact nature of the active gold(II) catalyst remains speculative, yet three[52] and four coordinate[17,18] gold(II) species are conceivable with coordination of counter ions, coordination of the substrate (*via* the amide oxygen atom) or aggregation *via* chlorido ligands and aurophilic interactions (Fig. 2). Attempts to get more insight into the structure of the active species using Mößbauer (iron) and X-ray absorption near edge structure spectroscopy at the gold L_3-edge were inconclusive as removing the solvent leads to the formation of elemental gold and several iron(II) and iron(III) species (ESI,† Fig. S22–S25). In the absence of coordinating solvents (DMF, THF) or substrates, a dark precipitate forms (ESI,† Fig. S26). Obviously, stabilising ligands (solvent, substrate) are required to keep the gold(II) catalyst active. The majority of the catalyst remains active for some time as a second batch of substrate is converted to the product with similar TOF but without induction period after a full initial conversion (ESI,† Fig. S27). The presence of [nBu$_4$N]Cl (42 eq.) inhibits the catalysis (ESI,† Fig. S28) suggesting that free coordination sites or only weakly coordinating donor ligands are required to enable catalysis. Activation of **1** using $AgSbF_6$ as halide scavenger initiates a conventional gold(I) catalysis with a smaller TOF = 3.2 × 10^{-3} s^{-1} but without induction period (ESI,† Fig. S29).

Addition of decamethylferrocene $FeCp^*_2$ as reductant stops catalytic turnover, while re-oxidation using Magic Blue re-starts the catalysis (Fig. 3). This second oxidation initiates catalysis almost instantaneously without induction period and with a similar TOF as during the first cycle. Hence, the catalytic mixture **1**/oxidant forms catalytically active gold(II) species which can be reversibly switched off and on by reduction and oxidation, respectively. The catalytically active species, however, still relates structurally to the precatalyst, as 84 ± 5% of **1** are recovered after *ca.* 63% conversion and quenching with $FeCp^*_2$ according to ^{1}H NMR spectroscopy (ESI,† Fig. S30).

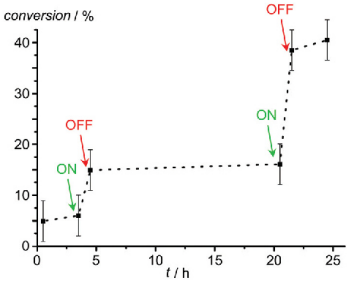

Fig. 3 Conversion *versus* time plot of the cyclisation (Scheme 1) during ON/OFF redox switching using Magic Blue (1.00/1.05 eq.; ON) and $FeCp^*_2$ (1.05/1.10 eq.; OFF).

Published on 01 March 2019. Downloaded on 5/6/2019 4:22:48 PM.

In summary, we report a redox-switchable gold-catalysed cyclisation with the gold centre of the precatalyst **1** reversibly switching between highly active, presumably coordinatively unsaturated gold(II)[17,18,52] and inactive, coordinatively saturated gold(I) centres. Our studies complement previous work on gold(I) pre-catalysts activated by redox-active ligands.[26–28,53] The very high activity may be due to the electrophilic nature of the gold(II) ion with free coordination sites. To prevent aggregation or disproportionation, the gold(II) centre must be stabilised by further donor ligands (counter ions, substrates) which should not coordinate too strongly. The Fc/Fc^+ couple temporarily stabilises $\mathbf{1}^+$ *via* valence isomerisation preventing aggregation or disproportionation of the unsaturated gold(II) centre in the absence of donor ligands. Detailed studies on Au^I complexes with carbene ligands using the $Au^{I/II}$ switch are ongoing.

Financial support from the Center for INnovative and Emerging MAterials (CINEMA) and the Forschungsinitiative Rheinland-Pfalz (LESSING) is gratefully acknowledged. Parts of this research were conducted using the supercomputer Mogon and advisory services offered by Johannes Gutenberg University Mainz (www.hpc.uni-mainz.de), which is a member of the AHRP and the Gauss Alliance e.V. PETRA III (Hamburg, Germany) is acknowledged for provision of beamtime.

Conflicts of interest

There are no conflicts to declare.

References

1 A. Fürstner, *Chem. Soc. Rev.*, 2009, **38**, 3208.
2 A. S. K. Hashmi, *Acc. Chem. Res.*, 2014, **47**, 864.
3 R. Dorel and A. M. Echavarren, *Chem. Rev.*, 2015, **115**, 9028.
4 A. S. K. Hashmi, *Angew. Chem., Int. Ed.*, 2010, **49**, 5232.
5 L.-P. Liu and G. B. Hammond, *Chem. Soc. Rev.*, 2012, **41**, 3129.
6 C. Obradors and A. M. Echavarren, *Chem. Commun.*, 2014, **50**, 16.
7 M. Joost, A. Amgoune and D. Bourissou, *Angew. Chem., Int. Ed.*, 2015, **54**, 15022.
8 B. Sahoo, M. N. Hopkinson and F. Glorius, *J. Am. Chem. Soc.*, 2013, **135**, 5505.
9 M. S. Winston, W. J. Wolf and F. D. Toste, *J. Am. Chem. Soc.*, 2014, **136**, 7777.
10 X.-z. Shu, M. Zhang, Y. He, H. Frei and F. D. Toste, *J. Am. Chem. Soc.*, 2014, **136**, 5844.
11 A. Tlahuext-Aca, M. N. Hopkinson, B. Sahoo and F. Glorius, *Chem. Sci.*, 2016, **7**, 89.
12 M. N. Hopkinson, A. Tlahuext-Aca and F. Glorius, *Acc. Chem. Res.*, 2016, **49**, 2261.
13 L. Huang, M. Rudolph, F. Rominger and A. S. K. Hashmi, *Angew. Chem., Int. Ed.*, 2016, **55**, 4808.
14 S. Kim, J. Rojas-Martin and F. D. Toste, *Chem. Sci.*, 2016, **7**, 85.
15 R. Kirmse, M. Kampf, R.-M. Olk, M. Hildebrand and H. Krautscheid, *Z. Anorg. Allg. Chem.*, 2004, **630**, 1433.
16 D. Huang, X. Zhang, E. J. L. McInnes, J. McMaster, A. J. Blake, E. S. Davies, J. Wolowska, C. Wilson and M. Schröder, *Inorg. Chem.*, 2008, **47**, 9919.
17 S. Preiß, J. Melomedov, A. Wünsche von Leupoldt and K. Heinze, *Chem. Sci.*, 2016, **7**, 596.
18 S. Preiß, C. Förster, S. Otto, M. Bauer, P. Müller, D. Hinderberger, H. H. Hashemi, L. Carella and K. Heinze, *Nat. Chem.*, 2017, **9**, 1249.
19 K. Heinze, *Angew. Chem., Int. Ed.*, 2017, **56**, 16126.
20 L. Hettmanczyk, D. Schulze, L. Suntrup and B. Sarkar, *Organometallics*, 2016, **35**, 3828.
21 R. Pretorius, M. R. Fructos, H. Müller-Bunz, R. A. Gossage, P. J. Pérez and M. Albrecht, *Dalton Trans.*, 2016, **45**, 14591.
22 N. Marion and S. P. Nolan, *Chem. Soc. Rev.*, 2008, **37**, 1776.
23 L. M. Slaughter, *ACS Catal.*, 2012, **2**, 1802.
24 V. P. Boyarskiy, K. V. Luzyanin and V. Y. Kukushkin, *Coord. Chem. Rev.*, 2012, **256**, 2029.
25 S. Ibáñez, M. Poyatos, L. N. Dawe, D. Gusev and E. Peris, *Organometallics*, 2016, **35**, 2747.
26 L. Hettmanczyk, S. Manck, C. Hoyer, S. Hohloch and B. Sarkar, *Chem. Commun.*, 2015, **51**, 10949.
27 L. Hettmanczyk, L. Suntrup, S. Klenk, C. Hoyer and B. Sarkar, *Chem. – Eur. J.*, 2017, **23**, 576.
28 S. Klenk, S. Rupf, L. Suntrup, M. van der Meer and B. Sarkar, *Organometallics*, 2017, **36**, 2026.
29 A. M. Allgeier and C. A. Mirkin, *Angew. Chem., Int. Ed.*, 1998, **37**, 894.
30 C. K. A. Gregson, V. C. Gibson, N. J. Long, E. L. Marshall, P. J. Oxford and A. J. P. White, *J. Am. Chem. Soc.*, 2006, **128**, 7410.
31 E. M. Broderick, N. Guo, C. S. Vogel, C. Xu, J. Sutter, J. T. Miller, K. Meyer, P. Mehrkhodavandi and P. L. Diaconescu, *J. Am. Chem. Soc.*, 2011, **133**, 9278.
32 E. M. Broderick, N. Guo, T. Wu, C. S. Vogel, C. Xu, J. Sutter, J. T. Miller, K. Meyer, T. Cantat and P. L. Diaconescu, *Chem. Commun.*, 2011, **47**, 9897.
33 R. Savka, S. Foro, M. Gallei, M. Rehahn and H. Plenio, *Chem. – Eur. J.*, 2013, **19**, 10655.
34 K. Arumugam, C. D. Varnado, S. Sproules, V. M. Lynch and C. W. Bielawski, *Chem. – Eur. J.*, 2013, **19**, 10866.
35 N. Debono, J.-C. Daran, R. Poli and A. Labande, *Polyhedron*, 2015, **86**, 57.
36 S. Ibáñez, M. Poyatos and E. Peris, *ChemCatChem*, 2016, **8**, 3790.
37 P. Neumann, H. Dib, A.-M. Caminade and E. Hey-Hawkins, *Angew. Chem., Int. Ed.*, 2015, **54**, 311.
38 A. Feyrer, M. K. Armbruster, K. Fink and F. Breher, *Chem. – Eur. J.*, 2017, **23**, 7402.
39 K. Hüttinger, C. Förster and K. Heinze, *Chem. Commun.*, 2014, **50**, 4285.
40 K. Hanauer, C. Förster and K. Heinze, *Eur. J. Inorg. Chem.*, 2018, 3537.
41 C. A. Tolman, *Chem. Rev.*, 1977, **77**, 313.
42 G. K. Ramollo, M. J. López-Gómez, D. C. Liles, L. C. Matsinha, G. S. Smith and D. I. Bezuidenhout, *Organometallics*, 2015, **34**, 5745.
43 D. I. Bezuidenhout, B. van der Westhuizen, A. J. Rosenthal, M. Wörle, D. C. Liles and I. Fernández, *Dalton Trans.*, 2014, **43**, 398.
44 J. A. Connor and J. P. Lloyd, *Dalton Trans.*, 1972, 1470.
45 P. Pyykkö, *Angew. Chem., Int. Ed.*, 2004, **43**, 4412.
46 H. Schmidbaur and A. Schier, *Chem. Soc. Rev.*, 2012, **41**, 370.
47 F. Balzano, A. Cuzzola, P. Diversi, F. Ghiotto and G. Uccello-Barretta, *Eur. J. Inorg. Chem.*, 2007, 5556.
48 X. Yang, S. Wang, I. Ghiviriga, K. A. Abboud and A. S. Veige, *Dalton Trans.*, 2015, **44**, 11437.
49 S. Sen and F. P. Gabbaï, *Chem. Commun.*, 2017, **53**, 13356.
50 J. C. Gallucci, G. Opromolla, L. A. Paquette, L. Pardi, P. F. T. Schirch, M. R. Sivik and P. Zanello, *Inorg. Chem.*, 1993, **32**, 2292.
51 A. Neidlinger, V. Ksenofontov and K. Heinze, *Organometallics*, 2013, **32**, 5955.
52 M. Baya, A. Pérez-Bitrián, S. Martínez-Salvador, A. Martín, J. M. Casas, B. Menjón and J. Orduna, *Chem. – Eur. J.*, 2018, **24**, 1514.
53 H. Yang and F. P. Gabbaï, *J. Am. Chem. Soc.*, 2015, **137**, 13425.

 This journal is © The Royal Society of Chemistry 2019

3.5 Unexpected C-C Bond Formation with a Ferrocenyl Fischer Carbene Complex

Philipp Veit, Sebastian Seibert, Christoph Förster* and Katja Heinze*

Z. Anorg. Allg. Chem., **2020**, *646*, 1–9.

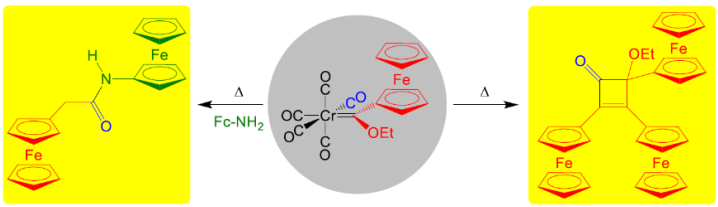

Ferrocenyl ethoxy Fischer carbene complex shows two unexpected products in the thermolysis, that were not reported so far. In the presence of aminoferrocene the formation of 2,*N*-diferrocenyl acetamide is observed which can be explained by nucleophilic attack on a carbonyl carbon. In the absence of any nucleophile three equivalents of Fischer carbene complex form 4-ethoxy-2,3,4-triferrocenyl-cyclobut-2-enone in a reaction that could be similar to the Dötz benzannulation reaction. Both products are confirmed by single crystal X-ray diffraction. Kinetic experiments by IR spectroscopy and mass spectrometry as well as DFT calculations help to find mechanistical proposals for both reactions.

Author contributions

2,*N*-diferrocenyl acetamide was first synthesized by Sebastian Seibert during a research internship in the Heinze group under the supervision of Christoph Förster. Single crystals suitable for XRD analysis were isolated by Sebastian Seibert. The optimization of the synthesis strategy for 2,*N*-diferrocenyl acetamide and the full characterization was done by Philipp Veit. 4-ethoxy-2,3,4-triferrocenyl-cyclobut-2-enone was synthesized and characterized by Philipp Veit. Single crystals suitable for XRD analysis were isolated by Philipp Veit. The crystal structures for both compounds were solved and refined by Christoph Förster. All DFT calculations were performed by Philipp Veit. The manuscript was written by Philipp Veit (60 %), Christoph Förster (10 %) and Katja Heinze (30 %).

Supporting Information

for this article is found in Chapter 6.5 at pp. 167. For full Supporting Information containing all relevant DFT calculated structures, refer to:

https://onlinelibrary.wiley.com/action/downloadSupplement?doi=10.1002%2Fzaac.201900350&file=zaac201900350-sup-0001-SupMat.pdf

“Reprinted with the permission of Veit, P.; Seibert, S.; Förster, C.; Heinze, K.; *Z. Anorg. Allg. Chem.* **2020**, *646*, 1–9. Copyright © 2020 WILEY-VCH Verlag GmbH & Co. KGaA, Weinheim”

Journal of Inorganic and General Chemistry
ZAAC
Zeitschrift für anorganische und allgemeine Chemie
DOI: 10.1002/zaac.201900350
ARTICLE

Unexpected C–C Bond Formation with a Ferrocenyl Fischer Carbene Complex

Philipp Veit,[a] Sebastian Seibert,[a] Christoph Förster,*[a] and Katja Heinze*[a]

Dedicated to Prof. Manfred Scheer on the Occasion of his 65th Birthday

Abstract. Thermolysis of $(OC)_5Cr(C(OEt)(Fc))$ (**1**) gives 2,*N*-diferrocenyl acetamide Fc–CH_2–CO–NH–Fc (**2**) in the presence of amino ferrocene Fc-NH_2. In the absence of a nucleophile, 4-ethoxy-2,3,4-triferrocenyl-cyclobut-2-enone (**3**) forms from **1** under thermal activation. Single crystal X-ray diffraction, NMR spectroscopy and mass spectrometry unambiguously confirm the structure of both unexpected products. Quantum chemical calculations and kinetic experiments by mass spectrometry and IR spectroscopy help to propose conceivable pathways to their formation.

Introduction

Fischer carbene complexes of group 6 metals[1] display a highly versatile follow-up chemistry (Scheme 1). This field has matured into well-established applications in organic synthesis.[2–6] For example, treating vinyl or aryl-substituted alkoxy carbenes with alkynes yields phenols and naphthols, respectively (Scheme 1a, Dötz benzannulation reaction).[7–13] Carbenes with 1,3-difluorphenyl-, cyclopropyl or ferrocenyl substituents furnish cyclobutenones (or cyclopentenones) in the presence of alkynes (Scheme 1a, Zora).[14–21]

In these cases, the initial steps comprise CO dissociation from the carbene complex. Hence, thermal activation is typically required. Coordination of the alkyne and insertion of the alkyne into the metal-carbene bond gives a vinyl carbene complex. CO insertion forms a vinyl ketene coordinated by a $Cr(CO)_3$ fragment. From this intermediate, the Dötz products (R = aryl or vinyl) or the cyclobutenones (R = cyclopropyl, Scheme 1a, Zora) evolve.

A classical reaction of alkoxy Fischer carbenes is the nucleophilic substitution of the alkoxide by primary or secondary amines giving the corresponding aminocarbene complexes (Scheme 1b).[22,23] However, using amino ferrocene Fc-NH_2 [24,25] as nucleophile and the carbene complex $(OC)_5Cr(C(OEt)(Fc))$ **1** (R^1 = Et, R^2 = Fc), the expected diferrocencyl carbene complex $(OC)_5Cr(C(NHFc)(Fc))$ could not be obtained.[26] The low nucleophilicity of Fc-NH_2 might be responsible for this failure. However, increasing the nucleophilicity of Fc-NH_2 by deprotonation with potassium hexamethyldisilazide resulted in the successful formation of $(OC)_5Cr(C(NHFc)(Fc))$ (Scheme 1c).[26]

On the other hand, using lithium morpholin-4-ide and alkoxy carbene complexes with bulky substituents (R^1 = menthyl, Scheme 1) results in a C–C coupling reaction to give α-alkoxy acetamides presumably via biscarbenes (Scheme 1d).[27] In the absence of a nucleophile or alkyne, simple thermolysis of carbene complexes yields the olefin as formal carbene-carbene coupling product as already reported by Fischer (Scheme 1e).[28,29]

In this study, we show that the thermally activated reaction of **1** with the weak nucleophile Fc-NH_2 gives 2,*N*-diferrocenyl acetamide Fc–CH_2–CO–NH–Fc (**2**) (Scheme 1f) instead of the initially intended (amino ferrocenyl)(ferrocenyl)carbene complex[26] (Scheme 1c). Beyond this thermal pathway, the photo-induced formation of a related compound MeOOC-CH_2-(η^5-C_5H_4)$Re(CO)_3$ of the Fischer carbene complex $(OC)_5Cr(C(OMe)(\eta^5\text{-}C_5H_4)Re(CO)_3)$ with MeOH had been reported by *Sierra*.[30] Obviously, the C-C coupling product **2** arises from two C_1 building blocks (carbene and CO). From the analogous reaction of the carbene complex **1** and adamantylamine only traces of the corresponding C-C coupling product 2-ferrocenyl-*N*-adamantyl acetamide Fc-CH_2-CO-NH-Ad (**2^{Ad}**) are detected. Instead, the triferrocenyl-substituted cyclobutenone **3** forms in significant amounts (Scheme 1g). **3** is obviously a C-C coupling product arising formally from four C_1 building blocks, namely from three ferrocenyl carbenes and CO. Cyclobutenone **3** even forms in the absence of adamantylamine by simple heating.

To the best of our knowledge, the formation of acetic acid derivatives by weak nucleophiles and the thermally induced formation of cylobutenones from carbene complexes in the ab-

* Dr. C. Förster
E-Mail: cfoerster@uni-mainz.de,
* Prof. Dr. K. Heinze
E-Mail: katja.heinze@uni-mainz.de
[a] Department of Chemistry
Johannes Gutenberg University of Mainz
Duesbergweg 10–14
55128 Mainz, Germany
Supporting information for this article is available on the WWW under **http://dx.doi.org/10.1002/zaac.201900350** or from the author.
© 2020 The Authors. Published by Wiley-VCH Verlag GmbH & Co. KGaA. · This is an open access article under the terms of the Creative Commons Attribution-NonCommercial-NoDerivs License, which permits use and distribution in any medium, provided the original work is properly cited, the use is non-commercial and no modifications or adaptations are made.

 © 2020 The Authors. Published by WILEY-VCH Verlag GmbH & Co. KGaA, Weinheim

Journal of Inorganic and General Chemistry
ZAAC
Zeitschrift für anorganische und allgemeine Chemie
ARTICLE

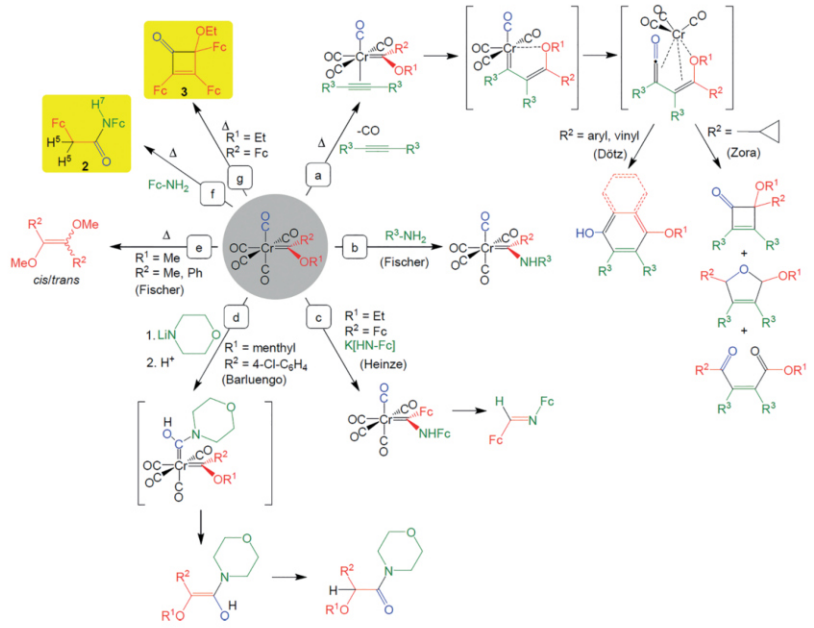

Scheme 1. Reactivity of chromium carbene complexes, which is relevant to this study.

sence of alkynes by formal coupling of CO and one and three carbene building blocks, respectively, have not been reported so far. Hence, we present our initial results on these unexpected C-C coupling reactions and discuss conceivable mechanistic aspects in the context of the well-established reactivity of Fischer carbene complexes.

Results and Discussion

Synthesis and Characterization of 2

The ferrocenyl-substituted chromium carbene complex **1** (prepared according to literature procedures)[26,31–33] was treated with amino ferrocene Fc-NH_2 [24,25] in toluene under reflux. After chromatographic workup, a brown solid was isolated and characterized (Figures S1–S4, Supporting Information).

Instead of the anticipated substituted carbene complex $(OC)_5Cr(C(NHFc)(Fc))$,[26] the acetic acid derivative **2** was isolated in 14% yield. Single crystals of **2** were obtained and the solid-state structure was determined by X-ray diffraction (Figure 1a). **2** crystallizes in the orthorhombic space group *Pbca* with one molecule in the asymmetric unit (Figure 1a). Selected bond lengths, bond angles and dihedral angles of the single-crystal X-ray diffraction data and the corresponding Density Functional Theory (DFT) calculation are collected in Table S1 (Supporting Information). The metrical data of the

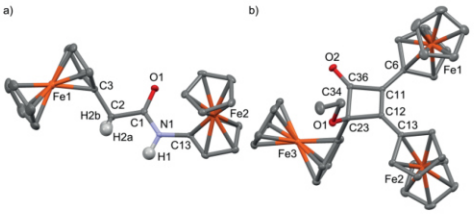

Figure 1. Molecular structures of (a) **2** and (b) **3** from single crystal XRD (hydrogen atoms are omitted for clarity except for NH and CH_2, thermal ellipsoids at 30% probability).

ferrocenyl moieties are unremarkable. The amides are linked by N–H···O=C hydrogen bonds between adjacent molecules [*d*(N···O) 2.894(5) Å] giving linear hydrogen bonded chains as commonly observed in ferrocenyl amides.[25,34–35] In the solid state, the characteristic amide-A, amide-I and amide-II bands for hydrogen-bonded amides appear at 3280, 1659, 1566 cm^{-1} in a similar range to those of Fc-$NHCOCH_3$ (3262, 1655, 1580 cm^{-1}).[25] In CD_2Cl_2 solution the chains disassemble into monomers as shown by the ^1H NMR resonance of the amide proton at δ_{H7} = 6.74 ppm (see Scheme 1 for atom numbering). In [D_8]THF, solvent coordinates to the amide (δ_{H7} = 8.23 ppm). The most unexpected observation is the presence of the additional CH_2 group in the molecule (Figure 1a). The

© 2020 The Authors. Published by WILEY-VCH Verlag GmbH & Co. KGaA, Weinheim

Journal of Inorganic and General Chemistry
ZAAC
Zeitschrift für anorganische und allgemeine Chemie
ARTICLE

methylene group is furthermore confirmed by its proton resonance at (δ_{H5} = 3.33 ppm in CD_2Cl_2, see Scheme 1 for atom numbering), the characteristic CH_2 stretching vibration at 2960 cm^{-1} and the FD mass spectrum of **2** (*m/z* = 427).

As this compound can be obtained by a much simpler route e.g. from ferrocenyl acetic acid and amino ferrocene using conventional amide coupling reactions[25,34–40] as described in the Supporting Information (experimental procedure, Figures S19–S21, Supporting Information), no attempts to optimize this reaction were undertaken. However, the CH_2 group formation from the initial carbene ligand is unusual and will be discussed next.

Mechanistic Considerations on the Formation of 2

As the *N*-ferrocenyl group is bound to a carbonyl group in the final product, nucleophilic attack of Fc-NH_2 onto a *cis*-CO ligand at **1** is highly probable. Indeed, biscarbene complexes have been reported by Fischer using $M(CO)_6$ and $LiPMe_2$ after methylation in very low yield.[41] More recently, *Barluenga* succeeded in isolating biscarbene complexes starting from chromium and tungsten alkoxy carbenes and strong heteronucleophiles such as amides or alkoxides after alkylation (Scheme 1d).[27] Heating these (aminoaryl)(alkoxyalkenyl)-biscarbene tungsten complexes to 35 °C furnished the olefinic carbene-carbene coupling products in good yields (Scheme 1d).[27]

A fully analogous reaction (without the intermediate alkylation step) might be operative here. Amino ferrocene, although a weak nucleophile, attacks a carbonyl ligand *cis* to the carbene ligand forming zwitterion **I** (Scheme 2). After tautomerization intermediate **II** forms. According to quantum chemical calculations, the resulting OH group forms a hydrogen bond to the ferrocenyl iron(II) center Fe2 of the initial amino ferrocene in intermediate **II** irrespective of the conformation (Figure 2). Possibly, **II** can also form directly from Fc-NH_2 **1** assisted by the evolving O1H1···Fe2 hydrogen bond. XH···Fe hydrogen bonds are meanwhile a well-established structural motif.[26,42–45] The XH···Fe bond dissociation energy can amount up to 13 kJ·mol^{-1}. Consequently, the ferrocenyl moiety might assist the nucleophilic attack acting as an internal base.[46]

After carbene-carbene coupling as the key C–C bond forming step, enol **III** forms (Scheme 2). Enol **III** would then tautomerize to the by 82 kJ·mol^{-1} more stable amide **IV** according to DFT calculations (Scheme 2 and Figure S5, Supporting Information).

Under the inert conditions employed, the chromium(0) species could be competent to reduce the alkoxy derivative **IV** to the final product **2** accounting for the formation of the CH_2 group. Indeed, secondary desalkoxylation reactions with chromium(0) carbenes have been reported in several cases,[47–50] likely forming chromium(II) alkoxides.[51–54]

Synthesis and Characterization of 3

To shed light onto the role of the incoming amine in the reaction discussed above, Fc-NH_2 was replaced by the bulky,

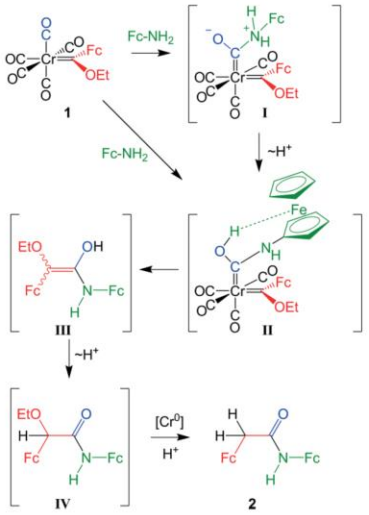

Scheme 2. Proposed mechanism for the formation of **2** via biscarbenes, carbene-carbene coupling and reduction.

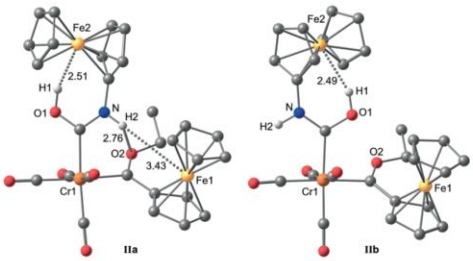

Figure 2. DFT optimized biscarbene intermediate **II** (distances given in Å). Conformer **IIa** is only slightly stabilized by 4 kJ·mol^{-1} with respect to **IIb**.

more nucleophilic adamantylamine Ad-NH_2 in the reaction with **1**. Naturally, Ad-NH_2 is incompetent to form an intramolecular, possibly rate-enhancing O1H1···Fe2 hydrogen bond.

In fact, only traces of the expected adamantyl derivative Ad–NHCO–CH_2–Fc (**2^{Ad}**) were detected by FD mass spectrometry (*m/z* = 377; Figure S6, Supporting Information) of the reaction mixture. Instead, the triferrocenyl cyclobutenone derivatives 4-ethoxy-2,3,4-triferrocenyl-cyclobut-2-enone (**3**; *m/z* = 664) and 4-(adamantylamide)-2,3,4-triferrocenyl-cyclobut-2-enone (**3^{Ad}**; *m/z* = 770) were identified (Figure S6, Supporting Information). The former was successfully isolated from the reaction mixture and characterized (Figures S7–S14, Supporting Information). Obviously, the amine was not incorporated into **3** in spite of its higher nucleophilicity. While Ad-NH_2 fails to attack a CO ligand of **1** at a significant rate, the

© 2020 The Authors. Published by WILEY-VCH Verlag GmbH & Co. KGaA, Weinheim

Journal of Inorganic and General Chemistry
ZAAC
Zeitschrift für anorganische und allgemeine Chemie
ARTICLE

assisting O1H1···Fe2 hydrogen bond (Figure 2) might be responsible for the special reactivity of Fc–NH_2 allowing its attack on the CO ligand.

As Ad–NH_2 appears non-essential for the formation of **3**, thermolysis of **1** was performed in the absence of any nucleophile. Indeed, in the FD mass spectrum of the reaction mixture, a peak at *m/z* = 664 appears corresponding to the molecular mass of **3** along with peaks assignable to carbene coupling products (*m/z* = 440, 442, 484) and traces of an oxidation product of **3** (*m/z* = 680). The latter might be assigned to a ring-opened keto ester 2,3,4-triferrocenyl-4-oxo-but-2-enoic acid ethyl ester (Scheme 1a, Zora pathway; with R^1 = Et, R^2 = R^3 = Fc). After chromatographic workup, cyclobutenone **3** was isolated in a remarkable 17% yield considering the formation of four C–C bonds in a single reaction.

Compound **3** crystallizes in the monoclinic space group $P2_1/c$ with one molecule in the asymmetric unit (Figure 1b) without significant intermolecular contacts. Table S2 (Supporting Information) reports selected bond lengths, bond angles and dihedral angles of the single-crystal X-ray diffraction data and the corresponding DFT calculation. The cyclobutenone ring is essentially planar, the C=C double bond [1.378(2) Å] is slightly longer than that found in the four other crystallographically characterized cyclobutenones with an alkoxy substituent (1.353–1.368 Å).[55–58] The Cp rings of the Fc substituents at the C=C double bond are quite coplanar to the four-membered ring (torsion angles C=C–C_{ipso}–C_{alpha} = 9.2° and 17.1°). The three bulky ferrocenyl substituents at the 2, 3 and 4 positions point up, down and down, respectively, relative to the cyclobutenone plane avoiding steric hindrance.

The ^{1}H and ^{13}C{^{1}H} NMR spectra exhibit all expected resonances of the chemically different ferrocenyl substituents although complete individual assignment was impossible (Figures S7–S12, Supporting Information). The CH_2 group of the ethoxy substituent possesses diastereotopic protons resulting in two doublets of quartets in the ^{1}H NMR spectrum. In the solid state and in heptane, the absorption band of the C=O stretching vibration appears at 1738 and 1751 cm^{-1}, respectively (Figure S13, Supporting Information). The value in the solid is rather low compared to the reported range for cyclobutenones (solid: 1757–1760 cm^{-1} solid. $CDCl_3$: 1753–1758 cm^{-1}).[14–18] Two intramolecular short CH···O distances of 2.90 and 2.81 Å, namely from the 2-ferrocenyl (α-CH) and 4-ferrocenyl (unsubstituted Cp-H) substituent, might be responsible for this finding especially in the solid state. According to quantum chemical calculations, these CH stretches indeed couple to the carbonyl stretching vibration (Figure S15, Supporting Information).

The three chemically different ferrocenyl substituents of **3** give rise to three individual quasi-reversible one-electron redox waves in the cyclic voltammogram at –80, 140 and 340 mV vs. the ferrocene/ferrocenium couple under our conditions (Figure S16, Supporting Information). Assignment of the oxidation processes to individual ferrocenes is impossible at this stage.

A conceivable mechanism to the formation of **3** is discussed next.

Mechanistic Considerations on the Formation of 3

In a formal retrosynthesis, the triferrocenyl cyclobutenone derivative **3** can be derived from a CO unit and three ferrocenyl carbenes (under partial desalkoxylation). As cyclobutenones are accessible from alkynes and Fischer carbene complexes (lacking conjugated aryl or vinyl carbene substituents which would enable the Dötz reaction, Scheme 1a) according to previous work by *Zora* and co-workers (Scheme 1a), the formation of **3** from **1** might be traced back to a thermally induced formation of the required diferrocenyl alkyne Fc–C≡C–Fc.[14–21]

Fischer reported the formation of carbene–carbene coupling products, i.e. *cis*/*trans*-dimethoxy stilbene and *cis*/*trans*-dimethoxy 2-butene, by thermolysis of chromium methoxy carbenes (Scheme 1e).[28,29] Similarly, heating **1** in toluene releases CO giving the unsaturated complex **V** (Scheme 3). Carbene transfer from **1** then could form biscarbene **VI**. Carbene-carbene coupling releases *cis*/*trans*-1,2-diethoxy-1,2-diferrocenyl ethylene **VII** (Scheme 3) which has been identified by a peak in the FD mass spectrum (*m/z* = 484; Figure 3).

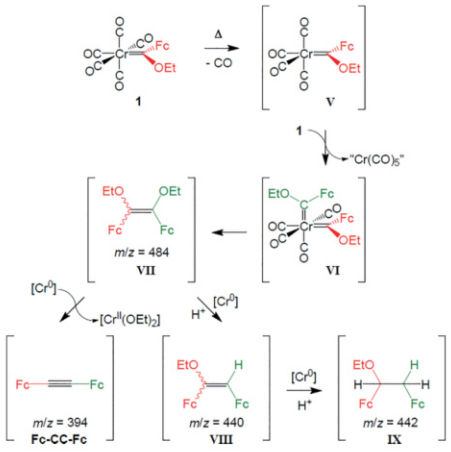

Scheme 3. Proposed mechanism for formation of 1,2-diferrocenyl alkenes **VII** and **VIII**, 1,2-diferrocenyl alkane **IX**, and diferrocenyl alkyne Fc–C≡C–Fc.

Furthermore, peaks at *m/z* = 440 and 442 are observed which can be assigned to *cis*/*trans*-1-ethoxy-1,2-diferrocenyl ethylene **VIII** and 1-ethoxy-1,2-diferrocenyl ethane **IX**, respectively (Figure 3). **VIII** could form via secondary desalkoxylation of **VII** by chromium(0) species similar to the proposed desalkoxylation of **IV** (Scheme 2) and literature precedents.[47–50] Further reduction of **VIII** then leads to the alkane **IX**. The latter is a dead-end in the reaction to **3** and indeed accumulates during the reaction, while **VII** and **VIII** are consumed over time (Figure 3). Concomitantly, the peak for the product **3** increases. The proposed diferrocenyl alkyne could form directly from diethoxy alkene **VII** with

© 2020 The Authors. Published by WILEY-VCH Verlag GmbH & Co. KGaA, Weinheim

Journal of Inorganic and General Chemistry
ZAAC
Zeitschrift für anorganische und allgemeine Chemie
ARTICLE

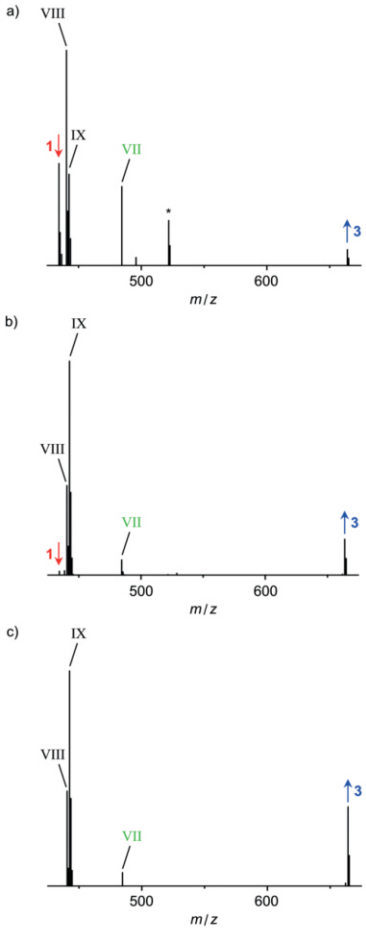

Figure 3. LIFDI mass spectra taken during the thermolysis of **1** after (a) 1 d, (b) 2 d, and (c) 8 d in toluene at 111 °C (* = unknown intermediate).

chromium(0) species[47–50] generating chromium(II) alkoxides.[51–54] However, Fc–C≡C–Fc (*m/z* = 394) is not observed by mass spectrometry during the reaction. Possibly, the formed alkyne reacts too fast with the unsaturated chromium carbene $(OC)_4Cr(C(OEt)(Fc))$ **V** (Scheme 3) to accumulate significantly in the reaction mixture. The alkyne complex then evolves further to the cyclobutenone **3** according to *Zora's* studies (Scheme 1a).[19–21] In agreement with the proposed fast reaction, tetracarbonyl chromium complex **V** could not be detected by mass spectrometry and IR spectroscopy (in *n*-heptane) during the thermolysis of **1**. IR spectra acquired during the thermolysis merely display absorption bands assignable to $Cr(CO)_6$ (1988 cm^{-1}) and **VII** (1724 cm^{-1})[59] (Figure S17, Supporting Information).

In a computational model reaction of the methoxy substituted carbene complex $\mathbf{1^{OMe}}$ with tolane we studied the course of the reaction towards the corresponding cyclobutenone (Scheme 4, Figure S18, Supporting Information). After CO loss, the alkyne coordinates to **V** giving the alkyne complex **X**. The tolane complex evolves to the thermodynamically preferred vinyl carbene complex **XI**. Coordination of the alkoxide substituent stabilizes the unsaturated chromium center in **XI** which evolves to the $Cr(CO)_3$ coordinated vinyl ketene[60–61] **XII**. Finally, ring closure yields the $Cr(CO)_3$ coordinated cyclobutenone **XIII**.

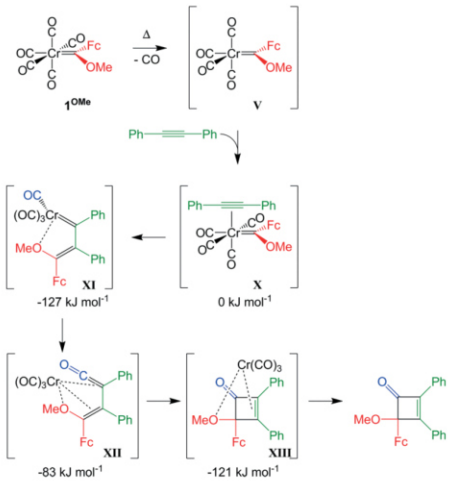

Scheme 4. Computational model reaction of $\mathbf{1^{OMe}}$ and Ph–C≡C–Ph. Relative energies of **X**, **XI**, **XII**, and **XIII** from the DFT calculations.

Conclusions

Products of carbene-carbene coupling reactions have been obtained by thermolysis of $(OC)_5Cr(C(OEt)(Fc))$ (**1**). In the presence of amino ferrocene Fc–NH_2, 2,*N*-diferrocenyl acetamide Fc–CH_2–CO–NH–Fc (**2**) was isolated. The initial attack of the rather weak nucleophile Fc-NH_2 at a CO ligand of **1** is possibly assisted by an OH···Fe hydrogen bond. In the absence of a nucleophile, CO dissociation, carbene transfer and carbene-carbene coupling yields diferrocenyl ethylenes, diferrocenyl ethane and possibly diferrocenyl alkyne. The diferrocenyl alkyne coordinates to **1** after CO dissociation. Alkyne and CO insertion finally releases 4-ethoxy-2,3,4-triferrocenylcyclobut-2-enone **3**. Key reactions in both scenarios are the intermediate formation of biscarbene complexes and carbene-carbene coupling.

 © 2020 The Authors. Published by WILEY-VCH Verlag GmbH & Co. KGaA, Weinheim

Journal of Inorganic and General Chemistry
ZAAC
Zeitschrift für anorganische und allgemeine Chemie
ARTICLE

Experimental Section

General Procedures: All reactions were performed in an argon atmosphere unless otherwise noted. A glovebox of the type UniLab/MBraun (Ar 4.8, $O_2 < 1$ ppm, $H_2O < 1$ ppm) was used for storage and weighing of sensitive compounds. All samples that required the absence of oxygen were prepared in the same glovebox. Dichloromethane was dried with CaH_2 and distilled prior to use. THF, xylenes and toluene were distilled from potassium. *n*-Heptane was dried with molecular sieves 4 Å for at least 48 h. Deuterated solvents were purchased from euriso-top. 1-Adamantylamine was received from Alfa Aesar. **1** [26,31–33] and amino ferrocene[24,25] were synthesized using literature procedures. NMR spectra were recorded on a Bruker Avance DRX 400 spectrometer at 400.31 MHz (^{1}H) and 100.07 MHz (^{13}C{^{1}H}). All resonances are reported in ppm vs. the solvent signal as internal standard. CD_2Cl_2 (^{1}H: δ = 5.32 ppm; ^{13}C: δ = 54.0 ppm), [D$_8$]THF (^{1}H: δ = 1.72, 3.58 ppm).[62] IR spectra were recorded with a Bruker ALPHA II FT-IR spectrometer with a platinum Di-ATR module as solid state samples or in *n*-heptane with a transmission module using KBr cells. UV/Vis/NIR spectra were recorded on a Varian Cary 5000 spectrometer by using 1.0 cm cells (Hellma, suprasil). Electrochemical experiments were carried out on a BioLogic SP-200 voltammetric analyzer using platinum wires as counter and working electrodes and a 0.01 M $Ag/AgNO_3$ electrode as reference electrode. Cyclic voltammetry measurements were carried out at scan rate of 100 mV•s^{-1} using 0.1 M [*n*Bu$_4$N][PF$_6$] as supporting electrolyte in CH_2Cl_2. Potentials are referenced to the decamethylferrocene/decamethylferrocenium couple ($E_{1/2}$ = –270 ± 5 mV under the experimental conditions; literature value $E_{1/2}$ = –590 mV vs. ferrocene[63]) and given vs. ferrocene. FD mass spectra were recorded on a Thermo Fisher DFS mass spectrometer with a LIFDI upgrade. Elemental analyses were performed by the microanalytical laboratory of the department of chemistry, University of Mainz.

Density Functional Theory Calculations: DFT calculations were carried out using the ORCA program package (version 4.1.1).[64] All calculations were performed using the B3LYP functional[65–67] and employ the RIJCOSX approximation.[68,69] Relativistic effects were calculated at the zeroth order regular approximation (ZORA) level.[70] The ZORA keyword automatically invokes relativistically adjusted basis sets. To account for solvent effects, a conductor-like screening model (CPCM) modelling dichloromethane was used in all calculations.[71,72] Geometry optimizations were performed using Ahlrichs' split-valence double-ξ basis set ZORA-def2-SVP which comprises polarization functions for all non-hydrogen atoms.[73] Auxiliary basis set for General-purpose Coulomb fitting SARC/J decontracted def2/J up to Kr was used.[74] Atom-pairwise dispersion correction was performed with the Becke-Johnson damping Scheme (D3BJ).[75,76] The presence of energy minima was checked by numerical frequency calculations. The approximate free energies at 298 K were obtained through thermochemical analysis of the frequency calculation, using the thermal correction to the Gibbs free energy as reported by ORCA.

Crystal Structure Determination: Intensity data were collected with a Bruker AXS Smart1000 CCD diffractometer with an APEX II detector and an Oxford cooling system and corrected for absorption and other effects using Mo-K_α radiation (λ = 0.71073 Å). The diffraction frames were integrated using the SAINT package[77] and most were corrected for absorption with MULABS[78] of the PLATON software package.[79] The structures were solved by direct methods and refined by the full-matrix method based on F^2 using the SHELXL software package.[80,81] All non-hydrogen atoms were refined anisotropically while the positions of all hydrogen atoms were generated with appropriate geometric constraints and allowed to ride on their respective parent carbon/nitrogen atoms with fixed isotropic thermal parameters. See Supporting Information for crystal data of **2** and **3**.

Crystallographic data (excluding structure factors) for the structures in this paper have been deposited with the Cambridge Crystallographic Data Centre, CCDC, 12 Union Road, Cambridge CB21EZ, UK. Copies of the data can be obtained free of charge on quoting the depository numbers CCDC-1962440 and CCDC-1962439. (Fax: +44-1223-336-033; E-Mail: deposit@ccdc.cam.ac.uk, http://www.ccdc.cam.ac.uk).

2,*N*-Diferrocenylacetamide (2): Amino ferrocene (422 mg, 2.1 mmol, 1.05 equiv.) and **1** (868 mg, 2.0 mmol, 1.0 equiv.) were heated under reflux in toluene (50 mL) for 120 h resulting in a dark solution and a dark precipitate. The reaction progress was monitored by TLC and LIFDI mass spectrometry. The solvent was removed under reduced pressure. Column chromatography (SiO_2, 42 × 3.5 cm, petroleum ether:THF, 6:4, R_f = 0.55) yielded a brown solid (119 mg, 0.28 mmol, 14 %). **^{1}H NMR** (CD_2Cl_2): δ = 6.74 (s, 1 H, H^7), 4.50 (pt, 2 H, H^9), 4.22 (pt, 4 H, H^2, H^3), 4.18 (s, 5 H, H$^{1/11}$), 4.09 (s, 5 H, H$^{1/11}$), 3.96 (pt, 2 H, H^{10}), 3.33 (s, 2 H, H^5) ppm. **^{1}H NMR** ([D$_8$]THF): δ = 8.23 (s, 1 H, H^7), 4.61 (pt, 2 H, Cp(subst.)), 4.23 (pt, 2 H, Cp(subst.)) 4.12 (s, 5 H, H$^{1/11}$), 4.07 (pt, 2 H, Cp(subst.)), 4.05 (s, 5 H, H$^{1/11}$), 3.88 (pt, 2 H, Cp(subst.)), 3.17 (s, 2 H, H^5) ppm. **MS** (FD): *m/z* (*int.* / %) = 427.4 (100) [M$^+$], 428.4 (30), 425.4 (9). Calcd. for $C_{22}H_{21}Fe_2NO$ (427.0). **IR** (KBr): $\tilde{\nu}$ = 3280 (m), 3209 (sh), 3090 (m), 2960 (m), 2909 (w), 1659 (s), 1566 (s), 1481 (m), 1389 (m), 1265 (s), 1196 (m), 1096 (vs), 1026 (vs), 802 (vs), 710 (m), 494 (vs) cm^{-1}. **UV/Vis** (CH_2Cl_2): λ_{max} (ε/M^{-1} cm^{-1}) = 270 (1260), 335 (65) 440 (50) nm.

4-Ethoxy-2,3,4-triferrocenyl-cyclobut-2-enone (3): **1** (1302 mg, 3 mmol) was heated under reflux in xylenes (120 mL) for three days resulting in a dark solution and a dark precipitate. The reaction was monitored by TLC and LIFDI-MS. After removal of the solvent under reduced pressure, the crude reaction mixture dissolved in dichloromethane was filtered using a short celite pad. Column chromatography of 694 mg brown oil (SiO_2, 57 × 4.5 cm, CH_2Cl_2, R_f = 0.71) yielded a red solid (110 mg, 0.17 mmol, 17 %). **^{1}H NMR** (CD_2Cl_2): δ = 4.95 (pt, 2 H, C_5H_4), 4.80 (pt, 1 H, C_5H_4), 4.57 (pt, 1 H, C_5H_4), 4.55 (pt, 2 H, C_5H_4), 4.45 (pt, 2 H, C_5H_4), 4.28 (s, 5 H, Cp), 4.25 (s, 5 H, Cp), 4.24 (pt, 2 H, C_5H_4), 4.16 (pt, 1 H, C_5H_4), 4.08 (pt, 1 H, C_5H_4), 4.03 (s, 5 H, Cp), 3.67–3.60 (dq, $^2J_{H,H}$ = 1.5, $^3J_{H,H}$ = 7.0 Hz, 1 H, CH$_2$, H^{6b}), 3.54–3.47(dq, $^2J_{H,H}$ = 1.5, $^3J_{H,H}$ = 7.0 Hz, 1 H, CH$_2$, H^{6a}), 1.25 (t, ^3J(H,H) = 6 Hz, 3 H, CH$_3$) ppm. **^{13}C{^{1}H} NMR** (CD_2Cl_2): δ = 191.24 (C^{10}), 172.63 (C$^{quat.}$), 141.99 (C$^{quat.}$), 98.40 (C^5), 87.81 (C$^{quat.}$), 72.93 (C$^{quat.}$), 72.53 (C$^{quat.}$), 72.35 (C$^{Cp(subst)}$), 72.26 (C$^{Cp(subst)}$), 70.88 (C$^{Cp(subst)}$), 70.59 (C$^{1/14/18}$), 70.22 (C$^{Cp(subst)}$), 70.15 (C$^{Cp(subst)}$), 70.04 (C$^{1/14/18}$), 69.89 (C$^{1/14/18}$), 69.31 (C$^{Cp(subst)}$), 69.01 (C$^{Cp(subst)}$), 68.85 (C$^{Cp(subst)}$), 68.26 (C$^{Cp(subst)}$), 68.17 (C$^{Cp(subst)}$), 68.06 (C$^{Cp(subst)}$), 66.82 (C$^{Cp(subst)}$), 60.56 (C^6), 16.2 (C^7) ppm. **MS** (FD): *m/z* (*int.* / %) = 663.9 (100) [M$^+$], 664.9 (44), 662.0 (19), 665.9 (12), 662.9 (8). calcd. for $C_{36}H_{32}Fe_3O_2$ (664.05). **IR** (ATR): $\tilde{\nu}$ = 3088 (w), 2963 (m), 2917(w), 2870 (w), 2851 (w), 1738 (m), 1724 (sh), 1614 (m), 1482 (w), 1443 (w), 1410 (w), 1379 (w), 1336 (w), 1260 (vs), 1103 (s), 1074 (s), 1018 (s), 1004 (s), 917 (w), 864 (w), 794 (vs), 742 (sh), 695 (m), 474 (s) cm^{-1}. **IR** (*n*-heptane): $\tilde{\nu}$ = 1751 (w) cm^{-1}. **UV/Vis** (CH_2Cl_2): λ_{max} (ε/M^{-1} cm^{-1}) = 264 (12850), 321 (10850), 338 (sh, 2400), 489 (2450) nm. **CV** (CH_2Cl_2, vs. FcH/FcH$^+$): $E_{1/2}$ = –80, 140, 340 mV. $C_{36}H_{32}Fe_3O_2$ (664.05): calcd. C, 65.10; H, 4.86 %; found: C, 64.73; H, 4.83 %.

Supporting Information (see footnote on the first page of this article): spectroscopic data of **2** and **3**, alternative synthesis of **2**, cyclic

© 2020 The Authors. Published by WILEY-VCH Verlag GmbH & Co. KGaA, Weinheim

Journal of Inorganic and General Chemistry
ZAAC
Zeitschrift für anorganische und allgemeine Chemie
ARTICLE

voltammogram of **3**, XRD data of **2** and **3**, additional DFT data and Cartesian coordinates of **2**, **3** and intermediates **IIa**, **IIb**, **III**, **IV**, **X**, **XI**, **XII**, **XII**.

Acknowledgements

We thank *Regine Jung-Pothmann* for collection of the diffraction data, *Dr. Mihail Mondeshki* for help with the NMR spectroscopic and LIFDI mass spectrometric experiments, *Taro Lieberth* for the independent synthesis of **2**, and the Johannes Gutenberg University of Mainz (Germany) for financial support to C. F. (Internal University Research Funding). DFT calculations were conducted using the supercomputer Mogon and advisory services offered by the Johannes Gutenberg University (www.hpc.uni-mainz.de), which is a member of the Gauss Alliance e.V. and the AHRP (Alliance for High Performance Computing in Rhineland Palatinate, www.ahrp.info).

Keywords: Carbene complexes; Chromium; C–C coupling; Cyclobutenone / Ferrocene

References

[1] E. O. Fischer, A. Maasböl, *Angew. Chem. Int. Ed. Engl.* **1964**, *3*, 580–581; *Angew. Chem.* **1964**, *76*, 645–646.
[2] H. G. Raubenheimer, *Dalton Trans.* **2014**, *43*, 16959–16973.
[3] D. I. Bezuidenhout, S. Lotz, D. C. Liles, B. van der Westhuizen, *Coord. Chem. Rev.* **2012**, *256*, 479–524.
[4] a) M. A. Sierra, *Chem. Rev.* **2000**, *100*, 3591–3638; b) M. Gómez-Gallego, M. J. Mancheño, M. A. Sierra, *Acc. Chem. Res.* **2005**, *38*, 44–53.
[5] K. H. Dötz, J. Stendel Jr., *Chem. Rev.* **2009**, *109*, 3227–3274.
[6] a) J. Barluenga, M. A. Fernández-Rodríguez, E. Aguilar, *J. Organomet. Chem.* **2005**, *690*, 539–587; b) J. Barluenga, J. Flórez, F. J. Fañanás, *J. Organomet. Chem.* **2001**, *624*, 5–17; c) A. de Meijere, H. Schirmer, M. Deutsch, *Angew. Chem. Int. Ed.* **2000**, *39*, 3964–4002; *Angew. Chem.* **2000**, *112*, 4124–4162.
[7] K. H. Dötz, *Angew. Chem. Int. Ed. Engl.* **1975**, *14*, 644–645; *Angew. Chem.* **1975**, *87*, 644–645.
[8] L. Chupak in *Wiley Series on Comprehensive Name Reactions* (Eds.: E. J. Corey, J. J. Li), Wiley, Hoboken, N. J, **2010**, 197–422.
[9] P. Hofmann, M. Hämmerle, *Angew. Chem. Int. Ed. Engl.* **1989**, *28*, 908–910; *Angew. Chem.* **1989**, *101*, 940–942.
[10] H. Fischer, P. Hofmann, *Organometallics* **1999**, *18*, 2590–2592.
[11] M. Torrent, M. Duran, M. Sol, *J. Am. Chem. Soc.* **1999**, *121*, 1309–1316.
[12] P. G. Wenthold, M. A. Lipton, *J. Am. Chem. Soc.* **2000**, *122*, 9265–9270.
[13] J. O. C. Jimenez-Halla, M. Solà, *Chem. Eur. J.* **2009**, *15*, 12503–12520.
[14] K. H. Dötz, *J. Organomet. Chem.* **1977**, *140*, 177–186.
[15] K. H. Dötz, W. Sturm, *J. Organomet. Chem.* **1986**, *310*, C22-C24.
[16] K. S. Chan, G. A. Peterson, T. A. Brandvold, K. L. Faron, C. A. Challener, C. Hyldahl, W. D. Wulff, *J. Organomet. Chem.* **1987**, *334*, 9–56.
[17] B. A. Anderson, J. Bao, T. A. Brandvold, C. A. Challener, W. D. Wulff, Y. C. Xu, A. L. Rheingold, *J. Am. Chem. Soc.* **1993**, *115*, 10671–10687.
[18] J. Bao, W. D. Wulff, M. J. Fumo, E. B. Grant, D. P. Heller, M. C. Whitcomb, S.-M. Yeung, *J. Am. Chem. Soc.* **1996**, *118*, 2166–2181.
[19] M. Zora, E. Ünsal Güngör, *Tetrahedron Lett.* **2001**, *42*, 4733–4735.
[20] M. Zora, C. Açıkgöz, M. Odabaşoğlu, O. Büyükgüngör, *J. Organomet. Chem.* **2007**, *692*, 1571–1578.
[21] M. Zora, T. Aslı Tumay, O. Büyükgüngör, *Tetrahedron* **2007**, *63*, 4018–4026.
[22] a) E. O. Fischer, B. Heckl, H. Werner, *J. Organomet. Chem.* **1971**, *28*, 359–365; b) E. O. Fischer, M. Leupold, *Chem. Ber.* **1972**, *105*, 599–608.
[23] D. B. Grotjahn, K. H. Dötz, *Synlett* **1991**, 381–390.
[24] B. Bildstein, M. Malaun, H. Kopacka, K. Wurst, M. Mitterböck, K.-H. Ongania, G. Opromolla, P. Zanello, *Organometallics* **1999**, *18*, 4325–4336.
[25] K. Heinze, M. Schlenker, *Eur. J. Inorg. Chem.* **2004**, 2974–2988.
[26] P. Veit, C. Förster, S. Seibert, K. Heinze, *Z. Anorg. Allg. Chem.* **2015**, *641*, 2083–2092.
[27] J. Barluenga, A. A. Trabanco, I. Pérez-Sánchez, R. de La Campa, J. Flórez, S. García-Granda, A. Aguirre, *Chem. Eur. J.* **2008**, *14*, 5401–5404.
[28] E. O. Fischer, B. Heckl, K. H. Dötz, J. Müller, H. Werner, *J. Organomet. Chem.* **1969**, *16*, P29–P32.
[29] E. O. Fischer, D. Plabst, *Chem. Ber.* **1974**, *107*, 3326–3331.
[30] M. L. Lage, I. Fernández, M. J. Mancheño, M. Gómez-Gallego, M. A. Sierra, *Chem. Eur. J.* **2010**, *16*, 6616–6624.
[31] a) J. G. López-Cortés, L. F. Contreras de la Cruz, M. C. Ortega-Alfaro, R. A. Toscano, C. Alvarez-Toledano, H. Rudler, *J. Organomet. Chem.* **2005**, *690*, 2229–2237; b) J. A. Connor, J. P. Lloyd, *J. Chem. Soc., Dalton Trans.* **1972**, 1470–1476.
[32] D. I. Bezuidenhout, W. Barnard, B. van der Westhuizen, E. van der Watt, D. C. Liles, *Dalton Trans.* **2011**, *40*, 6711–6721.
[33] G. A. Mose, E. O. Fischer, M. D. Rausch, *J. Organomet. Chem.* **1971**, *27*, 379–382.
[34] K. Heinze, D. Siebler, *Z. Anorg. Allg. Chem.* **2007**, *633*, 2223–2233.
[35] D. Siebler, M. Linseis, T. Gasi, L. M. Carrella, R. F. Winter, C. Förster, K. Heinze, *Chem. Eur. J.* **2011**, *17*, 4540–4551.
[36] K. Heinze, K. Hempel, M. Beckmann, *Eur. J. Inorg. Chem.* **2006**, 2040–2050.
[37] H. Huesmann, C. Förster, D. Siebler, T. Gasi, K. Heinze, *Organometallics* **2012**, *31*, 413–427.
[38] A. Neidlinger, V. Ksenofontov, K. Heinze, *Organometallics* **2013**, *32*, 5955–5965.
[39] J. Melomedov, J. R. Ochsmann, M. Meister, F. Laquai, K. Heinze, *Eur. J. Inorg. Chem.* **2014**, 1984–2001.
[40] A. Neidlinger, C. Förster, K. Heinze, *Eur. J. Inorg. Chem.* **2016**, 1274–1286.
[41] E. O. Fischer, F. R. Kreißl, C. G. Kreiter, E. W. Meineke, *Chem. Ber.* **1972**, *105*, 2558–2564.
[42] C. Förster, P. Veit, V. Ksenofontov, K. Heinze, *Chem. Commun.* **2015**, *51*, 1514–1516.
[43] T. Kienz, C. Förster, K. Heinze, *Organometallics* **2016**, *35*, 3681–3691.
[44] P. Veit, E. Prantl, C. Förster, K. Heinze, *Organometallics* **2016**, *35*, 249–257.
[45] K. Hanauer, M. T. Pham, C. Förster, K. Heinze, *Eur. J. Inorg. Chem.* **2017**, 433–445.
[46] M. Malischewski, K. Seppelt, J. Sutter, F. W. Heinemann, B. Dittrich, K. Meyer, *Angew. Chem. Int. Ed.* **2017**, *56*, 13372–13376; *Angew. Chem.* **2017**, *129*, 13557–13561.
[47] W. D. Wulff, R. W. Kaesler, G. A. Peterson, P.-C. Tang, *J. Am. Chem. Soc.* **1985**, *107*, 1060–1062.
[48] S. U. Turner, J. W. Herndon, L. A. McMullen, *J. Am. Chem. Soc.* **1992**, *114*, 8394–8404.
[49] M. Zora, J. W. Herndon, *Organometallics* **1993**,*12*, 248–249.
[50] M. Zora, Y. Li, J. W. Herndon, *Organometallics* **1999**, *18*, 4429–4436.
[51] J. J. H. Edema, S. Gambarotta, E. van Bolhuis, A. L. Spek, *J. Am. Chem. Soc.* **1989**, *111*, 2142–2147.
[52] O. L. Sydora, D. S. Kuiper, P. T. Wolczanski, E. B. Lobkovsky, A. Dinescu, T. R. Cundari, *Inorg. Chem.* **2006**, *45*, 2008–2021.
[53] P. Qiu, R. Cheng, B. Liu, B. Tumanskii, R. J. Batrice, M. Botoshansky, M. S. Eisen, *Organometallics* **2011**, *30*, 2144–2148.
[54] M. Yousif, A. C. Cabelof, P. D. Martin, R. L. Lord, S. Groysman, *Dalton Trans.* **2016**, *45*, 9794–9804.

 © 2020 The Authors. Published by WILEY-VCH Verlag GmbH & Co. KGaA, Weinheim

Journal of Inorganic and General Chemistry
ZAAC
Zeitschrift für anorganische und allgemeine Chemie

ARTICLE

[55] L. A. Paquette, L. H. Kuo, J. Tae, *J. Org. Chem.* **1998**, *63*, 2010–2021.
[56] S. Iwata, T. Hamura, K. Suzuki, *Chem. Commun.* **2010**, *46*, 5316–5318.
[57] M. W. Davies, J. P. A. Harrity, C. N. Johnson, *Chem. Commun.* **1999**, 2107–2108.
[58] A. R. Hergueta, H. W. Moore, *J. Org. Chem.* **2002**, *67*, 1388–1391.
[59] M. L. Lage, D. Curiel, I. Fernández, M. J. Mancheño, M. Gómez-Gallego, P. Molina, M. A. Sierra, *Organometallics* **2011**, *30*, 1794–1803.
[60] M. A. Huffman, L. S. Liebeskind, W. T. Pennington, *Organometallics* **1992**, *11*, 255–266.
[61] M. A. Huffman, L. S. Liebeskind, *J. Am. Chem. Soc.* **1990**, *112*, 8617–8618.
[62] G. R. Fulmer, A. J. M. Miller, N. H. Sherden, H. E. Gottlieb, A. Nudelman, B. M. Stoltz, J. E. Bercaw, K. I. Goldberg, *Organometallics* **2010**, *29*, 2176–2179.
[63] N. G. Connelly, W. E. Geiger, *Chem. Rev.* **1996**, *96*, 877–910.
[64] F. Neese, *WIREs Comput. Mol. Sci.* **2012**, *2*, 73–78.
[65] A. D. Becke, *J. Chem. Phys.* **1993**, *98*, 5648–5652.
[66] C. Lee, W. Yang, R. G. Parr, *Phys. Rev. B* **1988**, *37*, 785–789.
[67] B. Miehlich, A. Savin, H. Stoll, H. Preuss, *Chem. Phys. Lett.* **1989**, *157*, 200–206.
[68] F. Neese, F. Wennmohs, A. Hansen, U. Becker, *Chem. Phys.* **2009**, *356*, 98–109.
[69] R. Izsák, F. Neese, *J. Chem. Phys.* **2011**, *135*, 144105.
[70] D. A. Pantazis, X.-Y. Chen, C. R. Landis, F. Neese, *J. Chem. Theory Comput.* **2008**, *4*, 908–919.
[71] V. Barone, M. Cossi, *J. Phys. Chem. A* **1998**, *102*, 1995–2001.
[72] S. Miertuš, E. Scrocco, J. Tomasi, *Chem. Phys.* **1981**, *55*, 117–129.
[73] F. Weigend, R. Ahlrichs, *Phys. Chem. Chem. Phys.* **2005**, *7*, 3297–3305.
[74] F. Weigend, *Phys. Chem. Chem. Phys.* **2006**, *8*, 1057–1065.
[75] S. Grimme, J. Antony, S. Ehrlich, H. Krieg, *J. Chem. Phys.* **2010**, *132*, 154104.
[76] S. Grimme, S. Ehrlich, L. Goerigk, *J. Comput. Chem.* **2011**, *32*, 1456–1465.
[77] SMART Data Collection and SAINT-Plus Data Processing Software for the SMART System, Bruker Analytical X-ray Instruments, Inc.: Madison, WI **2000**.
[78] R. H. Blessing, *Acta Crystallogr., Sect. A* **1995**, *51*, 33–38.
[79] A. L. Spek, *Acta Crystallogr., Sect. D* **2009**, *65*, 148–155.
[80] G. M. Sheldrick, *Acta Crystallogr., Sect. C* **2015**, *71*, 3–8.
[81] G. M. Sheldrick, SHELXL-2014/7; University of Göttingen **2014**.

Received: December 20, 2019
Published Online: ■

 © 2020 The Authors. Published by WILEY-VCH Verlag GmbH & Co. KGaA, Weinheim

Journal of Inorganic and General Chemistry
ZAAC
Zeitschrift für anorganische und allgemeine Chemie

ARTICLE

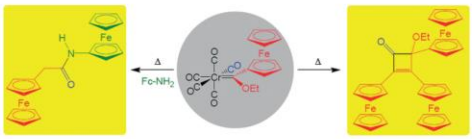

 © 2020 The Authors. Published by WILEY-VCH Verlag GmbH & Co. KGaA, Weinheim

3.6 Electrochemistry of the heterotrimetallic Fischer carbene complex (N-methylaminoferrocenyl) (ferrocenyl) carbene (pentacarbonyl) tungsten (0)

Philipp Veit, Christoph Förster* and Katja Heinze*

2020, Manuscript in submission process.

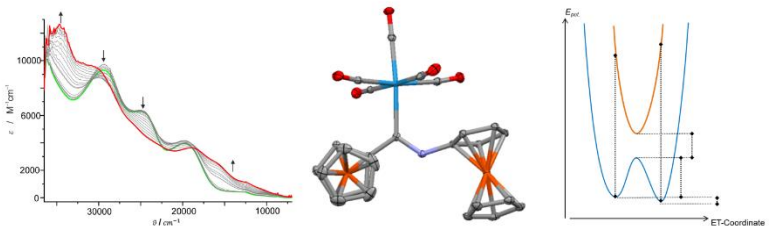

The heterotrimetallic Fischer carbene complex (N-methylaminoferrocenyl) (ferrocenyl) carbene (pentacarbonyl) tungsten(0) is synthesized and characterized by NMR- , IR-, UV-vis spectroscopy, cyclic voltammetry, spectroelectrochemical techniques, single crystal X-ray diffraction and DFT-calculations. The communication of the two iron centres in the mixed-valent mono cation is compared to the isolobal analogues diferrocenyl amide and thioamide and the role of the bridge is investigated (C=O, C=S, C=M(CO)$_5$).

Author contributions

The synthesis, characterization and all other experiments were performed by Philipp Veit. The crystal structure was solved and refined by Christoph Förster. All DFT calculations were performed by Philipp Veit. The manuscript was written by Philipp Veit (80 %), Christoph Förster (10 %), Katja Heinze (10 %).

Supporting Information

for this article is found in Chapter 6.6 at pp. 183.

“Reprinted with permission from Veit, P.; Förster, C.; Heinze, K.“

Electrochemistry of the heterotrimetallic Fischer carbene complex (*N*-methylaminoferrocenyl)(ferrocenyl)carbene(pentacarbonyl) tungsten(0)

Philipp Veit, Christoph Förster* and Katja Heinze*

Department of Chemistry, Johannes Gutenberg-University of Mainz, Duesbergweg 10-14, 55128 Mainz

Supporting Information Placeholder

ABSTRACT: Diferrocenyl amide and thio amide have been investigated before as short models for potential molecular wires. Here we present (aminoferrocenyl)(ferrocenyl)methylidene(pentacarbonyl)tungsten(0) and (*N*-methylaminoferrocenyl)(ferrocenyl)methylidene(pentacarbonyl)tungsten(0) as isolobal metallo analogues and study their electrochemical properties. The methylated trimetallic amino carbene complex is probed in detail by NMR-, IR-, UV-vis spectroscopy, cyclic voltammetry, spectroelectrochemical and theoretical techniques. The communication of the iron centres in dependence on the bridge (C=O, C=S, C=M(CO)$_5$) in the mixed-valent Fc/Fc$^+$ mono cations is studied and Robin Day classification is applied.

INTRODUCTION

Oligonuclear ferrocene amides can be seen as a prototype for iron containing molecular wires and are therefore of interest in organometallic chemistry.[1–27] In mixed valent systems the electron transfer between the metal centres can be investigated. The electron transfer can occur through space or with participation of the bridge.[2,15,28–32] The electronic structure of the bridge plays an important role in the influence on the electronic communication between two or more metal centres.[2,15,28–32] The simplest amide with two metal centres is diferrocenyl amide **1^O**. Substitution of the (C=O) fragment in the bridge of **1^O**[1] with (C=S) gives diferrocenyl thioamide **1^S**[33] (Scheme 1a). Both show two reversible oxidation waves in the cyclic voltammogram and are prominent to investigate the electronic communication of two ferrocenyl sites in the oxidized species **[1^O]$^{\cdot+}$** and **[1^S]$^{\cdot+}$**. Titration of **1^S** with substoichiometric amounts of iodine shows a shift of the *N*-Fc proton signals in the ^{1}H-NMR spectrum, localizing the site of the first oxidation on this ferrocenyl moiety. Classification after the Marcus theory[34,35] for electron transfer in mixed valence systems gives Robin-Day class II for both amides.[36,37] The heterotrimetallic Fischer carbene complex **1^{Cr}**[38] can be seen as isolobal to the latter amides by exchanging the (C=O)/(C=S) moieties in the bridge with a (C=M(CO)$_5$) fragment. This might totally change the electronic communication in the mixed valent species, as the energy of the C=X-π^*-molecular orbital for C=M is much lower than for C=O or C=S. Also, in **1^{Cr}** the electronegativity is should be higher at the carbene carbon atom, while in **1^O** and **1^S** the electronegativity is higher at the heteroatom. **1^{Cr}** was investigated previously by our group. Irreversible follow up reactions after oxidation prevented the elucidation of the electronic communication in **[1^{Cr}]$^{\cdot+}$**.

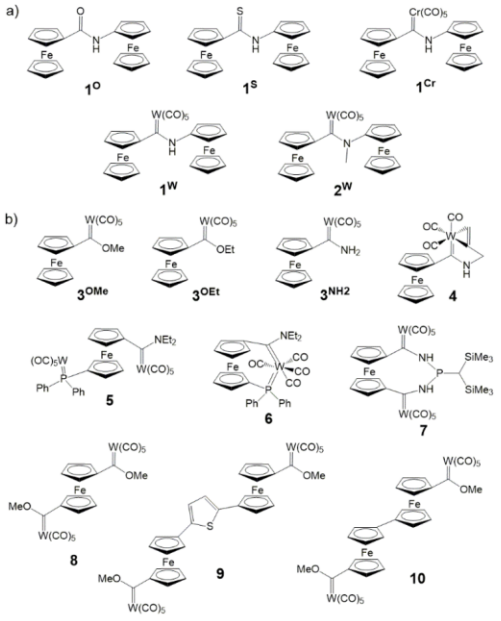

Scheme 1. a) diferrocenylamide 1$^{O[1]}$, -thioamide 1$^{S[33]}$ and isolobal heterotrimetallic Fischer carbene-complexes 1$^{Cr[38]}$, 1^W, 2^W and b) examples of tungsten ferrocenyl Fischer carbene complexes 3$^{OMe[39]}$, 3$^{OEt[40–42]}$, 3$^{NH2[43]}$, 4[44], 5[45], 6[45], 7[46], 8[39], 9[47], 10[39].

The tungsten homologue $\mathbf{1^W}$ shows quasi-reversibility for the first oxidation in the cyclic voltammogram, but shows thermal side reactions to *E*-1,2-diferrocenylimine.[48] Supressing the side reaction by using the *N*-methylated tungsten complex $\mathbf{2^W}$ is anticipated in this work (Scheme 1a). A wide variety of tungsten ferrocenyl Fischer carbene complexes has been reported so far. The Fischer carbene complexes $\mathbf{3^{OMe}}$[39,44], $\mathbf{3^{OEt}}$[40–42] and the amine $\mathbf{3^{NH2}}$[43] are simple representatives (Scheme 1b). Recently we reported two unexpected C-C bond formations of the chromium homologue of $\mathbf{3^{OEt}}$ leading to the chromium free products 2,*N*-diferrocenyl acetamide and the trimetallic 4-ethoxy-2,3,4-triferrocenyl-cyclobut-2-enone.[49] Cyclic Fischer carbene complexes are accessible by replacing two carbonyl ligands on the tungsten metal centre with a *N*-propenyl moiety **4**.[44] Phosphane groups can bond to additional tungsten pentacarbonyl like in **5** or replace a carbonyl bond and form a [3]ferrocenophane like in **6**.[45] Ferrocenophanes can also be generated by cyclization of an aminobiscarbene complex with chloro(bis(trimethylsilyl) methylene)phosphane to get the diaminophosphane-bridged [5]ferrocenophane **7** which can be used in further ring opening reactions.[46] Biscarbene complexes can be linked by one ferrocenyl group **8**[39], ferrocenyl and thiophene groups **9**[47] or by two ferrocenyl groups **10**.[39]

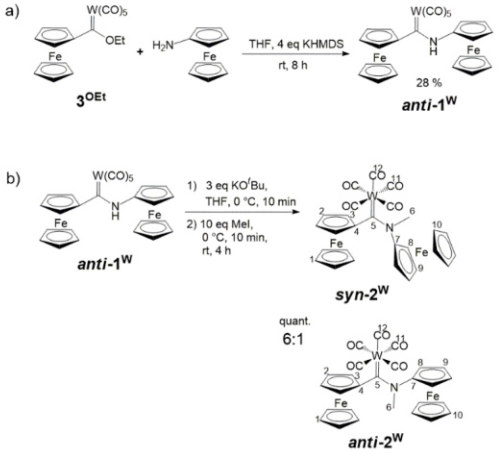

Scheme 2. a) Synthesis of $\mathbf{1^W}$ and b) *syn*/*anti*-$\mathbf{2^W}$ and numbering for NMR assignment.

RESULTS AND DISCUSSION

The treatment of the Fischer carbene-complex (ethoxy)-(ferrocenyl)carbene(pentacarbonyl)tungsten(0) $\mathbf{3^{OEt}}$ [40,41,50–52] with ferrocenylamine Fc-NH_2[53,54] in the presence of potassium hexamethyldisilazide (KHMDS) in tetrahydrofuran at room temperature yields the diferrocenyl NH–carbene complex $\mathbf{1^W}$[48] in quantitative yield (Scheme 2a) analogous to $\mathbf{1^{Cr}}$ [38]. In absence of KHMDS no reaction would be anticipated as aminoferrocene has a much lower nucleophilicity than the corresponding amide or than dimethylamine or pyrrolidine, which react with alkoxy Fischer carbene complexes to the corresponding amino Fischer carbene complexes without the presence of an additional base.[51] Unexpectedly Fischer carbene $\mathbf{1^{Cr}}$ shows reactivity with aminoferrocene in absence of KHMDS to 2,*N*-diferrocenyl acetamide in yields up to 14 % by attack of the amine on the carbonyl carbon instead of the carbene carbon atom as recently reported.[49]

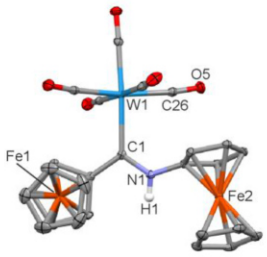

Figure 1. Molecular structure of ***anti*-$\mathbf{1^W}$** from single crystal XRD (CH hydrogen atoms omitted for clarity, thermal ellipsoids at 30 % probability level, for full numbering of all atoms see ESI Table S2).

$\mathbf{1^W}$ crystallizes as the *anti*-isomer[55–61] in the monoclinic space group *C*2/*c* with one molecule in the asymmetric unit (Figure 1, ESI Table S1, Table S2, Table S3). The central tungsten atom shows a slightly distorted octahedral coordination with a typical umbrella-like distortion[62] of the $W(CO)_5$ fragment (Figure 1) analogous to $\mathbf{1^{Cr}}$.[38] The carbene unit adopts a staggered conformation with respect to the $W(CO)_4$ plane. Expectedly, the W–C bond of the axial CO ligand is shorter and the corresponding C–O distance is larger than the respective distances of the equatorial CO ligands. The metrical data of $\mathbf{1^W}$ lies in range of that of the 18 known solid-state structures of related (ferrocenyl)(R)carbene(pentacarbonyl)-tungsten(0) complexes (W-CO = 2.003(3)–2.060(3), ESI Table S1).[39–41,43–47,63–67] The W-$C_{Carbene}$ distance is 2.268(3) Å, while the Cr-$C_{Carbene}$ distance in $\mathbf{1^{Cr}}$ is 2.097(2) Å due to the different covalent radii of 1.39(5) Å for chromium and 1.62(7) Å for tungsten[68]. In $\mathbf{3^{OEt}}$ [41] the W-$C_{Carbene}$ distance is 2.214(4) Å and in the amine $\mathbf{3^{NH2}}$ [43] it is 2.249(5) Å, which is both shorter than in $\mathbf{1^W}$. The $C_{Carbene}$-N distance in $\mathbf{1^W}$ is 1.325(3) Å and therefore longer than the distance in $\mathbf{3^{NH2}}$ with 1.306(5) Å. The same trend is observed in $\mathbf{1^{Cr}}$ and $(CO)_5Cr{=}C(Fc)(NH_2)$.[43] It seems like the *N*-ferrocenyl substituent does not increase the π-donor capability of the amine towards the carbene centre in $\mathbf{1^W}$. The cyclopentadienyl ring of the ferrocenyl group bound directly to the carbene carbon atom lies in plane with the carbene plane and allows interaction with the π-system of the carbene-tungsten bond as well as with the lone pair of the nitrogen atom (torsion angle C3-C2-C1-W1 −11.5(4)°). The out-of-plane orientation of the *N*-ferrocenyl moiety with respect to the carbene plane (torsion angle C16-C12-N1-C1 63.4(4)°) hinders a contribution to the π-system of the carbene-tungsten bond. Coplanar orientation is not possible due to steric interaction of the *N*-ferrocenyl moiety with the $W(CO)_5$-fragment. This is in contrast to the ferrocenyl amide $\mathbf{1^O}$ and thioamide $\mathbf{1^S}$, where the bound Cp rings of both ferrocenyl units are essentially co-planar with the (thio)amide bridges.[1,2,33] The trend of a shorter M-$C_{Carbene}$ bond in $\mathbf{1^{Cr}}$ compared to $(CO)_5Cr{=}C(Fc)(NH_2)$ is not present in the tungsten homologue. For chromium

Fischer carbene complexes the influence of the substituent on the carbene bond has been studied in detail by Solà et al. with 25 different complexes.[69] They used the Dewar-Chatt-Duncanson (DCD) model[70–72] in a DFT study to calculate the properties of chromium Fischer carbene complexes. For $(CO)_5Cr{=}C(X)R$ (X = OMe, OH, NHMe, NH_2, H) they found that stronger π electron donors lengthen the Cr-$C_{Carbene}$, shorten Cr-CO_{trans} and lengthen the C-O_{trans} bond distances while decreasing the chromium-carbene dissociation energies. The σ donation from the carbene carbon to the chromium is quite similar for all complexes studied, while the π back-donation from the chromium differs, making this the main influence of the geometrical and electronic parameters. For the same R the back-donation increases in the order H > OH > OMe > NH_2 > NHMe. The electrophilic character of the Fischer carbene complexes follow the same trend. The influence of the R group on the Cr-$C_{Carbene}$ bond is rather small comped to the change of the substituent X. The influence on the W-$C_{Carbene}$ bond by methylation of the amine group in **1^W** was investigated by DFT calculations. The DFT calculations of ***syn*-2^W** and ***anti*-2^W** show a lengthening of the carbene bond which could be assigned to the inductive effect of the methyl group increasing the electron density on the carbene carbon atom, weakening the π-backbonding from the tungsten atom to the carbene carbon atom.

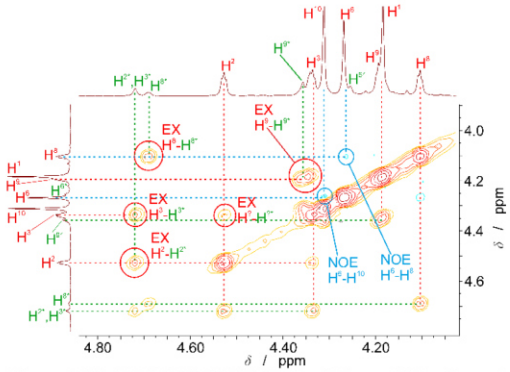

Figure 2. ^{1}H-^{1}H-NOESY / ^{1}H-^{1}H-EXSY of 6:1 ***syn*-2^W** (red):***anti*-2^W** (green) in CD_2Cl_2. NOE contacts marked in blue. Exchange signals of the isomers marked in red.

Similar to **1^{Cr}**[38] the tungsten homologue **1^W** shows two weak nonclassical NH···Fe intramolecular hydrogen bonds (IHB) in the solid state structure.[73–75] This was already suggested by the NMR and IR data of **1^W** reported before (10.5 ppm NH in the ^{1}H-NMR, 3439 cm^{-1} IR in CD_2Cl_2).[48] A five-membered ring with Fe1 [N1···Fe1: 3.655 Å, N1H···Fe1: 3.60 Å] and a four-membered ring with Fe2 [N1···Fe2: 3.070 Å, NH···Fe2: 3.15 Å] can be assigned. For **1^{Cr}** the corresponding distances are: Fe1 [N1···Fe1: 3.484(2) Å, N1H···Fe1: 3.13 Å] and Fe2 [N1···Fe2: 3.061(2) Å, NH···Fe2: 3.09 Å].[38] Compared to the ultra-strong NH···Fe IHB in diferrocenyl tosyl hydrazone[73] with NH···Fe: 2.67 Å the IHB in **1^W** is rather weak.

Both amino carbene complexes **1^{Cr}** and **1^W** undergo base induced follow up reaction to *trans*-1,2-diferrocenylimine. **1^W** also shows thermal reaction to the imine as investigated in detail with experimental and theoretical studies.[48] To prevent this side product, the nitrogen atom of **1^W** is alkylated. Deprotonation of **1^W** in tetrahydrofuran with potassium *tert*-butoxide (KO^{t}Bu) at low temperature and subsequent addition of iodomethane yields the methylated product in a 6:1 ratio of ***syn*/*anti*-2^W** (Scheme 2b) as analysis of the ^{1}H-NMR spectrum indicates (ESI Figure S02). Full methylation could be confirmed by the absence of the NH-signal at 10.5 ppm in the ^{1}H-NMR spectrum and appearance of the methyl protons at 4.27 ppm with the right integral ratio. Also, the NH band at 3271 cm^{-1} in the infrared spectrum is not visible after the methylation.

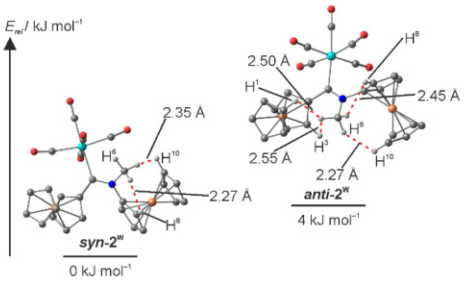

Figure 3. Possible NOE-contacts in ***syn*/*anti*-2^W** and DFT energies (B3LYP, LANL2DZ, IEF-PCM CH_2Cl_2).

The synthesis of **2^W** was also confirmed by mass spectrometry showing only the mono-cation **[2^W]$^{+}$** at *m/z* = 735.0 and the fragment **[2^W–CO]$^{+}$** at *m/z* = 706.0 (ESI Fig. S11). The carbene complex **2^W** is characterized by multinuclear and two-dimensional NMR techniques. All ^{1}H- and ^{13}C-NMR resonances of ***syn*-2^W** are assigned based on coupling patterns and NOE-contacts. Unfortunately, the resonances of C^5 and C^{12} of ***syn*-2^W** are out of the range of the measured ^{13}C-NMR spectrum. Literature values are **1^{Cr}** C^5 282.4 ppm, C^{12} 224.8 ppm[38] and **1^W** C^5 259.6 ppm, C^{12} 204.4 ppm[48]. ^{1}H-NMR resonances of ***anti*-2^W** are assigned based on exchange signals (Figure 2).

Assignment of the isomers was done by the number of possible NOE-contacts. As DFT-calculations (B3LYP, LANL2DZ, IEF-PCM CH_2Cl_2) indicate ***syn*-2^W** has two possible NOE-contacts from the methyl group to the cyclopentadienyl rings, namely $H^6\cdots H^8$ with 2.27 Å and $H^6\cdots H^{10}$ with 2.35 Å. In contrast the ***anti*-2^W** isomer has four possible NOE-contacts: $H^6\cdots H^8$ 2.45 Å, $H^6\cdots H^{10}$ 2.27 Å, $H^6\cdots H^1$ 2.50 Å, $H^6\cdots H^3$ 2.55 Å (Figure 3). The NOE-spectrum of ***syn*/*anti*-2^W** (Figure 2) shows two main NOE-contacts, suggesting the major isomer in this mixture is ***syn*-2^W**. Additionally, the spectrum shows the exchange between the two isomers as exchange peaks. This indicates that the 6:1 isomer ratio is of thermodynamically nature, according to an energy difference of 4.4 kJ mol^{-1}. The isomer ratio of ***syn*/*anti*-2^W** is also backed by the DFT calculations, which suggest that ***syn*-2^W** is 4 kJ mol^{-1} lower in energy than ***anti*-2^W** (Figure 3).

Electrochemical investigations show a significant difference between chromium and tungsten ferrocenyl Fischer carbenes in the first oxidation.[38,39,47,76–81] Ferrocenyl Fischer carbene

complexes containing chromium tend to follow up reactions upon oxidation while tungsten complexes show a reversible first oxidation with location of the spin density on the iron. The NH carbene complexes $\mathbf{1^{Cr}}$ and $\mathbf{1^{W}}$ show an irreversible first oxidation at 250 mV[38] and 260 mV[48] vs. FcH/FcH$^+$ respectively, followed by decomposition and follow up reactions. Methylation on the nitrogen atom tends to hinder these reactions as the cyclic voltammogram of $\mathbf{2^{W}}$ shows a quasi-reversible first oxidation at 170 mV (Figure 4). Increased electron density by the *+I*-effect of the methyl group lowers the potential for this oxidation. DFT calculations suggest that the NMeFc-moiety in $\mathbf{2^{W}}$ is oxidized at lower potential. Valence isomer *syn*-(CO)$_5$W=C(NMeFc$^+$)Fc is stabilized by 2 kJ mol^{-1} compared to the valence isomer *syn*-(CO)$_5$W=C(NMeFc)Fc$^+$, according to DFT calculations, which is isoenergetic on the accuracy of DFT calculations (Figure 5). Calculations for $\mathbf{[1^{W}]^{\cdot+}}$ show the same preference, with a difference of the valence tautomers in 3 kJ mol^{-1}. For $\mathbf{[1^{Cr}]^{\cdot+}}$ instead the valence isomer *anti*-(CO)$_5$Cr=C(NMeFc)Fc$^+$ is 3 kJ mol^{-1} lower in energy than *anti*-(CO)$_5$Cr=C(NMeFc$^+$)Fc.[38] All these energies are in the range of the precicion of DFT calculations and Bezuidenhout et al. showed that the calculated lower energy for one valence isomer of [(CO)$_5$Cr=C(OEt)Fc]$^{\cdot+}$ is highly dependent on the used basis set and functional.[77]

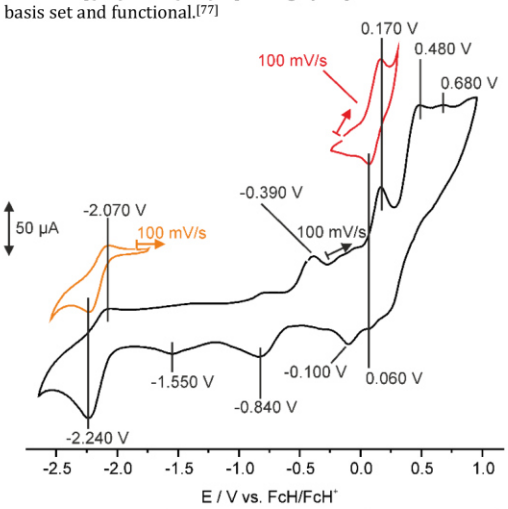

Figure 4. Cyclic voltammogram of 1 mM of $\mathbf{2^{W}}$ in THF with 100 mM [^{n}Bu$_4$N][BAr$^F_4$].

In the CO-region a distinct pattern is observed (Figure 6). Also, in CH_2Cl_2 solution this pattern is visible (ESI Fig. S09). The W(CO)$_5$ fragment has a pseudo C_{4v}-symmetry which should give three bands in total: two A_1 and one E vibration.[82] Lowering of the symmetry by the carbene fragment leads to five vibrational bands in total as confirmed by DFT calculations (scaling factor C = 1.03, $C = \sum(y_i \cdot w_i)/\sum w_i^2$, y_i = exp. frequency, w_i = calc. frequency)[83]: 2054 cm^{-1} (A_1), 1945 cm^{-1} (B_1), 1890 cm^{-1} (E), 1882 cm^{-1} (A_1), 1877 cm^{-1} (E). Overlapping of these bands gives the pattern visible in figure 6 with the peaks at: 2052 cm^{-1} (A_1), 1958 cm^{-1} (B_1) and 1908–1877 cm^{-1} (E, A_1). CO stretching vibrations of A_1 symmetry in M(CO)$_5$L complexes are a sensitive measure for the π-donor-/π-acceptor capability of the ligand L.[84] Substitution of an alkoxy carbene by an amino or thio carbene has a big difference in the A_1 vibration, while the effect of changing the substituents on an amino carbene itself has no significant influence as described in the literature.[84–87] Hence, the A_1 vibrations of all (CO)$_5$W=C(R)(NR'R'') carbene complexes are rather similar and $\mathbf{2^{W}}$ is no exemption.[41,43,51,77,84–88]

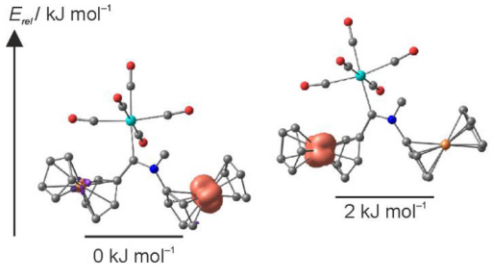

Figure 5. DFT optimized structure of the two valence tautomers **[*syn*-(CO)$_5$W=C(NMeFc$^+$)Fc]** (left) and **[*syn*-(CO)$_5$W=C(NMeFc)Fc$^+$]** (right) of $\mathbf{[\mathit{syn}\text{-}2^{W}]^+}$ with spin density at contour value 0.01 (B3LYP, LANL2DZ, IEF-PCM CH_2Cl_2).

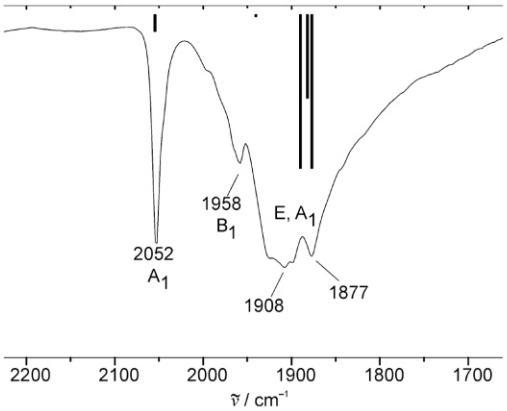

Figure 6. CO-region of the IR spectrum (KBr) of $\mathbf{2^{W}}$ and DFT-calculated vibrational spectrum (B3LYP, LANL2DZ, IEF-PCM CH_2Cl_2, scaling factor C = 1.03, $C = \sum(y_i \cdot w_i)/\sum w_i^2$, y_i = exp. frequency, w_i = calc. frequency)[83]

$\mathbf{2^{W}}$ can be chemically oxidized by 1 eq. of $AgSbF_6$ to $\mathbf{[2^{W}]^{\cdot+}}$ in CH_2Cl_2 solution while the change of the CO-bands is monitored by vibrational spectroscopy (ESI Fig. S10). A new band is rising at 1607 cm^{-1} while the intensity of the other peaks decreases and the maxima are shifting to higher wavenumbers: 2054→2062 cm^{-1}, 1958→1975 cm^{-1} and 1919→1927 cm^{-1}. In the DFT calculations the CO-bands also shift to higher wavenumbers: 2054→2057 cm^{-1} (A_1), 1945→1952 cm^{-1} (B_1), 1890→1905 cm^{-1} (E), 1882→1907 cm^{-1} (A_1), 1877→1884 cm^{-1} (E). The band at 1607 cm^{-1} is not reflected in the DFT calculations and might arise from a decomposition product that is not further characterized.

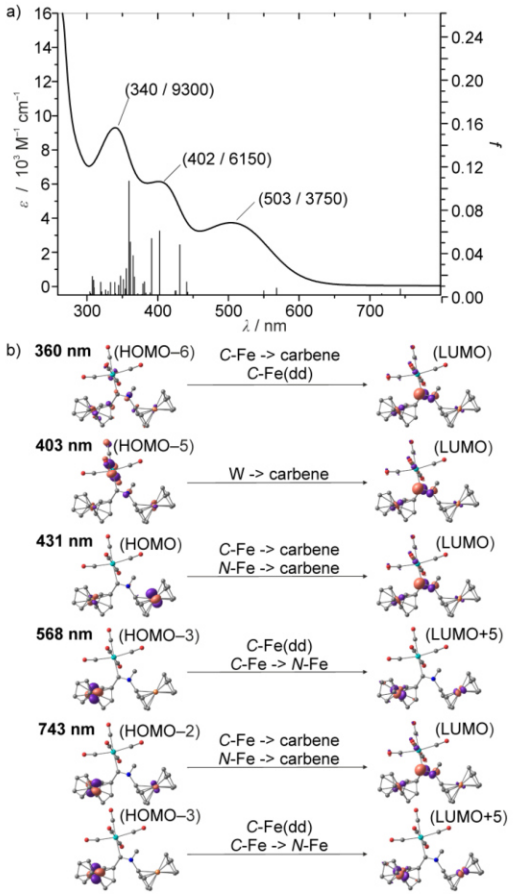

Figure 7. (a) UV-vis spectrum of $\mathbf{2^W}$ in DCM with TD-DFT calculated transitions and (b) major orbital contributions (isosurface value 0.08 a.u.) to the indicated transitions (B3LYP, LANL2DZ, IEF-PCM CH_2Cl_2).

The electronic spectrum of $\mathbf{2^W}$ in CH_2Cl_2 shows three prominent bands at λ_{max} = 340, 402 and 503 nm (Figure 7). The corresponding tungsten and chromium N-H carbene complexes show the following bands, $\mathbf{1^W}$: 290, 355, 387, 468 nm[48] and $\mathbf{1^{Cr}}$: 350, 392, 450 nm[38], while the characteristic ferrocene absorption bands of $\mathbf{1^O}$ and $\mathbf{1^S}$ are present at 445 and 470 nm, respectively.[1,33] Previous studies of Fischer carbene complexes show three absorptions, assigned to spin-allowed ligand-field (LF) bands around 300–350 nm and 350–450 nm as well as a spin-forbidden metal-to-ligand charge transfer (MLCT) band around 500 nm.[89,90] Time-dependent DFT calculations (B3LYP, LANL2DZ, IEF-PCM CH_2Cl_2) show the following main transitions in $\mathbf{2^W}$: MLCT from one iron centre (*C*-Fe) to the carbene ligand and *C*-Fe(dd) ligand field transition at 360 nm (HOMO–6→LUMO), MLCT from the tungsten centre to the carbene ligand at 403 nm (HOMO–5→LUMO) and MLCT from both iron centres to the carbene ligand at 431 nm (HOMO→LUMO). For the bands at lower energy the calculations show a *C*-Fe(dd) ligand field transition and a MM'CT from *C*-Fe to *N*-Fe at 568 nm (HOMO–3→LUMO+5). At 743 nm MLCT from both iron centres to the carbene ligand (HOMO–2→LUMO) and *C*-Fe(dd) ligand field transition and MM'CT from *C*-Fe to *N*-Fe at 568 nm (HOMO–3→LUMO+5) is predicted.

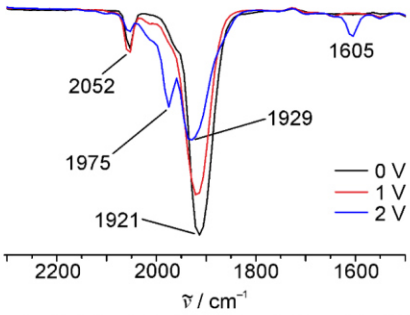

Figure 8. IR-SEC of 1 mM $\mathbf{2^W}$ in CH_2Cl_2 with 100 mM $[^nBu_4N][B(C_6F_5)_4]$, at 0 V, 1 V and 2 V.

Spectroelectrochemistry

To further study the electronic structure of $\mathbf{2^W}$ and the mono cation $\mathbf{[2^W]^{\cdot+}}$ spectroelectrochemical measurements with vibrational and optical spectroscopy were performed.

In the setting of the optically transparent thin-layer electrochemical cell (OTTLE-cell) the first reversible oxidation of 0.1 mM $\mathbf{2^W}$ in CH_2Cl_2 with 100 mM $[^nBu_4N][B(C_6F_5)_4]$ occurs at 0.8 V followed by an irreversible oxidation at 1.8 V. Therefore, the vibrational spectra were recorded from 0 V to 1 V and from 1 V to 2 V (Figure 8). In the series from 0 V to 1 V there is no significant shift in the CO-*A1* bands visible, indicating a first oxidation of the *N*-Fe site in accordance to the DFT calculations discussed above (Figure 5). When the voltage is increased to 2 V the CO-*A1* band at 1921 cm^{-1} is shifted to 1929 cm^{-1} and the CO-*B1* band is shifted from 1960 cm^{-1} to 1975 cm^{-1} in accordance to the spectrum of $\mathbf{2^W}$ after chemical oxidation (ESI Fig. S10). The CO-*A1* band at 2052 cm^{-1} is not shifted in contrast to the spectrum of $\mathbf{2^W}$ after chemical oxidation. An additional band at 1605 cm^{-1} is rising analogue to the vibrational spectrum of $\mathbf{2^W}$ after chemical oxidation discussed above (ESI Fig. S10).

In the optical spectrum of $\mathbf{2^W}$ with an applied voltage of 0.8 V for 50 min an IVCT band is rising at 831 nm as determined by Gaussian band shape analysis (Figure 9, Figure 10). The IVCT bands in $\mathbf{[1^O]^{\cdot+}}$ and $\mathbf{[1^S]^{\cdot+}}$ instead are located at lower energy with 1075 and 1150 nm.[33] TD-DFT calculations of $\mathbf{[2^W]^{\cdot+}}$ show a contribution of the carbene C π*-orbital in the IVCT (Figure 9) which could shift this transition to higher energy compared to the IVCT bands in $\mathbf{[1^O]^{\cdot+}}$ and $\mathbf{[1^S]^{\cdot+}}$. There are no isosbestic points observed suggesting reaction intermediates during the oxidation.

To calculate the electronic coupling parameter H_{AB}, the following equations were used: [36,37]

$$H_{AB} = 2.06 \cdot 10^{-2} (\tilde{\nu}_{max} \cdot \epsilon_{max} \cdot \Delta\tilde{\nu}_{0,5})^{0,5} \cdot r_{AB}^{-1} \quad \text{(Eq. 1)}$$

$$\Delta G_{ET}^{\neq} = \frac{\lambda}{4} + \frac{\Delta G^0}{2} + \frac{(\Delta G^0)^2}{(4(\lambda - 2H_{AB}))} - H_{AB} - \frac{{H_{AB}}^2}{(\lambda + \Delta G^0)} \quad \text{(Eq. 2)}$$

$$\lambda = E_{op} - \Delta G^0 \quad \text{(Eq. 3)}$$

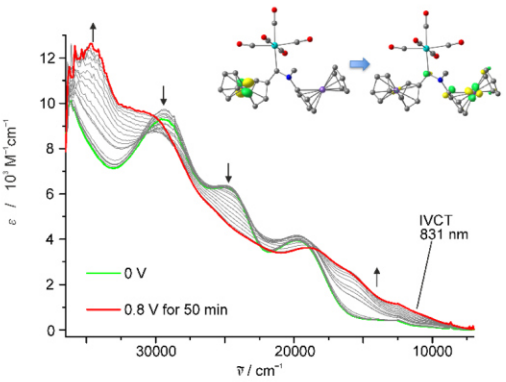

Figure 9. UV-SEC of 1 mM **2W** in CH_2Cl_2 with 100 mM [^{n}Bu$_4$N][B(C$_6$F$_5$)$_4$].

Gaussian band shape analysis of the UV-vis spectrum of **[2W]**$^{+}$ gives a maximum wavenumber of the IVCT at $\tilde{\nu}_{max}$ = 12050 cm^{-1}, a maximum extinction coefficient ε_{max} = 650 M^{-1} cm^{-1} and a full width at half maximum of $\Delta\tilde{\nu}_{0,5}$ = 4900 cm^{-1} (Figure 10). The Fe···Fe distance r_{AB} = 6.85 Å and the difference in energy of the two valence isomers ΔG^0 = 2 kJ mol^{-1} are estimated by DFT-calculations. This gives an electronic coupling of H_{AB} = 593 ± 10 cm^{-1} which assigns **[2W]**$^{+}$ to class II in the Robin-Day classification (Figure 11).[36,37] The corresponding electronic couplings in the amide **[1O]**$^{+}$ and the thioamide **[1S]**$^{+}$ are H_{AB} = 200 ± 10 and 190 ± 10 cm^{-1}, respectively.[33] The electronic coupling in the amide and thioamide are quite similar, which gives the conclusion that the electron transfer happens through space and not over the (thio)amide bridge.[33] The Fe···Fe distances estimated by DFT-Calculations for **[1O]**$^{+}$ and **[1S]**$^{+}$ are 7.20 and 7.18 Å respectively. For carbene complex **[2W]**$^{+}$ the Fe···Fe distance is significantly shorter with 6.85 Å. This could be one reason for the stronger electronic coupling. But also if 7.20 Å is used in the calculation an electronic coupling H_{AB} of 560 cm^{-1} is obtained, which is not that much smaller than in **[2W]**$^{+}$. Therefore the location of the IVCT in **[1O]**$^{+}$ at 1075 nm is not only dependent on the distance of the two iron centres, but also the role of the bridge has to be considered. In **[1O]**$^{+}$ and **[1S]**$^{+}$ $2 \cdot H_{AB}$ is significantly smaller (5 kJ mol^{-1}, 4 kJ mol^{-1}), while ΔG^0 is bigger (40 kJ mol^{-1}, 30 kJ mol^{-1}). It must be clarified, that ΔG^0 for **[2W]**$^{+}$ was estimated by DTF calculations, while for **[1O]**$^{+}$ and **[1S]**$^{+}$ it has been measured in the cyclic voltammogram by the splitting of the two reversible oxidation waves.[33] This could result in different outcomes.

The energy of the optical transition of the IVCT is calculated from the maximum wavenumber of the IVCT $\tilde{\nu}_{max}$ and gives E_{op} = 144 kJ mol^{-1}. With this, the activation barrier for the thermal electron transfer can be calculated to $\Delta G_{ET}^{\neq}$ = 29 mol^{-1}. The activation barriers for **[1O]**$^{+}$ and **[1S]**$^{+}$ are higher with 42 and 35 kJ mol^{-1}, respectively. An overview of all calculated electronic couplings H_{AB}, estimated metal to metal distances r_{AB}, difference in energy of the two valence isomers ΔG^0 and activation barrier for the thermal electron transfer $\Delta G_{ET}^{\neq}$ can be found in table 1. ΔG^0 for **[1O]**$^{+}$ and **[1S]**$^{+}$ was calculated from the distance of the two reversible oxidation waves in the cyclic voltammogram.[33]

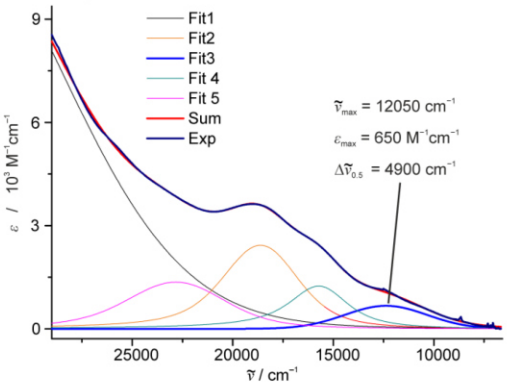

Figure 10. Gaussian band shape analysis of UV-vis spectrum of 1 mM **2W** electrochemically oxidized to **[2W]**$^{+}$ in CH_2Cl_2 with 100 mM [^{n}Bu$_4$N][B(C$_6$F$_5$)$_4$].

Table 1: Values for the electronic coupling in **[2W]**$^{+}$, **[1O]**$^{+}$[33] and **[1S]**$^{+}$[33]

	[2W]$^{+}$	**[1O]**$^{+}$ [33]	**[1S]**$^{+}$ [33]
H_{AB} / cm^{-1}	593	200	190
r_{AB} / Å	6.85 (DFT)	7.20 (DFT)	7.18 (DFT)
ΔG^0 / $kJ\ mol^{-1}$	2 (DFT)	40 (CV)	30 (CV)
$\Delta G_{ET}^{\neq}$ / $kJ\ mol^{-1}$	29	42	35

The properties of the bridge connecting the two ferrocenyl sites in **[1O]**$^{+}$ and **[1S]**$^{+}$ are quite similar, while in **[2W]**$^{+}$ it is different. In C=O and C=S the electronegativity is higher at the heteroatom while in C=W(CO)$_5$ the electronegativity is higher at the carbon atom. ΔG^0 in **[2W]**$^{+}$ is one order of magnitude smaller than in **[1O]**$^{+}$ and **[1S]**$^{+}$. The energetic location of the C=X-π^*-molecular orbital for C=M is much lower than for C=O or C=S. This could facilitate intramolecular electron hopping in **[2W]**$^{+}$ via the bridge and not though space.[32]

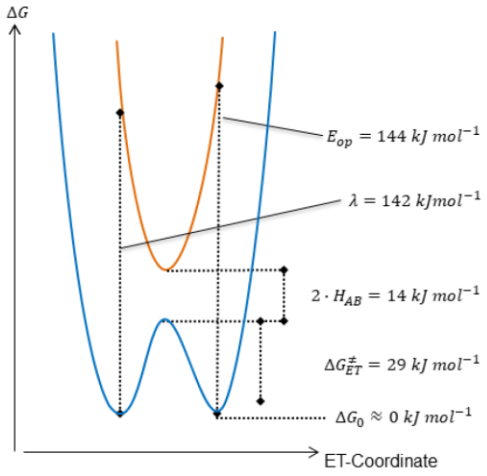

Figure 11. Visualisation of E_{op}, λ, H_{AB}, $\Delta G_{ET}^{\neq}$ and ΔG^0 of **[2W]**$^{\cdot+}$.

CONCLUSION

The pentacarbonyl tungsten carbene complex **1W** can be seen as an isolobal analogue to the amide **1O** and the thioamide **1S**. The metrics obtained from the single crystal structure of **1W** are similar to the lighter homologue **1Cr**. The amino group in the carbene complex **1W** undergoes further side reaction after oxidation, therefore the methylated complex **2W** is preferable for investigation of the electronic properties and the communication of the iron centres in the mixed valent mono cation **[2W]**$^{\cdot+}$. The methylated carbene complex is obtained as a dynamic 6:1 mixture of ***syn*/*anti*-2W**. NMR resonances are assigned by one- and two-dimensional techniques. The cyclic voltammogram of **2W** shows one reversible oxidation at $E_{1/2}$ = 115 mV. Spectroelectrochemical optical measurements give an electronic coupling of H_{AB} = 593 ± 10 cm^{-1} which assigns **[2W]**$^{\cdot+}$ to class II of the Robin-Day classification. Compared with the amide **[1O]**$^{\cdot+}$ and the thioamide **[1S]**$^{\cdot+}$, the electronic coupling in **[2W]**$^{\cdot+}$ is three times stronger which could result in part from the shorter Fe···Fe distance, but also in the electronic properties of the carbene bridge has to play a role to justify this big difference. The activation barrier for the thermal electron transfer $\Delta G_{ET}^{\neq}$ of the carbene complex **2W**, the amide and the thioamide are in the same range with 29, 42 and 35 kJ mol^{-1}. In **[1O]**$^{\cdot+}$ and **[1S]**$^{\cdot+}$ the properties of the bridge are similar, with higher electronegativity at the heteroatom, while in **[2W]**$^{\cdot+}$ the electronegativity of the carbene carbon atom is higher than the electronegativity of the tungsten atom. Considering the C=X-π^*-molecular orbital in the bridge, for C=M the energetic location is much lower than for C=O or C=S. This could open the possibility for an electron transfer in **[2W]**$^{\cdot+}$ over the bridge and not though space.

EXPERIMENTAL SECTION

General Procedures: All reactions were performed under argon atmosphere unless otherwise noted. A glovebox of the type *UniLab/MBraun* (Ar 4.8, O_2 < 1 ppm, H_2O < 1 ppm) was used for storage and weighing of sensitive compounds. All samples that required the absence of oxygen were prepared in the same glovebox. Dichloromethane was dried with CaH_2 and distilled prior to use. THF, was distilled from potassium. All reagents were used as received from commercial suppliers (ABCR, Acros Organics, Alfa Aesar, Fischer Scientific, Fluka and Sigma-Aldrich). Deuterated solvents were purchased from euriso-top. **3OEt**[40,41,51,52], aminoferrocene[53,54] and **1W**[48] were synthesized using literature procedures.

NMR spectra were recorded on a *Bruker Avance DRX 400* spectrometer at 400.31 MHz (^{1}H) and 100.07 MHz (^{13}C{^{1}H}). All resonances are reported in ppm vs. the solvent signal as internal standard. CD_2Cl_2 (^{1}H: δ = 5.32 ppm; ^{13}C: δ = 54.0 ppm).[91]

IR spectra were recorded with a *Varian 3100 FT-IR Excalibur Series* spectrometer. Solid state measurements were carried out with the sample as KBr pellet. Dissolved samples were investigated in a liquid cell with *Specac omni-cell* KBr windows.

UV/Vis/NIR spectra were recorded on a *Varian Cary 5000* spectrometer by using 1.00 cm cells (*Hellma, suprasil*).

Electrochemical experiments were carried out on a *BioLogic SP-50* voltammetric analyser using platinum wires as counter and working electrodes and a 0.01 M $Ag/AgNO_3$ electrode as reference electrode. The cyclic voltammetry measurements were carried out at scan rate of 100 mV s^{-1} using 0.1 M [nBu$_4$N][B(C$_6$F$_5$)$_4$][92] as supporting electrolyte in THF. Potentials are referenced to the decamethylcobaltocene/decamethylcobaltocenium couple (Cc*CH$_3$/Cc*CH$_3^+$) (E½ = −1940 ± 5 mV under the experimental conditions in THF compared to literature: E½ = −1940 mV (CH_2Cl_2), −1910 mV (MeCN)[93]).

FD mass spectra were recorded with a *FD Finnigan MAT90* spectrometer.

Spectroelectrochemical measurements were carried out using a optically transparent thin-layer electrochemical cell (OTTLE-cell)[94] by *Specac omni-cell* with CaF_2 windows equipped with a Pt-gauze working electrode, a Pt-gauze counter electrode and an Ag wire as pseudo-reference electrode, melt-sealed in a polyethylene spacer (approx. path length 0.5 mm) in CH_2Cl_2 with 0.1 M [^{n}Bu$_4$N][B(C$_6$F$_5$)$_4$] as supporting electrolyte.[92]

Density functional theory calculations were executed with the *Gaussian09/DFT*[95] series of programs. *B3LYP*[96] formulation of DFT and the *LanL2DZ*[97–100] basis set were used. For solvent modelling *IEF-PCM*[101,102] in CH_2Cl_2 was applied. No symmetry constrains were imposed in the initial molecule structure. The final structures were assigned to the minimum by numerical frequency analysis (N_{imag} = 0 respectively).

Crystal Structure Determination: Intensity data were collected with a *Bruker AXS Smart 1000 CCD* diffractometer with an *APEX II* detector and an Oxford cooling system and corrected for absorption and other effects using Mo K_α radiation (λ = 0.71073 Å) at 173(2) K. The diffraction frames were integrated using the SAINT package, and most were corrected for absorption with MULABS.[103,104] The structure was solved by direct methods and refined by the full-matrix method based on F^2 using the SHELXTL software package.[105–108] All non-hydrogen atoms were refined anisotropically, while the positions of carbon bonded hydrogen atoms were generated with appropriate geometric constraints and allowed to ride on their respective parent atoms with fixed isotropic thermal parameters. See Supporting Information for crystal data of **1W**. CCDC-XXXXXXX contains the supplementary crystallographic data for this paper. These data can be obtained

free of charge from The Cambridge Crystallographic Data Centre via www.ccdc.cam.ac.uk/data_request/cif.

Preparation: *syn/anti*-(*N*-Methylaminoferrocenyl) (ferrocenyl) carbene (pentacarbonyl) tungsten (0) **(2^{W})**: **1^{W}** (100 mg, 0.139 mmol, 1 eq) and KO^{t}Bu (47 mg, 0.417 mmol, 3 eq) were stirred at 0 °C in THF (20 mL) for 10 min. MeI (90 µL, 1.39 mmol, 10 eq) was added and stirred for 10 min at 0 °C. Stirring at room temperature for 4 h and removal of the solvent under reduced pressure yielded 111.4 mg of a dark red solid. NMR indicated a 6:1 ratio ***syn*/*anti*-2^{W}**.

^{1}H NMR (CD_2Cl_2): ***syn*-2^{W}**: δ = 4.53 (pt, 2 H, H^2), 4.34 (pt, 2 H, H^3), 4.31 (s, 5 H, H^{10}), 4,27 (s, 3 H, Me, H^6), 4.19 (pt, 2 H, H^9), 4.18 (s, 5 H, H^1), 4.10 (pt, 2 H, H^8) ppm. ***anti*-2^{W}**: δ = 4.72 (pt, 4 H, H^2, H^3), 4.69 (pt, 2 H, H^8), 4.36 (2 H, H^9), 4.34 (5 H, Cp), 4.25 (s, 3 H^6, Me), 4.22 (pt, 2 H, C_5H_4), 4.13 (pt, 2 H, C_5H_4) ppm. **^{13}C NMR** (CD_2Cl_2): δ = 201.12 (C^{11}), 108.11 (C^7), 97.24 (C^4), 76.61 (C^3), 73.18 (C^2), 71.83 (C^1), 70.32 (C^{10}), 66.79 (C^9), 65.69 (C^8), 58.17 (C^6) ppm (C^5 and C^{12} out of range). **MS (FD):** *m/z* (int. / %) = 735.0 (M^+, 100), 706.0 (M^+ - – CO). Calcd. for $C_{27}H_{21}Fe_2NO_5W$ (734.96).**IR (KBr):** $\tilde{\nu}$ = 3098 (w, CH), 2052 (vs, CO, A_1), 1958 (m, CO, B_1), 1908–1877 (br., CO, *E*, A_1) cm^{-1}. **IR (CH_2Cl_2):** $\tilde{\nu}$ = 2054 (vs, CO, A_1), 1958 (m, CO, B_1), 1919 (br., CO, *E*, A_1) cm^{-1}. **UV/vis (CH_2Cl_2):** λ_{max} (ε) = 340 (9300 M^{-1} cm^{-1}), 402 (6150 M^{-1} cm^{-1}), 502 (3750 M^{-1} cm^{-1}) nm. **CV** (THF, vs FcH/FcH$^+$): $E_{1/2}$ = –2325, 115 mV, E_{ox} = –390, 480, 680 mV, $E_{red.}$ = –100, –840, –1550 mV. Anal. Calcd for $C_{27}H_{21}Fe_2NO_5W$ (734,96)+$W(CO)_6$: C, 36.47; H, 1.95; N, 1,29. Found: C, 33.23; H, 1.83; N, 1,46.

ASSOCIATED CONTENTS

Supporting Information

The Supporting Information is available free of charge on the ACS Publications website and contains NMR, IR, mass spectra, crystal structure data and Cartesian coordinates of DFT optimized structures. CIF Files for **1^{W}** have been deposited at the Cambridge Crystallographic Data Centre and were allocated the deposition numbers CCDC-XXXXXXX.

AUTHOR INFORMATION

Corresponding Authors

* Dr. C. Förster, Prof. Dr. K. Heinze
Fax +49 6131 39-27277
E-Mail: cfoerster@uni-mainz.de, katja.heinze@uni-mainz.de

Notes

The authors declare no competing financial interest.

ACKNOWLEDGMENT

We thank Regine Jung-Pothmann and Dr. Dieter Schollmeyer for collection of the diffraction data, Dr. Mihail Mondeshki for help with the NMR experiments and the Johannes Gutenberg University of Mainz (Germany) for financial support to C. F. (Internal University Research Funding).

REFERENCES

[1] K. Heinze, D. Siebler, *Z. Anorg. Allg. Chem.* **2007**, *633*, 2223–2233.
[2] D. Siebler, M. Linseis, T. Gasi, L. M. Carrella, R. F. Winter, C. Förster, K. Heinze, *Chem. Eur. J.* **2011**, *17*, 4540–4551.
[3] K. A. Mahmoud, H.-B. Kraatz, *J Inorg Organomet Polym* **2006**, *16*, 201–210.
[4] S. F. Ekti, D. Hür, *Inorg. Chem. Commun.* **2008**, *11*, 1027–1029.
[5] D. P. Cormode, A. J. Evans, J. J. Davis, P. D. Beer, *Dalton Trans.* **2010**, *39*, 6532–6541.
[6] J. Ni, K.-J. Wei, Y.-W. Chen, Y. Liu, *J. Mol. Struct.* **2012**, *1011*, 76–80.
[7] K. Heinze, K. Hüttinger, D. Siebler, *Modeling of Molecular Properties (Ed. P. Comba), Wiley-VCH,* **2011**, 325–346.
[8] R. Trivedi, S. B. Deepthi, L. Giribabu, B. Sridhar, P. Sujitha, C. Ganesh Kumar, K. V. S. Ramakrishna, *Appl. Organomet. Chem.* **2012**, *26*, 369–376.
[9] P. O. Shipman, M. A. Lafreniere, C. D.S. Colquhoun, H.-B. Kraatz, *Inorg. Chim. Acta* **2012**, *391*, 195–200.
[10] M. Sarkar, P. Daw, T. Ghatak, J. K. Bera, *Chemistry* **2014**, *20*, 16537–16549.
[11] K. Heinze, M. Schlenker, *Eur. J. Inorg. Chem.* **2005**, 66–71.
[12] J. Lapić, D. Siebler, K. Heinze, V. Rapić, *Eur. J. Inorg. Chem.* **2007**, 2014–2024.
[13] V. Kovač, K. Radolović, I. Habuš, D. Siebler, K. Heinze, V. Rapić, *Eur. J. Inorg. Chem.* **2009**, 389–399.
[14] D. Siebler, C. Förster, T. Gasi, K. Heinze, *Organometallics* **2011**, *30*, 313–327.
[15] D. Siebler, C. Förster, K. Heinze, *Eur. J. Inorg. Chem.* **2010**, 3986–3992.
[16] M. Č. Semenčić, K. Heinze, C. Förster, V. Rapić, *Eur. J. Inorg. Chem.* **2010**, *2010*, 1089–1097.
[17] J. Lapić, S. Djaković, M. Cetina, K. Heinze, V. Rapić, *Eur. J. Inorg. Chem.* **2010**, *2010*, 106–114.
[18] H. Huesmann, C. Förster, D. Siebler, T. Gasi, K. Heinze, *Organometallics* **2012**, *31*, 413–427.
[19] A. Neidlinger, V. Ksenofontov, K. Heinze, *Organometallics* **2013**, *32*, 5955–5965.
[20] M. Lauck, C. Förster, K. Heinze, *Organometallics* **2017**, *36*, 4968–4978.
[21] Q.-Y. Cao, P.-S. Yao, X.-F. Zhao, J.-H. Liu, Z.-W. Wang, *Inorg. Chim. Acta* **2014**, *419*, 147–151.
[22] K. Heinze, M. Beckmann, *Eur. J. Inorg. Chem.* **2005**, 3450–3457.
[23] M. Č. Semenčić, D. Siebler, K. Heinze, V. Rapić, *Organometallics* **2009**, *28*, 2028–2037.
[24] K. Hanauer, M. T. Pham, C. Förster, K. Heinze, *Eur. J. Inorg. Chem.* **2017**, *2017*, 433–445.
[25] A. Neidlinger, C. Förster, K. Heinze, *Eur. J. Org. Chem.* **2016**, 4852–4864.
[26] D. Siebler, K. Heinze, *J. Organomet. Chem.* **2016**, *821*, 19–24.
[27] A. Neidlinger, C. Förster, K. Heinze, *Eur. J. Inorg. Chem.* **2016**, 1274–1286.
[28] A. S. Hazari, A. Indra, G. K. Lahiri, *RSC Adv.* **2018**, *8*, 28895–28908.
[29] K. Mahmoud, Y.-T. Long, G. Schatte, H.-B. Kraatz **2004**; Journal of Organometallic Chemistry, 689(13), 2250-2255.
[30] N. Ma, J. Gong, J. Zhang, S. Han, M. Song, G. Zhang **2018**; The Journal of Physical Chemistry C, 122(12), 6818-6825.
[31] S. W. Lehrich, A. Hildebrandt, T. Rüffer, M. Korb, P. J. Low, H. Lang, *Organometallics* **2014**, *33*, 4836–4845.
[32] S. P. Harmalker, M. T. Pope, *J. Am. Chem. Soc.* **1981**, *103*, 7381–7383.
[33] T. Kienz, C. Förster, K. Heinze, *Organometallics* **2014**, *33*, 4803–4812.
[34] R. A. Marcus, *J. Chem. Phys.* **1956**, *24*, 966–978.
[35] R. A. Marcus, *Angew. Chem. Int. Ed.* **1993**, *32*, 1111–1121; *Angew. Chem.*, **1993**, *105*, 1161–1172.

[36] M. B. Robin, P. Day, *Adv. Inorg. Chem. Radiochem.* **1968**, *10*, 247–422.
[37] B. S. Brunschwig, N. Sutin, *Coord. Chem. Rev.* **1999**, *187*, 233–254.
[38] P. Veit, C. Förster, S. Seibert, K. Heinze, *Z. Anorg. Allg. Chem.* **2015**, *641*, 2083–2092.
[39] B. van der Westhuizen, J. M. Speck, M. Korb, J. Friedrich, D. I. Bezuidenhout, H. Lang, *Inorg. Chem.* **2013**, *52*, 14253–14263.
[40] D. I. Bezuidenhout, W. Barnard, B. van der Westhuizen, E. van der Watt, D. C. Liles, *Dalton Trans.* **2011**, *40*, 6711–6721.
[41] J. G. López-Cortés, Contreras de la Cruz, Luis F., M. C. Ortega-Alfaro, R. A. Toscano, C. Alvarez-Toledano, H. Rudler, *J. Organomet. Chem.* **2005**, *690*, 2229–2237.
[42] M. E. Sánchez-Vergara, A. Ortiz, C. Álvarez-Toledano, A. Moreno, J. R. Alvarez, *Thin Solid Films* **2008**, *516*, 6382–6387.
[43] C. Sandoval-Chávez, J. G. López-Cortés, A. I. Gutiérrez-Hernández, M. C. Ortega-Alfaro, A. Toscano, C. Alvarez-Toledano, *J. Organomet. Chem.* **2009**, *694*, 3692–3700.
[44] R. Schobert, R. Kempe, T. Schmalz, A. Gmeiner, *J. Organomet. Chem.* **2006**, *691*, 859–868.
[45] L. Meca, D. Dvořák, J. Ludvík, I. Císařová, P. Štěpnička, *Organometallics* **2004**, *23*, 2541–2551.
[46] H. Helten, M. Beckmann, G. Schnakenburg, R. Streubel, *Eur. J. Inorg. Chem.* **2010**, 2337–2341.
[47] B. van der Westhuizen, J. Matthäus Speck, M. Korb, D. I. Bezuidenhout, H. Lang, *J. Organomet. Chem.* **2014**, *772-773*, 18–26.
[48] P. Veit, C. Förster, K. Heinze, *Beilstein J. Org. Chem.* **2016**, *12*, 1322–1333.
[49] P. Veit, S. Seibert, C. Förster, K. Heinze, *Z. Anorg. Allg. Chem.* **2020**.
[50] J. A. Connor, E. M. Jones, J. P. Lloyd, *J. Organomet. Chem.* **1970**, *24*, C20-C22.
[51] J. A. Connor, J. P. Lloyd, *J. Chem. Soc., Dalton Trans.* **1972**, 1470–1476.
[52] G. A. Mose, E. O. Fischer, M. D. Rausch, *J. Organomet. Chem.* **1971**, *27*, 379–382.
[53] B. Bildstein, M. Malaun, H. Kopacka, K. Wurst, M. Mitterböck, K.-H. Ongania, G. Opromolla, P. Zanello, *Organometallics* **1999**, *18*, 4325–4336.
[54] K. Heinze, M. Schlenker, *Eur. J. Inorg. Chem.* **2004**, 2974–2988.
[55] L. M. Slaughter, *ACS Catal.* **2012**, *2*, 1802–1816.
[56] J. Miller, A. L. Balch, J. H. Enemark, *J. Am. Chem. Soc.* **1971**, *93*, 4613–4614.
[57] G. B. Kauffman, *Naturwissenschaften* **1976**, *63*, 324–327.
[58] G. S. Hammond, R. C. Neuman, *J. Phys. Chem.* **1963**, *67*, 1655–1659.
[59] R. C. Neuman, G. S. Hammond, *J. Phys. Chem.* **1963**, *67*, 1659–1665.
[60] J. O. C. Jimenez-Halla, M. Solà, *Chemistry* **2009**, *15*, 12503–12520.
[61] C. G. Kreiter, E. O. Fischer, *Angew. Chem. Int. Ed.* **1969**, *8*, 761–762; *Angew. Chem.*, **1969**, *81*, 780–781.
[62] CCDC search (date: March 08, 2020) for W(CO)5L complexes with one Cr–C–O angle: 160–173°: 110 entries, e.g. CCDC no.: 949876, 611352, 959023, 819866, 105481, 1282934.
[63] CCDC search (date: March 06, 2020) for (ferrocenyl)(R)carbene(pentacarbonyl)tungsten(0) complexes: CCDC no.: 225471, 225470, 949875, 949876, 949877, 949878, 262966, 1133084, 969407, 969408, 278099, 904592, 810999, 729450, 697107, 769319, 766006, 252452.
[64] I. R. Butler, W. R. Cullen, F. W. B. Einstein, A. C. Willis, *Organometallics* **1985**, *4*, 603–604.
[65] P. Le Poul, B. Caro, N. Cabon, F. Robin-Le Guen, S. Golhen, *J. Organomet. Chem.* **2013**, *745-746*, 57–63.
[66] R. Streubel, M. Beckmann, C. Neumann, S. Fankel, H. Helten, O. Feier-Iova, P. G. Jones, M. Nieger, *Eur. J. Inorg. Chem.* **2009**, 2090–2095.
[67] J. G. López-Cortés, A. Samano-Galindo, M. C. Ortega-Alfaro, A. Toscano, H. Rudler, A. Parlier, C. Alvarez-Toledano, *J. Organomet. Chem.* **2005**, *690*, 3664–3668.
[68] B. Cordero, V. Gómez, A. E. Platero-Prats, M. Revés, J. Echeverría, E. Cremades, F. Barragán, S. Alvarez, *Dalton Trans.* **2008**, 2832–2838.
[69] M. Cases, G. Frenking, M. Duran, M. Solà, *Organometallics* **2002**, *21*, 4182–4191.
[70] M. J. S. Dewar, *Bull. Soc. Chim. Fr.* **1951**, C79.
[71] J. Chatt, L. A. Duncanson, *J. Chem. Soc.* **1953**, 2939.
[72] J. Chatt, L. A. Duncanson, L. M. Venanzi, *J. Chem. Soc.* **1955**, 4456.
[73] C. Förster, P. Veit, V. Ksenofontov, K. Heinze, *Chem. Commun.* **2015**, *51*, 1514–1516.
[74] L. Brammer, *Dalton Trans.* **2003**, 3145–3157.
[75] D. Braga, F. Grepioni, E. Tedesco, K. Biradha, G. R. Desiraju, *Organometallics* **1997**, *16*, 1846–1856.
[76] D. I. Bezuidenhout, I. Fernández, B. van der Westhuizen, P. J. Swarts, J. C. Swarts, *Organometallics* **2013**, *32*, 7334–7344.
[77] D. I. Bezuidenhout, B. van der Westhuizen, I. Strydom, P. J. Swarts, J. C. Swarts, I. Fernández, *Inorg. Chim. Acta* **2014**, *423*, 184–192.
[78] M. K. Lloyd, J. A. McCleverty, D. G. Orchard, J. A. Connor, M. B. Hall, I. H. Hillier, E. M. Jones, G. K. McEwen, *J. Chem. Soc., Dalton Trans.* **1973**, 1743–1747.
[79] B. van der Westhuizen, P. J. Swarts, I. Strydom, D. C. Liles, I. Fernández, J. C. Swarts, D. I. Bezuidenhout, *Dalton Trans.* **2013**, *42*, 5367–5378.
[80] B. van der Westhuizen, P. J. Swarts, van Jaarsveld, Louise M, D. C. Liles, U. Siegert, J. C. Swarts, I. Fernández, D. I. Bezuidenhout, *Inorg. Chem.* **2013**, *52*, 6674–6684.
[81] D. I. Bezuidenhout, B. van der Westhuizen, P. J. Swarts, T. Chatturgoon, O. Q. Munro, I. Fernández, J. C. Swarts, *Chem. Eur. J.* **2014**, *20*, 4974–4985.
[82] C. Elschenbroich, *Organometallchemie,* 6. Aufl., B. G. Teubner, Wiesbaden, **2008**.
[83] A. P. Scott, L. Radom, *J. Phys. Chem.* **1996**, *100*, 16502–16513.
[84] E. O. Fischer, M. Leupold, *Chem. Ber.* **1972**, *105*, 599–608.
[85] U. Klabunde, E. O. Fischer, *J. Am. Chem. Soc.* **1967**, *89*, 7141–7142.
[86] J. A. Connor, E. O. Fischer, *J. Chem. Soc. A* **1969**, 578–584.
[87] E. O. Fischer, B. Heckl, H. Werner, *J. Organomet. Chem.* **1971**, *28*, 359–365.
[88] A. I. Gutiérrez-Hernández, J. G. López-Cortés, M. C. Ortega-Alfaro, M. T. Ramírez-Apan, J. d. J. Cázares-Marinero, R. A. Toscano, *J. Med. Chem.* **2012**, *55*, 4652–4663.
[89] L. S. Hegedus, *Tetrahedron* **1997**, *53*, 4105–4128.
[90] M. L. Lage, I. Fernández, M. J. Mancheño, M. A. Sierra, *Inorg. Chem.* **2008**, *47*, 5253–5258.
[91] G. R. Fulmer, A. J. M. Miller, N. H. Sherden, H. E. Gottlieb, A. Nudelman, B. M. Stoltz, J. E. Bercaw, K. I. Goldberg, *Organometallics* **2010**, *29*, 2176–2179.
[92] R. J. LeSuer, C. Buttolph, W. E. Geiger, *Anal. Chem.* **2004**, *76*, 6395–6401.
[93] N. G. Connelly, W. E. Geiger, *Chem. Rev.* **1996**, *96*, 877–910.

[94] M. Krejčik, M. Daněk, F. Hartl, *J. Electroanal. Chem.* **1991**, *317*, 179–187.
[95] M. J. Frisch, G. W. Trucks, H. B. Schlegel, G. E. Scuseria, M. A. Robb, J. R. Cheeseman, G. Scalmani, V. Barone, B. Mennucci, G. A. Petersson et al., *gaussian09, Revision A.02, Gaussian, Inc., Wallingford CT* **2009**.
[96] A. D. Becke, *J. Chem. Phys.* **1993**, *98*, 5648–5652.
[97] C. E. Dykstra, *Chem. Phys. Lett.* **1977**, *45*, 466–469.
[98] P. J. Hay, W. R. Wadt, *J. Chem. Phys.* **1985**, *82*, 270.
[99] P. J. Hay, W. R. Wadt, *J. Chem. Phys.* **1985**, *82*, 299.
[100] W. R. Wadt, P. J. Hay, *J. Chem. Phys.* **1985**, *82*, 284.
[101] S. Miertuš, E. Scrocco, J. Tomasi, *Chem. Phys.* **1981**, *55*, 117–129.
[102] V. Barone, M. Cossi, *J. Phys. Chem. A* **1998**, *102*, 1995–2001.
[103] SMART Data Collection and SAINT-Plus Data Processing Software for the SMART System, *Bruker Analytical X-Ray Instruments, Inc.: Madison, WI* **2000**.
[104] R. H. Blessing, *Acta Cryst. A* **1995**, *51*, 33–38.
[105] G. M. Sheldrick, *SHELXTL, Version 5.1, Bruker AXS, Madison* **1998**.
[106] C. B. Hübschle, G. M. Sheldrick, B. Dittrich, *J. Appl. Crystallogr.* **2011**, *44*, 1281–1284.
[107] G. M. Sheldrick, *SHELXL-97, University of Göttingen* **1997**.
[108] G. M. Sheldrick, *Acta Cryst. A* **2008**, *64*, 112–122.

4 Summary and Outlook

In this work nonclassical intramolecular hydrogen bonds to ferrocenyl and ruthenocenyl groups are reported (Scheme 4.1, Section 3.1). The NH···Ru IHB to diruthenocenyl tosyl hydrazone **169** is 6 kJ mol^{-1} stronger than the NH···Fe IHB in diferrocenyl tosyl hydrazone **168** as confirmed by IR spectroscopy. In the synthesis of the mixed metal ferrocenyl ruthenocenyl tosyl hydrazone the NH···Ru IHB **170a** is preferred with a ratio of 10:1. Thermal and photochemical approaches lead to E → Z isomerization and conversion of the NH···Fe IHB **170b** to the preferred NH···Ru IHB **170a**. (Scheme 4.1)

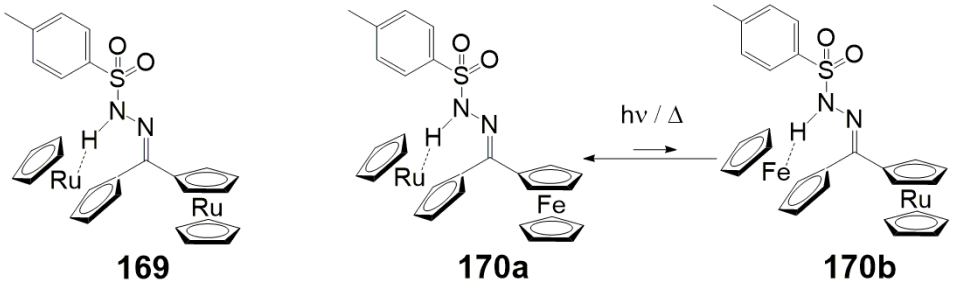

Scheme 4.1: NH···M IHB in tosyl hydrazones reported in this work.

The synthesis and characterization of ferrocenyl aminoferrocenyl Fischer carbene complexes of chromium **171** (Section 3.2) and tungsten **172** (Section 3.3 and 3.6) are reported (Scheme 4.2). They can be seen as the isolobal metal pentacarbonyl analogue of diferrocenyl amide and thioamide. Follow-up reactions of ferrocenyl aminoferrocenyl carbene pentacarbonyl metal complexes to diferrocenyl imine **173** hinder their use as ligands in redox switchable catalysis. Therefore, the nature of the side reaction to the imine was studied in detail (Section 3.3).

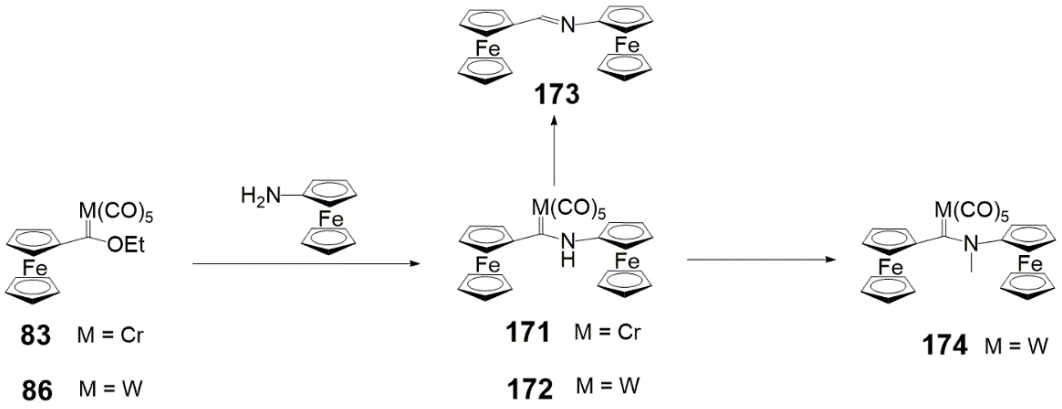

Scheme 4.2: Ferrocenyl Fischer Carbene complexes and their reactions presented in this work.

The most probable mechanism of three different proposed mechanisms for the thermal reaction of **172** to **173** includes the following steps: CO dissociation, *E*/*Z* isomerization, oxidative addition, pseudorotation, reductive elimination, imine dissociation and *E*/*Z* isomerization (Scheme 4.3). For the CO dissociation, *E*/*Z* isomerization and imine dissociation, *E*/*Z* isomerization also the reverse order might be possible. The most interesting proposed intermediates are the seven-coordinate hydrido W^{II} complexes **175** and **176** which facilitate the hydrogen shift. These intermediates are

not possible for the chromium Fischer carbene complex **171** and could give a hint why **171** needs basic reaction conditions to form **173**.

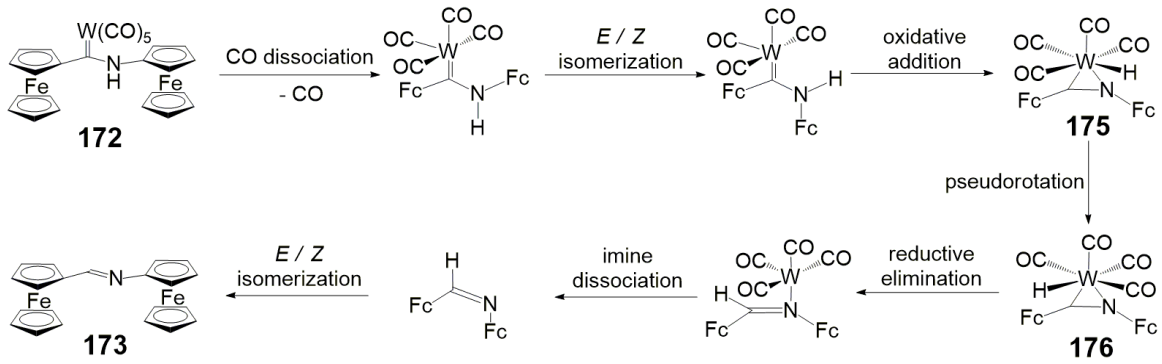

Scheme 4.3: Proposed mechanism for the thermal reaction of the Fischer carbene complex 172 to the imine 173.

The methylated complex ferrocenyl *N*-methylaminoferrocenyl carbene tungsten(0) pentacarbonyl **174** was studied in detail (Section 3.6, Scheme 4.2). Spectroelectrochemical measurements and Hush analysis of **174**$^{+}$ give a H_{AB} of 593 cm^{1} which is more than twice the strength compared to diferrocenylamide and thioamide. This suggest electronic communication of the mixed valent mono cation with almost degenerate Fe^{II} sites occurs via the bridge and not solely through space.

To study the principles of ferrocenyl carbenes in RSC the ferrocenyl ethoxy Fischer carbene was transferred to give gold complex **177** (Section 3.4). The cyclization of *N*-(2-propyn-1-yl) benzamide **180** to 5-methylene-2-phenyl-4,5-dihydrooxazole **181** with 1 mol% catalyst load was used to compare the catalyst to other redox switchable catalysts (Scheme 4.4). After 8 h full conversion was achieved with the oxidized catalyst **178**/**179** while the neutral species **177** showed no conversion. The catalysis could be turned on and off several times. EPR studies and DFT calculations of the oxidized species suggest an Au^{II} active species **179**.

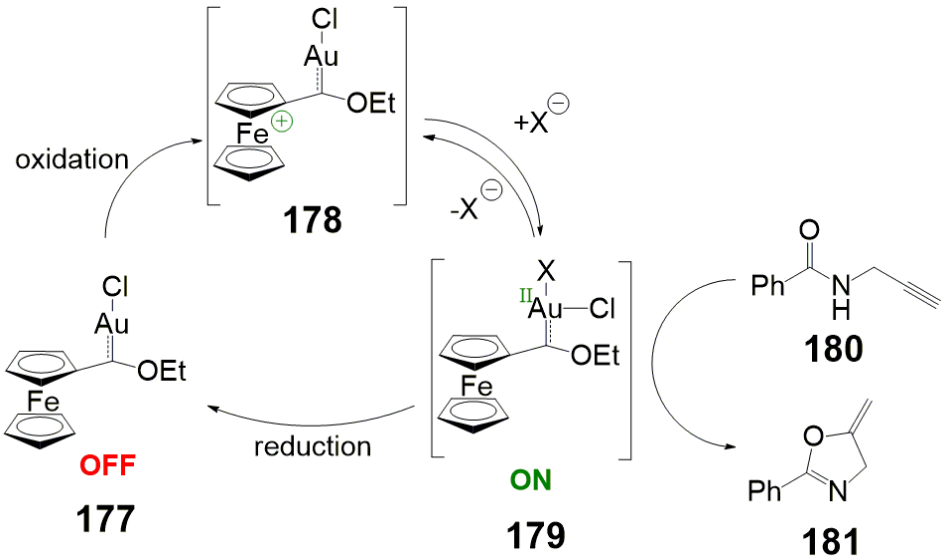

Scheme 4.4: Ferrocenyl Fischer carbene gold complex presented in this work and proposed catalytic cycle.

Two new reactions from chromium ferrocenyl Fischer carbene complex **83** to 2,*N*-diferrocenyl acetamide **182** and 4-ethoxy-2,3,4-triferrocenyl-cyclobut-2-enone **183** have been investigated in detail and mechanisms were proposed (Scheme 4.5–8, Section 3.5).

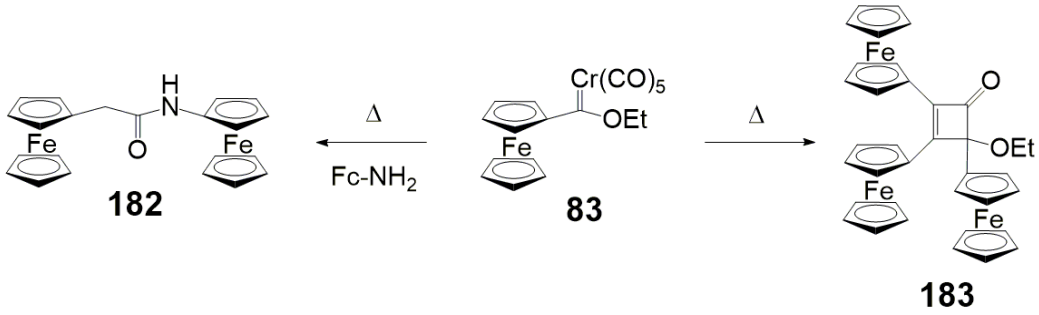

Scheme 4.5: Formation of 2,*N*-diferrocenyl acetamide 182 and 4-ethoxy-2,3,4-triferrocenyl-cyclobut-2-enone 183.

For the reaction of **83** with aminoferrocene to **182** the initial attack of the rather weak nucleophile aminoferrocene on the CO ligand of **83** might be assisted by an OH···Fe IHB present in the biscarbene **185** (Scheme 4.6). Carbene-carbene coupling and reduction gave the final product **182**.

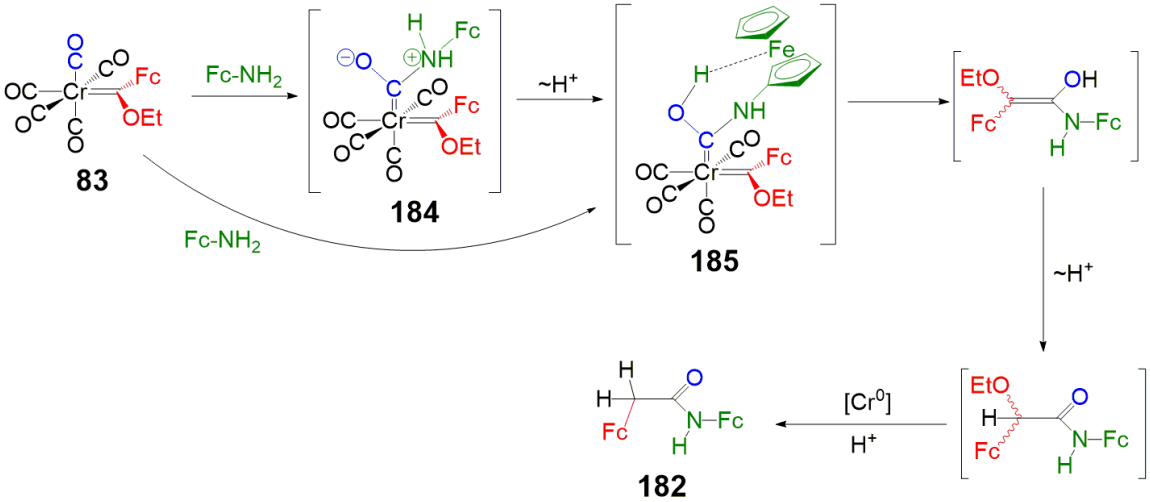

Scheme 4.6: Proposed mechanism for the formation of 182 from 83 via biscarbenes 184/185, carbene-carbene coupling and reduction.

For the proposed mechanism of the formation of **183** three equivalents of **83** are needed in total and the reaction can be divided into two parts (Scheme 4.7, Scheme 4.8).

In the first part two equivalents of **83** react to diferrocenyl alkyne **189** (Scheme 4.7). Thermal release of one CO ligand could form the unsaturated tetracarbonyl carbene complex **186**. By carbene transfer from **83** the biscarbene **187** might be formed. Carbene-carbene coupling releases an isomer mixture of the alkene **188** which was identified by FD mass spectrometry. In a last step the proposed alkyne **189** could be formed by reaction of the diethoxy alkene **188** with Cr^0 species giving Cr^{II} alkoxides as side products.

In the second part the alkyne **189** reacts with the third equivalent of **83** to the cyclobutenone **183** in a reaction which is similar to the Dötz benzannulation reaction (Scheme 4.8). This reaction is also initiated by thermal loss of one CO ligand to give the same unsaturated tetracarbonyl carbene complex **186**. This time the vacant coordination site is coordinated by the alkyne **189** to give the alkyne complex **190**. By insertion of the alkyne into the carbene bond the vinyl carbene complex **191** is formed. Coordination of one free electron pair of the alkoxy group to the chromium could stabilize this intermediate. Insertion of one CO ligand into the carbene bond could give the $Cr(CO)_3$ coordinated vinyl ketene **192**. In the final step the $Cr(CO)_3$ coordinated cyclobutenone **193** is formed by ring closure. During work up the free cyclobutenone **183** is obtained.

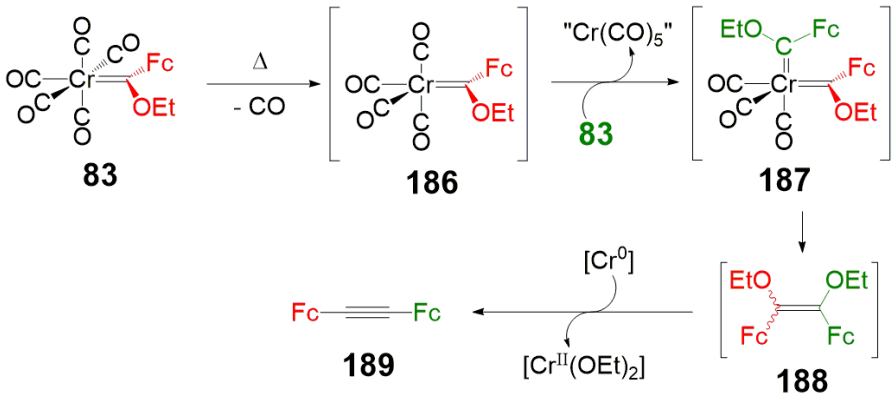

Scheme 4.7: Proposed mechanism for the thermal reaction of two equivalents of ferrocenyl Fischer carbene complex 83 to diferrocenyl alkyne 189.

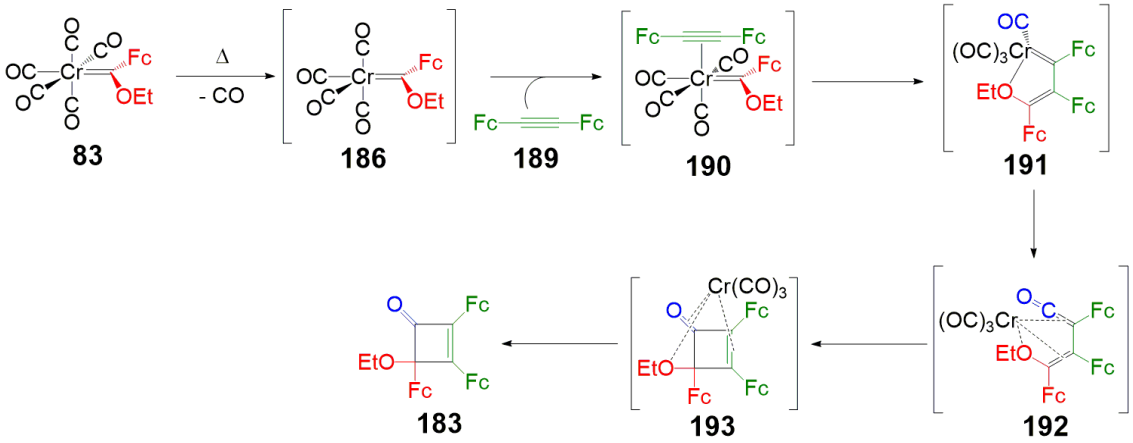

Scheme 4.8: Proposed mechanism for the thermal reaction of ferrocenyl Fischer carbene complex 83 to 4-ethoxy-2,3,4-triferrocenyl-cyclobut-2-enone 183

In future the ferrocenyl *N*-methylaminoferrocenyl carbene ligand will be investigated as redox switchable gold catalyst **189** to find out if one or both ferrocenyl sites can be oxidized and influence catalysis (Figure 4.5). Further investigation of the proposed active Au^{II} species are anticipated. More EPR studies of active species are planned to investigate the induction period at the beginning of the catalysis described in Section 3.4. ^{197}Au Mössbauer spectroscopy[159] could give some interesting insights into the reaction mechanism of the redox switchable gold catalysis, by showing the oxidation state and the coordination number of the gold atom. Therefore, a ^{197}Pt source is needed which can be produced in a nuclear reactor from ^{196}Pt with neutron capture. So

far, the synthesized gold catalyst **177** was only used for intermolecular test reactions. Further intramolecular test reactions with different alkynes will also be investigated. The synthesis of acyclic diamino carbene complexes (ADC) **190** and the comparison to **189** and NHCs is planned.

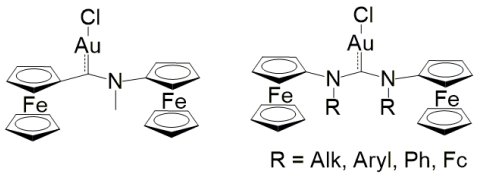

194 **195**

Scheme 4.8: Outlook.

5 References

[1] J. H. Richards, E. A. Hill, *J. Am. Chem. Soc.* **1959**, *81*, 3484–3485.
[2] D. S. Trifan, R. Bacskai, *J. Am. Chem. Soc.* **1960**, *82*, 5010–5011.
[3] D. S. Trifan, R. Bacskai, *Tetrahedron Lett.* **1960**, *1*, 1–8.
[4] E. A. Hill, J. H. Richards, *J. Am. Chem. Soc.* **1961**, *83*, 4216–4221.
[5] T. J. Kealy, P. L. Pauson, *Nature* **1951**, *168*, 1039–1040.
[6] S. A. Miller, J. A. Tebboth, J. F. Tremaine, *J. Chem. Soc.* **1952**, 632.
[7] E. A. Hill, J. H. Richards, *J. Am. Chem. Soc.* **1961**, *83*, 3840–3846.
[8] J. C. Ware, T. G. Traylor, *Tetrahedron Lett.* **1965**, *6*, 1295–1302.
[9] M. Cais, J. J. Dannenberg, A. Einsenstadt, M. I. Levenberg, J. H. Richards, *Tetrahedron Lett.* **1966**, *7*, 1695–1701.
[10] P. Ashkenazi, S. Lupan, A. Schwarz, M. Cais, *Tetrahedron Lett.* **1969**, *10*, 817–820.
[11] A. Sonoda, I. Moritani, T. Saraie, T. Wada, *Tetrahedron Lett.* **1969**, *10*, 2943–2946.
[12] W. R. Bamford, T. S. Stevens, *J. Chem. Soc.* **1952**, 4735–4740.
[13] A. Sonoda, I. Moritani, S. Yasuda, T. Wada, *Tetrahedron* **1970**, *26*, 3075–3081.
[14] A. Sonoda, I. Moritani, *Bull. Chem. Soc. Jpn.* **1970**, *43*, 3522–3527.
[15] A. Dehope, D. Mendoza-Espinosa, B. Donnadieu, G. Bertrand, *New J. Chem.* **2011**, *35*, 2037–2042.
[16] A. J. Arduengo, R. L. Harlow, M. Kline, *J. Am. Chem. Soc.* **1991**, *113*, 361–363.
[17] A. J. Arduengo, R. Krafczyk, *Chem. Unserer Zeit* **1998**, *32*, 6–14.
[18] D. A. Dixon, A. J. Arduengo, *J. Phys. Chem.* **1991**, *95*, 4180–4182.
[19] H. W. Wanzlick, *Angew. Chem. Int. Ed.* **1962**, *1*, 75–80; *Angew. Chem.*, **1962**, *74*, 129–134.
[20] H.-W. Wanzlick, F. Esser, H.-J. Kleiner, *Chem. Ber.* **1963**, *96*, 1208–1212.
[21] H.-W. Wanzlick, B. Lachmann, E. Schikora, *Chem. Ber.* **1965**, *98*, 3170–3177.
[22] A. J. Arduengo, H. V. R. Dias, R. L. Harlow, M. Kline, *J. Am. Chem. Soc.* **1992**, *114*, 5530–5534.
[23] A. J. Arduengo, H. V. R. Dias, D. A. Dixon, R. L. Harlow, W. T. Klooster, T. F. Koetzle, *J. Am. Chem. Soc.* **1994**, *116*, 6812–6822.
[24] D. Enders, K. Breuer, G. Raabe, J. Runsink, J. H. Teles, J.-P. Melder, K. Ebel, S. Brode, *Angew. Chem.* **1995**, *107*, 1119–1122; *Angew. Chem. Int. Ed. Engl.*, **1995**, *34*, 1021–1023.
[25] A. J. Arduengo, J. R. Goerlich, W. J. Marshall, *J. Am. Chem. Soc.* **1995**, *117*, 11027–11028.
[26] B. Bildstein, M. Malaun, H. Kopacka, K.-H. Ongania, K. Wurst, *J. Organomet. Chem.* **1999**, *572*, 177–187.
[27] B. Bildstein, M. Malaun, H. Kopacka, K. Wurst, M. Mitterböck, K.-H. Ongania, G. Opromolla, P. Zanello, *Organometallics* **1999**, *18*, 4325–4336.
[28] C. Bolm, M. Kesselgruber, G. Raabe, *Organometallics* **2002**, *21*, 707–710.
[29] D. Broggini, A. Togni, *Helv. Chim. Acta* **2002**, *85*, 2518–2522.
[30] Y. Yuan, G. Raabe, C. Bolm, *J. Organomet. Chem.* **2005**, *690*, 5747–5752.
[31] U. Siemeling, *Eur. J. Inorg. Chem.* **2012**, *2012*, 3523–3536.
[32] E. L. Rosen, C. D. Varnado, A. G. Tennyson, D. M. Khramov, J. W. Kamplain, D. H. Sung, P. T. Cresswell, V. M. Lynch, C. W. Bielawski, *Organometallics* **2009**, *28*, 6695–6706.
[33] C. Jutz, *Tetrahedron Lett.* **1959**, *1*, 1–4.

[34] S. Lupan, M. Kapon, M. Cais, F. H. Herbstein, *Angew. Chem. Int. Ed.* **1972**, *11*, 1025–1027; *Angew. Chem.*, **1972**, *84*, 1104–1106.
[35] M. Cais, S. Dani, F. H. Herbstein, M. Kapon, *J. Am. Chem. Soc.* **1978**, *100*, 5554–5558.
[36] B. Bildstein, P. Denifl, K. Wurst, *J. Organomet. Chem.* **1995**, *496*, 175–186.
[37] B. Bildstein, *J. Organomet. Chem.* **2001**, *617-618*, 28–38.
[38] K.-Y. Kay, L. H. Kim, I. C. Oh, *Tetrahedron Lett.* **2000**, *41*, 1397–1400.
[39] B. Bildstein, P. Denifl, K. Wurst, M. Andre, M. Baumgarten, J. Friedrich, E. Ellmerer-Mueller, *Organometallics* **1995**, *14*, 4334–4342.
[40] A. Sonoda, I. Moritani, *J. Organomet. Chem.* **1971**, *26*, 133–140.
[41] D. M. Khramov, E. L. Rosen, V. M. Lynch, C. W. Bielawski, *Angew. Chem. Int. Ed.* **2008**, *47*, 2267–2270; *Angew. Chem.*, **2008**, *120*, 2299–2302.
[42] U. Siemeling, C. Färber, C. Bruhn, *Chem. Commun.* **2009**, 98–100.
[43] U. Siemeling, C. Färber, M. Leibold, C. Bruhn, P. Mücke, R. F. Winter, B. Sarkar, M. von Hopffgarten, G. Frenking, *Eur. J. Inorg. Chem.* **2009**, *2009*, 4607–4612.
[44] A. M. Allgeier, C. A. Mirkin, *Angew. Chem. Int. Ed.* **1998**, *37*, 894–908; *Angew. Chem.*, **1998**, *110*, 936–952.
[45] U. Siemeling, T.-C. Auch, *Chem. Soc. Rev.* **2005**, *34*, 584–594.
[46] S. Rittinghaus, C. Färber, C. Bruhn, U. Siemeling, *Dalton Trans.* **2014**, *43*, 3508–3520.
[47] C. Thie, C. Bruhn, U. Siemeling, *Eur. J. Inorg. Chem.* **2015**, 5457–5466.
[48] A. R. Petrov, A. Derheim, J. Oetzel, M. Leibold, C. Bruhn, S. Scheerer, S. Oßwald, R. F. Winter, U. Siemeling, *Inorg. Chem.* **2015**, *54*, 6657–6670.
[49] D. S. Trifan, J. L. Weinmann, L. P. Kuhn, *J. Am. Chem. Soc.* **1957**, *79*, 6566–6567.
[50] M. Rosenblum, J. O. Santer, *J. Am. Chem. Soc.* **1959**, *81*, 5517–5518.
[51] T. J. Curphey, J. O. Santer, M. Rosenblum, J. H. Richards, *J. Am. Chem. Soc.* **1960**, *82*, 5249–5250.
[52] U. T. Mueller-Westerhoff, T. J. Haas, G. F. Swiegers, T. K. Leipert, *J. Organomet. Chem.* **1994**, *472*, 229–246.
[53] M. Rosenblum, J. O. Santer, W. G. Howells, *J. Am. Chem. Soc.* **1963**, *85*, 1450–1458.
[54] M. Malischewski, K. Seppelt, J. Sutter, F. W. Heinemann, B. Dittrich, K. Meyer, *Angew. Chem. Int. Ed.* **2017**, *56*, 13372–13376.
[55] A. W. Baker, D. E. Bublitz, *Spectrochimica Acta* **1966**, *22*, 1787–1799.
[56] Y.S. Shubina, L. M. Epstein, *J. Mol. Struct.* **1992**, *265*, 367–384.
[57] E. S. Shubina, A. N. Krylov, A. Z. Kreindlin, M. I. Rybinskaya, L. M. Epstein, *J. Mol. Struct.* **1993**, *301*, 1–5.
[58] N. V. Belkova, E. S. Shubina, E. I. Gutsul, L. M. Epstein, I. L. Eremenko, S. E. Nefedov, *J. Organomet. Chem.* **2000**, *610*, 58–70.
[59] L. M. Epstein, E. S. Shubina, *Coord. Chem. Rev.* **2002**, *231*, 165–181.
[60] L. M. Epstein, L. N. Saitkulova, E. S. Shubina, *J. Mol. Struct.* **1992**, *270*, 325–337.
[61] H. Schottenberger, M. Buchmeiser, C. Rieker, P. Jaitner, K. Wurst, *J. Organomet. Chem.* **1997**, *541*, 249–260.
[62] V. Dimitrov, A. Linden, M. Hesse, *Tetrahedron: Asymmetry* **2001**, *12*, 1331–1335.
[63] E. I. Klimova, T. Klimova Berestneva, L. R. Ramirez, A. Cinquantini, M. Corsini, P. Zanello, S. Hernández-Ortega, M. M. García, *Eur. J. Org. Chem.* **2003**, *2003*, 4265–4272.
[64] V. Albrow, A. J. Blake, A. Chapron, C. Wilson, S. Woodward, *Inorg. Chim. Acta* **2006**, *359*, 1731–1742.

[65] M. Lotz, R. Schuecker, K. Mereiter, P. Knochel, *Organometallics* **2010**, *29*, 6503–6508.
[66] A. Eloi, M. Poizat, A. Hautecoeur, A. Panossian, F. Rose-Munch, E. Rose, *Organometallics* **2011**, *30*, 5564–5567.
[67] D. Enders, R. Lochtman, G. Raabe, *Synlett* **1996**, *1996*, 126–128.
[68] J. R. Hagadorn, J. Arnold, *J. Organomet. Chem.* **2001**, *637-639*, 521–530.
[69] Y. Tanaka, N. Taniguchi, T. Kimura, M. Uemura, *J. Org. Chem.* **2002**, *67*, 9227–9237.
[70] L. Brammer, *Dalton Trans.* **2003**, 3145–3157.
[71] D. Braga, F. Grepioni, E. Tedesco, K. Biradha, G. R. Desiraju, *Organometallics* **1997**, *16*, 1846–1856.
[72] L. M. Epstein, A. N. Krylov, E. S. Shubina, *J. Mol. Struct.* **1994**, *322*, 345–352.
[73] L. Brammer, *J. Organomet. Chem.* **2000**, *609*, 36–43.
[74] L. Brammer in *NATO science series Series E, Applied sciences*, *Vol. 360* (Hrsg.: F. H. Allen, J. A. K. Howard, G. P. Shields), Kluwer Acad. Publ, Dordrecht, **1999**, S. 197–210.
[75] D. Braga, F. Grepioni, G. R. Desiraju, *Chem. Rev.* **1998**, *98*, 1375–1406.
[76] D. Braga, F. Grepioni, *Acc. Chem. Res.* **2000**, *33*, 601–608.
[77] D. Braga, *Chem. Commun.* **2003**, 2751–2754.
[78] J. A. Connor, E. M. Jones, J. P. Lloyd, *J. Organomet. Chem.* **1970**, *24*, C20-C22.
[79] G. A. Mose, E. O. Fischer, M. D. Rausch, *J. Organomet. Chem.* **1971**, *27*, 379–382.
[80] J. A. Connor, J. P. Lloyd, *J. Chem. Soc., Dalton Trans.* **1972**, 1470–1476.
[81] M. K. Lloyd, J. A. McCleverty, D. G. Orchard, J. A. Connor, M. B. Hall, I. H. Hillier, E. M. Jones, G. K. McEwen, *J. Chem. Soc., Dalton Trans.* **1973**, 1743–1747.
[82] J. G. López-Cortés, Contreras de la Cruz, Luis F., M. C. Ortega-Alfaro, R. A. Toscano, C. Alvarez-Toledano, H. Rudler, *J. Organomet. Chem.* **2005**, *690*, 2229–2237.
[83] D. I. Bezuidenhout, E. van der Watt, D. C. Liles, M. Landman, S. Lotz, *Organometallics* **2008**, *27*, 2447–2456.
[84] E. O. Fischer, A. Maasböl, *Angew. Chem. Int. Ed.* **1964**, *3*, 580–581.
[85] D. I. Bezuidenhout, W. Barnard, B. van der Westhuizen, E. van der Watt, D. C. Liles, *Dalton Trans.* **2011**, *40*, 6711–6721.
[86] D. I. Bezuidenhout, S. Lotz, M. Landman, D. C. Liles, *Inorg. Chem.* **2011**, *50*, 1521–1533.
[87] D. I. Bezuidenhout, S. Lotz, D. C. Liles, B. van der Westhuizen, *Coord. Chem. Rev.* **2012**, *256*, 479–524.
[88] B. van der Westhuizen, P. J. Swarts, I. Strydom, D. C. Liles, I. Fernández, J. C. Swarts, D. I. Bezuidenhout, *Dalton Trans.* **2013**, *42*, 5367–5378.
[89] B. van der Westhuizen, P. J. Swarts, van Jaarsveld, Louise M, D. C. Liles, U. Siegert, J. C. Swarts, I. Fernández, D. I. Bezuidenhout, *Inorg. Chem.* **2013**, *52*, 6674–6684.
[90] D. I. Bezuidenhout, B. van der Westhuizen, I. Strydom, P. J. Swarts, J. C. Swarts, I. Fernández, *Inorg. Chim. Acta* **2014**, *423*, 184–192.
[91] D. I. Bezuidenhout, I. Fernández, B. van der Westhuizen, P. J. Swarts, J. C. Swarts, *Organometallics* **2013**, *32*, 7334–7344.
[92] B. van der Westhuizen, J. M. Speck, M. Korb, J. Friedrich, D. I. Bezuidenhout, H. Lang, *Inorg. Chem.* **2013**, *52*, 14253–14263.
[93] B. van der Westhuizen, J. Matthäus Speck, M. Korb, D. I. Bezuidenhout, H. Lang, *J. Organomet. Chem.* **2014**, *772-773*, 18–26.
[94] M. B. Robin, P. Day, *Adv. Inorg. Chem. Radiochem.* **1968**, *10*, 247–422.

[95] D. I. Bezuidenhout, B. van der Westhuizen, P. J. Swarts, T. Chatturgoon, O. Q. Munro, I. Fernández, J. C. Swarts, *Chem. Eur. J.* **2014**, *20*, 4974–4985.
[96] C. A. Tolman, *Chem. Rev.* **1977**, *77*, 313–348.
[97] G. Bouquet, A. Loutellier, M. Bigorgne, *J. Mol. Struct.* **1968**, *1*, 211–237.
[98] W. Strohmeier, F.-J. Müller, *Chem. Ber.* **1967**, *100*, 2812–2821.
[99] S. Díez-González, S. P. Nolan, *Coord. Chem. Rev.* **2007**, *251*, 874–883.
[100] R. A. Kelly III, H. Clavier, S. Giudice, N. M. Scott, E. D. Stevens, J. Bordner, I. Samardjiev, C. D. Hoff, L. Cavallo, S. P. Nolan, *Organometallics* **2008**, *27*, 202–210.
[101] A. R. Chianese, X. Li, M. C. Janzen, J. W. Faller, R. H. Crabtree, *Organometallics* **2003**, *22*, 1663–1667.
[102] S. Wolf, H. Plenio, *J. Organomet. Chem.* **2009**, *694*, 1487–1492.
[103] T. Dröge, F. Glorius, *Angew. Chem.* **2010**, *122*, 7094–7107; *Angew. Chem. Int. Ed.*, **2010**, *49*, 6940–6952.
[104] G. Giordano, R. H. Crabtree, R. M. Heintz, D. Forster, D. E. Morris in *Inorganic Syntheses* (Hrsg.: R. J. Angelici), John Wiley & Sons, Inc, Hoboken, NJ, USA, **1990**, S. 88–90.
[105] G. K. Ramollo, M. J. López-Gómez, D. C. Liles, L. C. Matsinha, G. S. Smith, D. I. Bezuidenhout, *Organometallics* **2015**, *34*, 5745–5753.
[106] S. Klenk, S. Rupf, L. Suntrup, M. van der Meer, B. Sarkar, *Organometallics* **2017**, *36*, 2026–2035.
[107] L. Hettmanczyk, L. Suntrup, S. Klenk, C. Hoyer, B. Sarkar, *Chemistry* **2017**, *23*, 576–585.
[108] O. R. Luca, R. H. Crabtree, *Chem. Soc. Rev.* **2013**, *42*, 1440–1459.
[109] D. Tapu, D. A. Dixon, C. Roe, *Chem. Rev.* **2009**, *109*, 3385–3407.
[110] O. Back, M. Henry-Ellinger, C. D. Martin, D. Martin, G. Bertrand, *Angew. Chem.* **2013**, *125*, 3011–3015; *Angew. Chem. Int. Ed.*, **2013**, *52*, 2939–2943.
[111] G. P. Junor, J. Lorkowski, C. M. Weinstein, R. Jazzar, C. Pietraszuk, G. Bertrand, *Angew. Chem. Int. Ed.* **2020**, *59*; *Angew. Chem.*, **2020***, 132*.
[112] A. Liske, K. Verlinden, H. Buhl, K. Schaper, C. Ganter, *Organometallics* **2013**, *32*, 5269–5272.
[113] S. V. C. Vummaleti, D. J. Nelson, A. Poater, A. Gómez-Suárez, D. B. Cordes, A. M. Z. Slawin, S. P. Nolan, L. Cavallo, *Chem Sci.* **2015**, *6*, 1895–1904.
[114] K. Verlinden, H. Buhl, W. Frank, C. Ganter, *Eur. J. Inorg. Chem.* **2015**, 2416–2425.
[115] J. E. Parks, A. L. Balch, *J. Organomet. Chem.* **1973**, *57*, C103-C106.
[116] G. Minghetti, F. Bonati, *J. Organomet. Chem.* **1973**, *54*, C62-C63.
[117] J. E. Parks, A. L. Balch, *J. Organomet. Chem.* **1974**, *71*, 453–463.
[118] R. Aumann, E. O. Fischer, *Chem. Ber.* **1981**, *114*, 1853–1857.
[119] E. O. Fischer, M. Böck, R. Aumann, *Chem. Ber.* **1983**, *116*, 3618–3623.
[120] E. O. Fischer, M. Böck, *J. Organomet. Chem.* **1985**, *287*, 279–285.
[121] G. Banditelli, F. Bonati, S. Calogero, G. Valle, *J. Organomet. Chem.* **1984**, *275*, 153–160.
[122] R. Usón, A. Laguna, M. D. Villacampa, *Inorg. Chim. Acta* **1984**, *81*, 25–31.
[123] G. Banditelli, F. Bonati, S. Calogero, G. Valle, F. E. Wagner, R. Wordel, *Organometallics* **1986**, *5*, 1346–1352.
[124] B. Bovio, S. Calogero, F. E. Wagner, A. Burini, B. R. Pietroni, *J. Organomet. Chem.* **1994**, *470*, 275–283.
[125] P. G. Jones, A. G. Maddock, M. J. Mays, M. M. Muir, A. F. Williams, *J. Chem. Soc., Dalton Trans.* **1977**, 1434–1439.

[126] S. Doherty, J. G. Knight, A. S. K. Hashmi, C. H. Smyth, N. A. B. Ward, K. J. Robson, S. Tweedley, R. W. Harrington, W. Clegg, *Organometallics* **2010**, *29*, 4139–4147.
[127] A. S. K. Hashmi, M. Rudolph, *Chem. Soc. Rev.* **2008**, *37*, 1766–1775.
[128] A. S. K. Hashmi, T. Häffner, M. Rudolph, F. Rominger, *Eur. J. Org. Chem.* **2011**, *2011*, 667–671.
[129] N. Huguet, D. Lebœuf, A. M. Echavarren, *Chem. Eur. J.* **2013**, *19*, 6581–6585.
[130] H. Schmidbaur, A. Schier, *Organometallics* **2010**, *29*, 2–23.
[131] D. S. Weinberger, M. Melaimi, C. E. Moore, A. L. Rheingold, G. Frenking, P. Jerabek, G. Bertrand, *Angew. Chem. Int. Ed.* **2013**, *52*, 8964–8967; *Angew. Chem.*, **2013**, *125*, 9134–9137.
[132] M. W. Hussong, F. Rominger, P. Krämer, B. F. Straub, *Angew. Chem. Int. Ed.* **2014**, *53*, 9372–9375; *Angew. Chem.*, **2014**, *126*, 9526–9529.
[133] G. Seidel, A. Fürstner, *Angew. Chem. Int. Ed.* **2014**, *53*, 4807–4811; *Angew. Chem.*, **2014**, *126*, 4907–4911.
[134] G. Seidel, B. Gabor, R. Goddard, B. Heggen, W. Thiel, A. Fürstner, *Angew. Chem. Int. Ed.* **2014**, *53*, 879–882; *Angew. Chem.*, **2014**, *126*, 898–901.
[135] D. I. Bezuidenhout, B. van der Westhuizen, A. J. Rosenthal, M. Wörle, D. C. Liles, I. Fernández, *Dalton Trans.* **2014**, *43*, 398–401.
[136] Y. Wang, M. E. Muratore, A. M. Echavarren, *Chem. Eur. J.* **2015**, *21*, 7332–7339.
[137] Nunes Dos Santos Comprido, Laura, Klein, Johannes E. M. N., G. Knizia, J. Kästner, A. S. K. Hashmi, *Angew. Chem. Int. Ed.* **2015**, *54*, 10336–10340; *Angew. Chem.*, **2015**, *127*, 10477–10481.
[138] C. Werlé, R. Goddard, A. Fürstner, *Angew. Chem. Int. Ed.* **2015**, *54*, 15452–15456; *Angew. Chem.*, **2015**, *127*, 15672–15676.
[139] J. F. Arambula, R. McCall, K. J. Sidoran, D. Magda, N. A. Mitchell, C. W. Bielawski, V. M. Lynch, J. L. Sessler, K. Arumugam, *Chem Sci.* **2016**, *7*, 1245–1256.
[140] R. Pretorius, M. R. Fructos, H. Müller-Bunz, R. A. Gossage, P. J. Pérez, M. Albrecht, *Dalton Trans.* **2016**, *45*, 14591–14602.
[141] D. Marchione, M. A. Izquierdo, G. Bistoni, R. W. A. Havenith, A. Macchioni, D. Zuccaccia, F. Tarantelli, L. Belpassi, *Chem. Eur. J.* **2017**, *23*, 2722–2728.
[142] J. Schießl, J. Schulmeister, A. Doppiu, E. Wörner, M. Rudolph, R. Karch, A. S. K. Hashmi, *Adv. Synth. Catal.* **2018**, *360*, 3949–3959.
[143] I. M. Lorkovic, M. S. Wrighton, W. M. Davis, *J. Am. Chem. Soc.* **1994**, *116*, 6220–6228.
[144] I. M. Lorkovic, R. R. Duff, M. S. Wrighton, *J. Am. Chem. Soc.* **1995**, *117*, 3617–3618.
[145] M. Süssner, H. Plenio, *Angew. Chem. Int. Ed.* **2005**, *44*, 6885–6888; *Angew. Chem.*, **2005**, *117*, 7045–7048.
[146] C. K. A. Gregson, V. C. Gibson, N. J. Long, E. L. Marshall, P. J. Oxford, A. J. P. White, *J. Am. Chem. Soc.* **2006**, *128*, 7410–7411.
[147] A. G. Tennyson, V. M. Lynch, C. W. Bielawski, *J. Am. Chem. Soc.* **2010**, *132*, 9420–9429.
[148] C. D. Varnado, E. L. Rosen, M. S. Collins, V. M. Lynch, C. W. Bielawski, *Dalton Trans.* **2013**, *42*, 13251–13264.
[149] S. Ibáñez, M. Poyatos, L. N. Dawe, D. Gusev, E. Peris, *Organometallics* **2016**, *35*, 2747–2758.
[150] E. Peris, *Chemical reviews* **2017**, *118*, 9988–10031.

[151] E. M. Broderick, N. Guo, C. S. Vogel, C. Xu, J. Sutter, J. T. Miller, K. Meyer, P. Mehrkhodavandi, P. L. Diaconescu, *J. Am. Chem. Soc.* **2011**, *133*, 9278–9281.
[152] L. Hettmanczyk, S. Manck, C. Hoyer, S. Hohloch, B. Sarkar, *Chem. Commun.* **2015**, *51*, 10949–10952.
[153] S. Vanicek, M. Podewitz, J. Stubbe, D. Schulze, H. Kopacka, K. Wurst, T. Müller, P. Lippmann, S. Haslinger, H. Schottenberger et al., *Chem. Eur. J.* **2018**, *24*, 3742–3753.
[154] D. Aucamp, T. Witteler, F. Dielmann, S. Siangwata, D. C. Liles, G. S. Smith, D. I. Bezuidenhout, *Eur. J. Inorg. Chem.* **2017**, 1227–1236.
[155] D. Aucamp, S. V. Kumar, D. C. Liles, M. A. Fernandes, L. Harmse, D. I. Bezuidenhout, *Dalton Trans.* **2018**, *47*, 16072–16081.
[156] K. O. Marichev, S. A. Patil, A. Bugarin, *Tetrahedron* **2018**, *74*, 2523–2546.
[157] J. Popp, A.-M. Caminade, E. Hey-Hawkins, *Eur. J. Inorg. Chem.* **2020**, *37*, 894.
[158] C. Förster, P. Veit, V. Ksenofontov, K. Heinze, *Chem. Commun.* **2015**, *51*, 1514–1516.
[159] R. V. Parish, *Gold Bull* **1982**, *15*, 51–63.

6 Appendix

6.1 Supporting Information: Competitive NH···Ru/Fe Hydrogen Bonding in Ferrocenyl Ruthenocenyl Tosyl Hydrazone

Competitive NH···Ru/Fe Hydrogen Bonding in Ferrocenyl Ruthenocenyl Tosyl Hydrazone

Philipp Veit, Ephraim Prantl, Christoph Förster* and Katja Heinze*

Institute of Inorganic Chemistry and Analytical Chemistry, Johannes Gutenberg-University of Mainz, Duesbergweg 10-14, 55128 Mainz

Supporting Information

Table S1. X-ray crystallographic data of **1**[1], **2** and **3a**

	1	**2**	**3a**
empirical formula	$C_{28}H_{26}N_2O_2SFe_2$	$C_{28}H_{26}N_2O_2SRu_2$	$C_{28}H_{26}N_2O_2SFeRu$
Formula weight	566.27	656.71	611.49
cryst system	monoclinic	monoclinic	monoclinic
space group	$P2_1/c$	$P2_1/c$	$P2_1/c$
a / Å	7.1125(6)	7.4062(6)	7.2898(9)
b / Å	11.3143(8)	11.3262(9)	11.3748(14)
c / Å	29.525(2)	29.215(2)	29.218(4)
β / °	95.838(2)	96.701(2)	95.627(2)
volume / Å^3	2363.6(3)	2433.9(3)	2411.1(5)
Z	4	4	4
density (calcd) / Mg m^{-3}	1.591	1.792	1.685
absorp coeff / mm^{-1}	1.346	1.357	1.345
F(000)	1168	1312	1240
cryst size / mm^3	0.46×0.06×0.01	0.55×0.18×0.12	0.59×0.29×0.12
θ range for data collection / °	2.27 – 27.94	2.28 – 27.87	2.27 – 27.91
index ranges	$-9 \le h \le 9$	$-9 \le h \le 9$	$-9 \le h \le 9$
	$-14 \le k \le 11$	$-14 \le k \le 14$	$-14 \le k \le 14$
	$-36 \le l \le 38$	$-38 \le l \le 25$	$-37 \le l \le 38$
no. of reflns collected	26075	22483	17484
no. of indep reflns	5663	5778	5748
R_{int}	0.0650	0.0488	0.1080
completeness to θ_{max} / %	99.7	99.5	99.5
max. / min transmission	0.9867 / 0.5764	0.8541 / 0.5224	0.8553 / 0.5043
goodness-of-fit on F^2	0.913	1.066	1.003
final R indices [$I > 2\sigma(I)$]	$R_1 = 0.0320$	$R_1 = 0.0273$	$R_1 = 0.0453$
	$wR_2 = 0.0649$	$wR_2 = 0.0646$	$wR_2 = 0.1124$
R indices (all data)	$R_1 = 0.0551$	$R_1 = 0.0320$	$R_1 = 0.0594$
	$wR_2 = 0.0691$	$wR_2 = 0.0663$	$wR_2 = 0.1191$
Largest diff. peak and hole / e Å^{-3}	0.434 / –0.330	0.434 / –0.684	1.053 / –1.161

Figure S1. Experimental FD-mass spectra and calculated isotopic pattern of a) **2** and b) **3a/3b**.

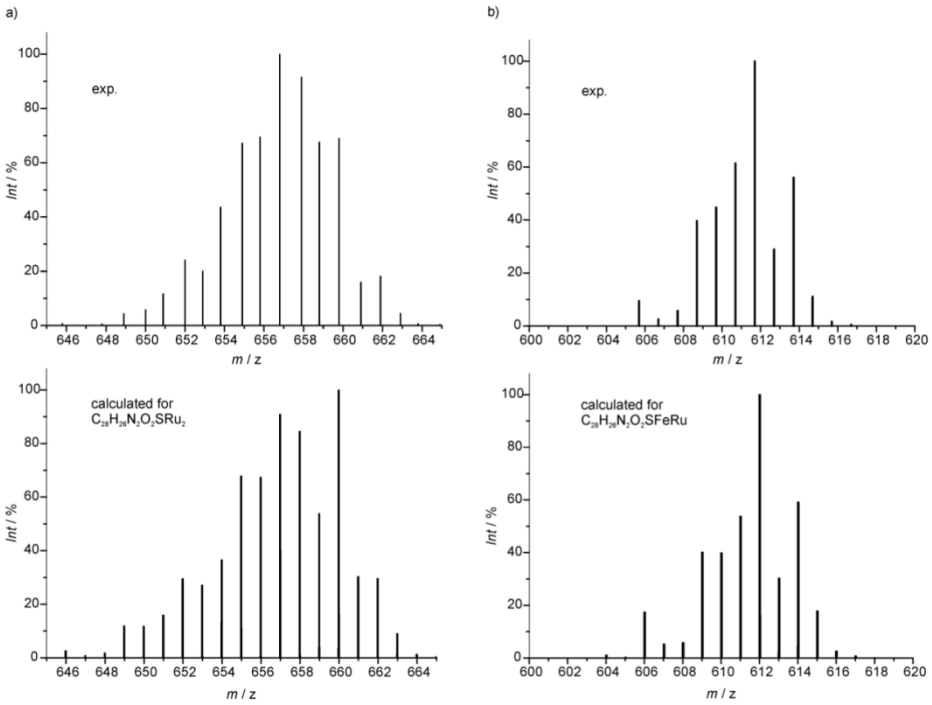

Figure S2. UV/Vis spectrum of **2** in CH_2Cl_2 together with the major transitions calculated by TD-DFT.

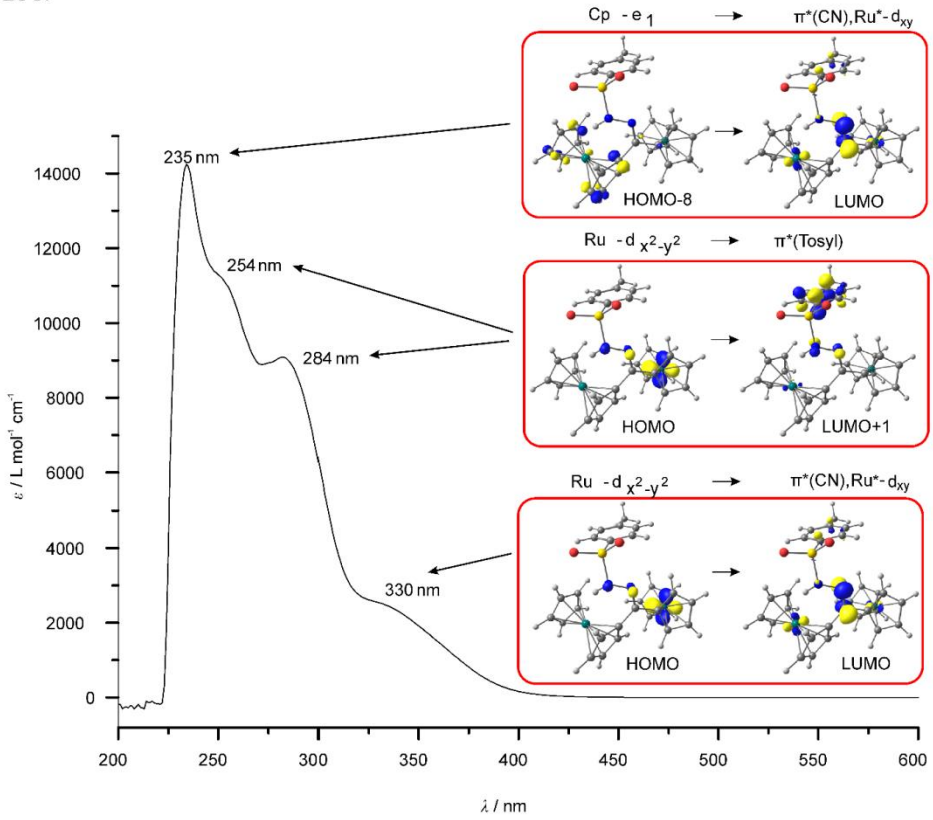

Figure S3. UV/Vis spectrum of **3a/3b** in CH_2Cl_2 together with the major transitions of **3a** calculated by TD-DFT.

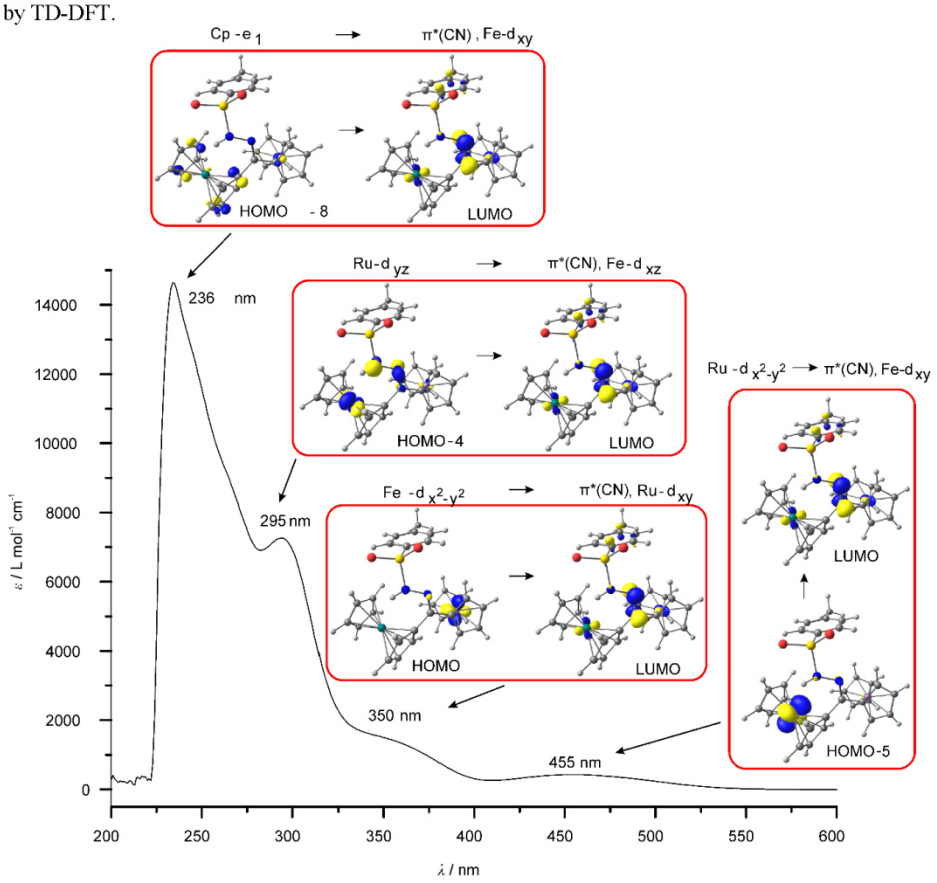

Figure S4. ^{1}H NMR spectrum of **2** in $CDCl_3$, a) full spectrum and b) zoom into Cp region.

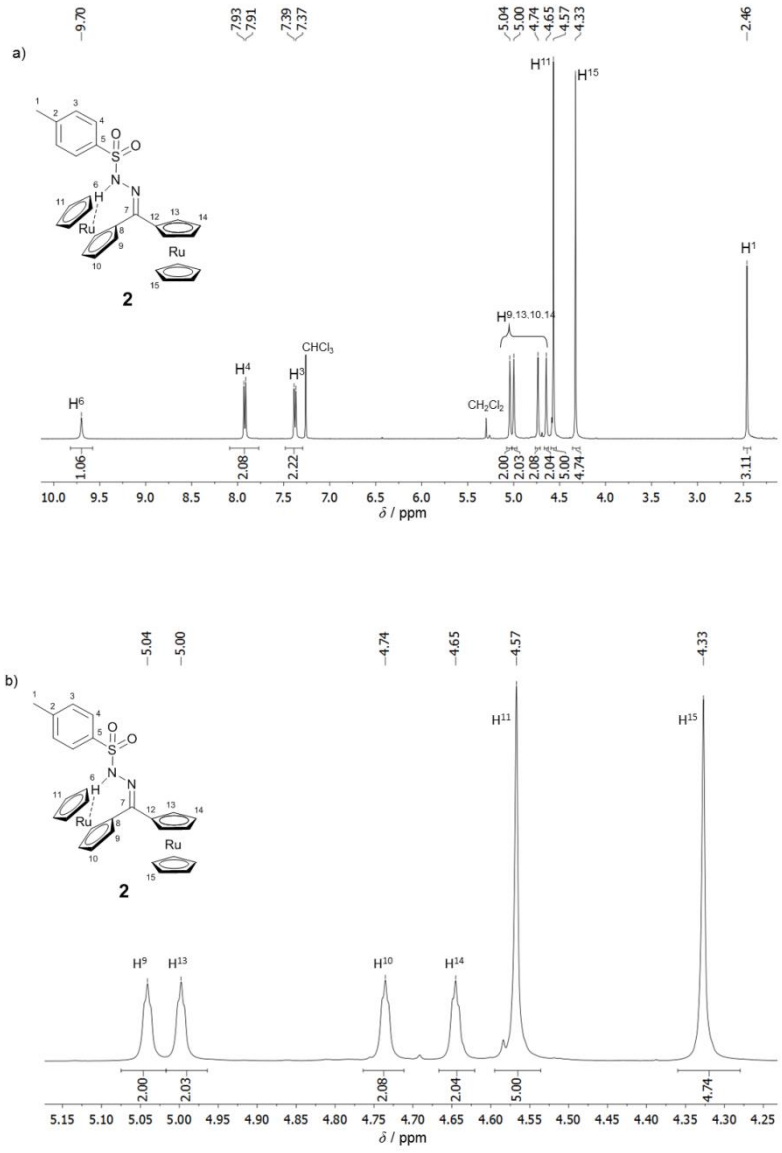

Figure S5. ^{13}C NMR spectrum of **2** in $CDCl_3$, a) full spectrum and b) zoom into Cp region.

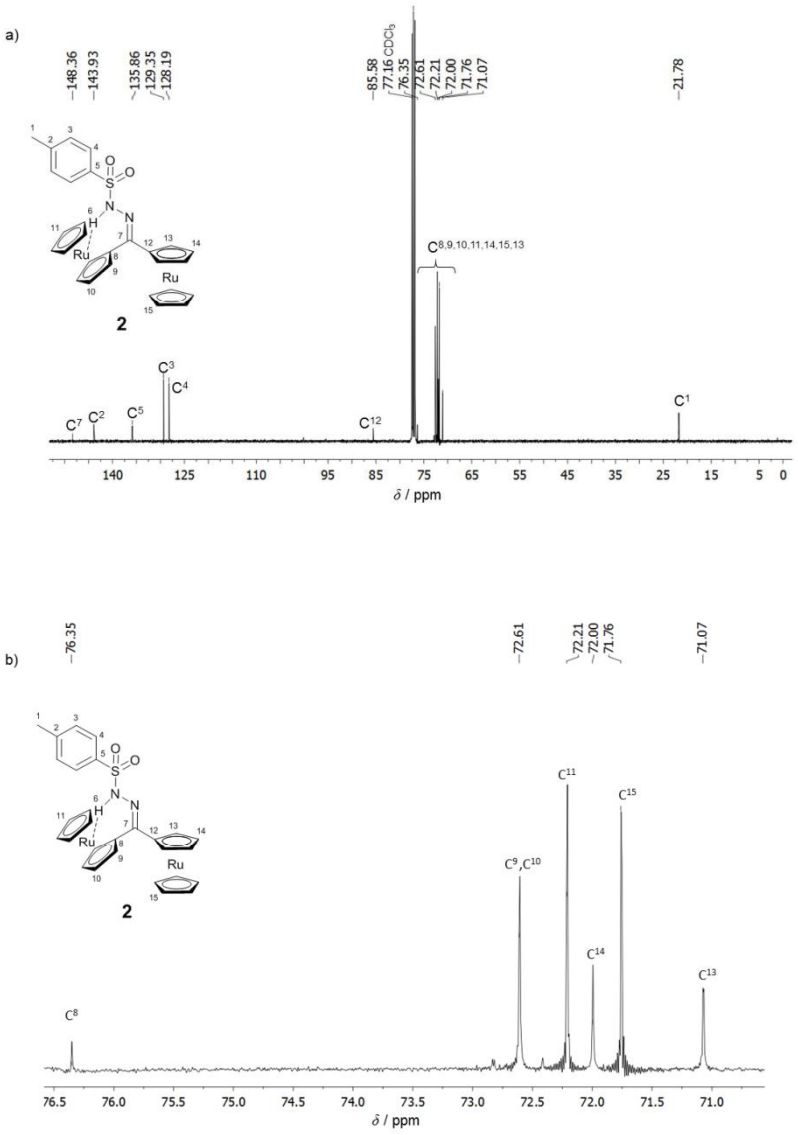

Figure S6. Part of the ^{1}H-^{1}H NOE NMR spectrum of **2** in $CDCl_3$.

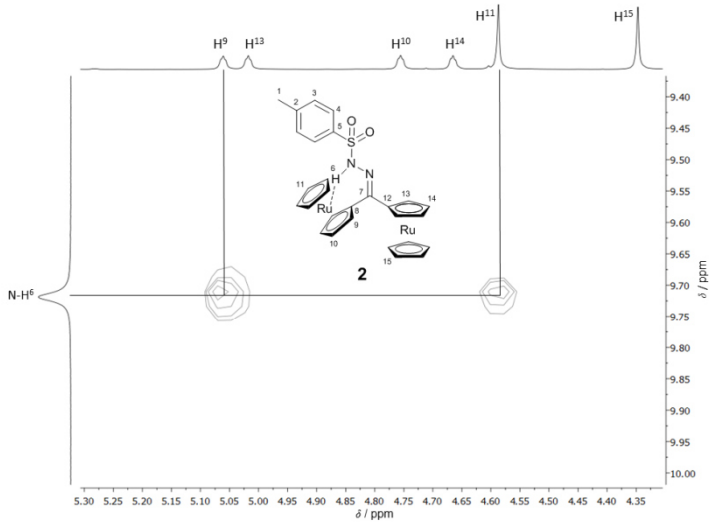

Figure S7. ^{1}H NMR spectra of a) **2** and b) a 10:1 mixture of **3a/3b** in DMSO-d_6.

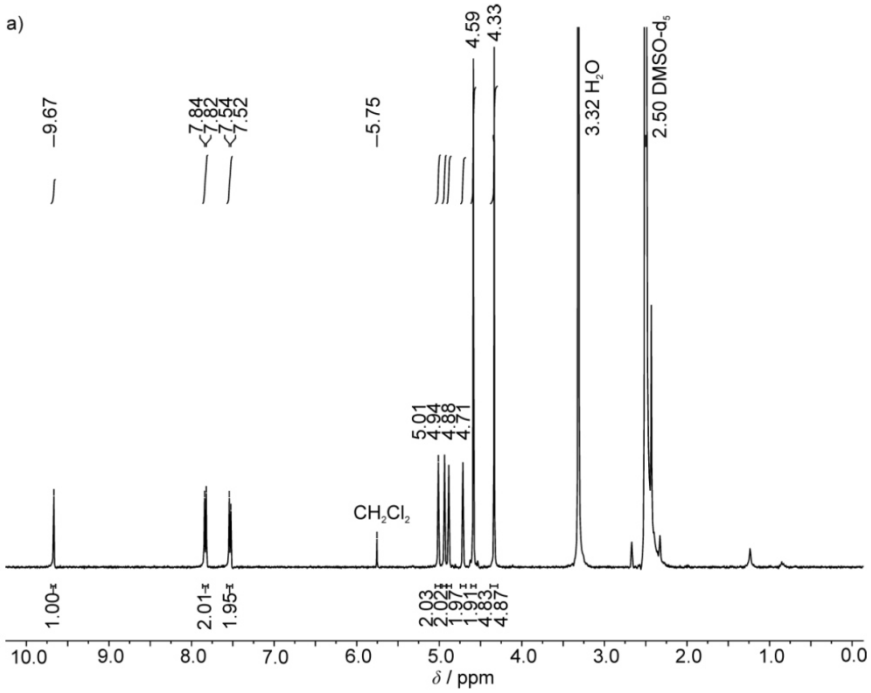

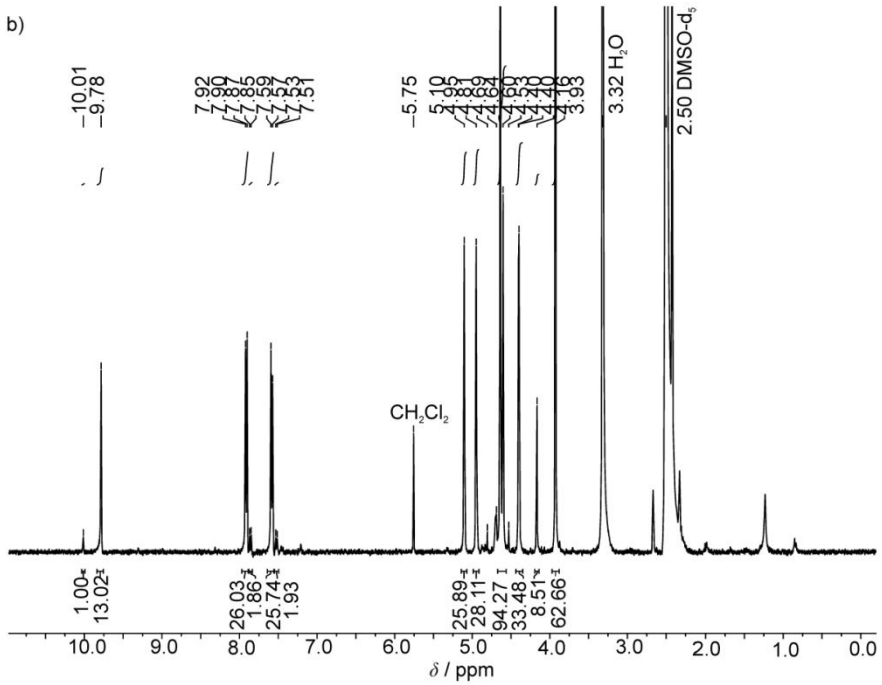

Figure S8. ^{1}H NMR spectra of a) **1**[1], b) **2** and c) a 10:1 mixture of **3a/3b** in $CDCl_3$.

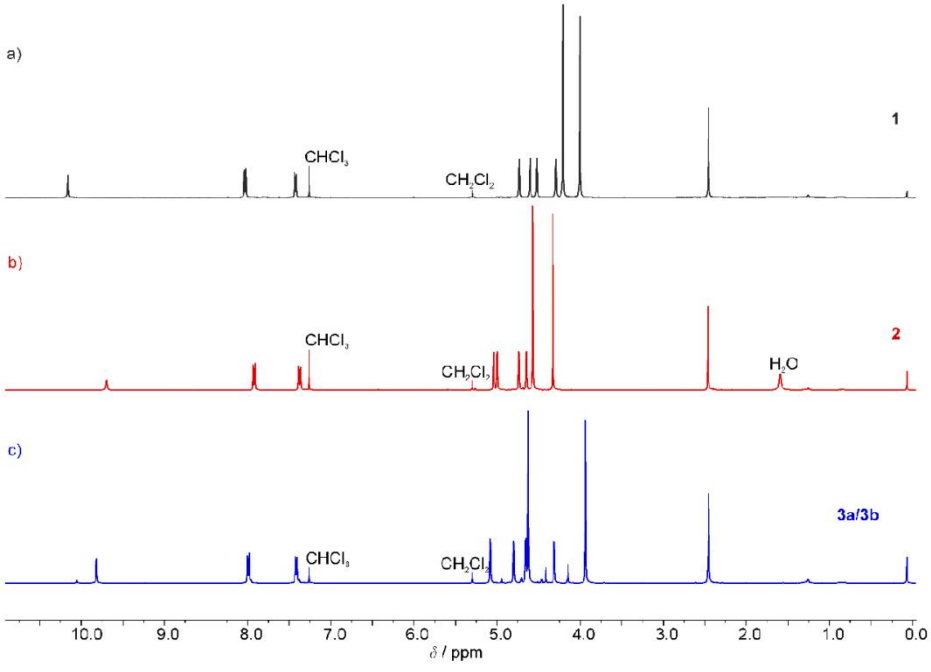

Figure S9. ^{1}H NMR spectra of a 10:1 mixture of **3a/3b** in $CDCl_3$, a) full spectrum with assignment of **3a** (H^x) and **3b** (H'^x) nuclei, b) zoom into Cp region with assignment of **3a** nuclei and c) zoom into Cp region with assignment of **3b** nuclei.

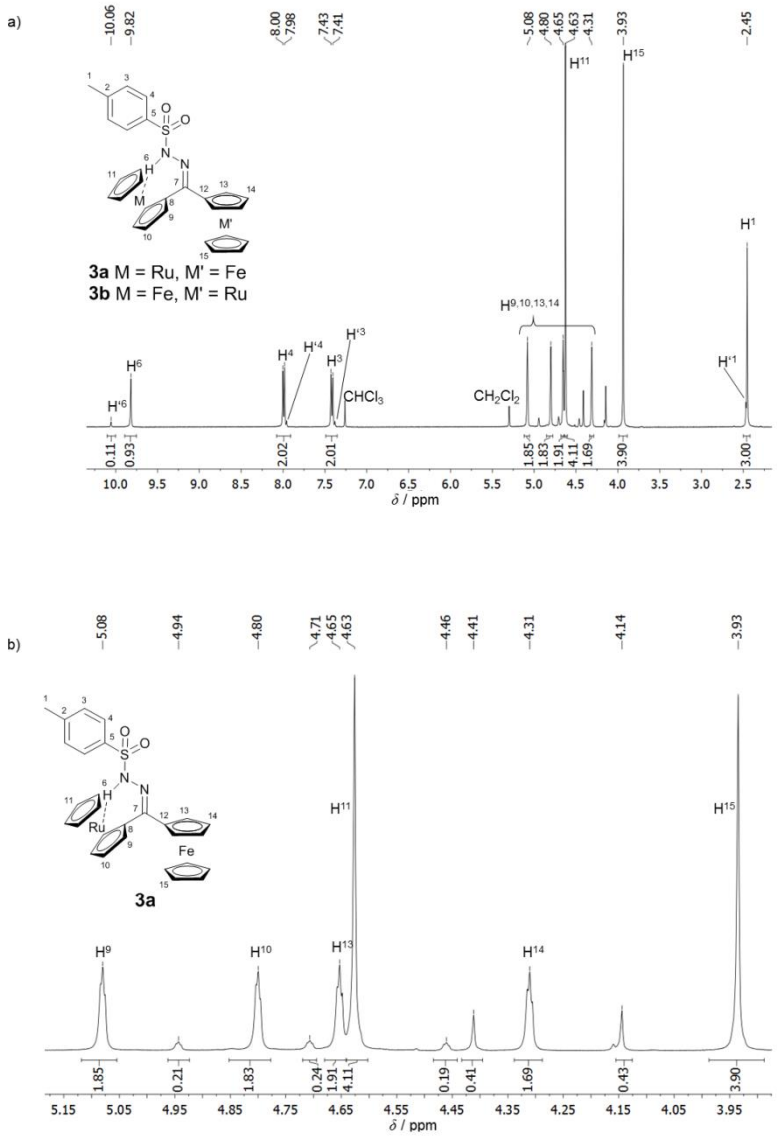

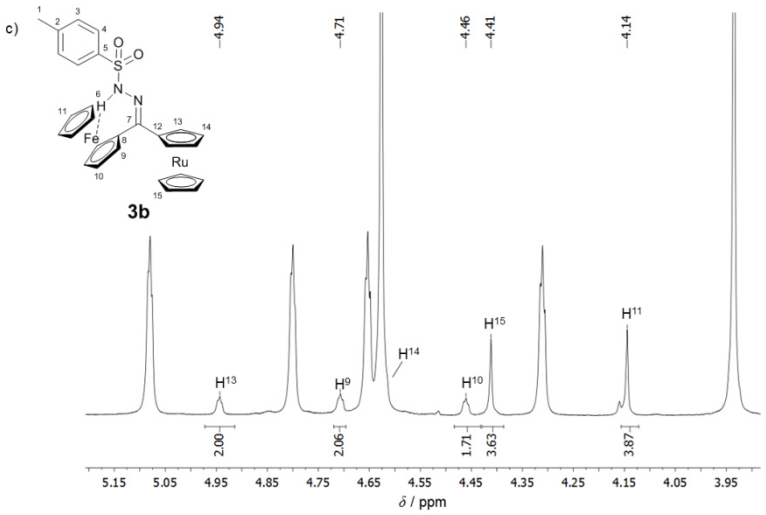

Figure S10. ^{13}C NMR spectrum of a 10:1 mixture of **3a/3b** in $CDCl_3$. Assignment of **3a** ^{13}C nuclei.

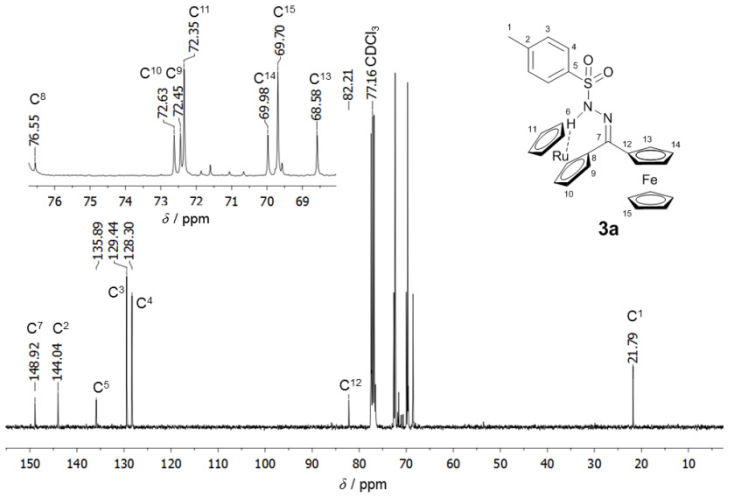

Figure S11. Part of the ^{1}H-^{1}H NOE NMR spectrum of **3a/3b** in $CDCl_3$.

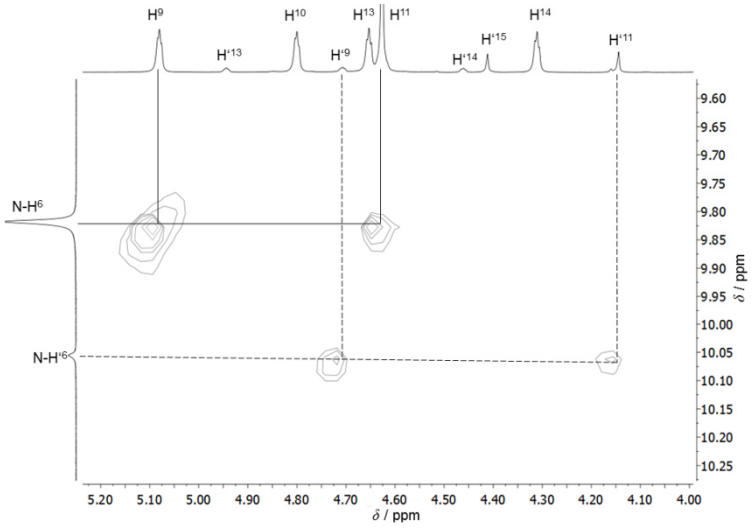

Figure S12. Variable temperature ^{1}H NMR spectra of a 10:1 mixture of **3a/3b** in toluene-d_8.

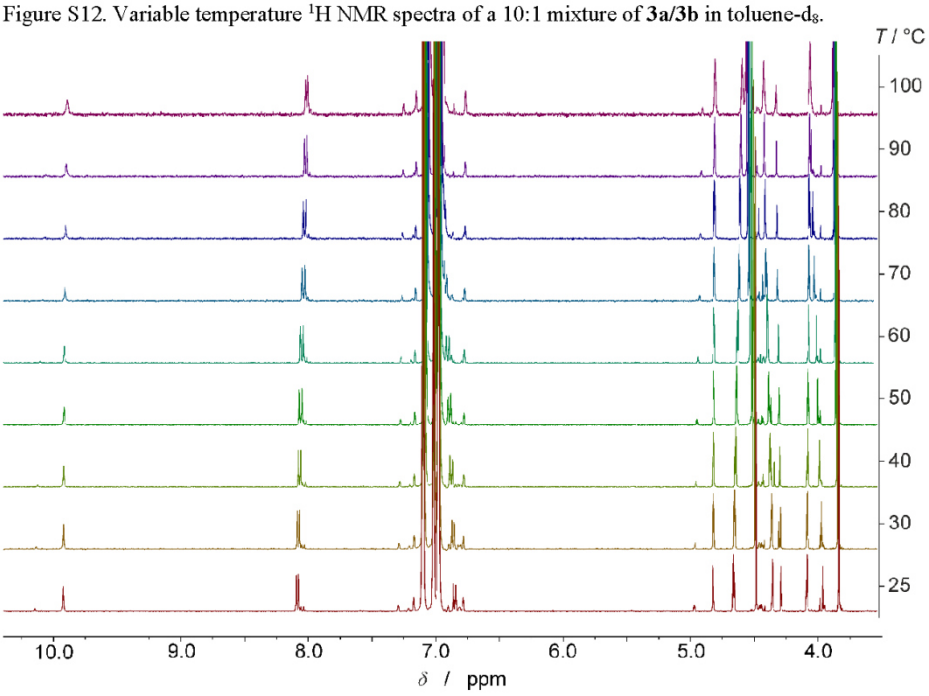

Figure S13. Change in the ratio **3a**:**3b** upon irradiation at 400 nm in CD_2Cl_2 determined by ^1H NMR spectroscopy (integration of proton resonances H^6 and $H^{6'}$).

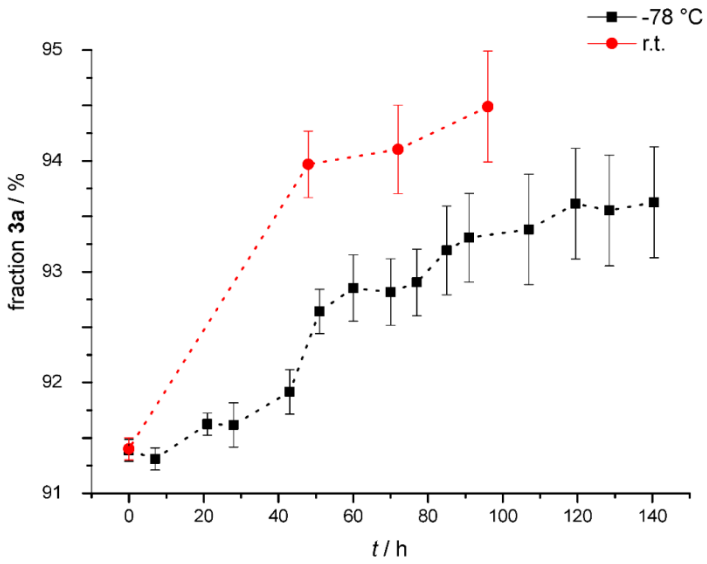

Figure S14. UV/Vis spectrum of a 10:1 mixture of **3a/3b** before and after addition of 1 eq TFA and 1 eq K_2CO_3 in CH_2Cl_2.

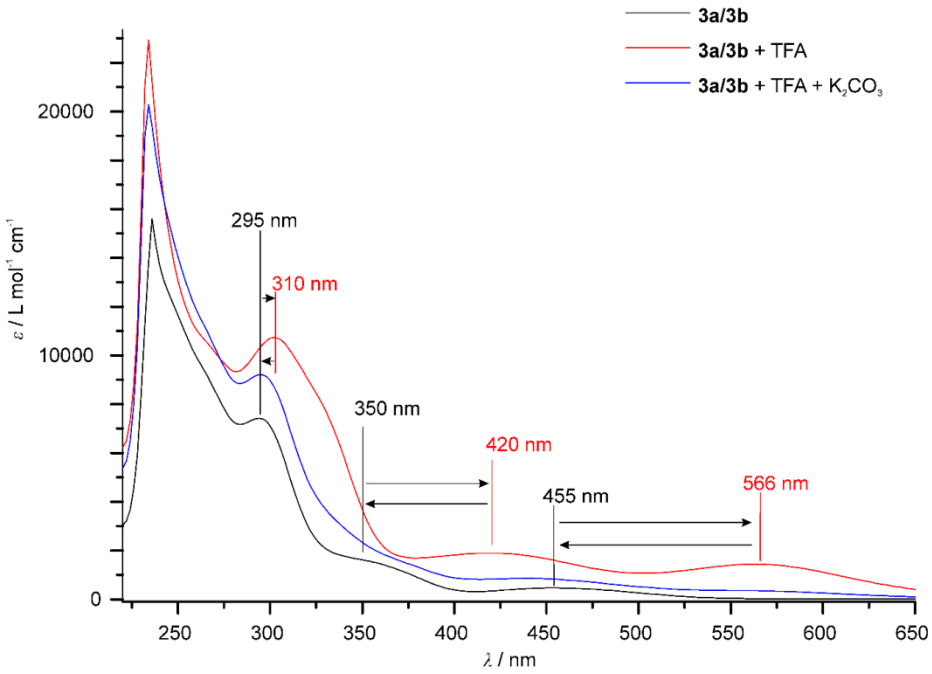

Figure S15. ^{1}H NMR spectra of a) a 10:1 mixture of **3a/3b** b) **3a/3b** + 1 eq TFA and c) **3a**/**3b** + 1 eq TFA + 1 eq K_2CO_3 in CD_2Cl_2.

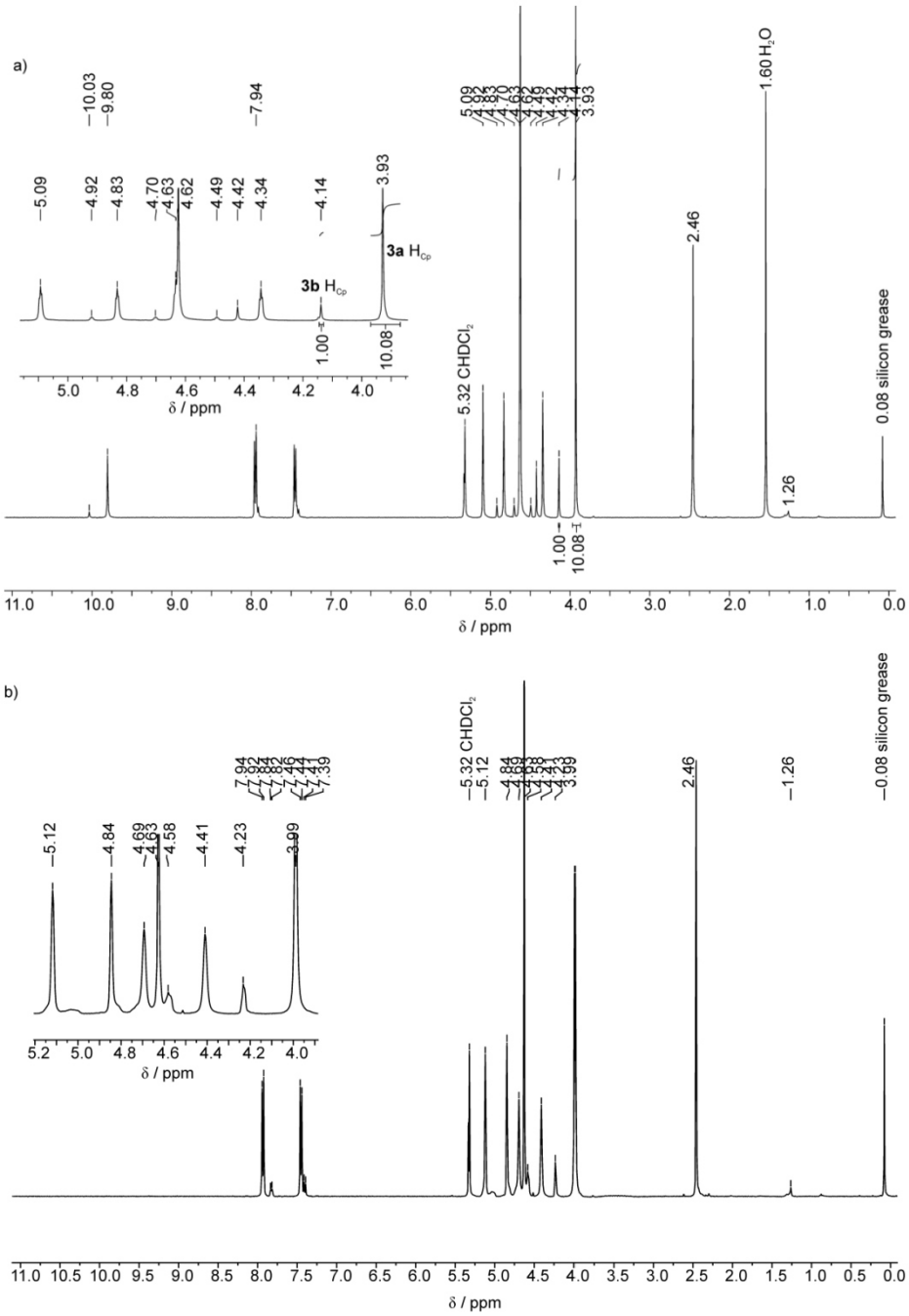

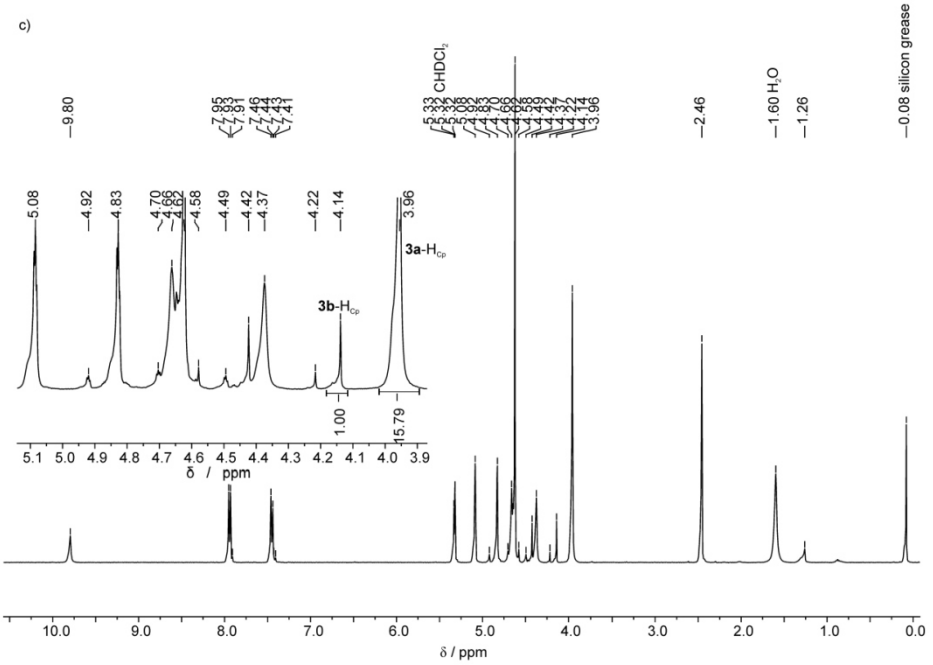

Figure S16. IR spectra of **1**[1], **2** and **3a/b** as KBr disk (NH-region).

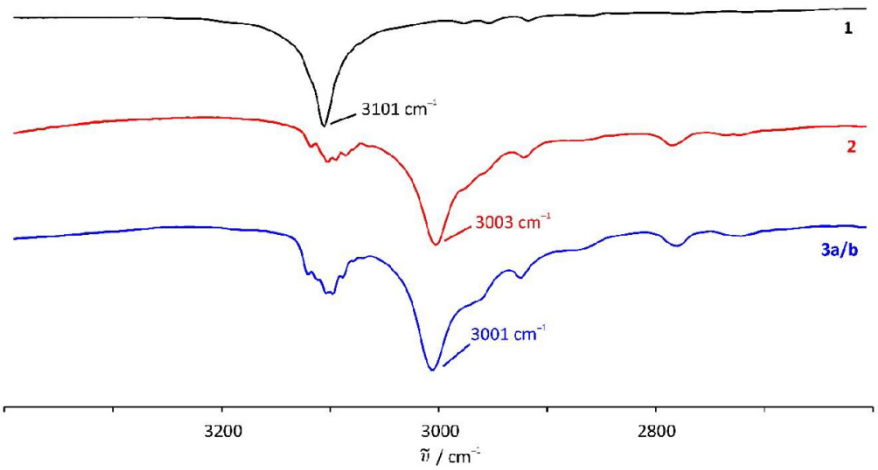

(1) Förster, C.; Veit, P.; Ksenofontov, V.; Heinze, K. *Chem. Commun.* **2015**, *51*, 1514–1516.

6.2 Supporting Information: Preparation, Properties, and Reactivity of (Aminoferrocenyl) (ferrocenyl) carbene (penta-carbonyl) chromium(0) as Bulky Isolobal Trimetallo-amide

Z. Anorg. Allg. Chem. **2015** · ISSN 0044–2313

SUPPORTING INFORMATION

Title: Preparation, Properties, and Reactivity of (Aminoferrocenyl)(ferrocenyl)carbine(pentacarbonyl)-chromium(0) as Bulky Isolobal Trimetallo-amide
Author(s): P. Veit, C. Förster,* S. Seibert, K. Heinze*
Ref. No.: Z201500562

Preparation, properties and reactivity of (aminoferrocenyl)(ferrocenyl)carbene(pentacarbonyl)chromium(0) as bulky isolobal trimetallo-amide

Philipp Veit, Christoph Förster, Sebastian Seibert and Katja Heinze

Supporting Information

Figure S1. FD mass spectrum of **3** and experimental/calculated isotope pattern of the molecular ion peak $[\mathbf{3}]^{\bullet+}$.

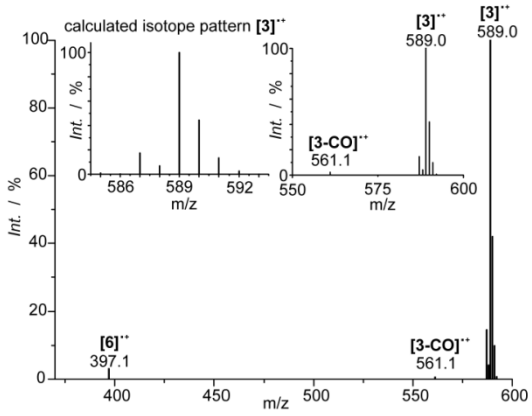

Figure S2. ^{1}H NMR spectrum of **3** in CD_2Cl_2.

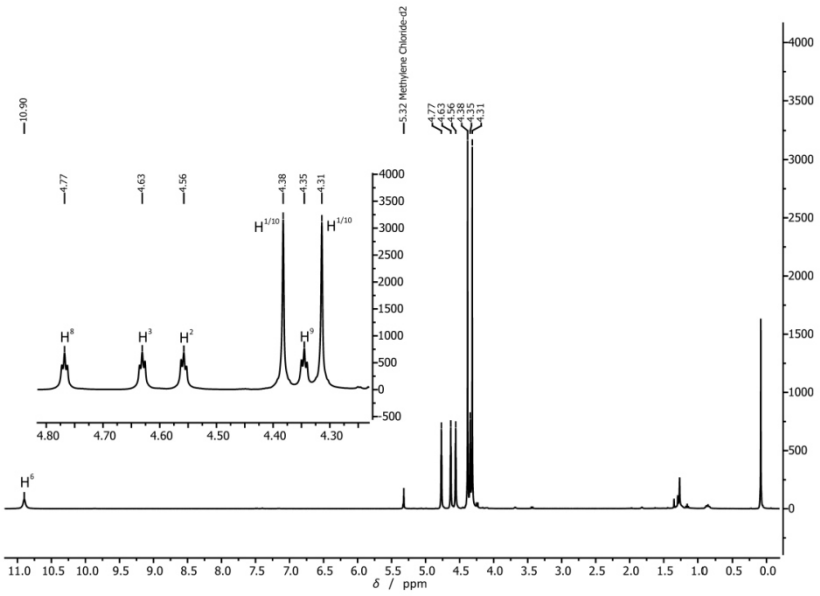

Figure S3. $^{13}C\{^{1}H\}$ NMR spectrum of **3** in CD_2Cl_2.

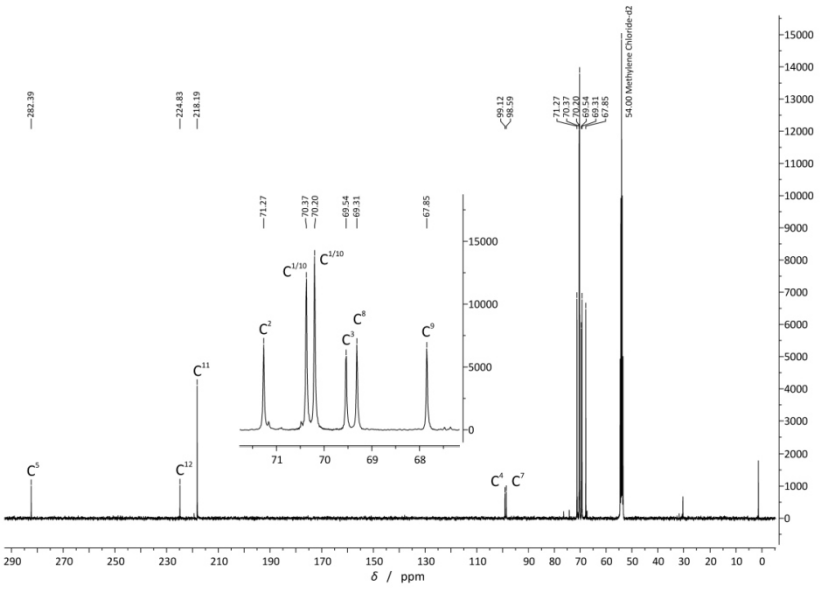

Figure S4. ^{1}H-^{1}H COSY of **3** in CD_2Cl_2.

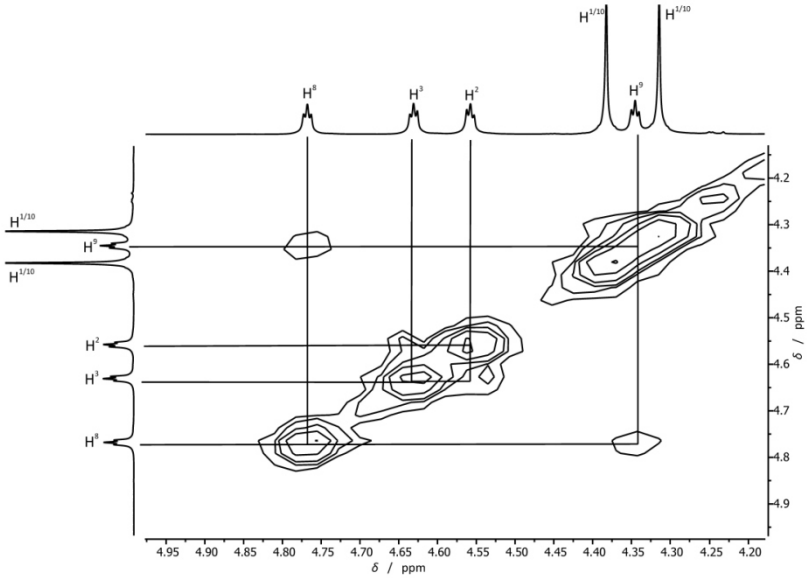

Figure S5. ^{1}H-^{13}C HSQC of **3** in CD_2Cl_2.

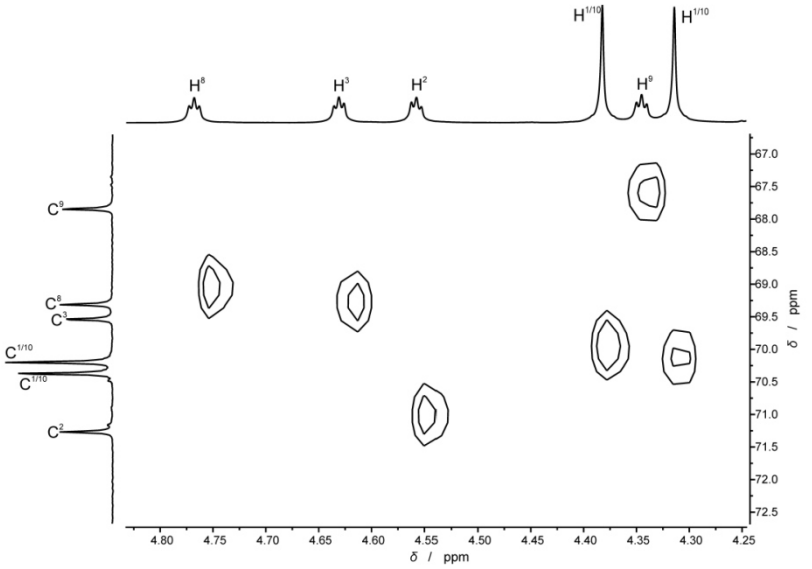

Figure S6. ^{1}H-^{13}C HMBC of **3** in CD_2Cl_2.

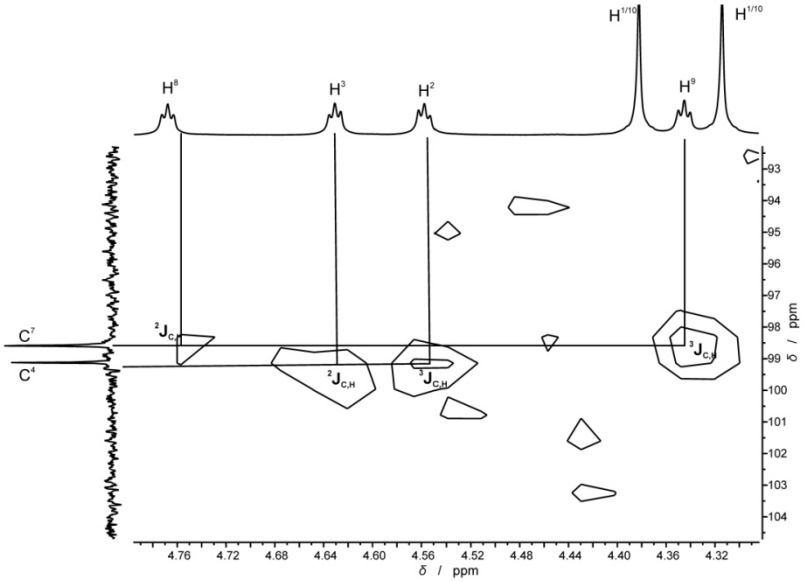

Figure S7. IR spectrum of **3** as KBr disk.

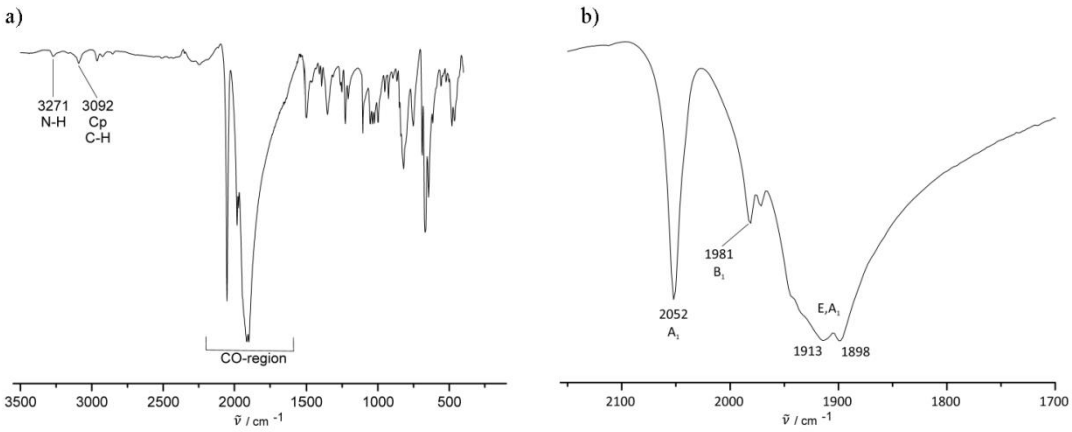

Figure S8. IR spectrum of **3** in CD_2Cl_2 (NH region).

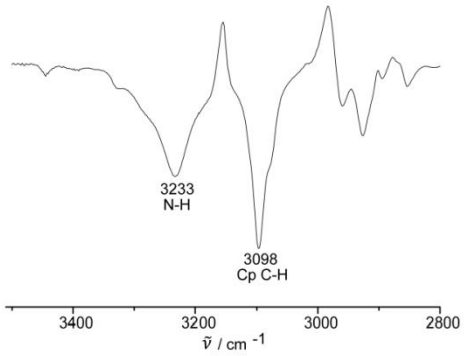

Figure S9. IR spectrum of **3** (black) and **3** with one equivalent of magic blue (red) in THF (CO region).

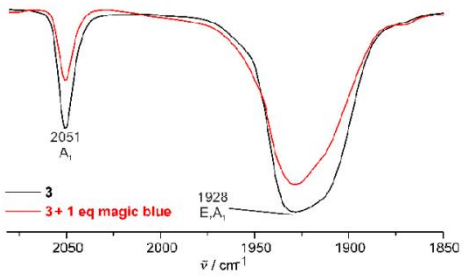

Figure S10. Relevant Kohn-Sham molecular orbitals of **3** (isosurface value 0.1 a.u.).

Orbital 127: HOMO-7

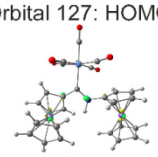

Orbital 128: HOMO-6

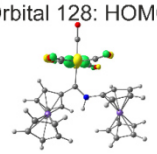

Orbital 129: HOMO-5

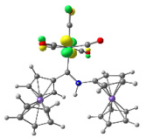

Orbital 130: HOMO-4

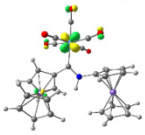

Orbital 131: HOMO-3

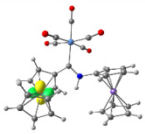

Orbital 132: HOMO-2

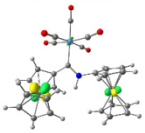

Orbital 133: HOMO-1

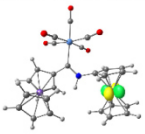

Orbital 134: HOMO

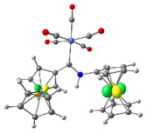

Orbital 135: LUMO

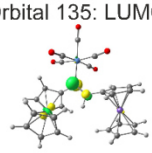

Orbital 136: LUMO+1

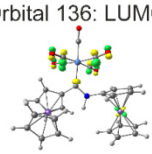

Orbital 137: LUMO+2

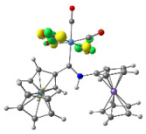

Orbital 138: LUMO+3

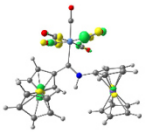

Orbital 139: LUMO+4

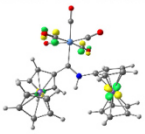

Orbital 140: LUMO+5

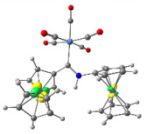

Orbital 141: LUMO+6

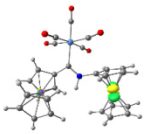

Orbital 142: LUMO+7

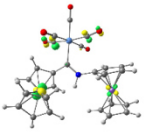

Figure S11. ^{1}H NMR spectrum of a mixture of **3** and **3^{Me}** in CD_2Cl_2.

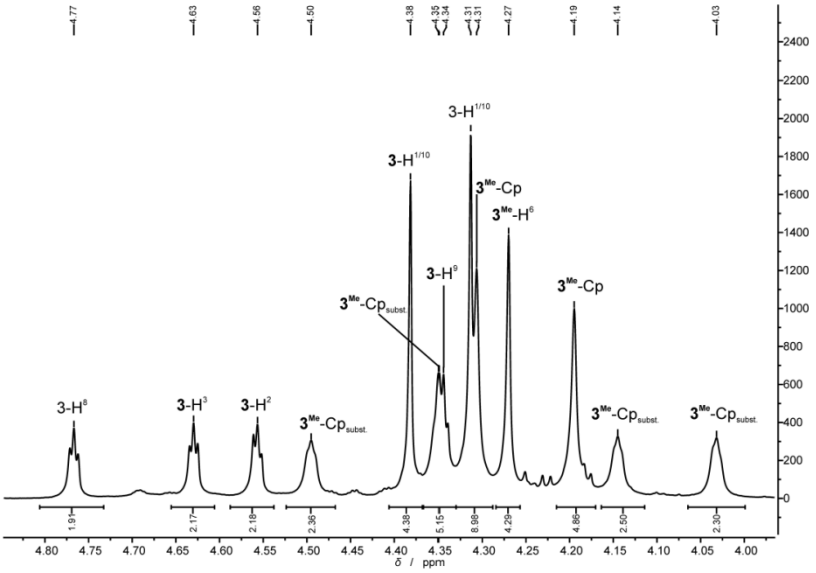

Figure S12. FD mass spectrum of a mixture of **3** and **3^{Me}** and experimental/calculated isotope pattern of the molecular ion peak $[\mathbf{3^{Me}}]^{\bullet+}$.

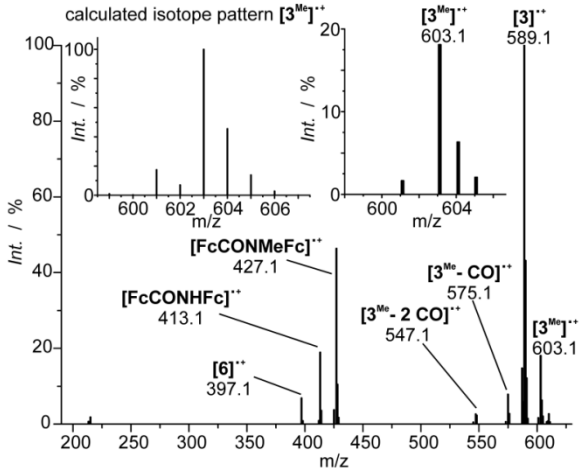

6.3 Supporting Information: On the mechanism of imine elimination from Fischer tungsten carbene complexes

Supporting Information File

for

On the mechanism of imine elimination from Fischer tungsten carbene complexes

Philipp Veit[1], Christoph Förster[1*] and Katja Heinze[1*]

Address: [1]Institute of Inorganic and Analytical Chemistry, Johannes Gutenberg-University, Duesbergweg 10-14, 55128 Mainz, Germany

Email: Christoph Förster - cfoerster@uni-mainz.de; Katja Heinze - katja.heinze@uni.mainz.de

* Corresponding authors

In memoriam Prof. Dr. Peter Hofmann

Experimental spectra and DFT derived data

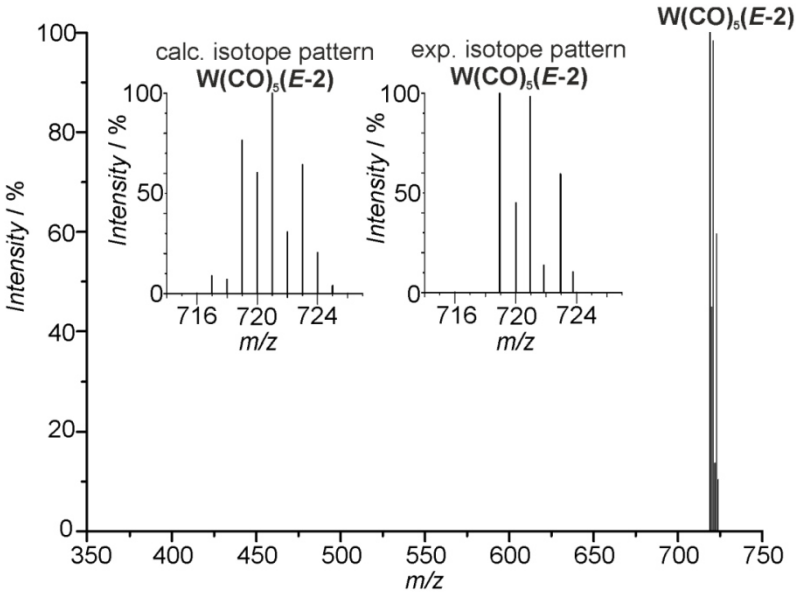

Figure S1: FD mass spectrum of **W(CO)$_5$(*E*-2)** in toluene.

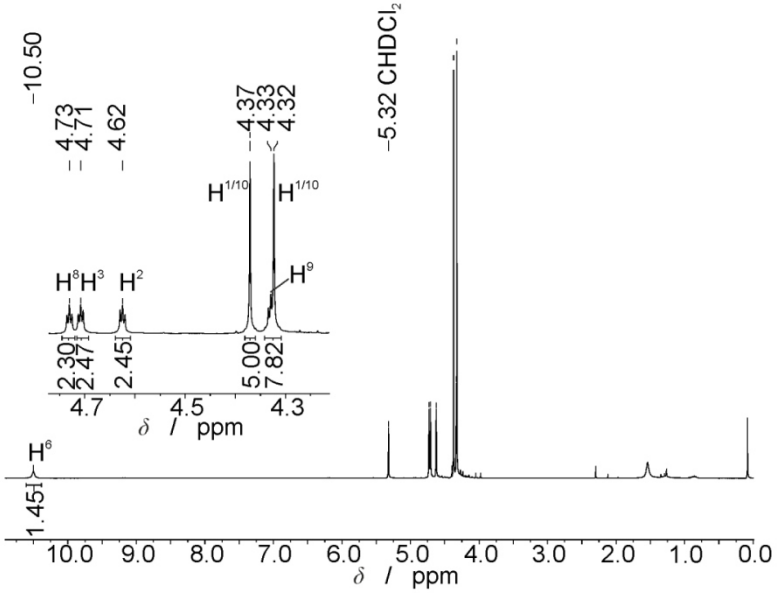

Figure S2: ^{1}H NMR spectrum of **W(CO)$_5$(*E*-2)** in CD_2Cl_2.

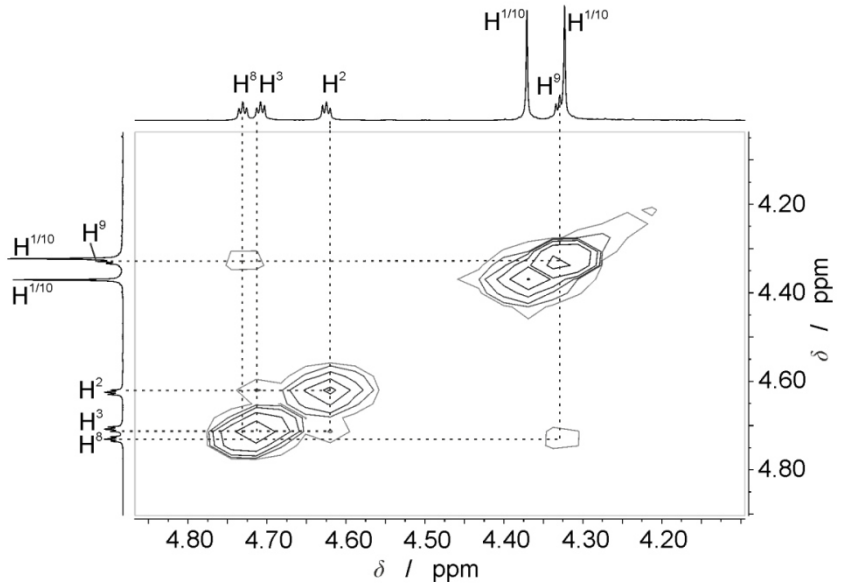

Figure S3: $^{1}H–^{1}H$ COSY of **W(CO)$_5$(*E*-2)** in CD_2Cl_2.

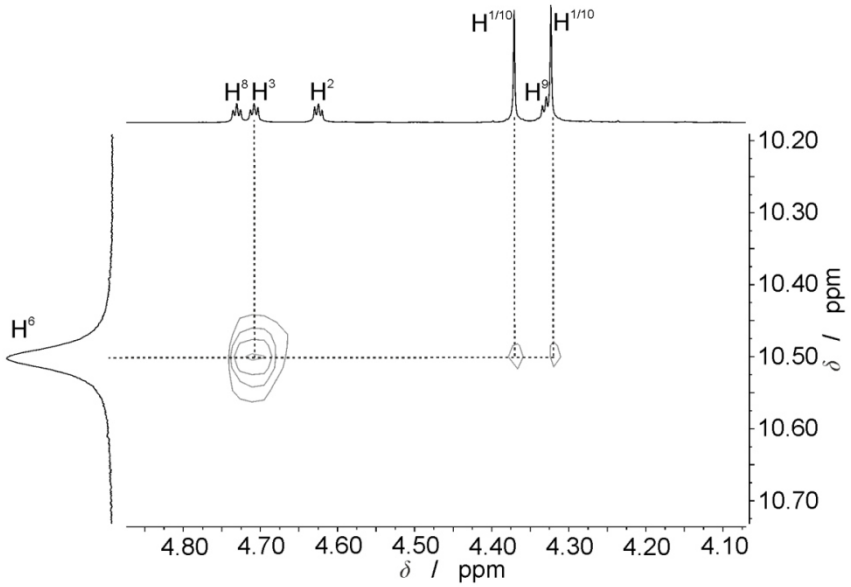

Figure S4: $^{1}H–^{1}H$ NOESY of **W(CO)$_5$(*E*-2)** in CD_2Cl_2.

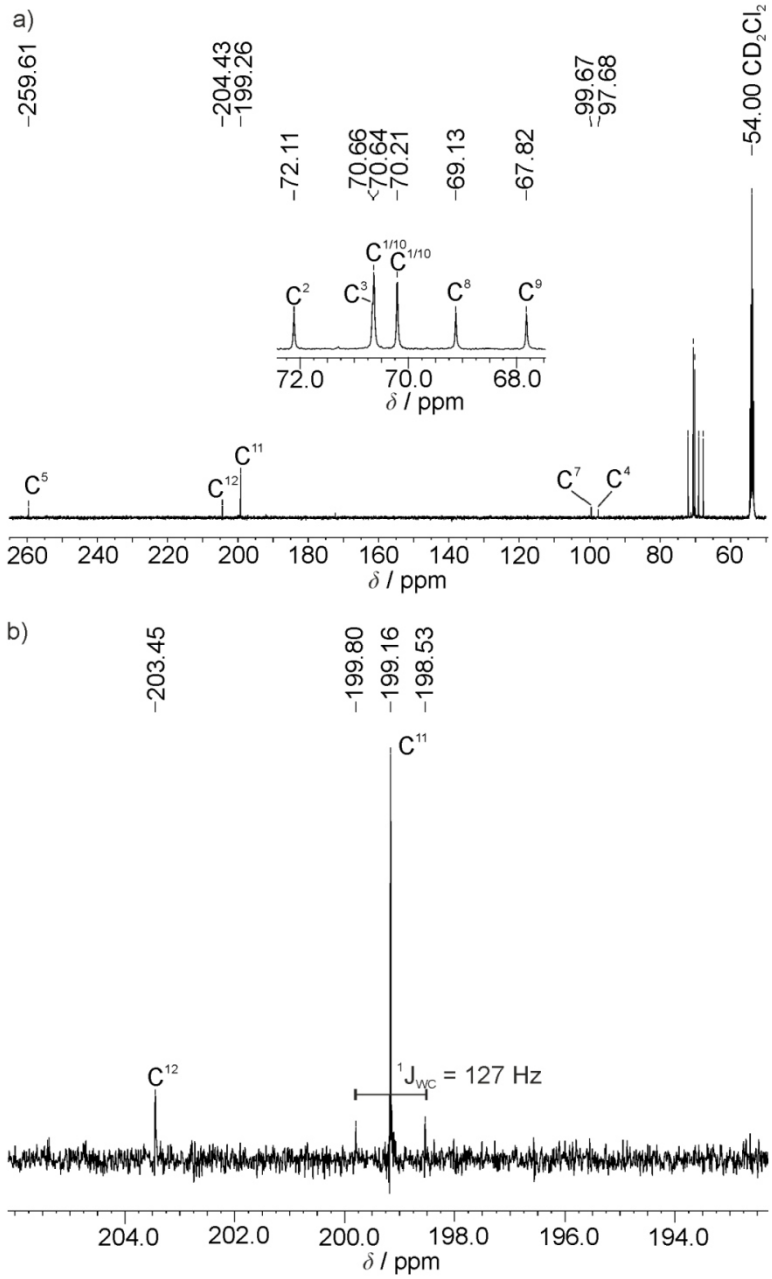

Figure S5: a) $^{13}C\{^1H\}$ NMR spectrum of **W(CO)$_5$(*E*-2)** in CD_2Cl_2 and b) zoom into the CO region showing the ^{183}W satellites in the $^{13}C\{^1H\}$ NMR spectrum of **W(CO)$_5$(*E*-2)** in d_8-toluene.

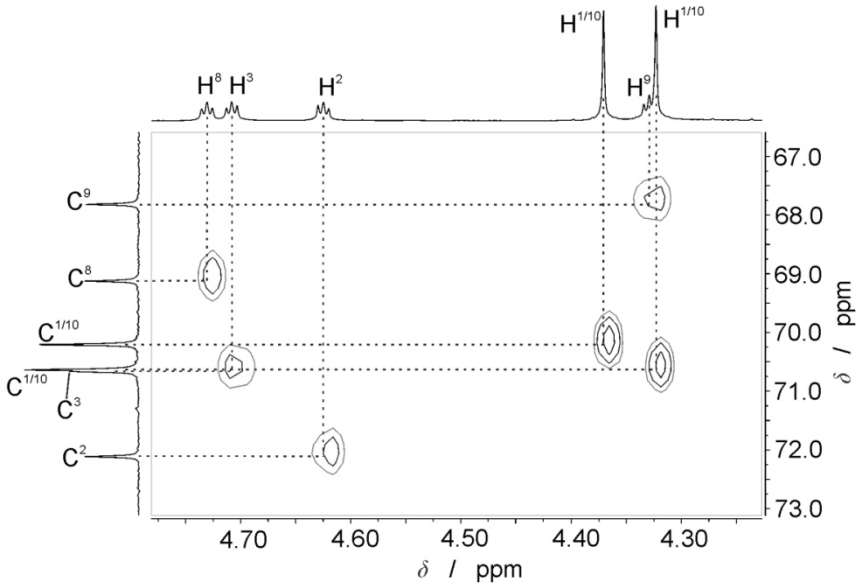

Figure S6: ^{13}C–^{1}H HSQC of **W(CO)$_5$(*E*-2)** in CD_2Cl_2.

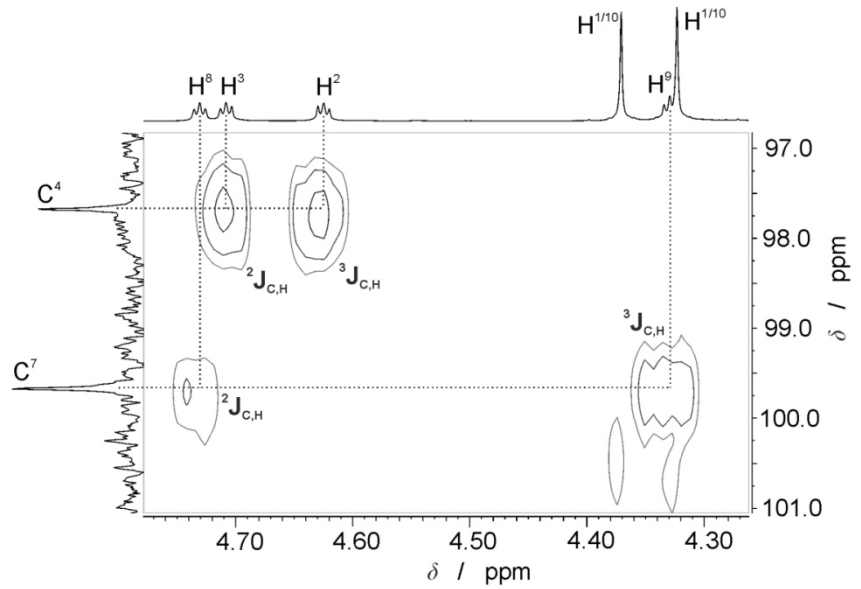

Figure S7: ^{13}C–^{1}H HMBC of **W(CO)$_5$(*E*-2)** in CD_2Cl_2.

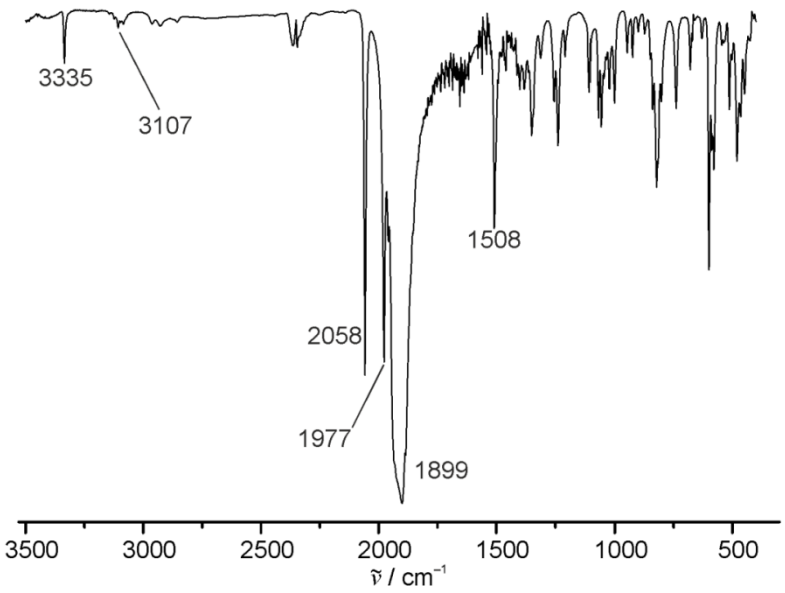

Figure S8: IR spectrum of **W(CO)$_5$(*E*-2)** as KBr disk.

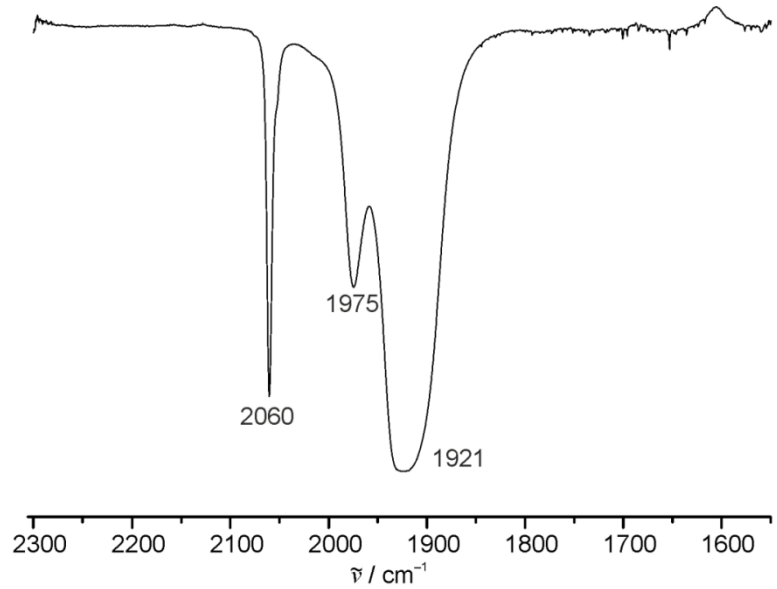

Figure S9: IR spectrum of **W(CO)$_5$(*E*-2)** in CH_2Cl_2 (CO region).

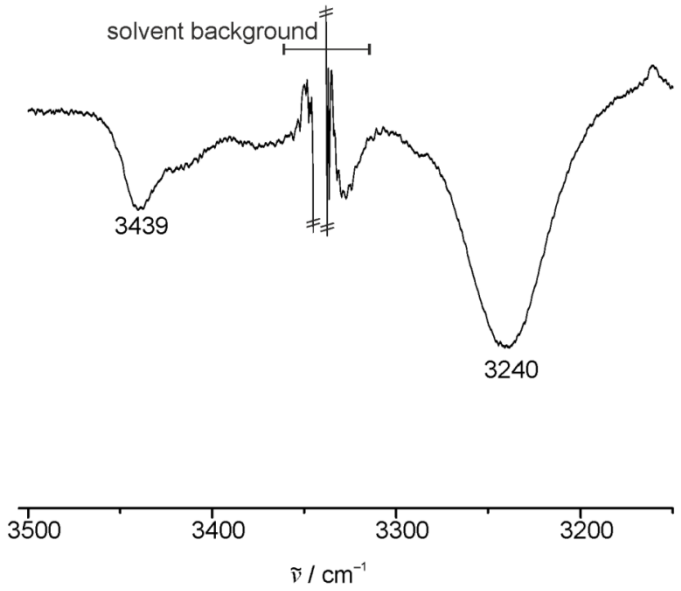

Figure S10: IR spectrum of **W(CO)$_5$(*E*-2)** in CD_2Cl_2 (NH region).

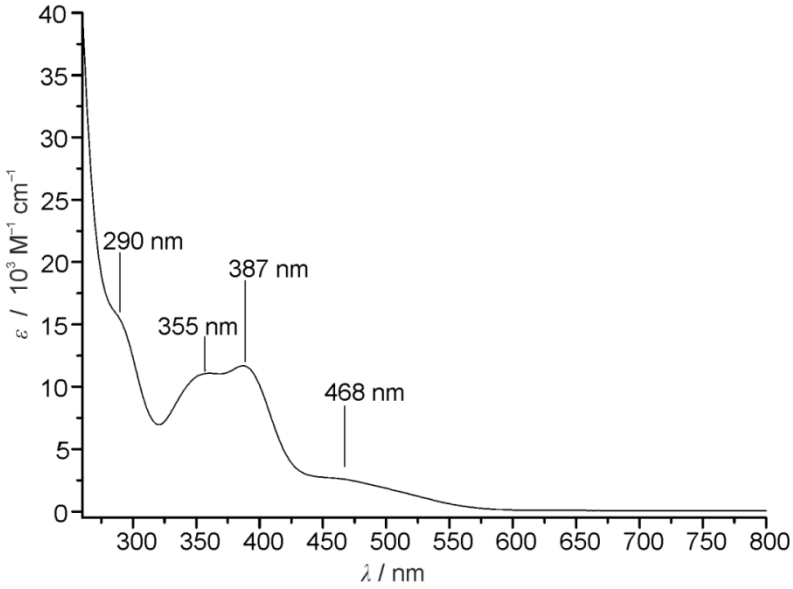

Figure S11: UV–vis spectrum of **W(CO)$_5$(*E*-2)** in CH_2Cl_2.

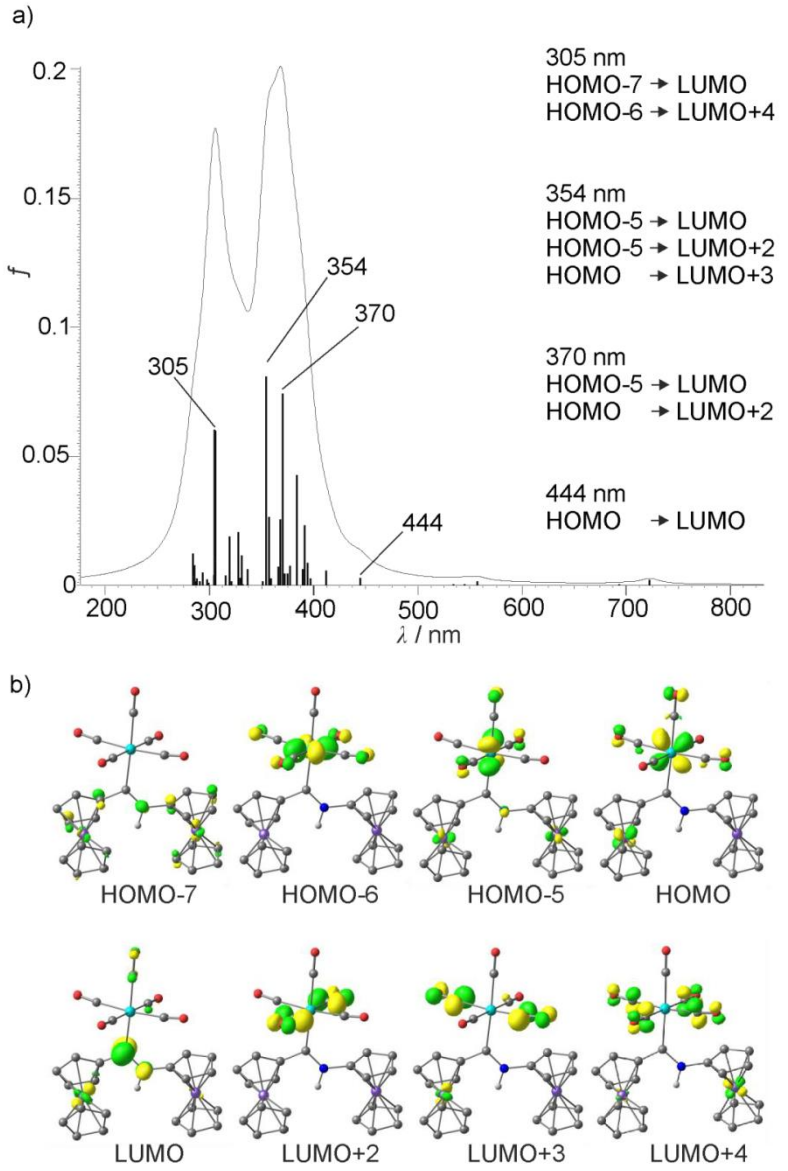

Figure S12: (a) TD-DFT calculated UV/Vis spectrum of **W(CO)$_5$(*E*-2)** with major orbital contributions to the indicated transitions and (b) corresponding orbitals (isosurface values 0.08 a.u.).

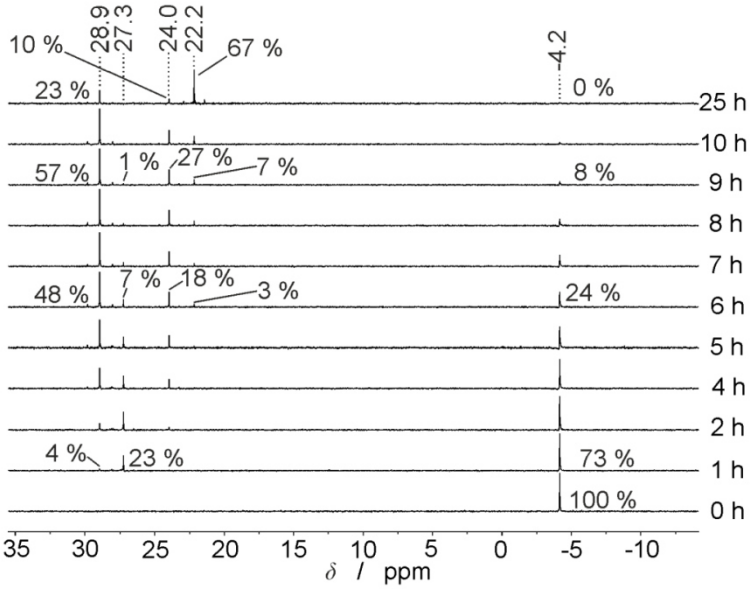

Figure S13: $^{31}P\{^{1}H\}$ NMR spectra of a solution of **W(CO)$_5$(*E*-2)** and 1 equiv PPh_3 in d_8-toluene during heating to 100 °C.

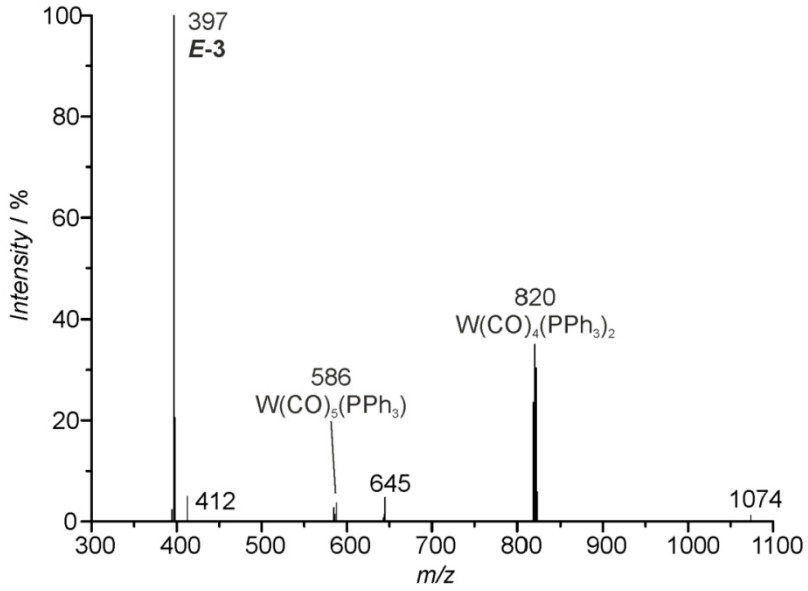

Figure S14: FD mass spectrum of a solution of **W(CO)$_5$(*E*-2)** and 1 equiv PPh_3 in d_8-toluene after heating to 100 °C for 25 h.

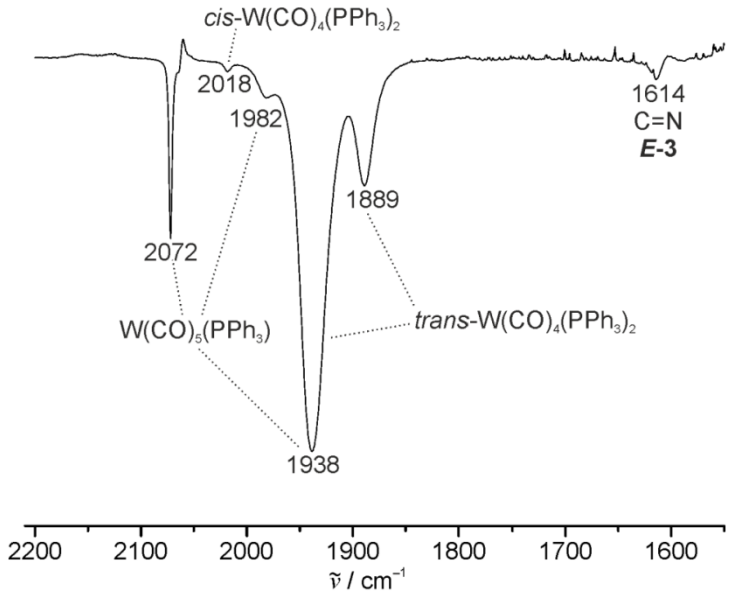

Figure S15: IR spectrum of a solution of **W(CO)$_5$(*E*-2)** and 1 equiv PPh_3 in d_8-toluene after heating to 100 °C for 25 h.

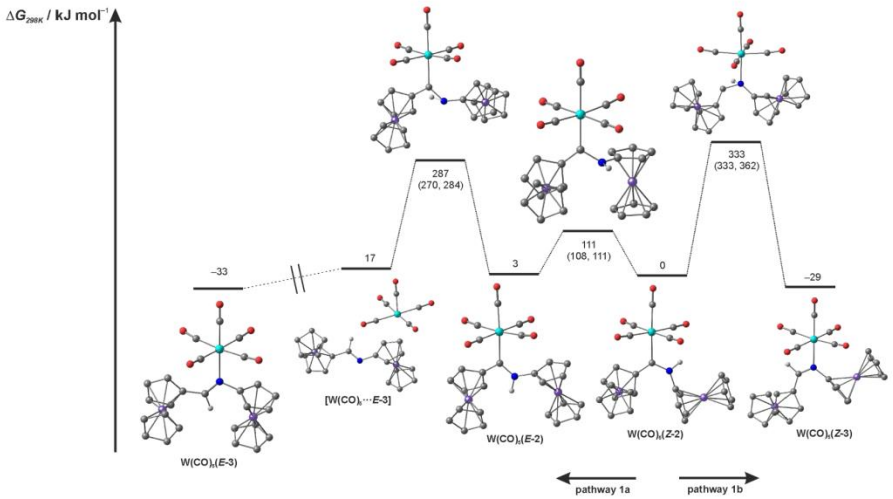

Figure S16: DFT calculated reaction pathway 1a from **W(CO)$_5$(*Z*-2)** to **W(CO)$_5$(*E*-3)** (left) and pathway 1b from **W(CO)$_5$(*Z*-2)** to **W(CO)$_5$(*Z*-3)** (right).

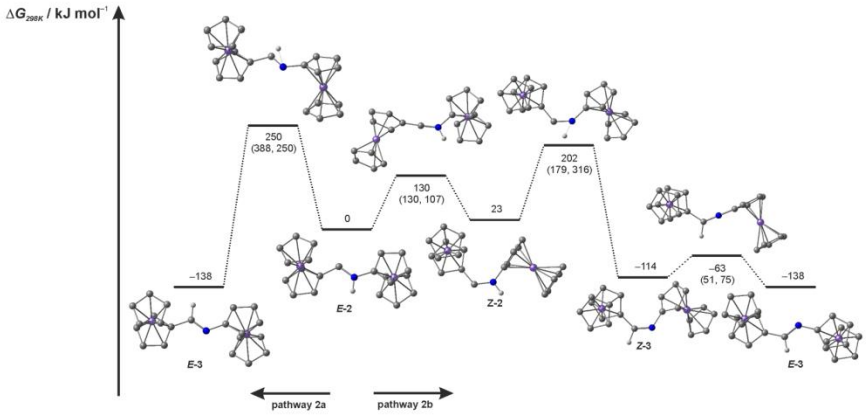

Figure S17: DFT calculated reaction pathway 2a from carbene ***E*-2** to imine ***E*-3** (left) and pathway 2b from carbene ***E*-2** to imine ***E*-3** via imine ***Z*-3** (right).

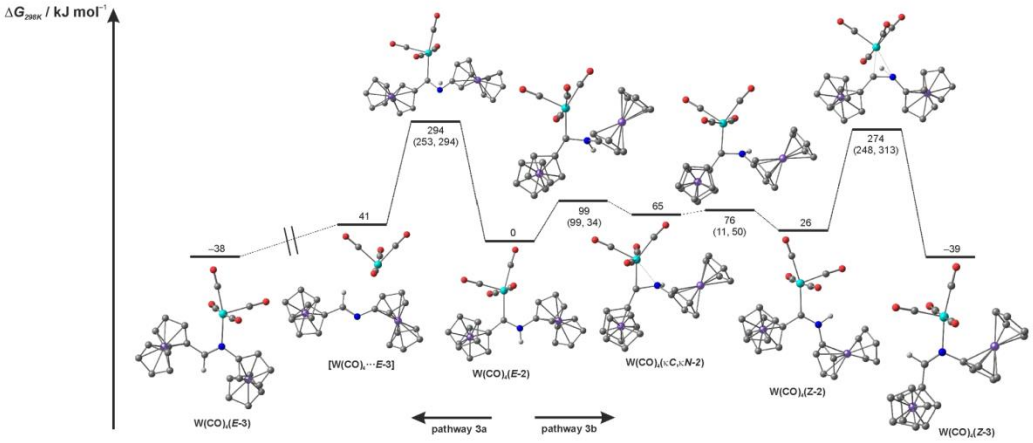

Figure S18: DFT calculated reaction pathway 3a from **W(CO)$_4$(*E*-2)** to **W(CO)$_4$(*E*-3)** (left) and pathway 3b **W(CO)$_4$(*E*-2)** to **W(CO)$_4$(*Z*-3)** (right).

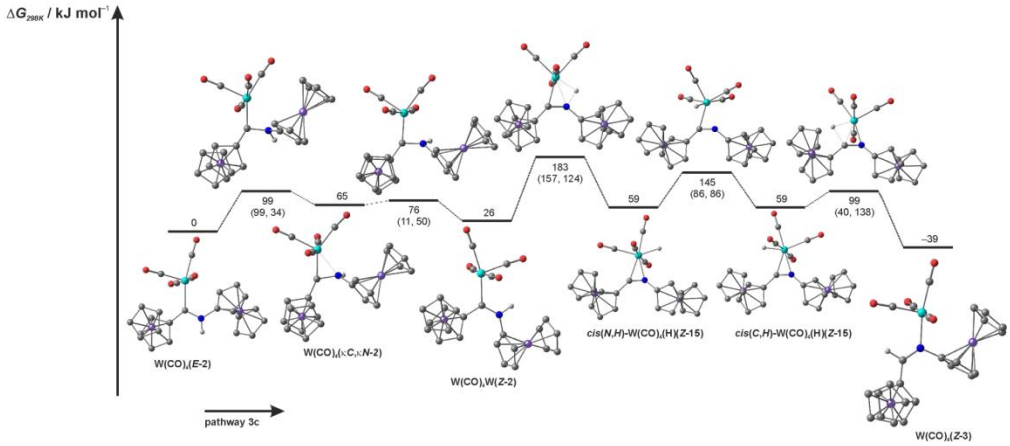

Figure S19: DFT calculated reaction pathway 3c from **W(CO)$_4$(*E*-2)** to **W(CO)$_4$(*Z*-3)** via oxidative addition/reductive elimination.

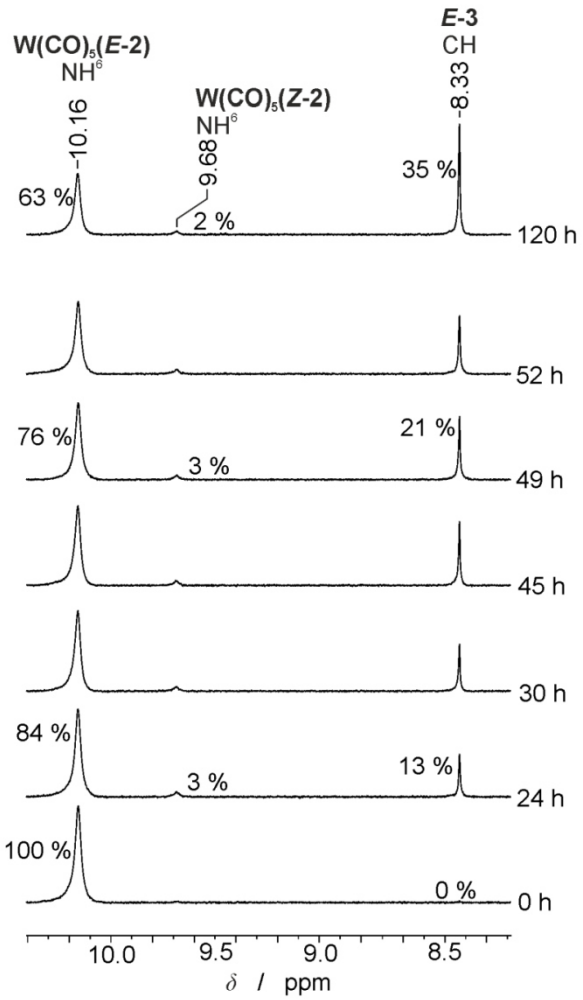

Figure S20: ^{1}H NMR spectroscopic reaction monitoring of the thermolysis of **W(CO)$_5$(*E*-2)** in d_8-toluene at 60 °C.

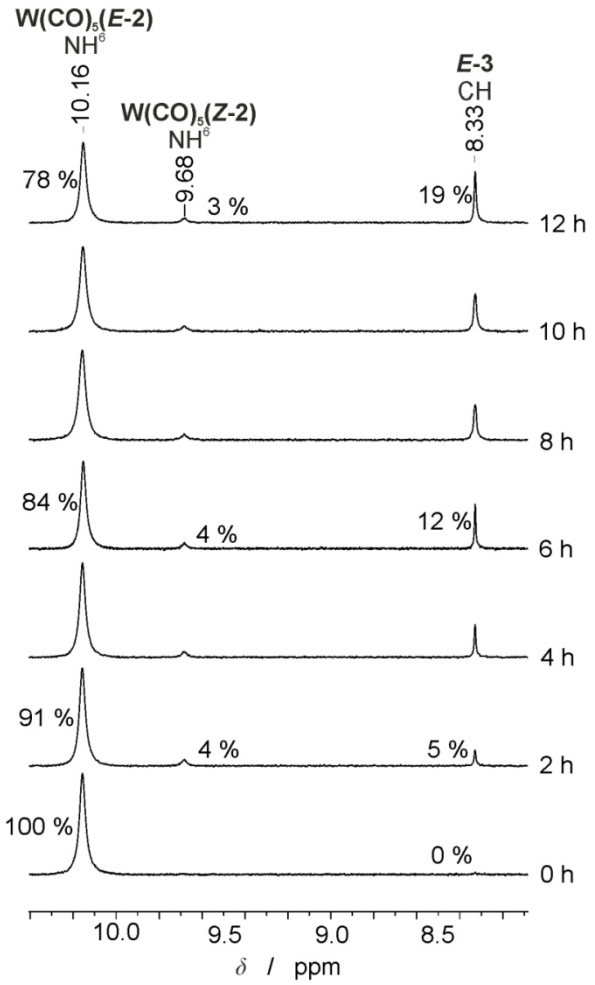

Figure S21: ^{1}H NMR spectroscopic reaction monitoring of the thermolysis of **W(CO)$_5$(*E*-2)** in d_8-toluene at 70 °C.

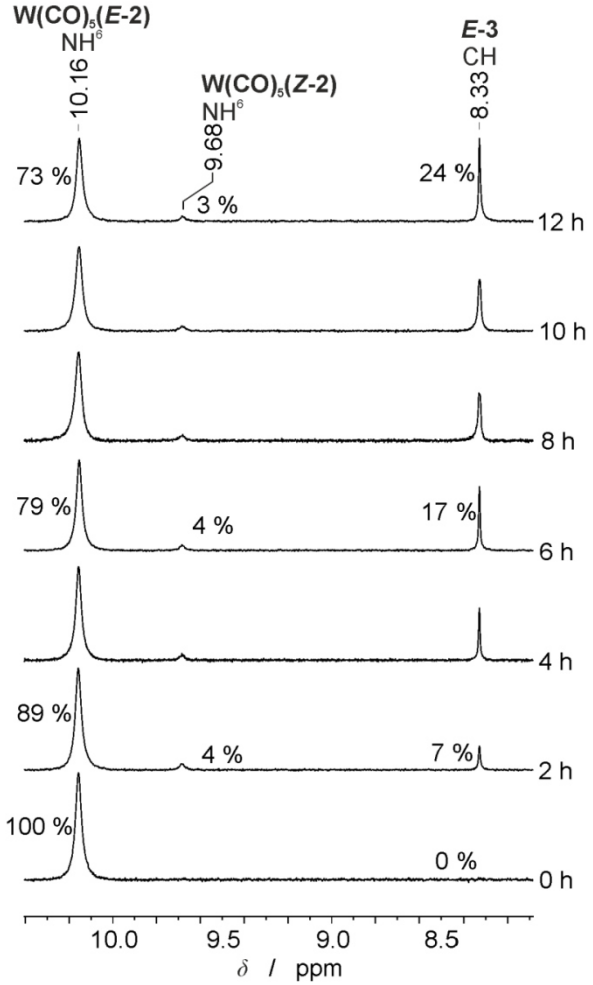

Figure S22: ^{1}H NMR spectroscopic reaction monitoring of the thermolysis of **W(CO)$_5$(*E*-2)** in d_8-toluene at 80 °C.

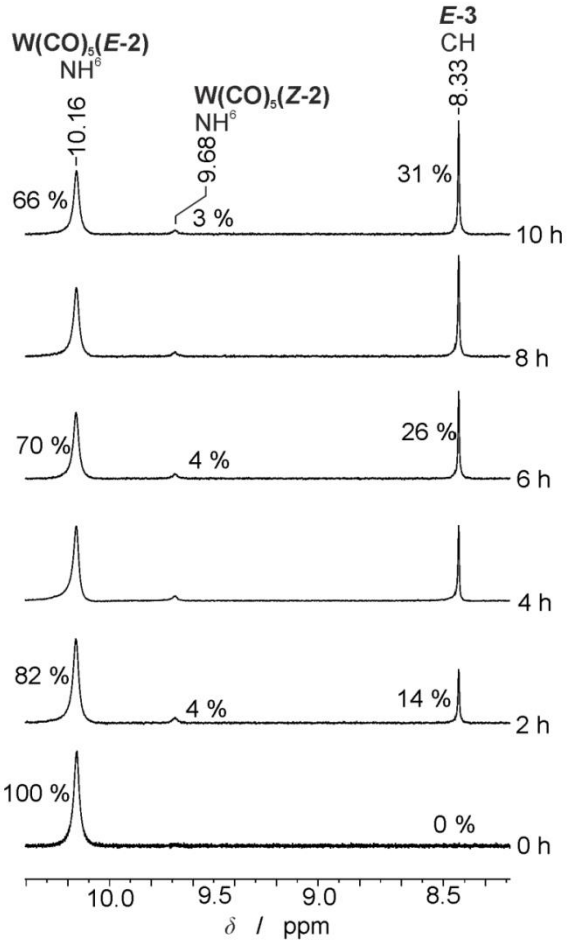

Figure S23: ^{1}H NMR spectroscopic reaction monitoring of the thermolysis of **W(CO)$_5$(*E*-2)** in d_8-toluene at 90 °C.

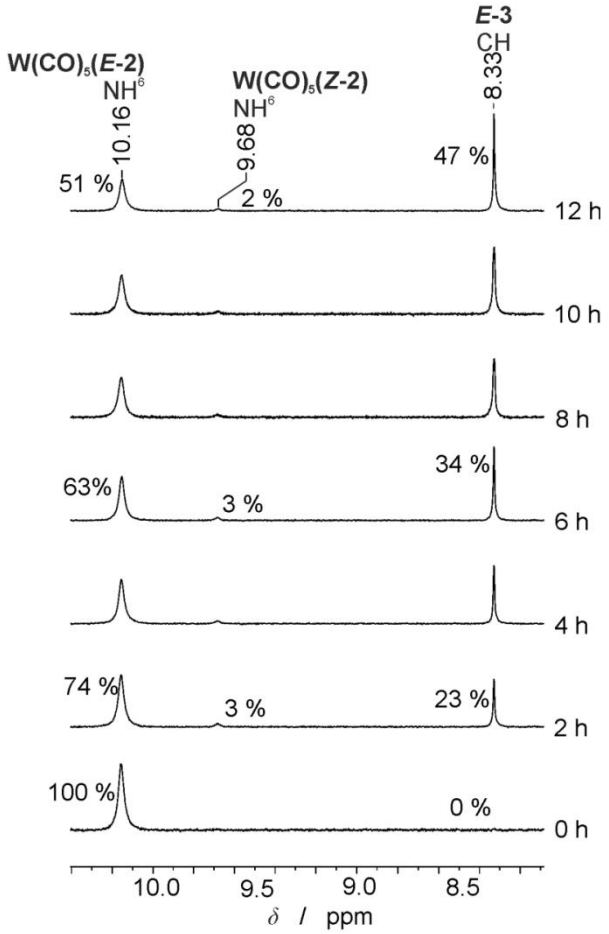

Figure S24: ^{1}H NMR spectroscopic reaction monitoring of the thermolysis of **W(CO)$_5$(*E*-2)** in d_8-toluene at 100 °C.

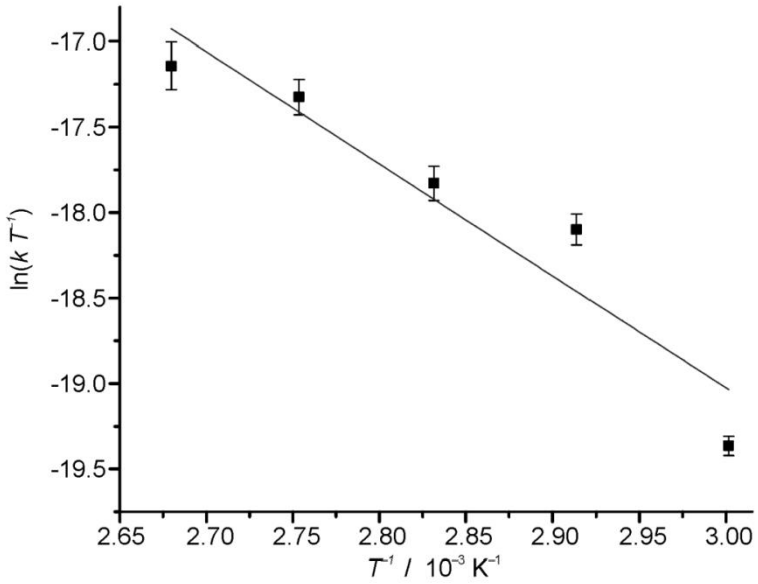

Figure S25: Eyring analysis of the ^{1}H NMR spectroscopic reaction monitoring of the thermolysis of **W(CO)$_5$(*E*-2)** in d_8-toluene at 60 °C, 70 °C, 80 °C, 90 °C and 100 °C.

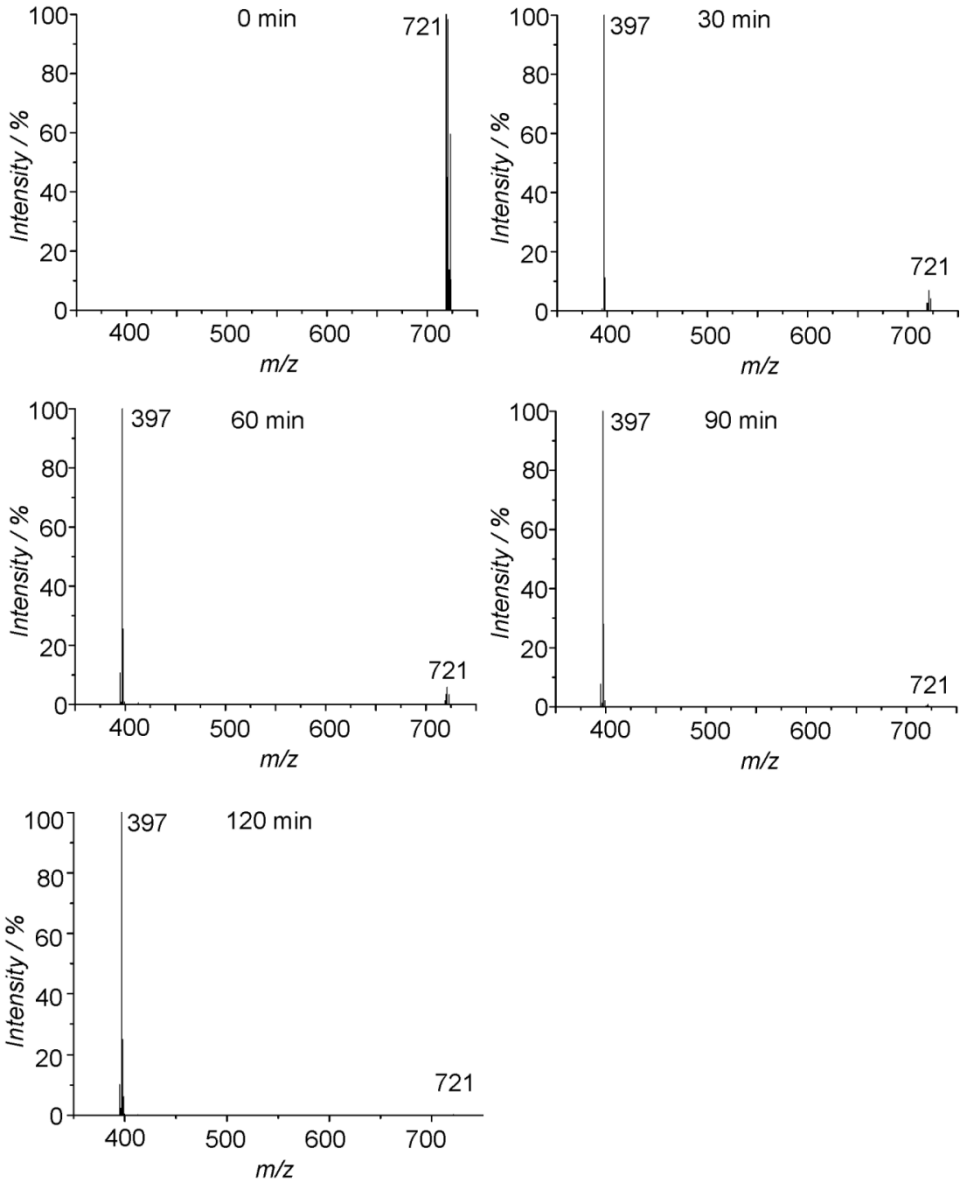

Figure S26: FD mass spectrometric reaction monitoring of the thermolysis of **W(CO)$_5$(*E*-2)** in toluene at 100 °C.

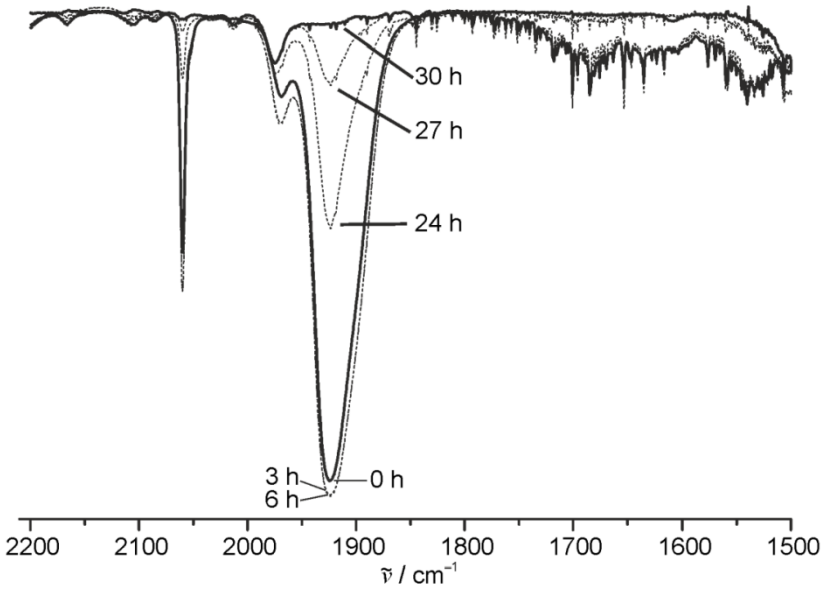

Figure S27: IR spectroscopic reaction monitoring of the thermolysis of **W(CO)$_5$(*E*-2)** in 1,2-dichloroethane at 84 °C.

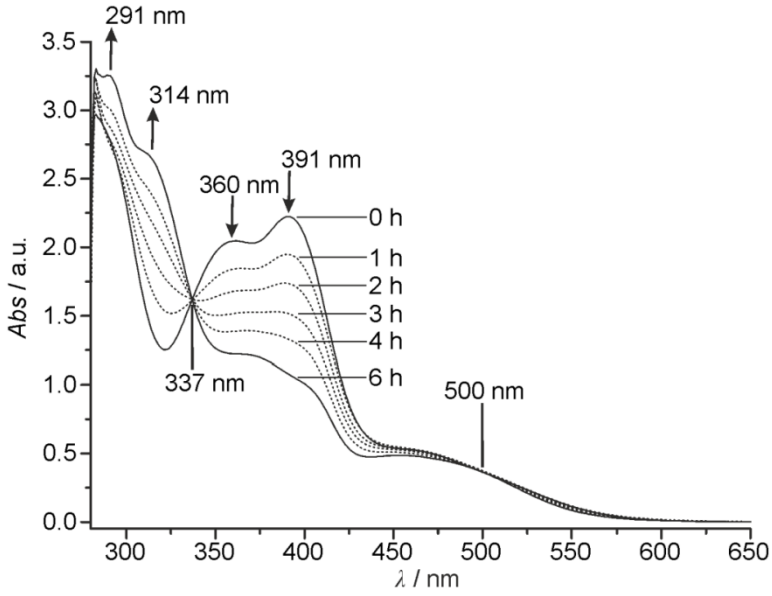

Figure S28: UV–vis spectroscopic reaction monitoring of the thermolysis of **W(CO)$_5$(*E*-2)** in toluene at 100 °C.

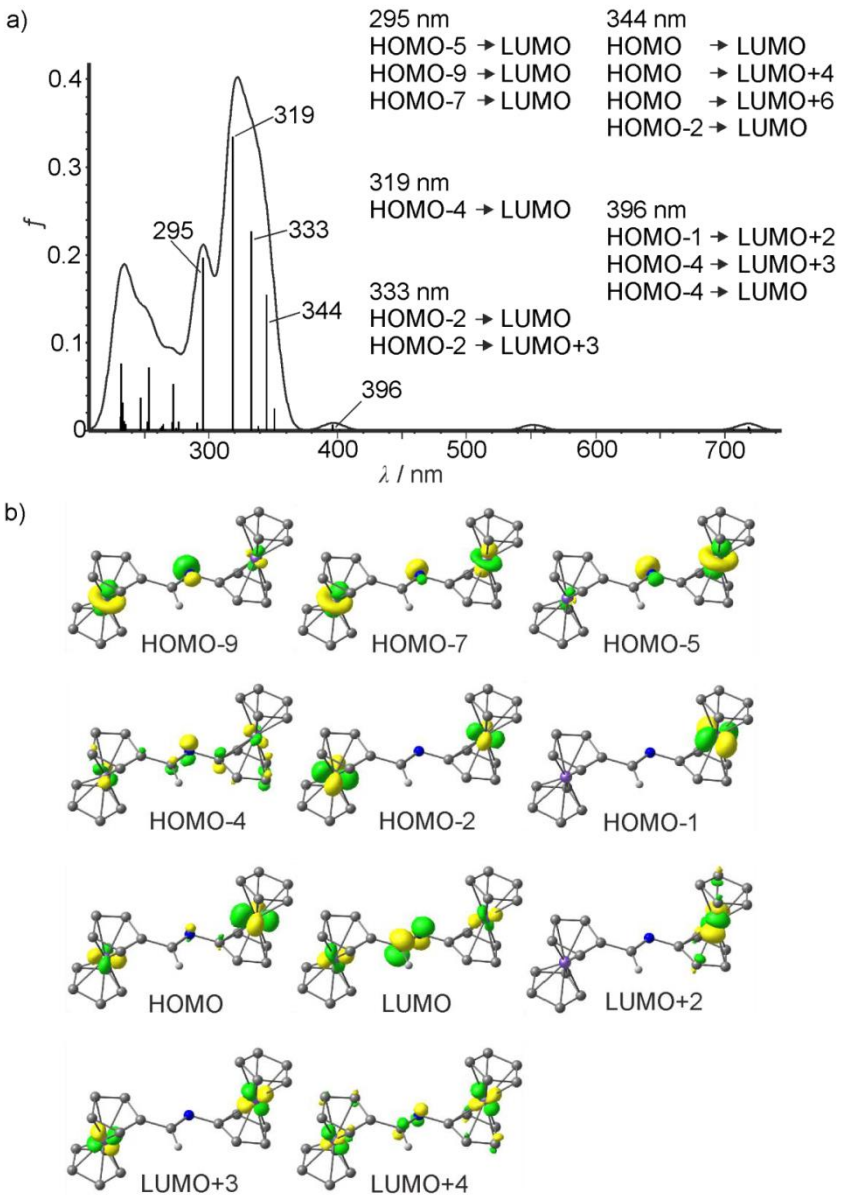

Figure S29: (a) TD-DFT calculated UV–vis spectrum of ***E*-3** with major orbital contributions to the indicated transitions and (b) corresponding orbitals (isosurface values 0.08 a.u.).

6.4 Supporting Information: Gold(II) in redox-switchable gold(I) catalysis

Electronic Supplementary Material (ESI) for ChemComm.
This journal is © The Royal Society of Chemistry 2019

General Procedures

All reactions were performed under argon atmosphere unless otherwise noted. A glovebox of the type UniLab/MBraun (Ar 4.8, O_2 < 1 ppm, H_2O < 1 ppm) was used for storage and weighing of sensitive compounds. All analytical samples that required the absence of oxygen were prepared in the same glovebox. Dichloromethane was dried with CaH_2 and distilled prior to use. THF was distilled from potassium. All reagents were used as received from commercial suppliers (ABCR, Acros Organics, Alfa Aesar, Fischer Scientific, Fluka and Sigma-Aldrich). Deuterated solvents were purchased from eurisotop. $W(CO)_5$[C(Fc)OEt] was synthesized using literature procedures.[1] NMR spectra were recorded on a Bruker Avance DRX 400 spectrometer at 400.31 MHz (^{1}H) and 100.07 MHz ($^{13}C\{^1H\}$). All resonances are reported in ppm versus the solvent signal as internal standard [CD_3CN (^{1}H: δ = 1.94), CD_2Cl_2 (^{1}H: δ = 5.32 ppm; ^{13}C: δ = 54.0 ppm)].[2] IR spectra were recorded as solid state samples with a Bruker ALPHA II FT-IR spectrometer with a platinum Di-ATR module. Electrochemical experiments were carried out on a BioLogic SP-50 voltammetric analyser using platinum wires as counter and working electrodes and a 0.01 M Ag/$AgNO_3$ electrode as reference electrode. The cyclic voltammetry measurements were carried out at scan rate of 50–100 mV s^{-1} using 0.1 M [nBu$_4$N][B(C_6F_5)$_4$] or 0.1 M [nBu$_4$N][PF_6] as supporting electrolytes in CH_2Cl_2 of THF. Potentials are referenced to the ferrocene/ferrocenium couple ($E_{½}$ = 220 ± 5 mV under the experimental conditions). UV/Vis/NIR spectra were recorded on a Varian Cary 5000 spectrometer using 1.0 cm cells (Hellma, suprasil). FD mass spectra were recorded on a Thermo Fisher DFS mass spectrometer with a LIFDI upgrade. Elemental analyses were performed by the microanalytical laboratory of the chemical institutes of the University of Mainz. ^{57}Fe Mößbauer measurements of powder samples were performed in transmission geometry using a constant-acceleration spectrometer and the source ^{57}Co(Rh). The Recoil 1.03 Mössbauer Analysis Software was used to fit the experimental spectra with Lorentzian peaks.[3] Isomer shift values are quoted relative to α-Fe at 293 K. X-band CW EPR spectra were measured on a Miniscope MS 300 at 77 K cooled by liquid nitrogen in a finger Dewar and at 298 K (Magnettech GmbH, Berlin, Germany). g factors are referenced to external Mn^{2+} in ZnS (g = 2.118, 2.066, 2.027, 1.986, 1.946, 1.906). Simulations of EPR spectra were performed with EasySpin (v 5.0.0) for MatLab (R2016b).[4] XAS spectral measurements were performed at beamline P64 of PETRA III (Hamburg, Germany) under ambient conditions at 293 K. A Si(111) double crystal monochromator was used for measurements at the Au L_3-edge (11.918 keV). The second monochromator crystal was tilt for optimal harmonic rejection. Energy calibration was performed with a gold metal foil. The samples were handled in a glove box. All samples were prepared as self supporting wafers using degassed BN as binder.

DFT calculations

Density functional theory calculations were carried out using the ORCA program package (version 4.0.1).[5] All calculations were performed using the B3LYP functional[6–8] and employ the RIJCOSX approximation.[9,10] Relativistic effects were calculated at the zeroth order regular approximation (ZORA) level.[11] The ZORA keyword automatically invokes relativistically adjusted basis sets. To account for solvent effects, a conductor-like screening model (CPCM) modelling dichloromethane was used in all calculations.[12,13] Geometry optimizations were performed using Ahlrichs' split-valence triple-ξ basis set ZORA-def2-TZVP.[14] The auxiliary basis set for General-purpose Coulomb fitting SARC/J decontracted def2/J up to Kr was used.[15] The segmented all-electron relativistically contracted (SARC) auxiliary basis set beyond Kr, SARC-ZORA-TZVP, was used for gold and a special grid of 7 (default 4).[11,16–19] Atom-pairwise dispersion correction was performed with the Becke-Johnson damping scheme (D3BJ).[20,21] The presence of energy minima was checked by numerical frequency calculations.

Synthesis of 1, AuCl[C(Fc)OEt]

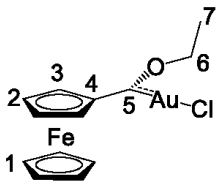

A slightly modified literature procedure for the synthesis of AuCl[C(Fc)OMe] was used for the synthesis of **1**.[22] To a solution of $W(CO)_5$[C(Fc)(OEt)][23] (1 mmol, 565.5 mg, 1 eq) in THF (10 mL) chlorido(dimethylsulfide)gold(I) (1 mmol, 294.6 mg, 1 eq) was added under stirring at 0 °C. The deep red solution was stirred at this temperature for 6 h. After filtration, *n*-heptane (10 mL) was added and the red-purple solution was stored at −28 °C for 3 days. Filtration yielded a deep purple solid. Yield 340.4 mg (0.72 mmol 72 %). ^{1}H NMR (400.32 MHz, CD_2Cl_2): δ = 5.17 (pt, 2H, H^2), 5.00 (q, $^3J_{HH}$ = 8 Hz, 2H, H^6), 5.00 (pt, 2H, H^3; under the q of the OCH_2 group confirmed by COSY), 4.47 (s, 5H, H^1), 1.56 (t, $^3J_{HH}$ = 8 Hz, 3H, H^7) ppm. ^{1}H NMR (400.32 MHz, CD_3CN) δ = 5.25 (pt, 2H, H^2), 5.03 (pt, 2H, H^3), 4.96 (q, $^3J_{HH}$ = 8 Hz, 2H, H^6), 4.50 (s, 5H, H^1), 1.54 (t, $^3J_{HH}$ = 8 Hz, 3H, H^7) ppm. ^{13}C NMR (100.07 MHz, CD_2Cl_2): δ = 250.9 (C^5), 87.2 (C^4), 80.3 (C^3), 79.5 (C^2), 79.0 (C^6; confirmed by HSQC), 72.1 (C^1), 15.3 (C^7) ppm. MS (FD): *m/z* (%) = 474.3 (100) $[M]^+$. IR (ATR) $\tilde{\nu}$ = 3092 (w), 2933 (w), 1364 (m) 1107 (m), 826 (m), 823 (m), 480 (s) cm^{-1}. UV/Vis (CH_2Cl_2): λ_{max} (ε) = 266 (2270), 304 (3550), 374 (1010), 521 (1040 M^{-1} cm^{-1}) nm. Anal. Calcd for $C_{13}H_{14}FeAuClO$ (473.97): C, 32.90; H, 2.97. Found: C, 32.60; H 2.87.

General Procedure for the Catalytic Cyclization of *N*(2-propyn-1-yl)benzamide to 2-phenyl-5-vinylidene-2-oxazoline

N-Prop-2-yne-benzamide (15.9 mg, 0.1 mmol, 1 eq) was dissolved in CD_2Cl_2 (1 mL) in an inert-gas NMR tube, **1** (0.5 mg, 1.0×10^{-3} mmol, 1 mol-%), tris(4-bromophenyl)ammoniumyl hexachloroantimonate (Magic Blue; 1.0 mg, 1.25×10^{-3} mmol, 1.25 mol %) and *n*-hexadecane (3 µL) as internal standard were added. ^{1}H NMR spectra were recorded over time. The proton resonances (*ortho* protons of phenyl ring, H^3) of the starting material (δ = 7.77) and the product (δ = 7.98) were integrated.

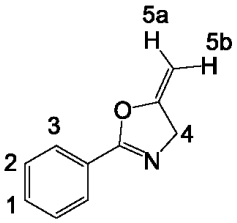

EPR calibration

Quantification of the EPR signals was performed via an adapted literature procedure.[24,25] For quantification measurements, EPR tubes with an internal diameter of 2.0 mm were used. The calibration curve was determined using commercially available tetraphenylporphyrinato copper(II) (CuTPP) as standard. The samples were prepared in a glovebox under argon, and the EPR tubes were filled with 400 µL of the solution and sealed with Critoseal. They were inserted 10.4 cm (measured at the Teflon holder) into the EPR spectrometer. Four concentrations (c = 1.67, 0.84, 0.42 and 0.21 mM) in THF were used for the calibration. The settings for the calibration curve and the sample EPR spectra were as follows: temperature = 298 K, field = 3360 G, sweep = 800 G, sweep time = 300 s, modulation = 2000 mG, MW attenuation = 6 db, and number of passes = 3. The double integral of the experimental, baseline corrected spectra was plotted against the concentration. The resulting calibration (linear regression; $y = (2.97 \pm 0.03) \times 10^6 \times c$(mM); $R^2 = 0.9986$) was used to quantify the experimental spectra of **1** after oxidation with Magic Blue.

References

[1] J. G. López-Cortés, L. F. La Contreras de Cruz, M. C. Ortega-Alfaro, R. A. Toscano, C. Alvarez-Toledano and H. Rudler, *J. Org. Chem.*, 2005, **690**, 2229–2237.

[2] G. R. Fulmer, A. J. M. Miller, N. H. Sherden, H. E. Gottlieb, A. Nudelman, B. M. Stoltz, J. E. Bercaw and K. I. Goldberg, *Organometallics*, 2010, **29**, 2176–2179.

[3] K. Lagarec and D. G. Rancourt, *Nucl. Instrum. Methods Phys. Res. B*, 1997, **129**, 266–280.

[4] S. Stoll and A. Schweiger, *J. Magn. Reson.*, 2006, **178**, 42–55.

[5] F. Neese, *WIREs Comput Mol Sci* 2012, **2**, 73–78.

[6] A. D. Becke, *J. Chem. Phys.* 1993, **98**, 5648–5652.

[7] C. Lee, W. Yang and R. G. Parr, *Phys. Rev. B* 1988, **37**, 785–789.

[8] B. Miehlich, A. Savin, H. Stoll and H. Preuss, *Chem. Phys. Lett.* 1989, **157**, 200–206.

[9] F. Neese, F. Wennmohs, A. Hansen and U. Becker, *Chem. Phys.* 2009, **356**, 98–109.

[10] R. Izsák and F. Neese, *J. Chem. Phys.* 2011, **135**, 144105.

[11] D. A. Pantazis, X.-Y. Chen, C. R. Landis and F. Neese, *J. Chem. Theory Comput.*, 2008, **4**, 908–919.

[12] V. Barone and M. Cossi, *J. Phys. Chem. A*, 1998, **102**, 1995–2001.

[13] S. Miertuš, E. Scrocco and J. Tomasi, *Chem. Phys.*, 1981, **55**, 117–129.

[14] F. Weigend and R. Ahlrichs, *Phys. Chem. Chem. Phys.*, 2005, **7**, 3297–3305.

[15] F. Weigend, *Phys. Chem. Chem. Phys.*, 2006, **8**, 1057–1065.

[16] D. A. Pantazis and F. Neese, *J. Chem. Theory Comput.*, 2009, **5**, 2229–2238.

[17] D. A. Pantazis, X. Y. Chen, C. R. Landis and F. Neese, *J. Chem. Theory Comput.* 2008, **4**, 908–919.

[18] D. A. Pantazis and F. Neese, *Theor. Chem. Acc.*, 2012, **131**, 1292–1298.

[19] D. A. Pantazis and F. Neese, *J. Chem. Theory Comput.*, 2011, **7**, 677–684.

[20] S. Grimme, J. Antony, S. Ehrlich and H. Krieg, *J. Chem. Phys.* 2010, **132**, 154104.

[21] S. Grimme, S. Ehrlich and L. Goerigk, *J. Comput. Chem.* 2011, **32**, 1456–1465.

[22] D. I. Bezuidenhout, B. van der Westhuizen, A. J. Rosenthal, M. Wörle, D. C. Liles and I. Fernández, *Dalton Trans.*, 2014, **43**, 398-401.

[23] J. A. Connor and J. P. Lloyd, *Dalton Trans.*, 1972, 1470–1476.

[24] A. Neidlinger, T. Kienz and K. Heinze, *Organometallics*, 2015, **34**, 5310–5320.

[25] G. R. Eaton, S. S. Eaton, D. P. Barr and R. T. Weber, *Quantitative EPR*; Springer: Wien, NY, 2010.

Fig. S01. ^{1}H NMR spectrum of **1** in CD_2Cl_2.

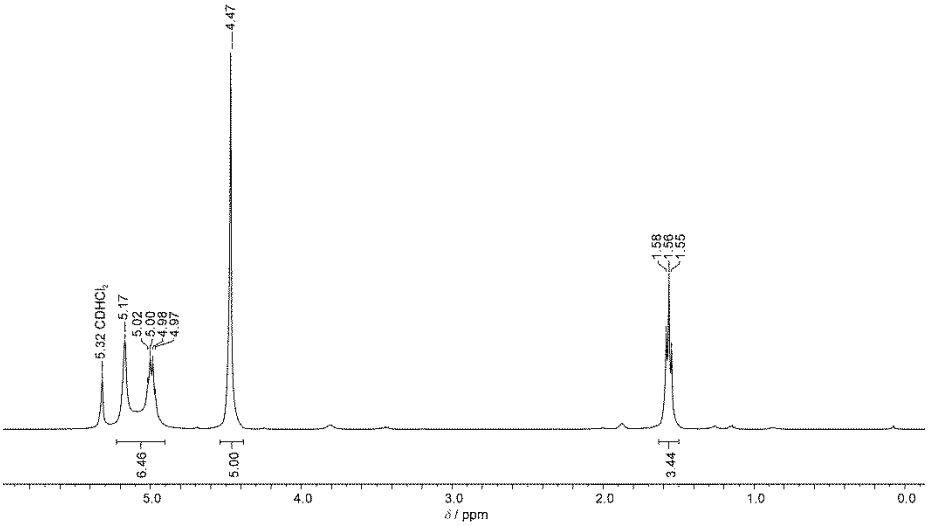

Fig. S02. $^{13}C\{^{1}H\}$ NMR spectrum of **1** in CD_2Cl_2.

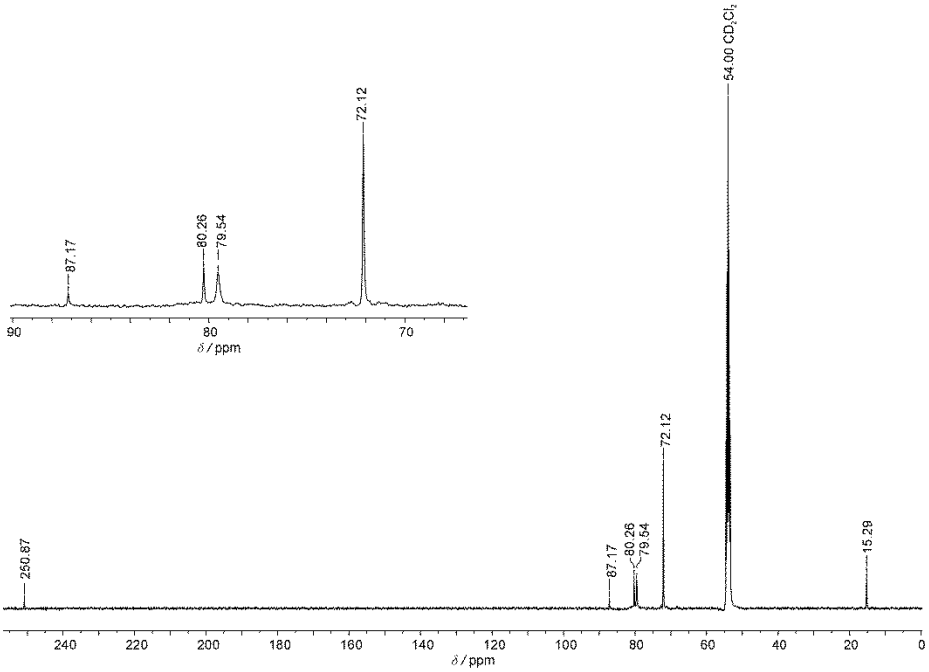

Fig. S03. ATR IR spectrum of **1**.

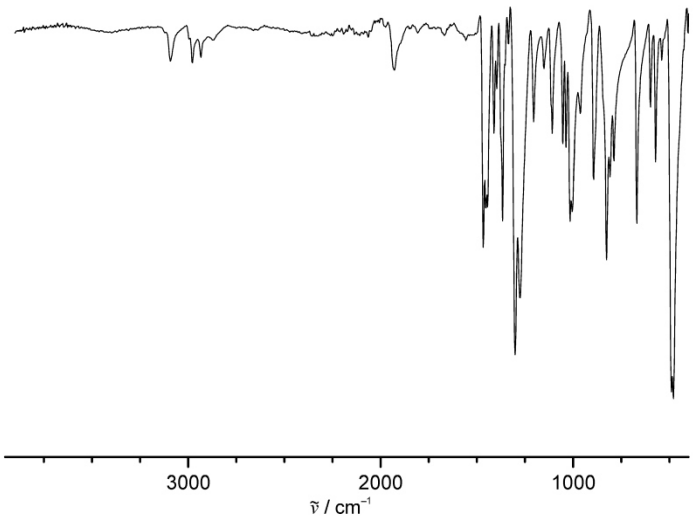

Fig. S04. UV/Vis absorption spectrum of **1** in CH_2Cl_2; oscillator strengths of DFT calculated transitions; difference electron densities (purple = depletion; orange = gain; contour value 0.01 a.u.) of the major transitions.

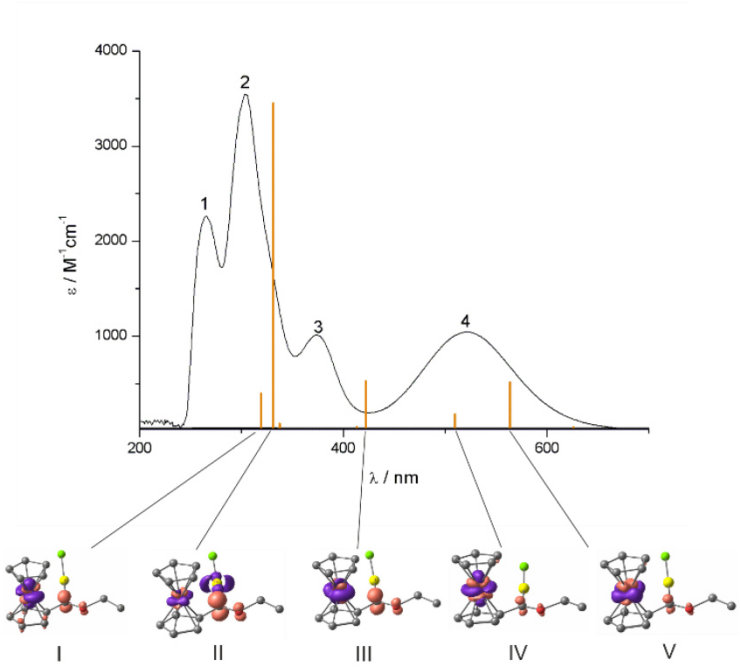

Fig. S05. LIFDI mass spectrum of **1** in CH_2Cl_2.

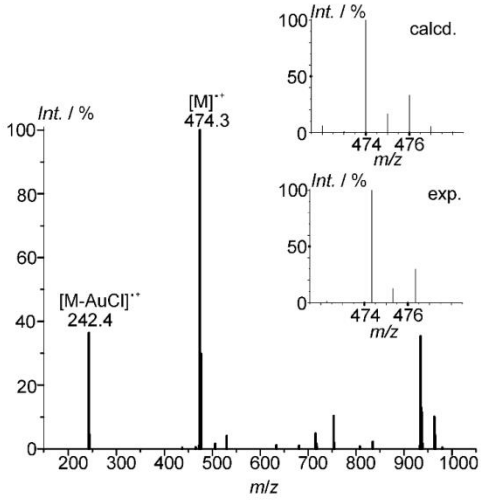

Fig. S06. Cyclic voltammogram of **1** in CH_2Cl_2 / $[^nBu_4N][PF_6]$.

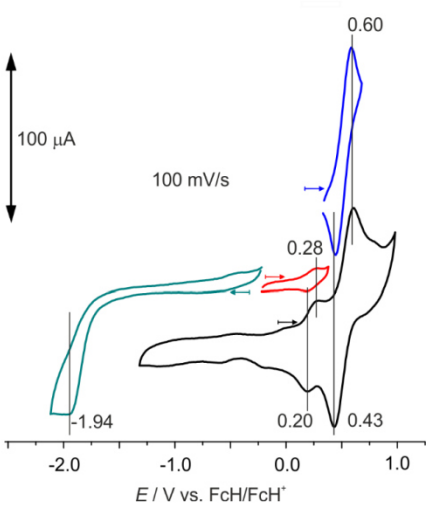

Fig. S07. Cyclic voltammogram of **1** in CH_2Cl_2 / $[^nBu_4N][BAr^F{}_4]$.

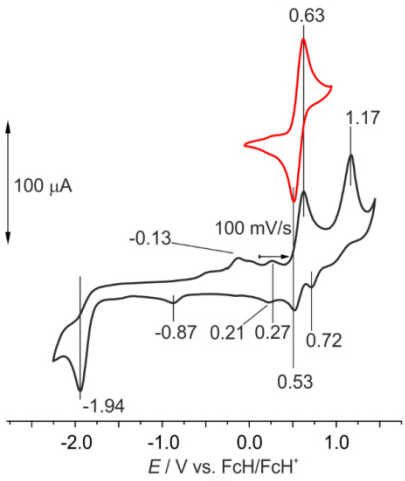

Fig. S08. Cyclic voltammogram of **1** in THF / [^{n}Bu$_4$N][PF$_6$].

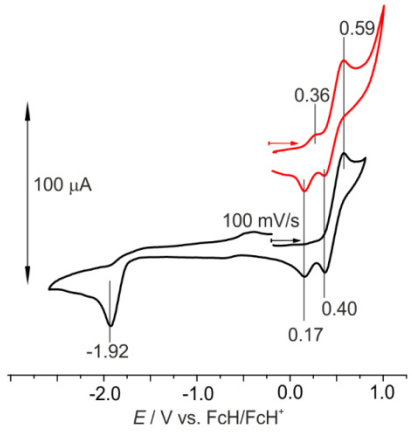

Fig. S9. Cyclic voltammogram of **1** in CH_2Cl_2 / [^{n}Bu$_4$N][BAr$^{F}_4$].

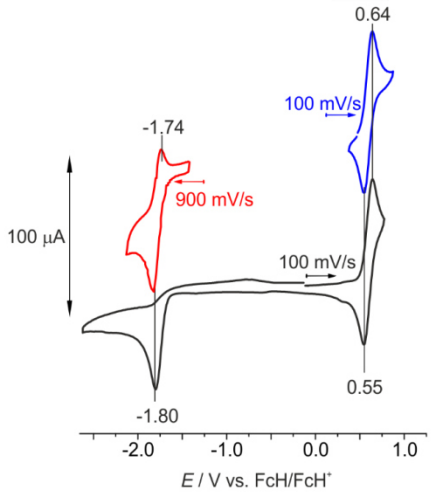

Fig. S10. ^{1}H DOSY of a mixture of **1** and $W(CO)_5[C(Fc)OEt]$ in CD_2Cl_2 at 298 K; diffusion values in $m^2\ s^{-1}$ obtained from the respective sufficiently different Cp resonances (H^1).

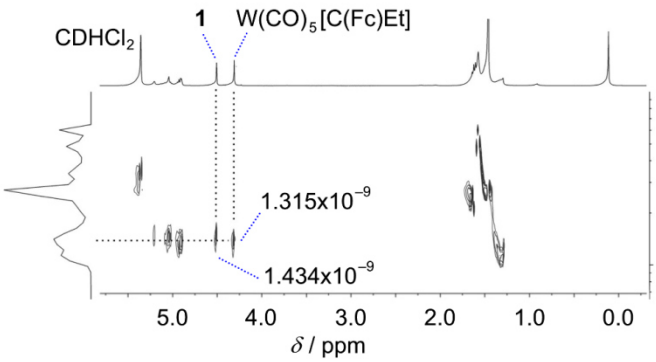

Fig. S11. X-band EPR spectrum of **1** (1.67 mM) and Magic Blue (0.95 eq) in THF after 162 h at 77 K.

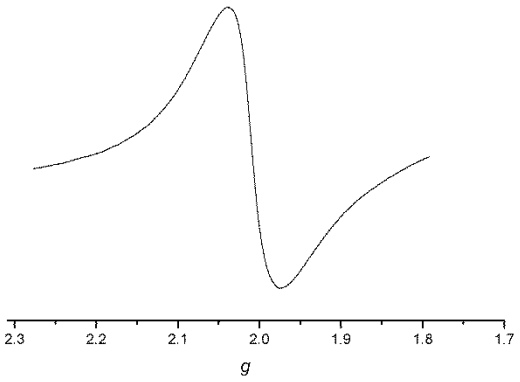

Fig. S12. X-band EPR spectrum of **1** (1.67 mM) and Magic Blue (0.95 eq) in THF after 160 h at 298 K.

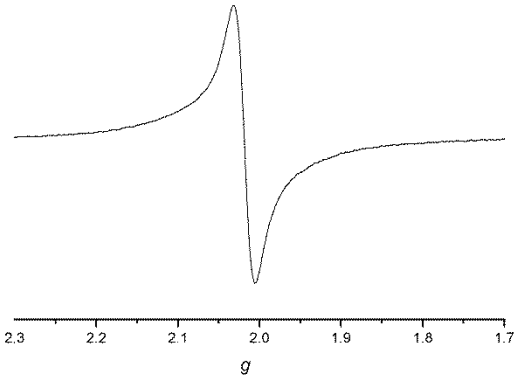

Fig. S13. X-band EPR spectrum of **1** (1.67 mM) and Magic Blue (0.95 eq) in CH_2Cl_2 (and 1 eq DMF as stabilizer) after 16 h at 77 K.

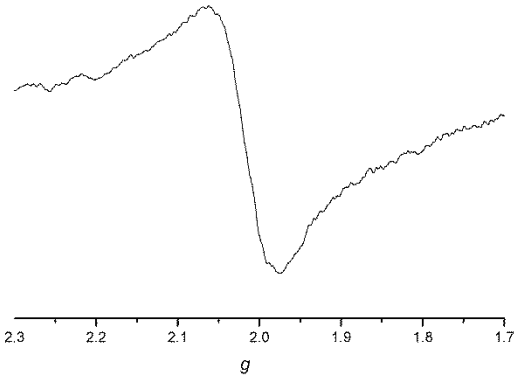

Fig. S14. X-band EPR spectrum of **1** (1.67 mM) and CAN (0.95 eq) in THF after 2 h at 77 K.

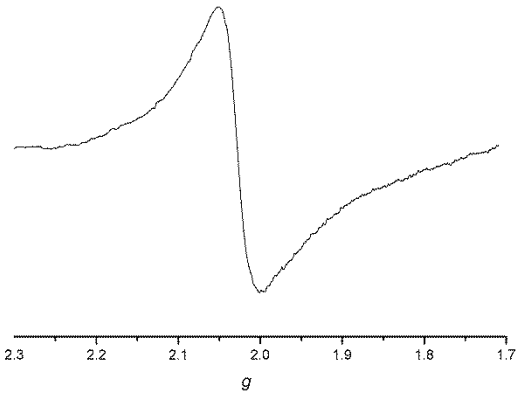

Fig. S15. X-band EPR spectrum of **1** (0.5 mM) and CAN (0.95 eq) in THF after 2.5 h at 298 K.

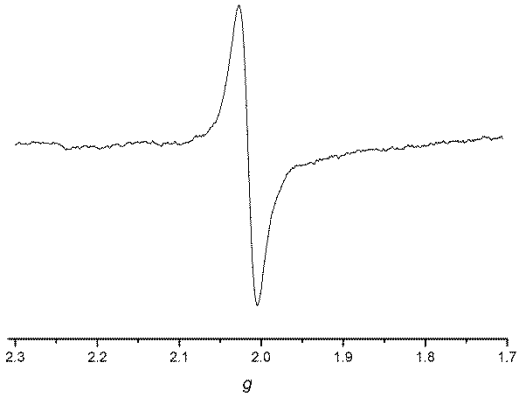

Fig. S16. X-band EPR spectrum of Magic Blue (5 mM) in THF at 298 K.

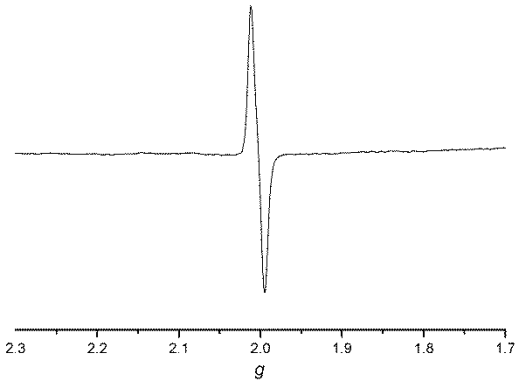

Fig. S17. X-band EPR spectra of Cu(TPP) in THF at different concentrations.

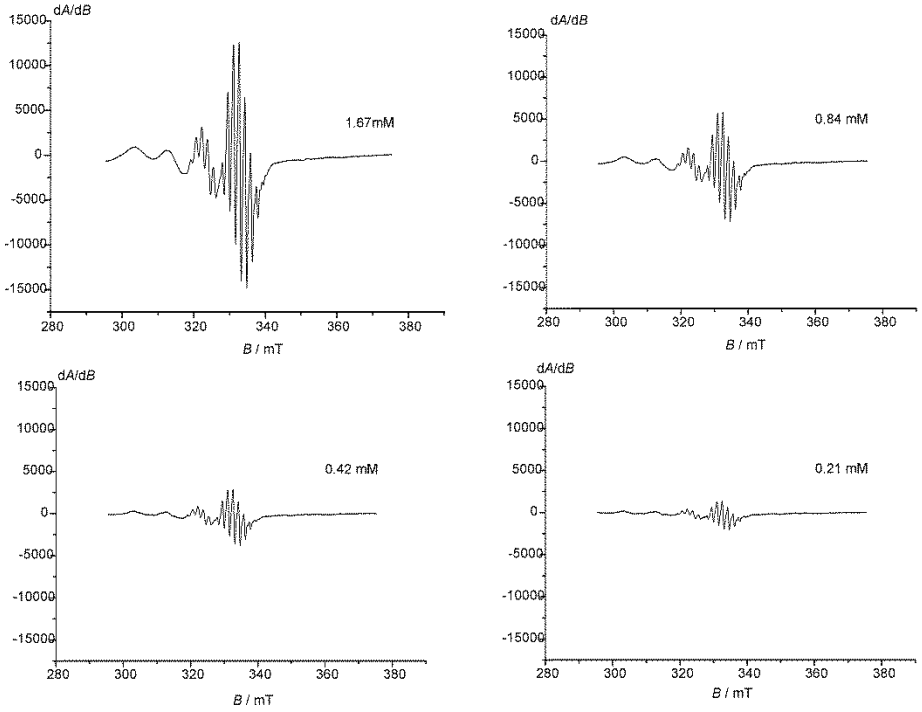

Fig. S18. Linear regression of the double integral of the EPR resonances of CuTPP versus concentration.

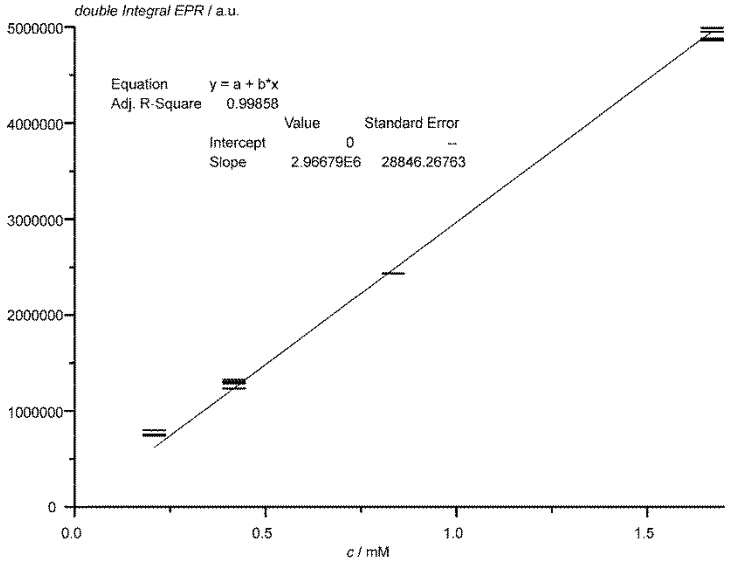

Fig. S19. Conversion versus time plot for the catalytic reaction using **1** (1 mol-%) and Magic Blue (1.25 eq) in CD_2Cl_2. The determined TOF = $(8.3\pm1.1)\times10^{-3}$ s^{-1} is based on the conversion versus time plot without the induction period (ca. 2 h – 5 h).

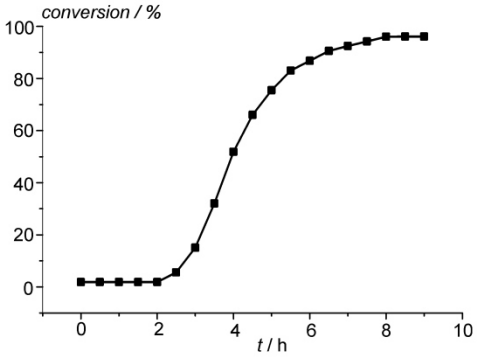

Fig. S20. Conversion versus time plots for the attempted reactions using **1** (1 mol-%) or Magic Blue (1 mol-%) alone in CD_2Cl_2.

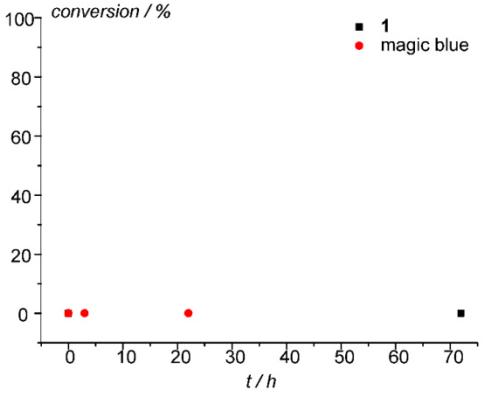

Fig. S21. ^{1}H NMR spectra of **1** and Magic Blue (1.0 eq) in CD_2Cl_2 over time.

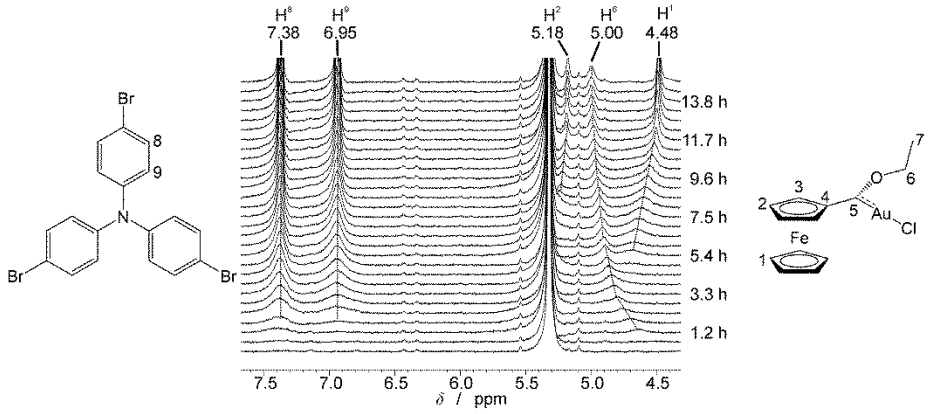

Fig. S22. ^{57}Fe Mößbauer spectrum of **1** and Magic Blue (0.95 eq) after 0.5 h in CH_2Cl_2 and removal the solvent by evaporation (Fc: δ= 0.520 mm s^{-1}; ΔE_Q = 2.107 mm s^{-1}; Fc$^+$: δ= 0.457 mm s^{-1}; ΔE_Q = 0.243 mm s^{-1}).

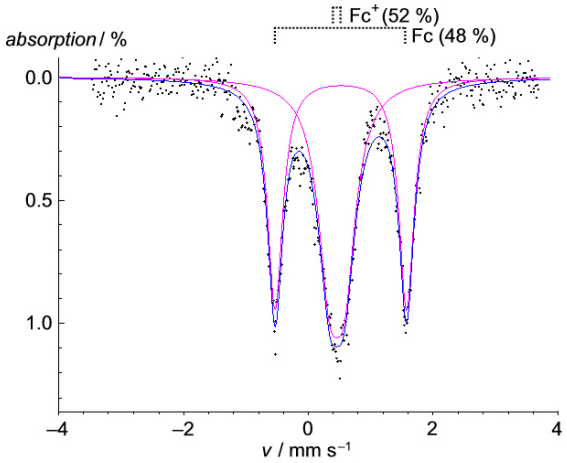

Fig. S23. ^{57}Fe Mößbauer spectrum of **1** and Magic Blue (0.95 eq) after 5 h in CH_2Cl_2 and removal of the solvent by evaporation (Fc: δ= 0.525 mm s^{-1}; ΔE_Q = 2.291 mm s^{-1}; Fc$^+$: δ= 0.47 mm s^{-1}; ΔE_Q = 0.240 mm s^{-1}; Fe^{II}: δ= 1.311 mm s^{-1}; ΔE_Q = 2.650 mm s^{-1}.

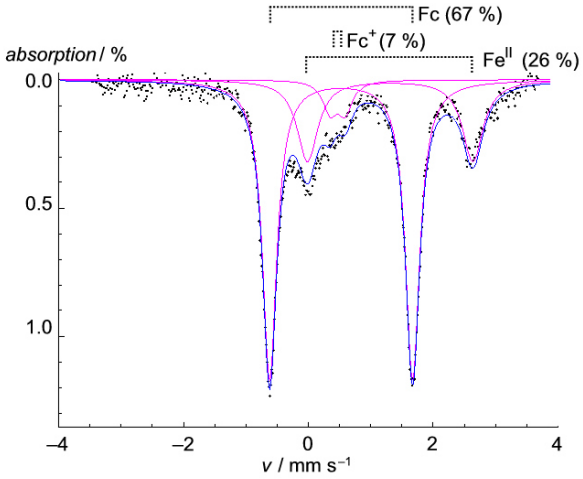

Fig. S24. Au L_3-edge XANES spectrum of **1**.

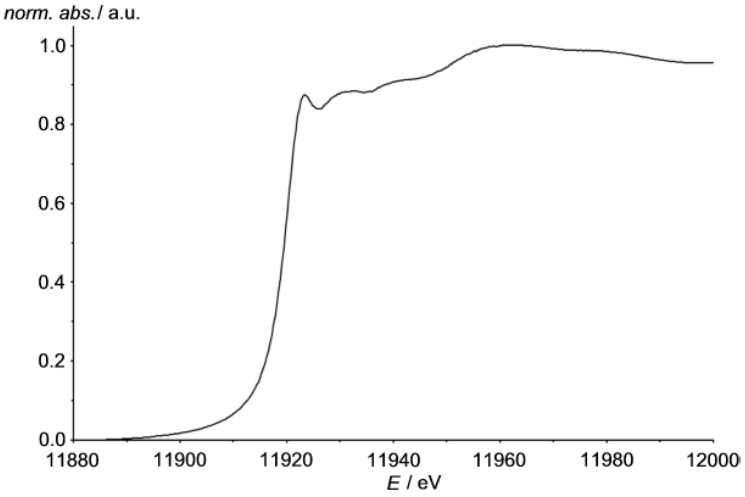

Fig. S25. Au L_3-edge XANES spectrum of **1** and Magic Blue (1.25 eq) after 5 h in CH_2Cl_2 and removal of the solvent (blue) and the spectrum of gold foil (red) for comparison.

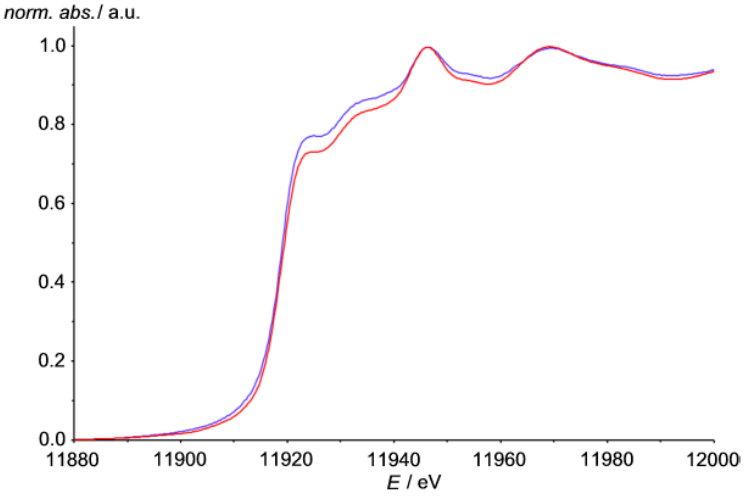

Fig. S26. Photographs of **1** in CH_2Cl_2 (left) and of the mixture of **1** and Magic Blue (1.0 eq) plus DMF (1 eq) after 14 h in CD_2Cl_2 (right) showing the precipitate.

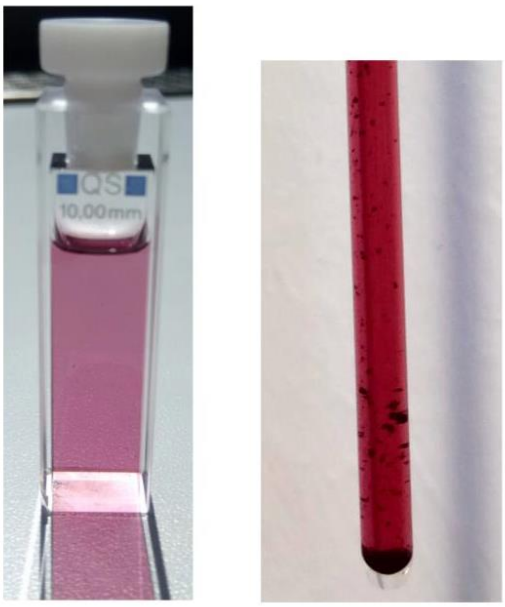

Fig. S27. Conversion versus time plot for the catalytic reaction using **1** (1 mol-%) and Magic Blue (1.25 eq) in CD_2Cl_2; second batch of substrate added.

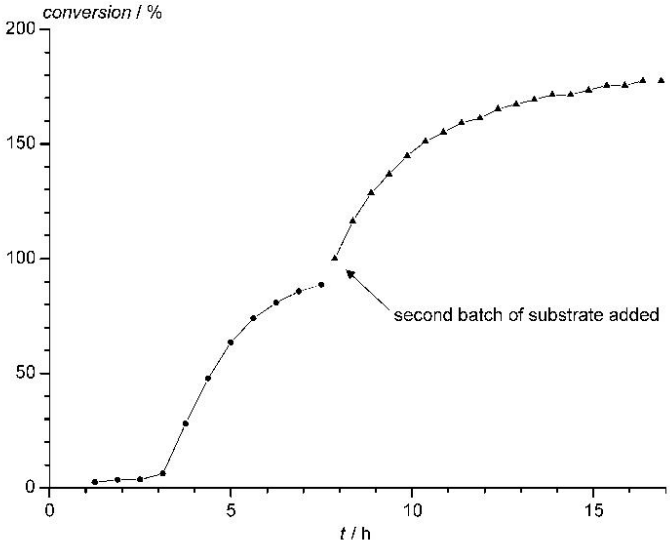

Fig. S28. Conversion versus time plot for the catalytic reaction using **1** (1 mol-%) and Magic Blue (1.25 eq) in the presence of [^{n}Bu$_4$N]Cl (42 eq) in CD_2Cl_2.

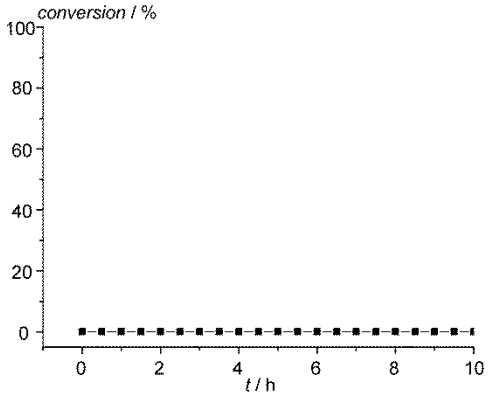

Fig. S29. Conversion versus time plot for the catalytic reaction using **1** (1 mol-%) and $AgSbF_6$ (1.25 eq) in CD_2Cl_2. The determined TOF = 3.2×10^{-3} s^{-1} is based on the conversion versus time plot (ca. 0 h – 5 h).

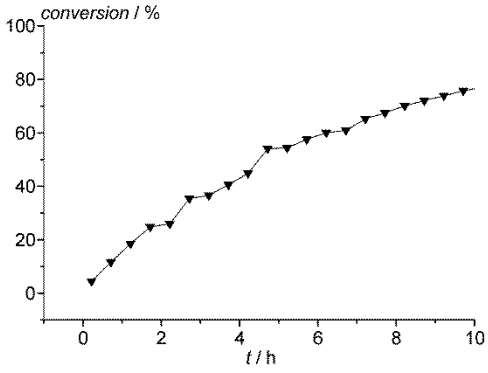

Fig. S30. ^{1}H NMR spectrum of **1** (0.01 mM; 10 mol-%) and Magic Blue (1.0 eq) at the beginning of the catalytic reaction and after ca. 63 % conversion stopped by addition of $FeCp^*_2$ (1.05 eq) indicating a 84±5 % recovery.

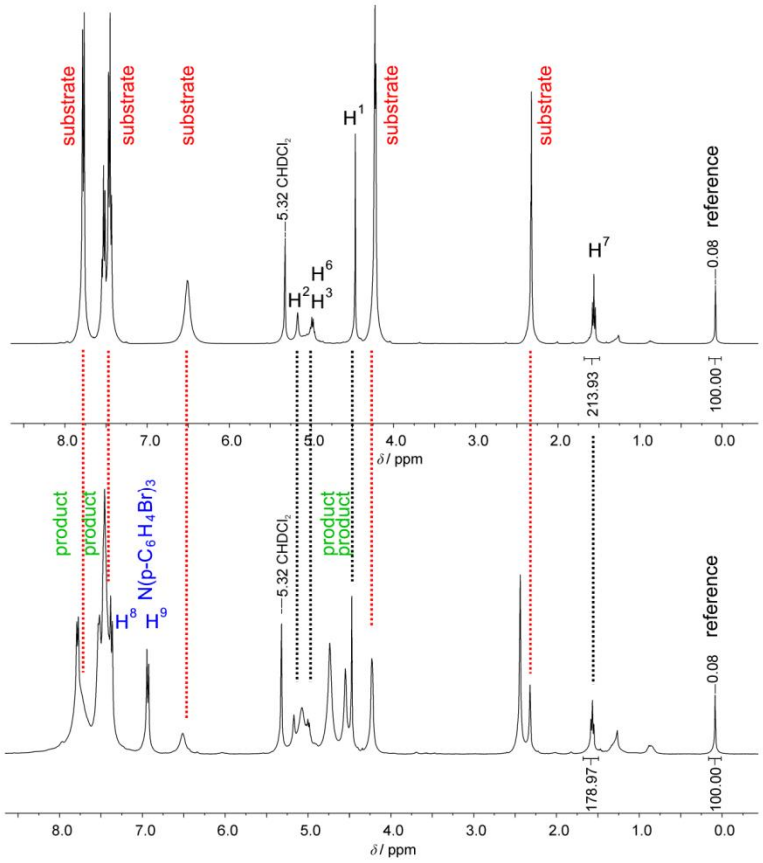

6.5 Supporting Information: Unexpected C-C Bond Formation with a Ferrocenyl Fischer Carbene Complex

Z. Anorg. Allg. Chem. **2020** · ISSN 0044–2313

SUPPORTING INFORMATION

Title: Unexpected C–C Bond Formation with a Ferrocenyl Fischer Carbene Complex
Author(s): P. Veit, S. Seibert, C. Förster,* K. Heinze*
Ref. No.: z201900350

Unexpected C-C Bond Formation with a Ferrocenyl Fischer Carbene Complex

Philipp Veit, Sebastian Seibert, Christoph Förster, Katja Heinze

Supporting Information

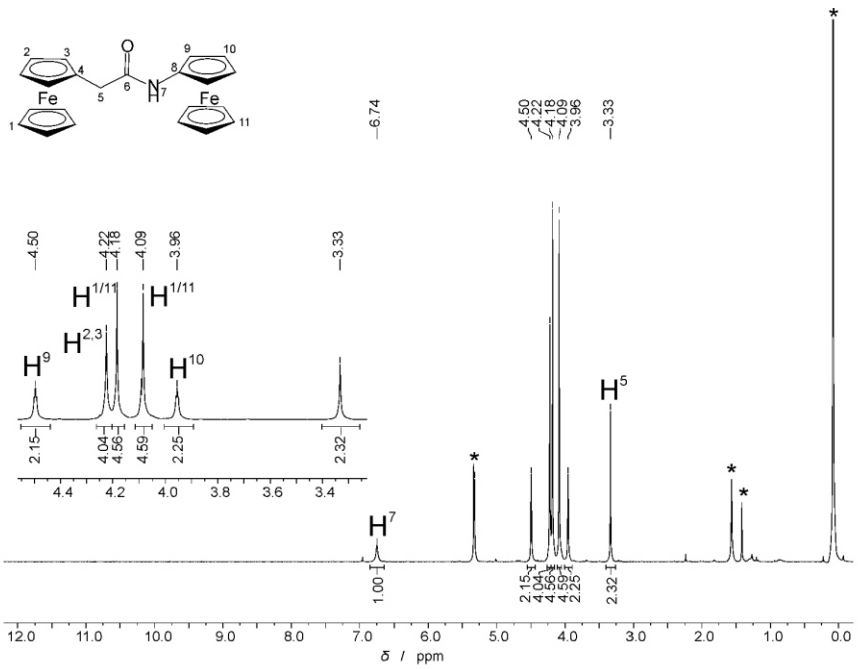

Figure S01. ^{1}H NMR spectrum of **2** in CD_2Cl_2 (* denotes residual solvent resonances or grease).

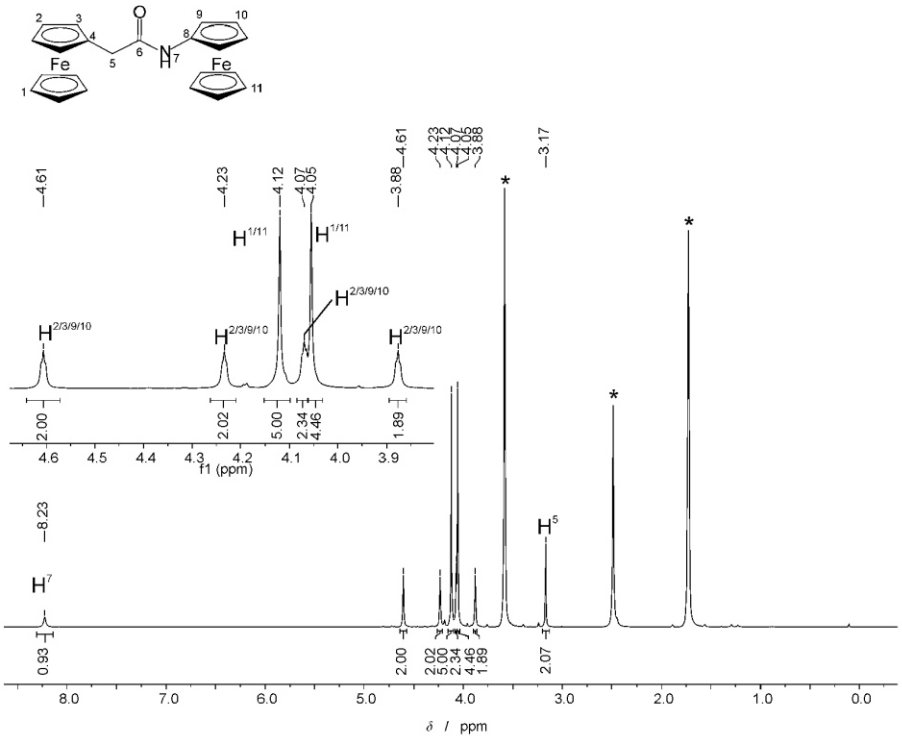

Figure S02. ^{1}H NMR spectrum of **2** in d_8-THF (* denotes residual solvent resonances).

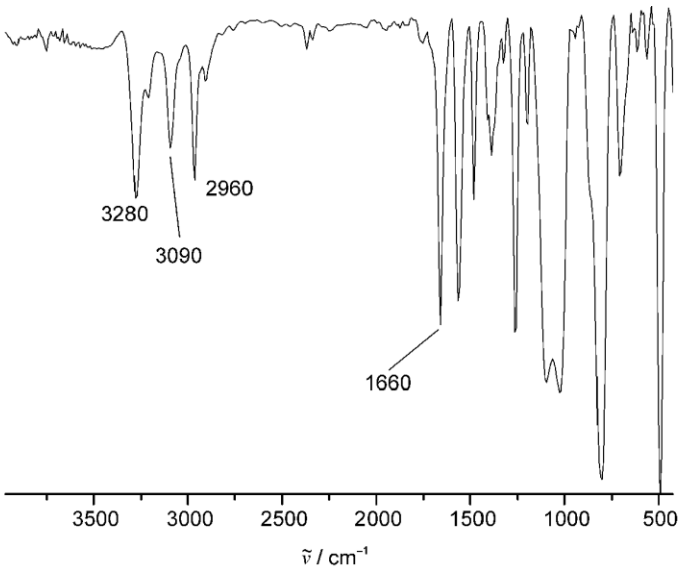

Figure S03. IR spectrum (KBr) of **2**.

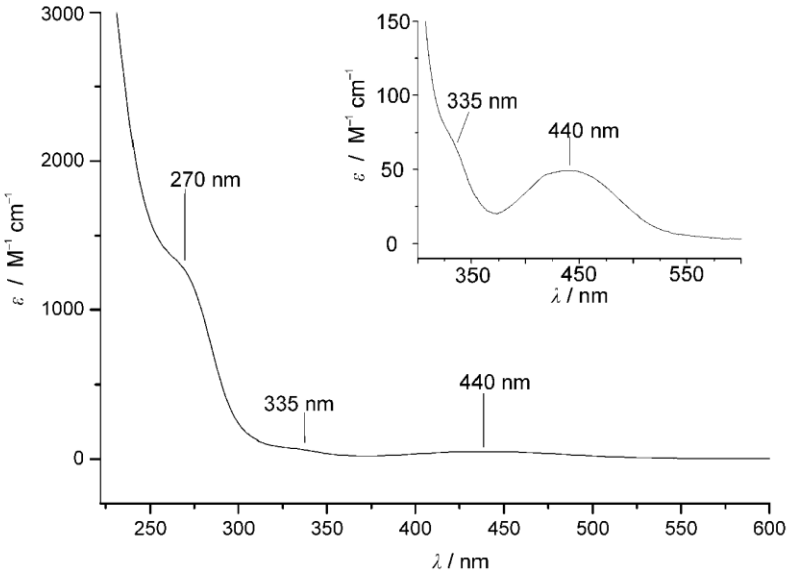

Figure S04. UV/Vis spectrum of **2** in CH_2Cl_2; the inset shows a zoom into the 300 – 600 nm region.

Table S1. Selected bond lengths / Å and angles /° of **2** determined by XRD and by DFT calculations.

	2 (XRD)	**2** (DFT)
C1-O1	1.224(6)	1.225
C1-C2	1.520(6)	1.525
C2-C3	1.502(6)	1.499
N1-C1	1.343(6)	1.358
N1-C13	1.421(5)	1.401
C1-N1-C13	124.9(4)	127.2
N1-C1-C2	113.9(4)	113.9
C3-C2-C1	112.2(4)	110.6
Fe1-C3-C2-C1	–169.0(3)	171.5
Fe2-C13-N1-C1	70.0(5)	83.0
Fe1-X1[a)]	1.637(3)	1.669
Fe1-X2[b)]	1.634(2)	1.663
Fe2-X1[a)]	1.649(2)	1.668
Fe2-X2[b)]	1.650(2)	1.668
τ(Fe1)[c)]	179.65(14)	179.7
τ(Fe2)[c)]	177.81(10)	178.4

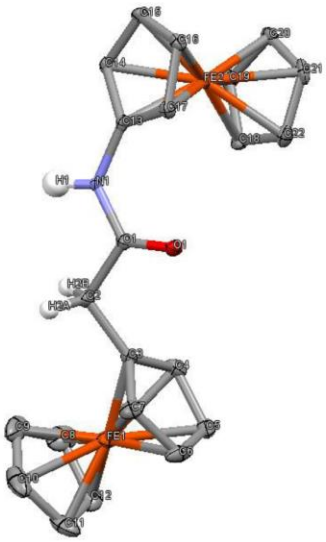

a) X1 = centroid of coordinated C_5H_5 ring.

b) X2 = centroid of coordinated C_5H_4 ring.

c) τ = X1-M-X2.

Figure S05. DFT calculated tautomers **III** and **IV**.

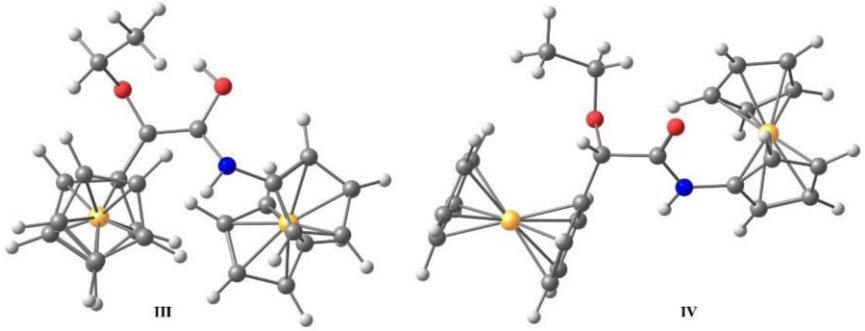

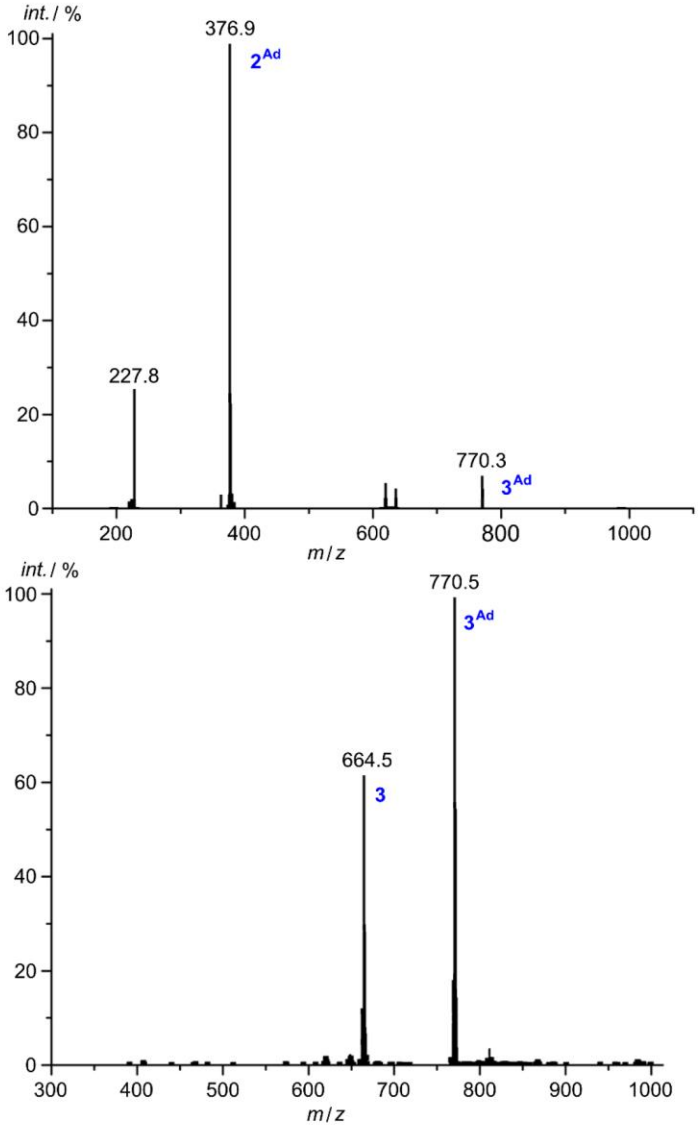

Figure S06. LIFDI mass spectra taken during the thermolysis of **1** in the presence of adamantyl amine in toluene.

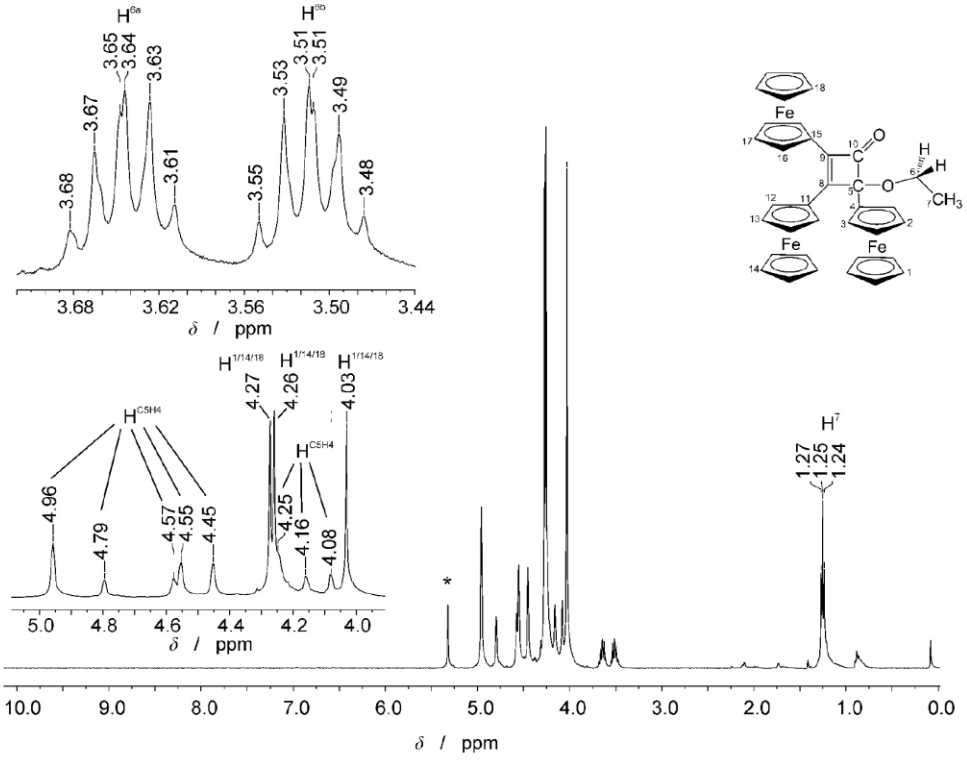

Figure S07. ^{1}H NMR spectrum of **3** in CD_2Cl_2 (* denotes residual solvent resonances).

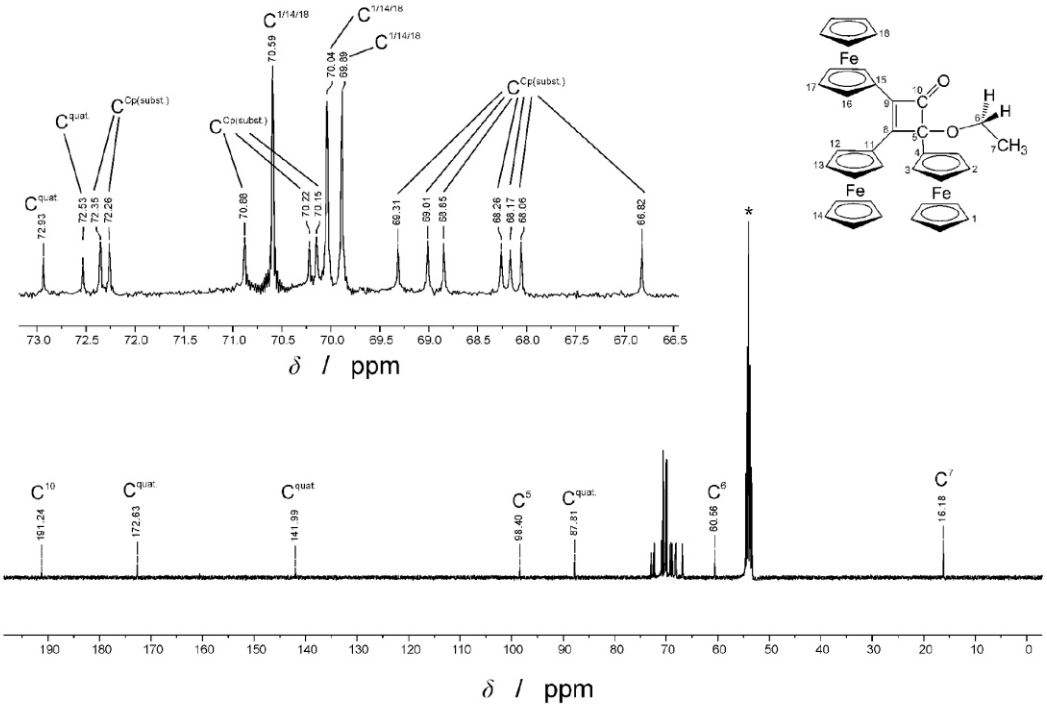

Figure S08. $^{13}C\{^{1}H\}$ NMR spectrum of **3** in CD_2Cl_2 (* denotes residual solvent resonances).

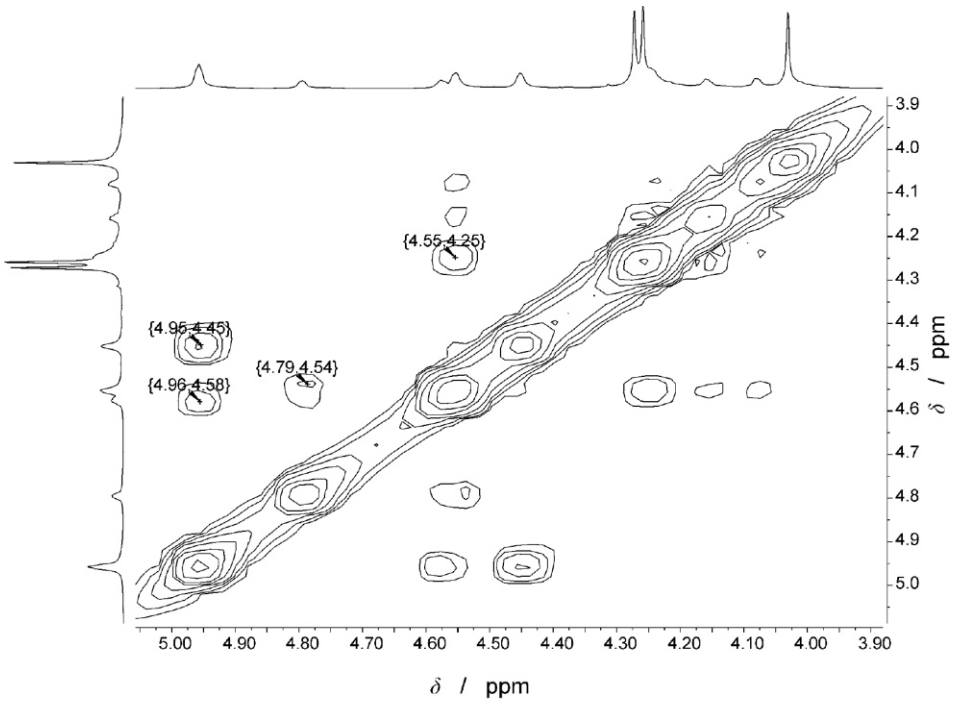

Figure S09. ^{1}H-^{1}H COSY of **3** in CD_2Cl_2.

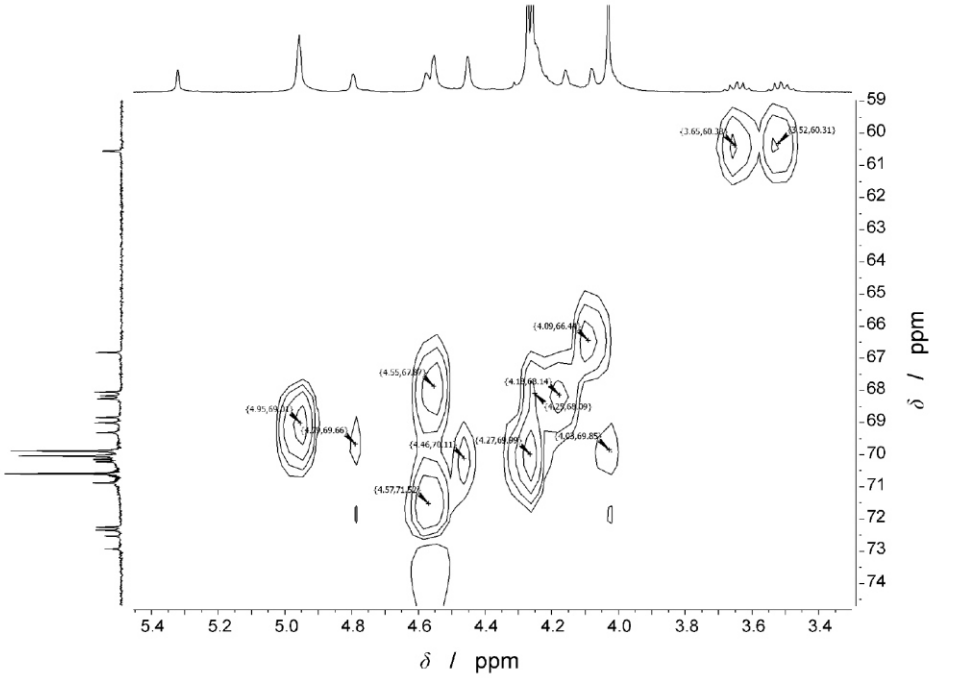

Figure S10. ^{1}H-^{13}C HSQC of **3** in CD_2Cl_2.

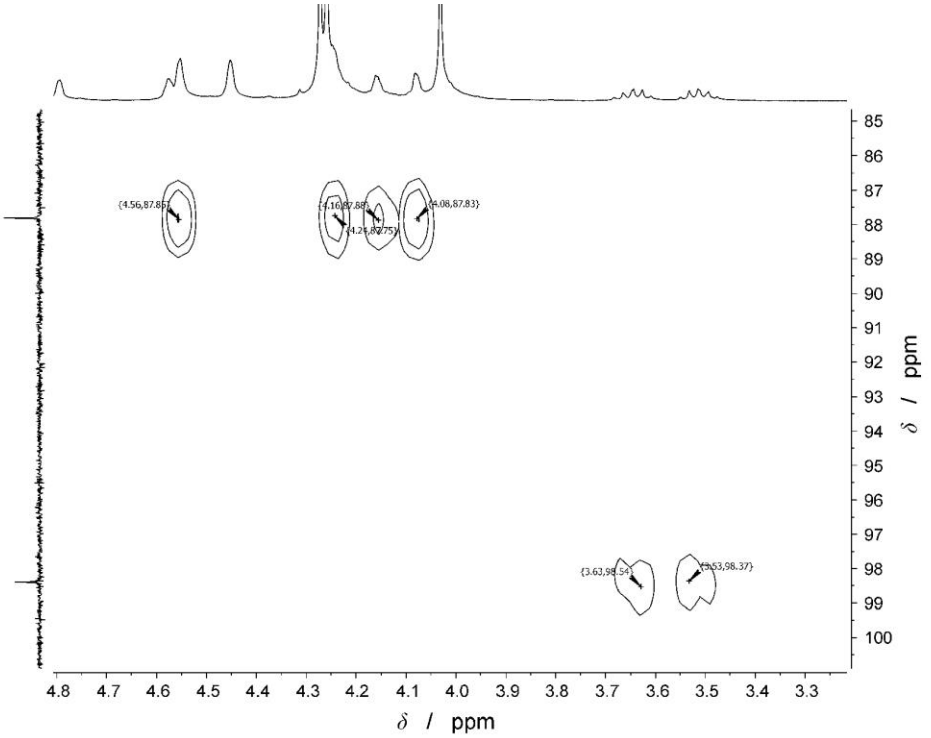

Figure S11. ^{1}H-^{13}C HMBC of **3** in CD_2Cl_2.

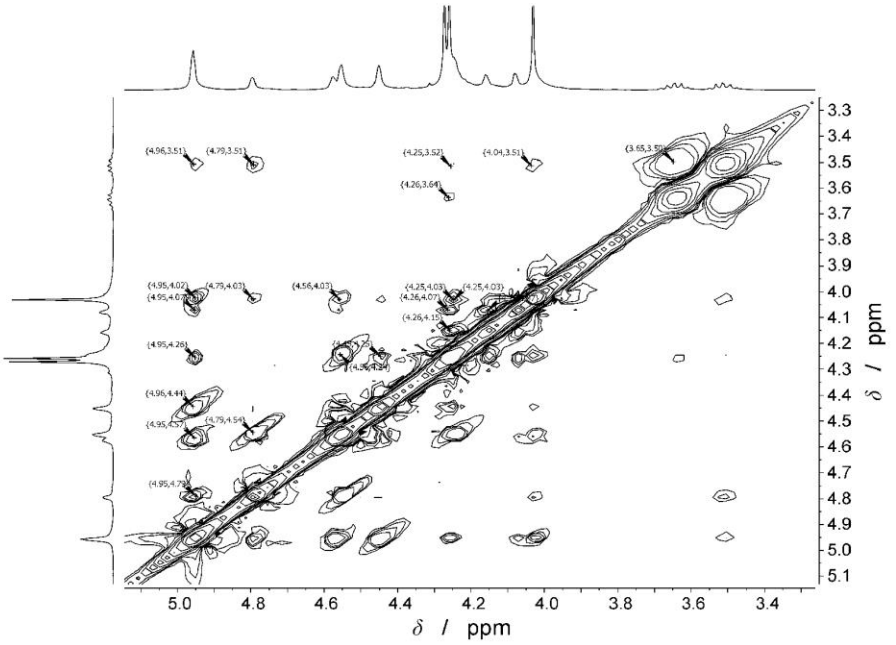

Figure S12. ^{1}H-^{1}H NOESY of **3** in CD_2Cl_2 (t_{mix} = 1.5 s).

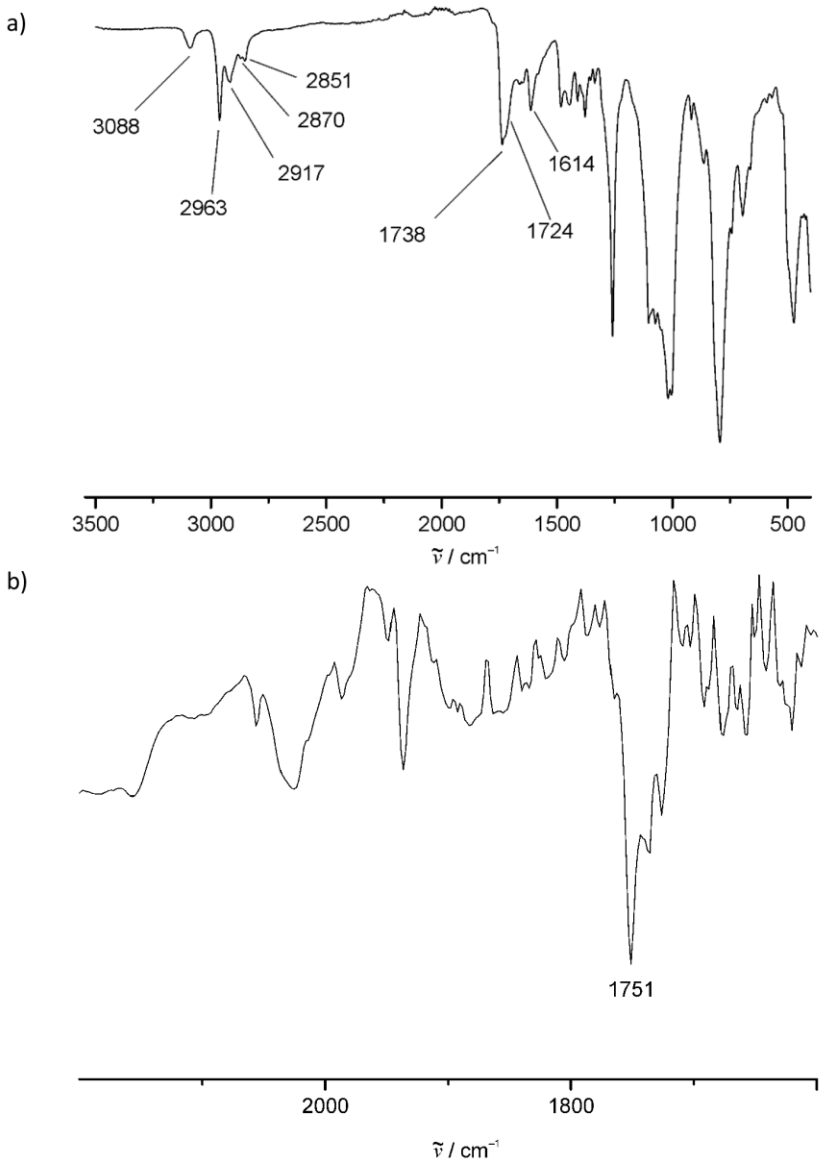

Figure S13. a) ATR-IR spectrum of **3** and b) IR spectrum of **3** in *n*-heptane.

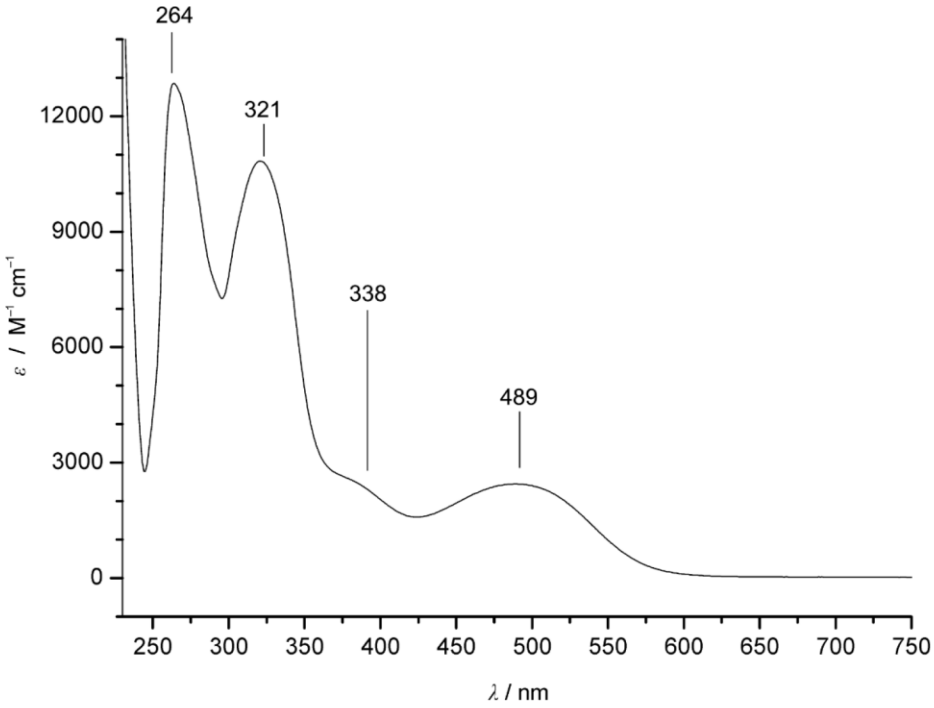

Figure S14. UV/Vis spectrum of **3** in CH_2Cl_2.

Table S2. Selected bond lengths / Å and angles /° of 3 determined by XRD and by DFT calculations.

	3 (XRD)	**3** (DFT)
C6-C11	1.452(2)	1.449
C12-C13	1.4427(19)	1.434
C23-C24	1.502(2)	1.500
O1-C23	1.4079(18)	1.401
C11-C36	1.476(2)	1.473
C11-C12	1.378(2)	1.381
C12-C23	1.547(2)	1.549
C23-C36	1.571(2)	1.577
O2-C36	1.2100(18)	1.214
O1-C23-C12	118.41(12)	117.5
C11-C12-C23	95.19(12)	94.6
C12-C23-C36	82.06(11)	82.5
C11-C36-C23	90.35(11)	89.9
C12-C11-C36	91.60(12)	92.4
Fe1-C6-C11-C36	107.96(16)	109.0
Fe2-C13-C12-C11	–87.5(2)	–89.8
Fe3-C24-C23-C36	–62.35(17)	–65.6
C6-C11-C12-C13	11.5(3)	9.1
C36-C11-C12-C23	7.15(12)	6.39
Fe1-X1[a)]	1.6514(9)	1.657
Fe1-X2[b)]	1.6460(8)	1.654
Fe2-X1[a)]	1.6587(8)	1.656
Fe2-X2[b)]	1.6513(8)	1.653
Fe3-X1[a)]	1.6545(9)	1.652
Fe3-X2[b)]	1.6495(8)	1.647
τ(Fe1)[c)]	177.9	179.0
τ(Fe2)[c)]	179.3	179.2
τ(Fe3)[c)]	177.3	178.4

a) X1 = centroid of coordinated C_5H_5 ring.

b) X2 = centroid of coordinated C_5H_4 ring.

c) τ = X1-M-X2.

Figure S15. Geometry of DFT optimized **3** and indication of close CH···O=C contacts. The blue arrows indicate the displacement vectors associated with the $C{=}O^2$ stretching vibration.

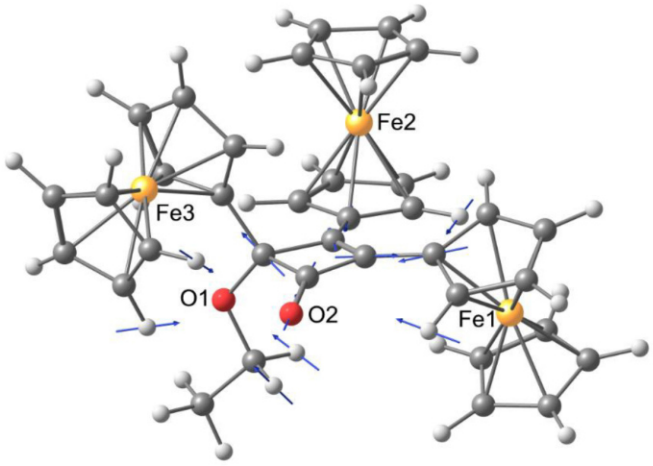

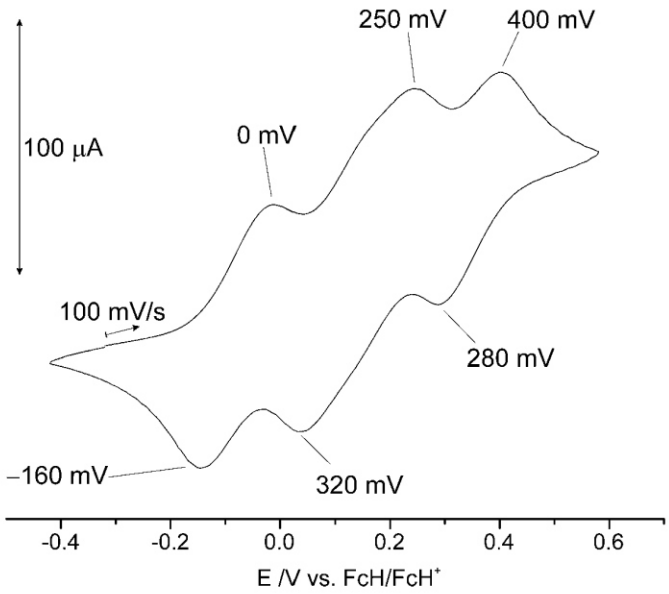

Figure S16. Cyclic voltammogram of **3** in $CH_2Cl_2/[n Bu_4N][PF_6]$. Potentials are given versus ferrocene.

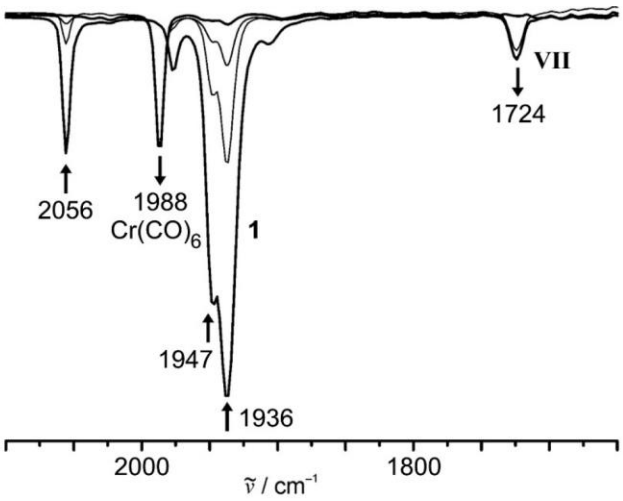

Figure S17. IR spectra of **1** during thermolysis in *n*-heptane (98°C) over 3 h.

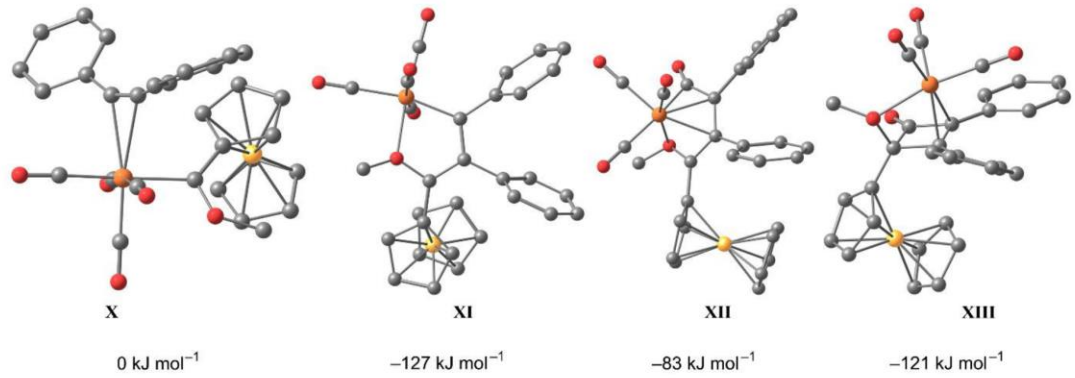

Figure S18. DFT calculated model reaction of **X** → **XI** → **XII** → **XIII** (hydrogen atoms omitted for clarity).

Synthesis of 2,*N*-diferrocenylamide (2) via an amide coupling reaction

Ferrocenyl acetic acid (122 mg, 0.50 mmol) was dissolved in dry dichloromethane (5 mL) and 1-chloro-*N*,*N*,2-trimethyl1-1-propenylamine (Ghosez' reagent, 75 μL, 0.57 mmol) was added under argon. The mixture was stirred overnight resulting in a dark orange solution of ferrocenyl acetic acid chloride. Dry triethylamine (77 μL, 0.55 mmol) was added to a solution of amino ferrocene (100 mg, 0.50 mmol) in dry dichloromethane (5 mL) under argon. This mixture was added to the solution of ferrocenyl acetic acid chloride. Within a few minutes a light brown solid precipitated. To complete the reaction, the mixture was stirred overnight at room temperature. Water (30 mL) and diethylether (20 mL) were added. The coupling product was extracted with ethyl acetate. The combined organic layers were washed with aqueous solutions of HCl (2 %), NaCl (saturated), $NaHCO_3$ (4 %), NaCl (saturated) and dried over Na_2SO_4. The solvents were removed under reduced pressure. **2** was obtained as a brown solid (92 mg, 44 %). The formation of **2** was confirmed by ^1H, $^{13}C\{^1H\}$ and IR spectroscopy (Figures S19–21).

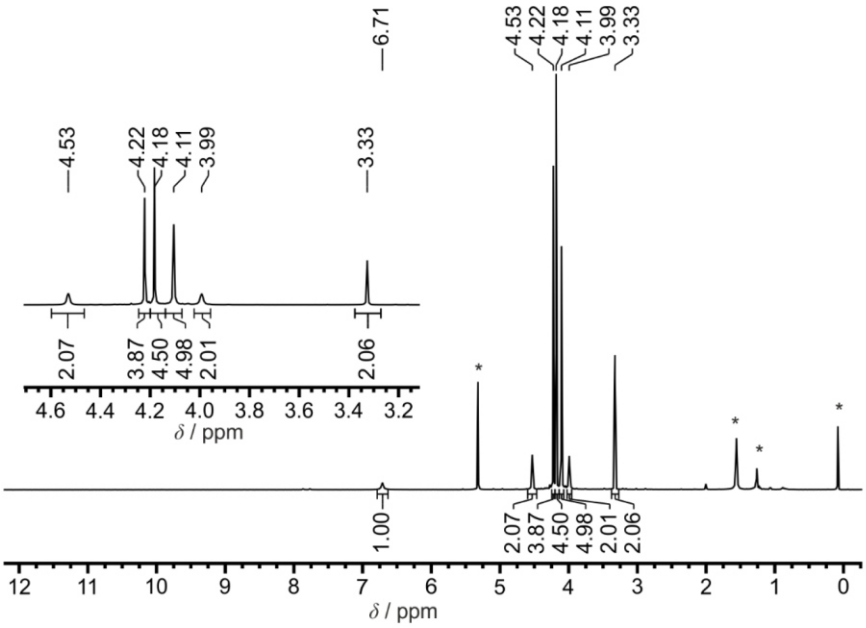

Figure S19. ^1H NMR spectrum of **2** (as obtained from an amide coupling reaction) in CD_2Cl_2 (* denotes residual solvent resonances or grease).

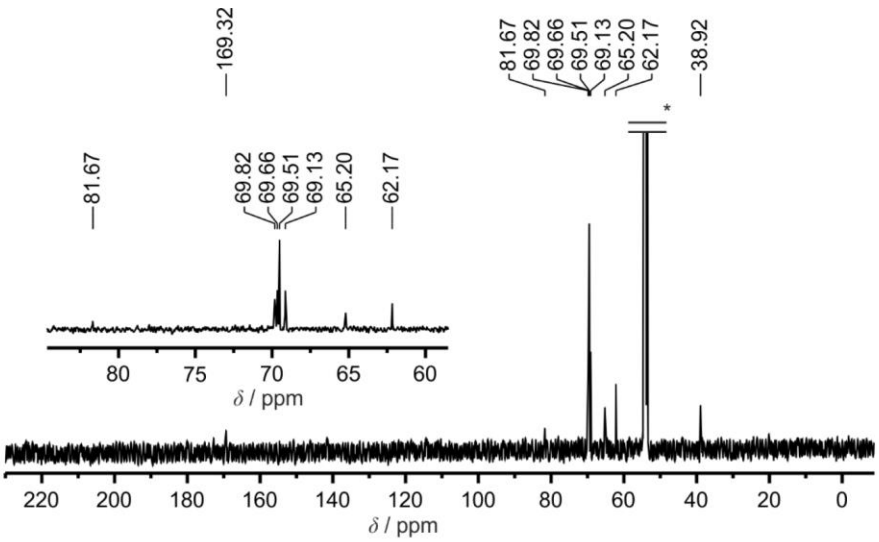

Figure S20. $^{13}C\{^{1}H\}$ NMR spectrum of **2** (as obtained from an amide coupling reaction) in CD_2Cl_2 (* denotes solvent resonances).

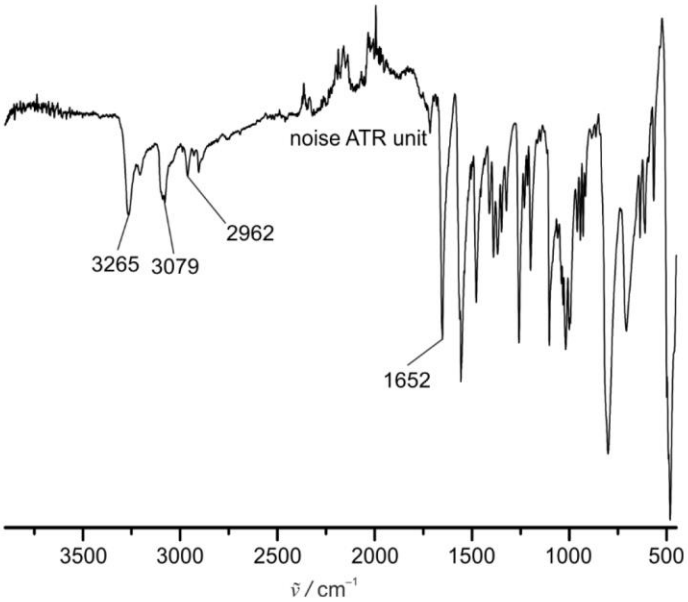

Figure S21. ATR-IR spectrum of **2** (as obtained from an amide coupling reaction).

6.6 Supporting Information: Electrochemistry of the heterotrimetallic Fischer carbene complex (N-methylaminoferrocenyl) (ferrocenyl) carbene (pentacarbonyl) tungsten (0)

Supporting Information for

Electrochemistry of the heterotrimetallic Fischer carbene complex (N-methylaminoferrocenyl) (ferrocenyl) carbene (pentacarbonyl) tungsten (0)

Philipp Veit, Christoph Förster* and Katja Heinze*

Department of Chemistry, Johannes Gutenberg University of Mainz, Duesbergweg 10–14, 55128 Mainz, Germany. E-Mail: katja.heinze@uni-mainz.de

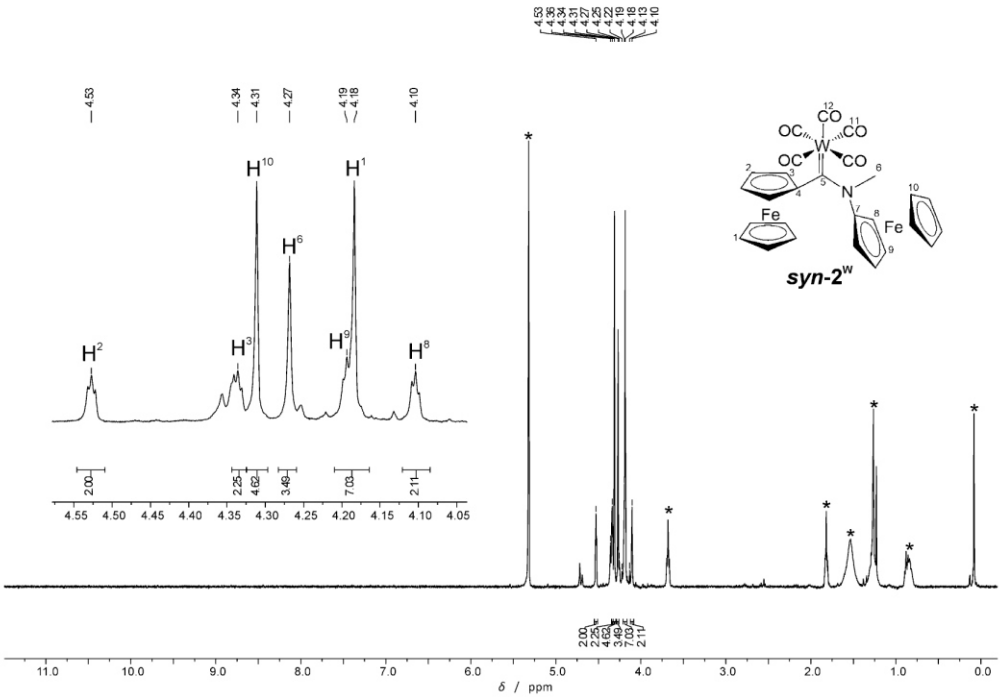

Fig. S01: ^{1}H-NMR spectrum of 6:1 ***syn/anti*-2^W** in CD_2Cl_2. Only signals of ***syn*-2^W** marked, residual solvent resonances and grease marked with asterisk.

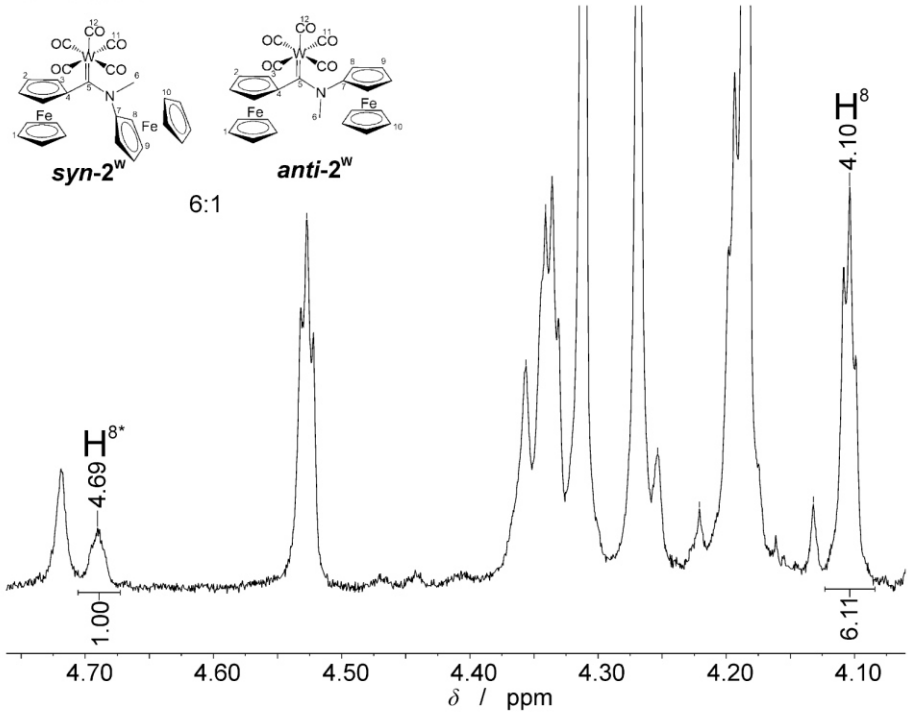

Fig. S02: ^{1}H-NMR spectrum of 6:1 ***syn/anti*-2^W** in CD_2Cl_2. Integral ratio 6:1 *syn/anti* highlighted at resonance H^8 of ***syn*-2^W** and H^{8*} of ***anti*-2^W**.

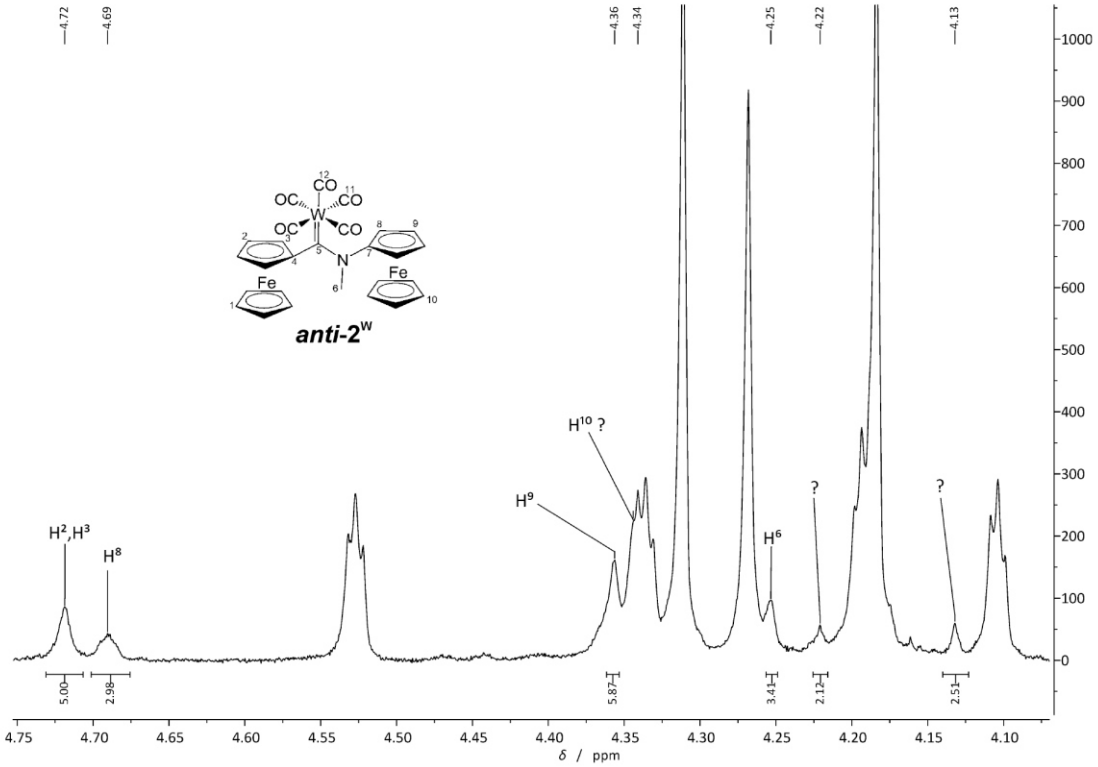

Fig. S03: ^{1}H-NMR spectrum of 6:1 ***syn/anti*-2^{W}** in CD_2Cl_2. Zoom into Cp-region of ***anti*-2^{W}**.

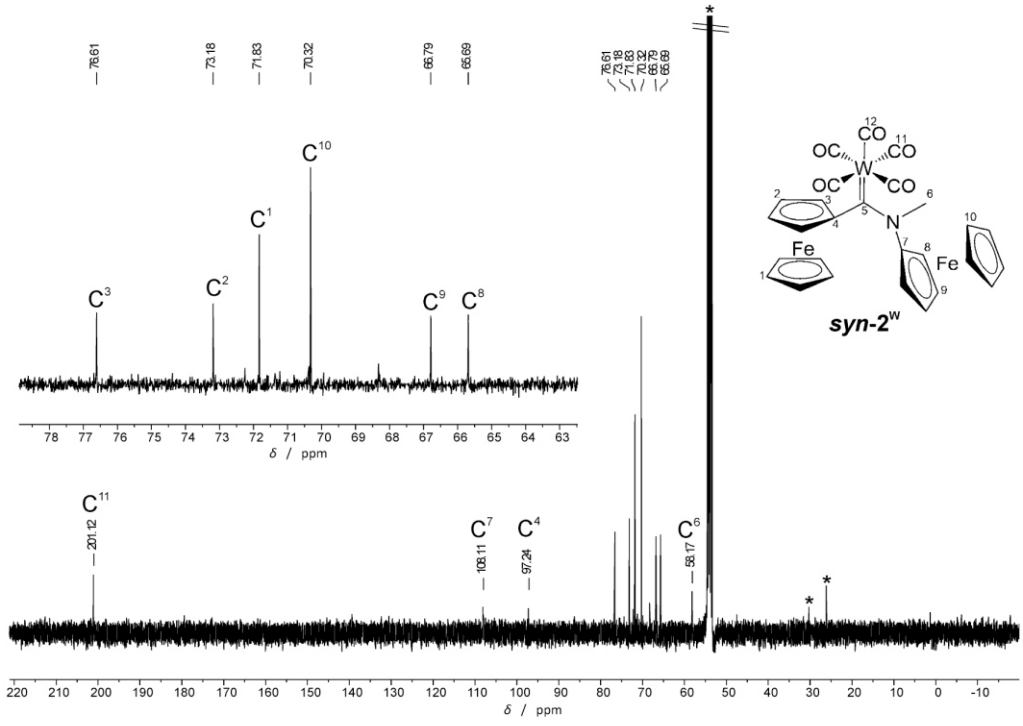

Fig. S04: $^{13}C\{^{1}H\}$-NMR spectrum of **2^{W}** in CD_2Cl_2.

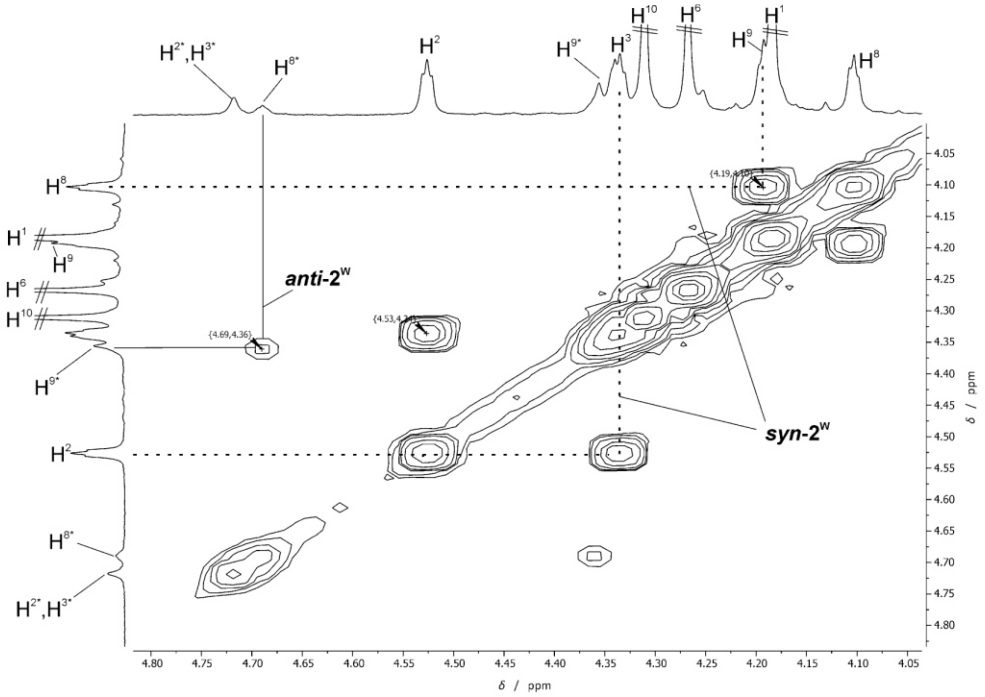

Fig. S05: ^{1}H-^{1}H-COSY of 2^{W} in CD_2Cl_2.

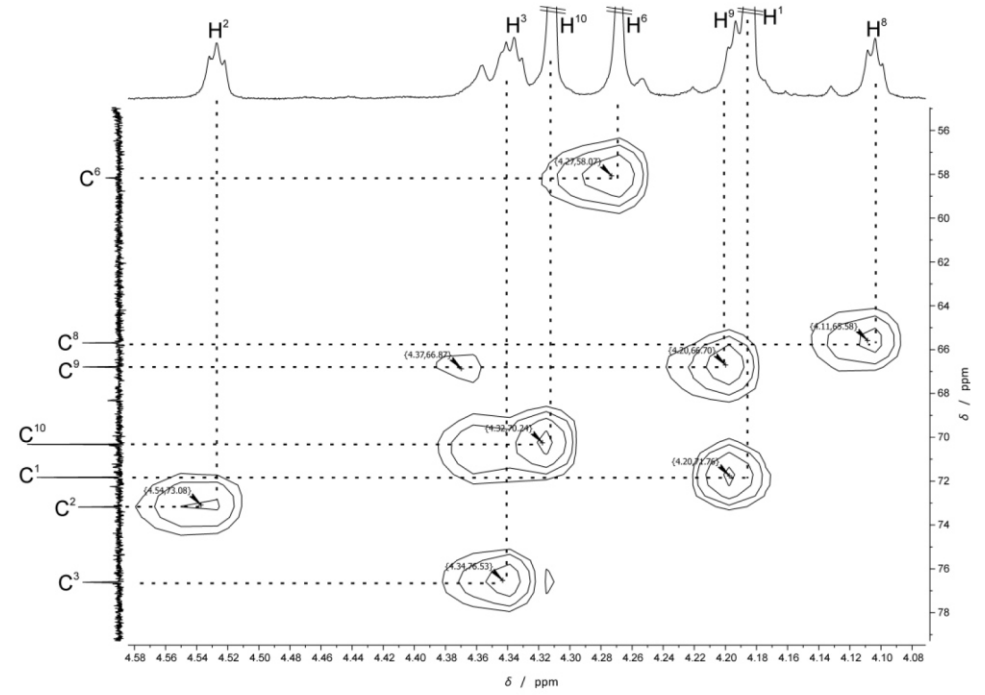

Fig. S06: ^{1}H-^{13}C-HSQC NMR spectrum of 2^{W} in CD_2Cl_2.

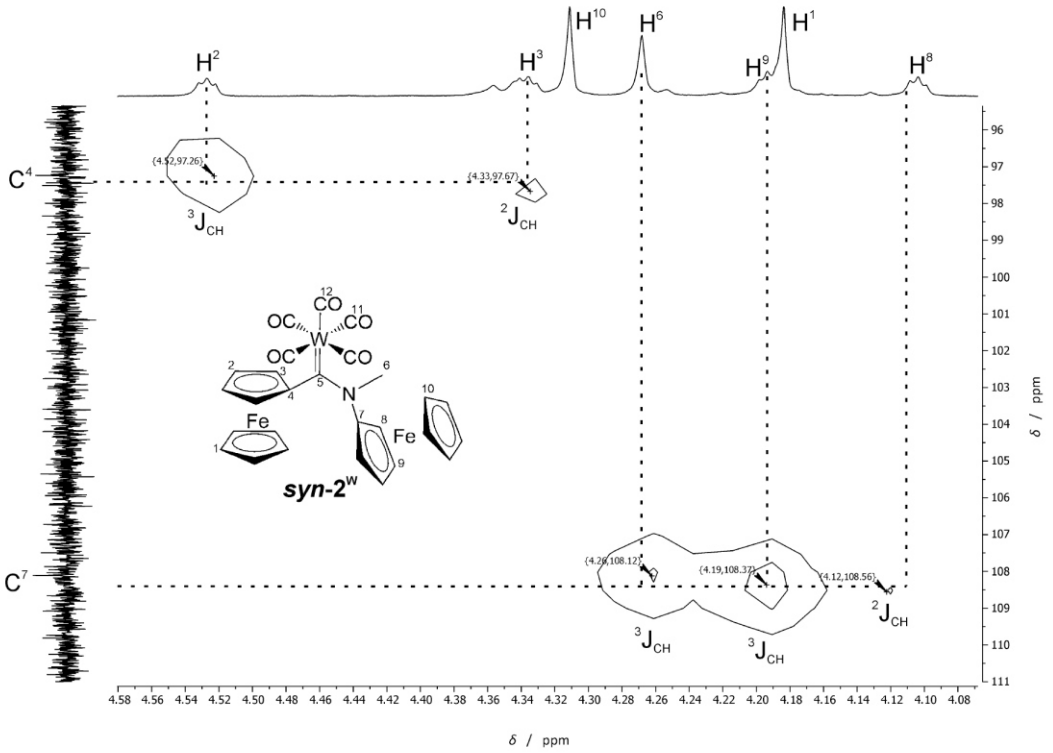

Fig. S07: ^{1}H-^{13}C-HMBC NMR spectrum of 2^{W} in CD_2Cl_2.

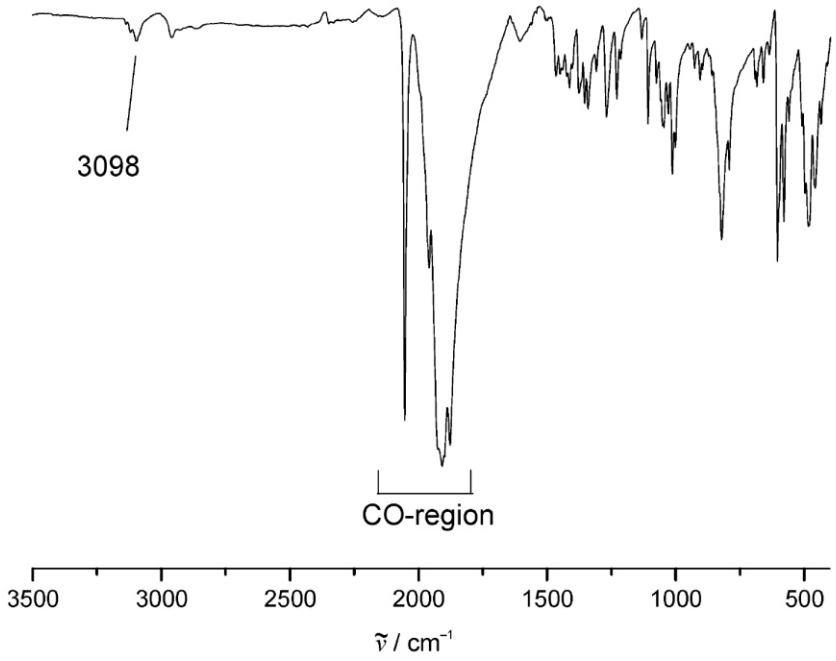

Fig. S08: IR spectrum (KBr) of 2^{W}.

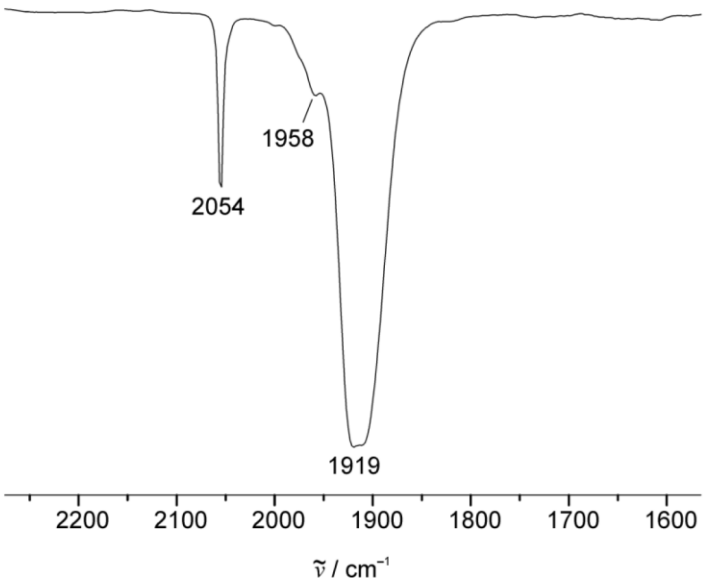

Fig. S09: IR spectrum of 2^W in DCM.

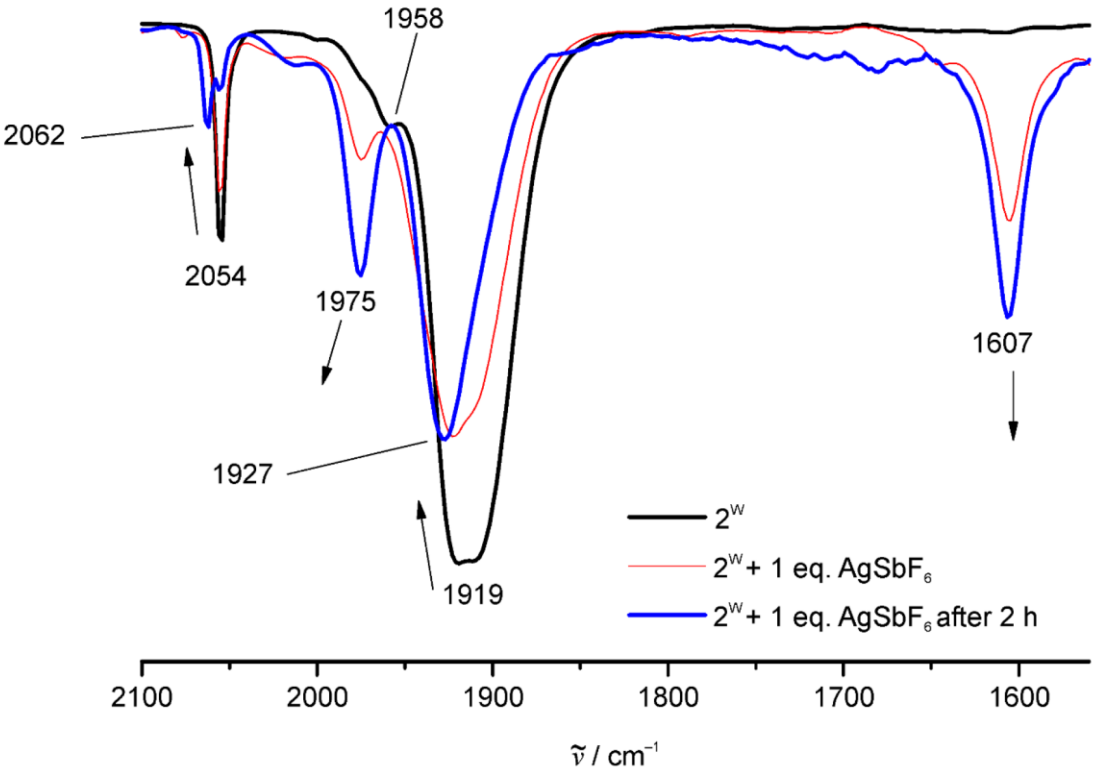

Fig. S10: IR spectrum of 2^W in DCM with 1 eq $AgSbF_6$.

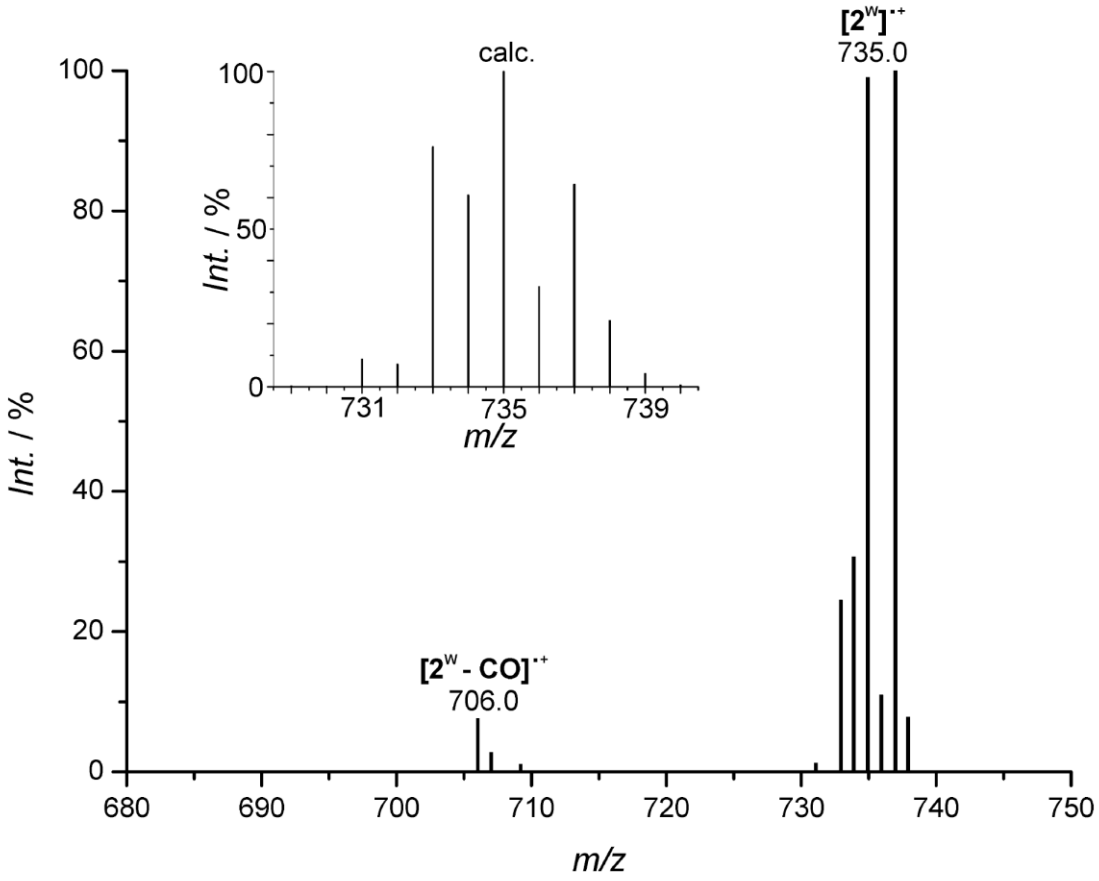

Fig. S11: FD-MS of 2^W in CH_2Cl_2.

Table S1. Selected bond lengths / Å and angles /° of $\mathbf{1}^{W}$, $\mathbf{1}^{Cr}$ [1], $\mathbf{3}^{OEt}$ [2], $\mathbf{3}^{NH2}$ [3] determined by XRD and $\mathbf{1}^{W}$ and ***syn/anti*-2**^{W} determined by DFT calculations.

	$\mathbf{1}^{W}$ (XRD)	$\mathbf{1}^{W}$ (DFT)	***syn*-2**^{W} (DFT)	***anti*-2**^{W} (DFT)	$\mathbf{1}^{Cr}$ (XRD)[1]	$\mathbf{3}^{OEt}$ (XRD)[2]	$\mathbf{3}^{NH2}$ (XRD)[3]
R1[a]-H1	0.8800	1.023	–	–	0.8800	–	0.88(5)/ 0.89(3)
R1[a]-Me	–	–	1.485	1.496	–	–	–
C1-C2	1.476(4)	1.486	1.479	1.492	1.477(3)	1.466(5)	1.488(7)
R1[a]-C1	1.325(3)	1.349	1.370	1.357	1.322(3)	1.315(5)	1.306(5)
R1[a]-C12	1.430(4)	1.431	1.443	1.446	1.424(3)	1.429(6)	–
M1[b]-C1	2.268(3)	2.242	2.309	2.306	2.097(2)	2.214(4)	2.249(5)
M1[b]-C22	2.003(3)	2.011	2.003	2.001	1.865(3)	2.018(5)	1.986(5)
M1[b]-C23	2.034(3)	2.038	2.036	2.036	1.903(3)	2.054(6)	2.035(5)
M1[b]-C24	2.024(3)	2.036	2.037	2.037	1.900(3)	2.021(6)	2.031(5)
M1[b]-C25	2.048(3)	2.037	2.034	2.036	1.910(3)	2.043(6)	2.034(5)
M1[b]-C26	2.060(3)	2.041	2.037	2.040	1.907(3)	2.034(6)	2.045(5)
C1-R1[a]-C12	126.4(2)	129.0	124.5	122.5	129.1(2)	124.1(4)	–
C1-M1[b]-C22	170.86(11)	177.2	174.8	174.9	176.48(11)	176.0(2)	177.2(2)
C3-C2-C1	125.3(2)	128.9	126.8	126.8	128.0(2)	124.5(4)	125.8(4)
C16-C12-R1[a]	125.0(3)	124.5	125.1	125.2	123.5(2)	–	–
C24-M1[b]-C26	170.95(12)	174.5	170.1	171.4	178.33(10)	175.4(2)	176.8(2)
C23- M1[b]-C25	177.94(11)	179.7	178.6	177.7	172.47(11)	178.0(2)	174.1(2)
M1[b]-C1-R1[a]-H1	-161.24	171.1	–	–	178.37	–	-2(4)/ -180(3)
M1[b]-C1-R1[a]-Me	–	–	34.7	163.2	–	–	–
Fe1-C2-C1- M1[b]	–96.7(2)	–130.5	–78.6	–121.7	–112.07(18)	99.9(3)	-89.4(4)
Fe2-C12-R1[a]-C1	151.2(2)	–155.0	128.0	–152.7	–157.9(2)	–	–
C3-C2-C1- M1[b]	–11.5(4)	–36.6	9.1	–25.4	–22.0(3)	-176.9(3)	-2.3(6)
C16-C12-R1[a]-C1	63.4(4)	117.5	39.3	117.3	115.2(3)	–	–
Fe1-X1[c]	1.6560(16)	1.729	1.734	1.737	1.653	1.657	1.649
Fe1-X2[d]	1.6420(14)	1.730	1.732	1.740	1.644	1.643	1.646
Fe2-X1[c]	1.6532(14)	1.729	1.732	1.735	1.658	–	–
Fe2-X2[d]	1.6539(12)	1.726	1.733	1.735	1.654	–	–
τ(Fe1)[e]	178.03(8)	177.6	175.4	174.4	178.83	178.58	177.92
τ(Fe2)[e]	178.99(7)	178.6	177.0	176.1	179.80	–	–

a) R = N for $\mathbf{1}^{W}$, $\mathbf{2}^{W}$, $\mathbf{1}^{Cr}$, $\mathbf{3}^{NH2}$, O for $\mathbf{3}^{OEt}$ b) M = W, Cr c) X1 = centroid of coordinated C_5H_5 ring.
d) X2 = centroid of coordinated C_5H_4 ring. e) τ = X1-M-X2.

Table S2: X-ray structures and DFT calculated geometries for: $\mathbf{1}^{\mathbf{W}}$ (XRD), $\mathbf{1}^{\mathbf{W}}$ (DFT), ***syn*-2**$^{\mathbf{W}}$ (DFT), ***anti*-2**$^{\mathbf{W}}$ (DFT), $\mathbf{1}^{\mathbf{Cr,NHFc}}$ (XRD)[1], $\mathbf{3}^{\mathbf{OEt}}$ (XRD) [2], $\mathbf{3}^{\mathbf{NH2}}$ (XRD) [3].

$\mathbf{1}^{\mathbf{W}}$ (XRD)	$\mathbf{1}^{\mathbf{W}}$ (DFT)	***syn*-2**$^{\mathbf{W}}$ (DFT)	***anti*-2**$^{\mathbf{W}}$ (DFT)
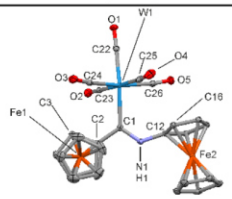	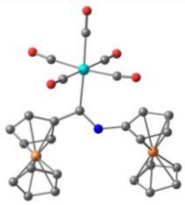	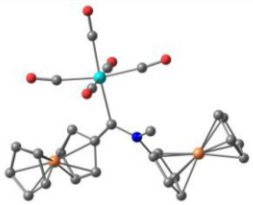	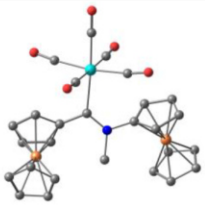
$\mathbf{1}^{\mathbf{Cr}}$ (XRD)[1]	$\mathbf{3}^{\mathbf{OEt}}$ (XRD)[2]	$\mathbf{3}^{\mathbf{NH2}}$ (XRD)[3]	
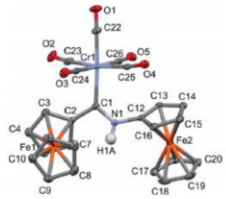	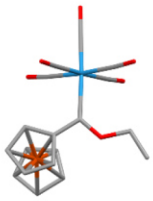		

Table S3: X-ray crystallographic data of $\mathbf{1}^{\mathbf{W}}$.

	$\mathbf{1}^{\mathbf{W}}$
empirical formula	$C_{26}H_{19}Fe_2NO_5W$
Fw	720.97
cryst syst	monoclinic
space group	*C2/c*
a / Å	12.0435(3)
b / Å	23.3639(7)
c / Å	17.3559(5)
α / deg	90
β / deg	104.4490(10)
γ / deg	90
volume / Å^3	4729.2(2)
Z	8
density (calcd) / Mg/m^3	2.025
absorption coefficient / mm^{-1}	6.102
F(000)	2784
crystal size / mm^3	0.260 x 0.120 x 0.020
θ range for data collection	2.424 to 28.000°
index ranges	$-15 \le h \le 15$
	$-30 \le k \le 29$
	$-22 \le l \le 22$
no. of reflns collected	33364
no. of indep. reflns	5703
R_{int}	0.0530
completeness to θ_{max}	99.9 %
max. / min. transmission	1.28882 / 0.59650
goodness-of-fit on F^2	0.907
final *R* indices [$I>2\sigma(I)$]	R1 = 0.0212
	wR2 = 0.0425
R indices (all data)	R1 = 0.0300
	wR2 = 0.0445
Largest diff. peak and hole, e / Å^3	1.224 / –0.510

References

[1] P. Veit, C. Förster, S. Seibert, K. Heinze, *Z. Anorg. Allg. Chem.* **2015**, *641*, 2083.
[2] J. G. López-Cortés, Contreras de la Cruz, Luis F., M. C. Ortega-Alfaro, R. A. Toscano, C. Alvarez-Toledano, H. Rudler, *J. Organomet. Chem.* **2005**, *690*, 2229.
[3] R. Streubel, M. Beckmann, C. Neumann, S. Fankel, H. Helten, O. Feier-Iova, P. G. Jones, M. Nieger, *Eur. J. Inorg. Chem.* **2009**, *2009*, 2090.

Cartesian coordinates of DFT optimized structures:

1^{W}

26	-0.304866000	3.476248000	0.069847000
8	-4.391537000	-3.488471000	-0.471781000
8	-4.016329000	0.003361000	2.148680000
26	3.681948000	-1.182484000	-0.006963000
74	-2.051922000	-1.349895000	-0.013506000
6	-0.485948000	0.226917000	0.280195000
6	-0.828651000	1.558883000	0.841738000
6	-2.021598000	2.353684000	0.634431000
1	-2.841011000	2.109463000	-0.023521000
8	-3.267447000	0.441763000	-2.400250000
6	-1.926702000	3.539624000	1.439319000
1	-2.663849000	4.328234000	1.489357000
8	-0.453838000	-3.063938000	-2.223637000
6	-0.677624000	3.497375000	2.160798000
1	-0.323357000	4.236960000	2.864665000
8	-0.881803000	-3.184161000	2.361702000
6	0.012748000	2.295448000	1.784885000
1	0.950238000	1.949838000	2.198215000
6	0.670950000	3.304050000	-1.809621000
1	0.879481000	2.376192000	-2.324381000
6	1.537721000	3.967402000	-0.862889000
1	2.517995000	3.633848000	-0.550761000
6	0.871397000	5.168609000	-0.417183000
1	1.256854000	5.880710000	0.299259000
6	-0.404464000	5.246253000	-1.087855000
1	-1.144721000	6.023168000	-0.956255000
6	-0.528661000	4.093425000	-1.948162000
1	-1.374884000	3.857702000	-2.578081000
6	1.605953000	-0.998952000	-0.369153000
6	1.866423000	-2.178579000	0.422475000
1	1.496240000	-2.371934000	1.417465000
6	2.716965000	-3.039297000	-0.357515000
1	3.090748000	-4.004691000	-0.047659000
6	2.994254000	-2.385520000	-1.613732000
1	3.604934000	-2.779740000	-2.413239000
6	2.315950000	-1.115736000	-1.621540000
1	2.299586000	-0.395629000	-2.427153000
6	4.424950000	0.530511000	1.001822000
1	3.857661000	1.407568000	1.282684000
6	5.139330000	0.342294000	-0.239154000
1	5.187458000	1.044998000	-1.059359000
6	5.780665000	-0.950188000	-0.192019000
1	6.382216000	-1.390238000	-0.975224000
6	5.462312000	-1.560350000	1.077206000
1	5.783607000	-2.537454000	1.410475000
6	4.624534000	-0.645576000	1.815580000
1	4.217067000	-0.813283000	2.802900000

7 Acknowledgments

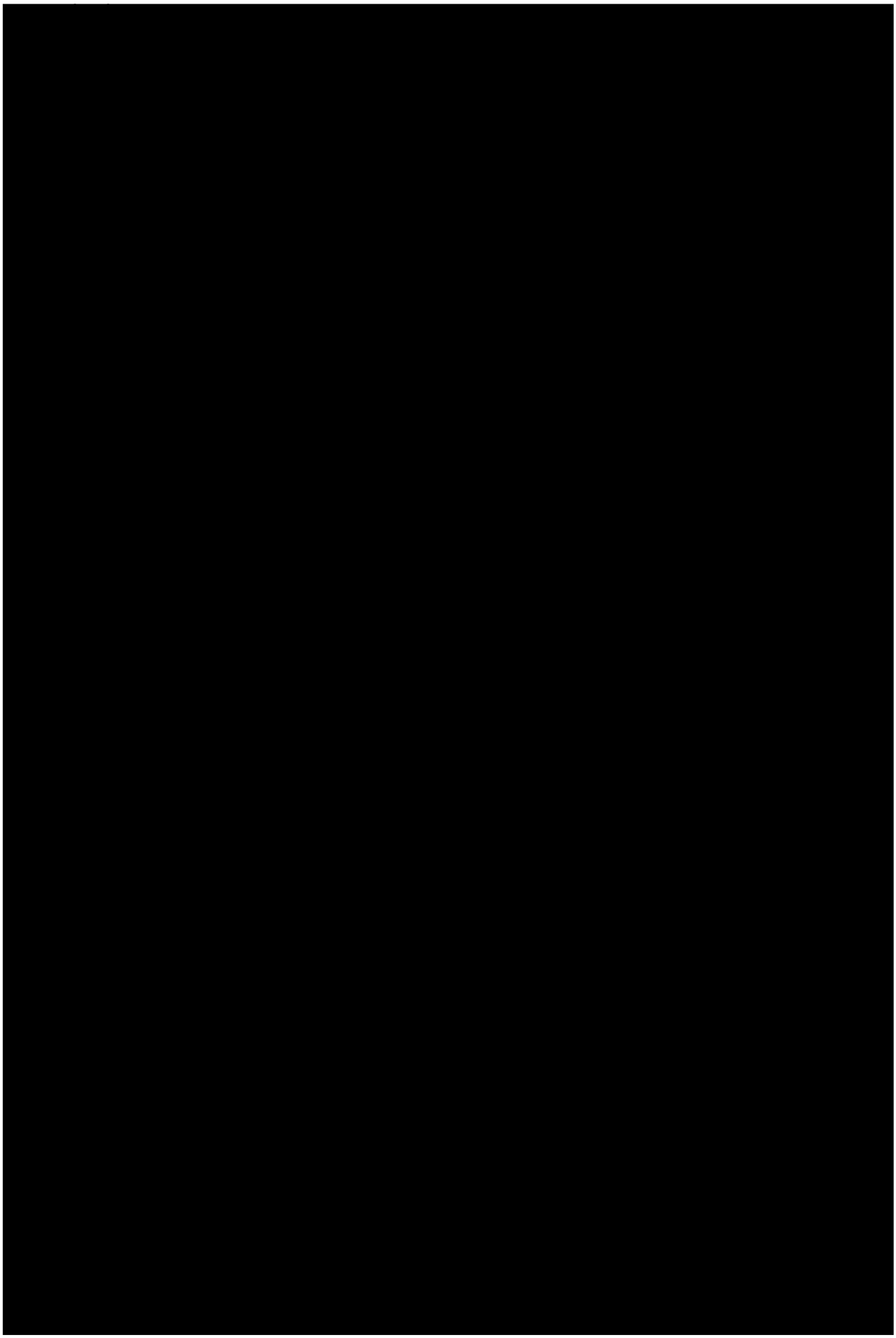

8 Curriculum Vitae

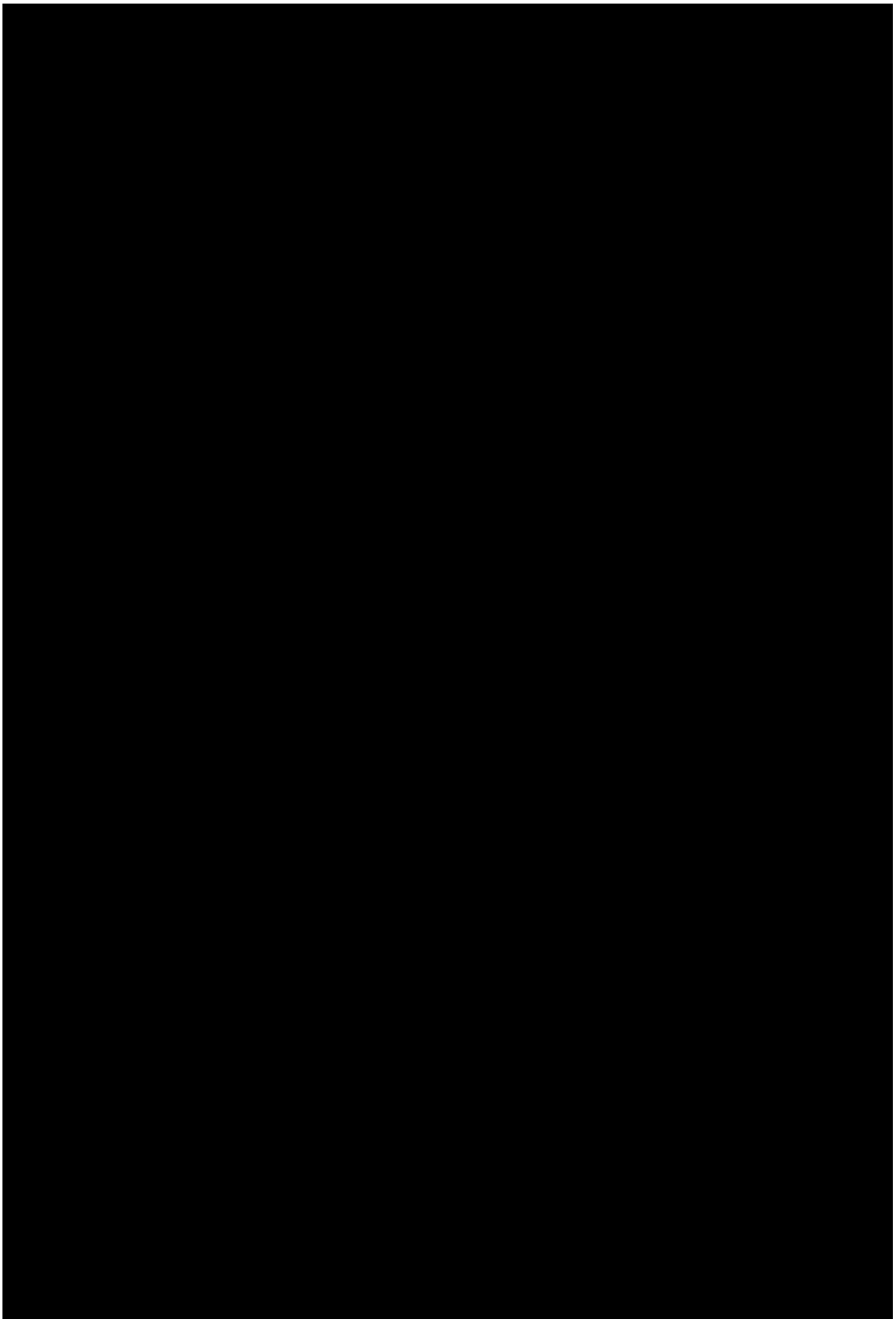

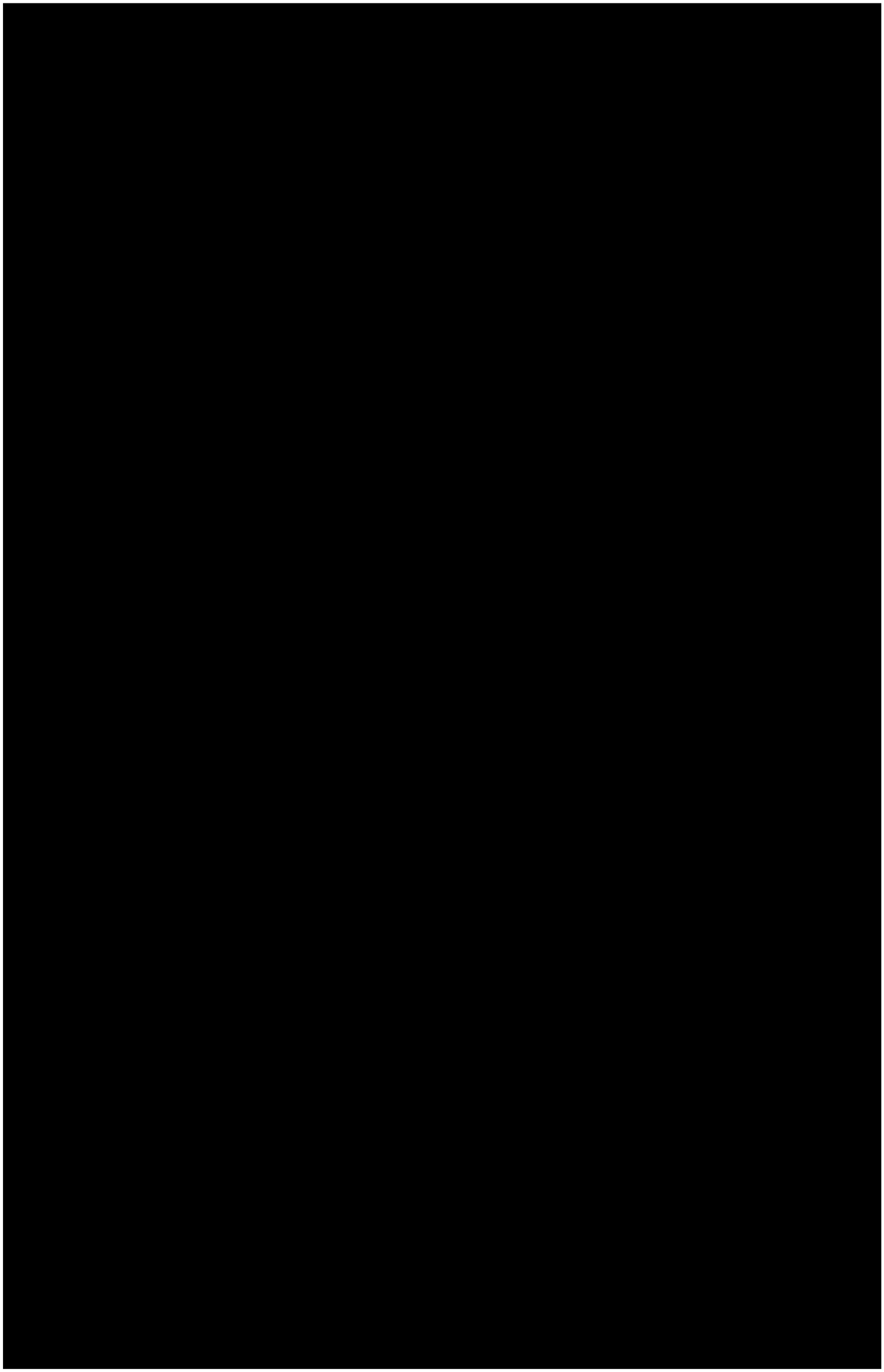

8.1 List of Publications

[7] **P. Veit**, C. Förster, K. Heinze, **2020**, Electrochemistry of the heterotrimetallic Fischer carbene complex (*N*-methylaminoferrocenyl)(ferrocenyl)carbene(pentacarbonyl)-tungsten(0), Manuscript in preparation.

[6] **P. Veit**, S. Seibert; C. Förster, K. Heinze, *Z. Anorg. Allg. Chem.*, **2020**, *646*, 1–9: Unexpected C-C Bond Formation with a Ferrocenyl Fischer Carbene Complex.

[5] **P. Veit**, C. Volkert, C. Förster, V. Ksenofontov, S. Schlicher, M. Bauer, K. Heinze, *Chem Commun.* **2019**, *55*, 4615–4618: Gold(II) in Redox-Switchable Gold(I) Catalysis.

[4] **P. Veit**, C. Förster, K. Heinze, *Beilstein J. Org. Chem.* **2016**, *12*, 1322–1333: On the mechanism of imine elimination from Fischer tungsten carbene complexes.

[3] **P. Veit**, E. Prantl, C. Förster, K. Heinze, *Organometallics* **2016**, *35*, 249–257: Competitive NH···Ru/Fe Hydrogen Bonding in Ferrocenyl Ruthenocenyl Tosyl Hydrazone.

[2] **P. Veit**, C. Förster, S. Seibert, K. Heinze, *Z. Anorg. Allg. Chem.* **2015**, *12–13*, 2083–2092: Preparation, Properties, and Reactivity of (Aminoferrocenyl) (ferrocenyl) carbene (pentacarbonyl)chromium(0) as Bulky Isolobal Trimetallo-amide.

[1] C. Förster, **P. Veit**, V. Ksenofontov, K. Heinze, *Chem. Commun.* **2015**, *51*, 1514–1519: Diferrocenyl tosyl hydrazone with an ultrastrong NH···Fe hydrogen bond as double click switch.

8.2 Conference Contributions

02/2018 **16th Ferrocene Colloquium**, Berlin
Poster presentation:
"Thermal Cyclization of Ferrocenyl Fischer Carbene Complexes"

09/2017 **GDCh-Wissenschaftsforum Chemie 2017**, Berlin
Poster presentation:
"New Reactivity of Group 6 Ferrocenyl Fischer Carbene Complexes"

02/2017 **15th Ferrocene Colloquium**, Mainz
Poster presentation:
"On the mechanism of imine elimination from trimetallic Fischer tungsten carbene complexes"

09/2016 **3rd International Conference on Bimetallic Complexes**, Kaiserslautern, 3MET
Poster presentation:
"On the mechanism of imine elimination from trimetallic Fischer tungsten carbene complexes"

02/2016 **14th Ferrocene Colloquium**, Konstanz
Oral presentation:
"Ferrocenyl Fischer-Carbene Complexes: Stability and Redox Ambiguity"

06/2015 **Heidelberg Forum of Molecular Catalysis**, Heidelberg
Poster presentation:
"Diferrocenyl Tosyl Hydrazone With a Rare N-H···Fe Hydrogen Bond"

02/2015 **13th Ferrocene Colloquium**, Leipzig
Oral presentation:
"Diferrocenyl tosyl hydrazone with an unusual hydrogen bond"